Synthesis of Nitrogen-Containing Carbohydrate Derivatives and Their Use Toward Inhibiting Ice Recrystallization and Gas Hydrate Formation

Malay Doshi

B. Sc. Honours Biopharmaceutical Science,
Medicinal Chemistry (Co-op) – University of Ottawa, 2010

Thesis submitted to the
Faculty of Graduate and Postdoctoral Studies
in partial fulfillment of the requirements
for the Doctorate in Philosophy degree in Chemistry

Department of Chemistry
Faculty of Science
University of Ottawa

Candidate

Malay Doshi

Supervisor

Professor Robert Ben

Acknowledgements

I would like to firstly thank Dr. Robert Ben for accepting me into his lab and giving me the amazing opportunity to pursue my Ph.D studies. He constantly encouraged me to be a better researcher, problem solver and to think critically about my work. He always taught me the invaluable lesson of thinking "big picture" about the work I did and presented. He also made me a better person overall. Thank you so much for your constant guidance and mentorship throughout my studies.

The next people I need to thank are my lab mates and this list is by no means in any order. I sincerely want to thank Dr. Anna Balcerzak for all of her help in the laboratory and outside it. I will never forget everything you did for me. You weren't just a lab mate but a true friend. Julia Meyer, thanks for all of the hilarious conversations about everything from chemistry to hilarious discussions on life. Mostly, via texts. Maddy Adam, thank you so much for editing the thesis and being an awesome friend and for the great football talks. Dr. Mathieu Leclère for teaching me and helping me learn so many techniques in the lab. Dr. John Trant for being an awesome mentor throughout my honour's thesis and teaching me lots of useful laboratory techniques. You also instilled your enthusiasm for chemistry in me. Devin Tonelli, thanks for always having utterly useless talks about life and for all your help on the gas hydrate project. Frank Loiseau, you weren't in the Ben lab but it was so much fun having your around. Your passion for chemistry always made me strive for more. Chantelle Capicciotti, thank you for always inspiring me to continue to push myself and learn as much as I could about my work. You really showed me what attention to detail really means and I'll never forget that. Matt Alteen, you are always around to talk chemistry and just have chats about life. You are truly the biggest yet cool nerd I know. Jennie Briard, thank you for all of your help on the umbilical cord blood experiments and all of the fun times we have had especially at the cottage. Thomas Charlton (aka "TChar"), thanks for making me laugh and being able to discuss chemistry and geeky things. You are the biggest hipster of the lab. Jessica Poisson thanks for being a great lab mate and all the great hiking and camping talks we have had. Don't forget those ear plugs while camping. Steph, you were a good friend in the lab and someone who would always listen to everything I had to say about life and chemistry. You always remembered dates and occasions which was something I couldn't do. Vanessa Musca, we were bay mates and it was definitely fun having discussions about life with you. It was never boring with you around. Kyle McClymont,

your love for chemistry was contagious. Thanks for all the memories outside the lab. The last day for your co-op session is something I won't forget. Amanda Saikaley, thanks for all the fun chemistry and non-chemistry chats we have had. Your constant energy in the lab was contagious. To the undergraduate students I was grateful to work with: Tiffany Tuen, Vikrant Singh and Allan Grant. All of your help has gone a long way towards the completion of this thesis. I'll never forget it. To the other undergrads which were part of Ben Laboratory whilst I was there. Amanda Commons, thanks for all the one liners. You were an awesome listener. Evan Perley-Robertson, you are one hell of a baker. Melody, you always had some story to talk about. I always got sucked into the stories. I would love to have you as my doctor someday.

Lastly, and most importantly, I need to thank my parents. You were there for me when I needed you the most. This thesis couldn't have been completed without you. You have been there every step of the way and have been my true inspiration for everything. Thank you.

Abstract

Ice recrystallization during cryopreservation results in cell death and decreased cell viabilities due to cellular damage. This is a significant problem particularly in regenerative medicine where decreased cell viabilities post-thaw affect the success of the therapy. Given the success of these therapies to treat various diseases, the development of novel cryprotectants which have the ability to inhibit ice recrystallization during freezing and thawing are urgently required. Current cryoprotectant such as dimethyl sulfoxide, is associated with cytotoxicity in the clinical settings and thus are not optimal cryoprotectants. Our laboratory is interested in the rational synthesis of non-cytotoxic small molecules which possess the property of ice recrystallization inhibition (IRI) activity.

Previously, the Ben laboratory has demonstrated that simple monosaccharides possess moderate ice recrystallization inhibition activity and that this activity is linked to hydration. The "compatibility" of the carbohydrate within the three-dimensional hydrogen bonded network of water is inversely proportional to its IRI activity. Hydration has previously been directly linked to the stereochemical relationship of individual hydroxyl groups on the carbohydrate. Additionally, it has been proposed that intramolecular hydrogen bond formation and hydrogen bonding cooperativity has a large effect on the water structure thus impacting hydration. Structure-function work has suggested that the presence of an amine as a hydrogen donor at the endocyclic position within the pyranose ring maybe beneficial to IRI activity. Thus, the first part of this thesis describes the synthesis and IRI activity of D-glucose and D-galactose based azasugars and its analogues. These azasugars have replaced the endocyclic ring oxygen with an amine. These azasugars and their analogues were found to possess moderate to potent IRI activity suggesting that hydrogen bond donation may be important for hydration and thus, IRI activity at the endocyclic ring oxygen.

During the development of these azasugars, the Ben laboratory developed carbohydrate-based surfactants and hydrogelators possessing unprecedented IRI activity. A potential use of molecules possessing IRI activity is towards the inhibition of gas hydrate formation. Gas hydrates are ice-like solids containing gases within a highly ordered network of water molecules. These gas hydrates tend to accumulate in oil and gas pipelines posing significant dangers as the build-up of solid material leads to blockages in the pipeline reducing flow. Previous work had demonstrated the use of antifreeze proteins possessing potent IRI activity in inhibiting gas

hydrate formation. However, their complex structure limits commercial use. Thus, the second part of the thesis describes the use of the azasugars, carbohydrate-based surfactants and hydrogelators in inhibiting gas hydrate formation. The effectiveness of the small molecules is compared to a commercial inhibitor PVP 10. Some of these small molecules were significantly better inhibitors of gas hydrate formation than the currently utilized inhibitor PVP 10. The low molecular weights of these small molecules, easy synthesis and potency make them excellent alternatives to PVP 10. However it was found that while some of the structural features in the small molecules may be amenable to both activities, it seems that the ability to inhibit ice recrystallization is not a good indicator of a compounds ability to inhibit gas hydrate formation.

In a continuing effort to develop novel small molecule IRIs, the Ben laboratory has develop three classes of compounds. These include: carbohydrate-based surfactants and hydrogelators, lysine-based surfactants and truncated *C*-linked glycopeptides. Structure-function work utilizing these compounds revealed that presence of long alkyl chains, an amide linkage and the presence of an open-alditol chain are all important to IRI activity. However, the surfactant-like nature limits their use in cryopreservation and thus prompted the discovery of phenoxyglycosides as IRI active molecules. The structural features of these recently developed small molecules were combined to generate novel small molecule IRIs which do not resemble surfactants. These novel small molecules included "disaccharides" which possessed an aryl group at the anomeric position of a pyranose ring and an open-alditol chain linked via an amide bond. Additionally, *N*-cycloalkyl-D-aldonamides and *N*-phenyl-D-aldonamides were also synthesized. Of these novel small molecules, two very potent IRI active molecules were discovered: a "disaccharide" possessing an aryl group at the anomeric position with the open-alditol chain of D-galactose linked via an amide bond at C3 and *N*-phenyl-D-arbonamide. Both of these small molecules were assessed for their ability to cryopreserve hematopoietic stem cells. Unfortunately, the additional of these compounds failed to improved percent cell viabilities as compared to DMSO.

Table of Contents

Table of Contents

List of Figures

List of Tables

List of Schemes

List of Abbreviation

7-AAD	7-Aminoacetinomycin D
α	Alpha
β	Beta
δ	Delta
ε	Epsilon
^{1}H	Proton
^{13}C	Carbon
AAs	Anti-agglomeration agents
Ac_2O	Acetic Anhydride
ACN	Acetonitrile
Ac	Acetate
Ara	Arabinose
AFP	Antifreeze protein
AFGP	Antifreeze glycoprotein
Atm	Atmosphere
Bn	Benzyl
Br	Broad
BzCl	Benzoyl Chloride
$BF_3{\cdot}OEt_2$	Boron trifluoride diethyl etherate
CMC	Critical micelle concentration
CSA	Camphorsulfonic acid
Cat	Catalyst
DCM	Dicholormethane
DIAD	Diisopropyl azodicarboxylate
DMF	*N*,*N*-diemthylformamide
DMSO	Dimethyl sulfoxide
DSC	Differential scanning calorimeter
dt	Doublet of triplets
EtOH	Ethanol
Gal	Galactose
Glu	Glucose
Hep G2	Human liver hepatocellular carcinoma cells

HSC	Hematopoietic stem cells
IC_{50}	Half maximal inhibitory concentration
IFP	French Petroleum Institute
IRI	Ice recrystallization inhibition
KHIs	Kinetic hydrate inhibitors
LDHI	Low-dosage hydrate inhibitor
Lc	Leukocyte
m	Multiplet
M	Molar
M^+	Parent molecular ion
Man	Mannose
mCPBA	*meta*-Chloroperbenzoic acid
MeOH	Methanol
Me	Methyl
MGS	Mean grain size
MHz	Megahertz
mM	Millimolar
MPa	Megapascal
MS	Mass spectrometry
MTT	3-(4,5-dimethylthiazol-2-yl)-2,5-diphenyltetrazolium bromide
NaOMe	Sodium Methoxide
NMO	*N*-methylmorpholine *N*-oxide
OMe	*O*-Methoxy
*p*BrPh	*para*-Bromophenyl
PBS	Phosphate-buffered saline
PhMe	Toluene
PMP	*para*-methoxylphenyl
Psi	Pound per square inch
PVP	Polyvinylpyrrolidone
sI	Structure I
sII	Structure II
sH	Structure H
SEM	Standard error of mean
*t*BuOH	*tert*-Butanol
Tal	Talose
Tf	Triflate
TBSOTf	*tert*-Butyldimethylsilyl Trifluoromethanesulfonate
Tf_2O	Trifluoromethanesulfonic anhydride
TH	Thermal Hysteresis
THF	Teterahydrofuran
THI	Thermodynamic hydrate inhibitor
TPAP	Tetrapropylammonium perruthenate
TsCl	*p*-Toluenesulfony Chloride
QLL	Quasi-liquid layer
UCB	Umbilical cord blood
WAXS	Wide-angle X-ray scattering

wt	Weight percent

Chapter 1. Introduction to Ice and Ice Recrystallization Inhibitors

1.1 Application of Ice Recrystallization Inhibition

Ice recrystallization is defined as the growth of large ice crystals at the expense of small ones. It is a thermodynamically driven process resulting in an overall reduction in the free energy of the system (this process is further explained in 1.3). [1] The phenomenon of ice recrystallization has been problematic in areas of cryopreservation of cells, tissues and frozen foods.[2, 3]

Cryostorage is an important process to preserve precious cell types such red blood cells and different progenitor cells. Ice recrystallization is known to be a significant cause of cell damage and cell death especially during the thaw process of cryopreservation.[2, 3] The same process has been responsible for changes in texture, taste and quality in frozen foods. [4] Freezing of foods is another well-established process used to decrease the rates of deterioration. In order to fully understand the relationship between ice recrystallization and cell damage, an explanation of cryo injury suffered during cryopreservation is required.

During cryopreservation, the formation of ice is inevitable but different cooling rates have been applied to mitigate the damage associated with ice formation. There is an optimal cooling and warming rate for each cell type that is dependent on cell permeability to water and cyroprotectants. In general, either a fast or slow cooling rate is employed during cryopreservation depending on the cell type. Usually, ice will prefer to form in the extracellular medium.[5] The formation extracellular ice causes an osmotic pressure across the cell membrane. All solutes are excluded from the ice lattice of extracellular ice and concentrated in the extracellular medium.[6-9] This causes the cell to undergo dehydration (intracellular water to external medium).[10] Cells with less permeable membrane will rupture with increasing pressure if they cannot dehydrate fast enough. This process of dehydration is necessary as decreased intracellular water reduces the chance for lethal intracellular ice formation. However, dehydration combined with exposure to high concentrations of electrolytes is also lethal to cells.[11] This is referred to the "solute effect" which causes irreparable damage to cell membranes.[5, 11] Excessive dehydration can be prevented using cryoprotectants. Two classes of cryoprotectants are commonly employed. Non-penetrating cryoprotectants do not cross the cell membrane and thus, increase the osmolality of the extracellular medium, facilitating dehydration. Penetrating cryoprotectants readily cross the cell membrane and decrease the concentration of intracellular electrolytes while maintain greater cell volumes.[12] In summary, cryopreservation of

cells under slow-freezing results in dehydration of the cell in response to increasing osmotic pressure. This dehydration has been shown to be detrimental to the cell.

Cryopreservation using high cooling rates traps water inside the cell promoting lethal intracellular ice formation.[13] High cooling rates generally lead to the formation of smaller ice crystals.[5] A high cooling rate must be accompanied by appropriate dehydration of the cell to mitigate cell death.[14] As mentioned above, a non-penetrating cryoprotectant can be employed to facilitate cell dehydration during fast-cooling protocols. Interestingly, while intracellular ice formation has been correlated to cell death, there is evidence that intracellular ice formation is not solely responsible for cell death.[15] Studies have indicated that the survival of cells post-cryopreservation is dependent on the warming rate utilized during thaw. It has been concluded that the cell death associated with intracellular ice formation is occurring as a result of ice recrystallization.[16-18] It is reported that at -100 °C, ice recrystallization can occur, and the rate of recrystallization is proportional to temperature and inversely proportional to ice crystal size.[19] Thus, while ice recrystallization can occur during freezing, the largest cell damage occurs during the thawing process during which higher temperatures and smaller ice crystals are present. Upon warming, the enthalpically favoured recrystallization of ice (discussed in 1.3) will occur outside and inside the cell causing stress on the membrane.[5] Therefore, the less thermodynamically stable and smaller ice crystals will merge into larger ones which then apply stress on the cytoplasmic and plasma membranes. The result is a ruptured membrane which undoubtedly induces cell death.[5] Ice recrystallization is not limited to cryopreservation protocols utilizing a high cooling rate. Cells with low water permeability require slow cooling rates to allow for sufficient dehydration to inhibit intracellular ice formation. However, it is often difficult to obtain a slow enough cooling rate to completely inhibit intracellular ice formation and therefore ice recrystallization will always occur and cause cell death.[5]

Recently, the cryopreservation of certain progenitor cells such as hematopoietic stem cells has become increasingly important with recent advances in regenerative medicine therapies.[20, 21] Regenerative therapies have been utilized during the treatment of many medical complications such as spinal cord injury,[22] coronary artery disease,[22] heart attacks,[23] stroke,[24] various cancers, genetic diseases, immune deficiencies and blood disorders.[25] However, the success of regenerative therapy is closely correlated to the quality and number of cells recovered post-thaw.[26] Reduced post-thaw cell viabilities due to cryo injury caused by ice recrystallization

remains a major problem. The mechanism of recrystallization has been extensively studied in the metallurgical and material science literature.[1, 27-29] However, the reasons that some compounds are better inhibitors of ice recrystallization that other are not known. Additionally, the key structural features necessary for effective ice recrystallization inhibition have not been elucidated. In order to fully understand the mechanism of ice recrystallization, an understanding of properties of ice is required.

1.2 Properties of Ice

The many different forms of ice are dependent on temperature and pressure. The most common form of ice, hexagonal (I_h), is formed at atmospheric pressure and below 0 °C.[30, 31] The basic structure of I_h consists of six water molecules forming a chair-form when viewing from the *z*-axis. When viewing from the vertical axis, the structure is a boat-form containing six water molecules (**Figure 1-1**). Each water molecule is typically hydrogen bonded with four other surrounding water molecules. The typical distance between oxygen nuclei in 2.76 Å; covalently bonded hydrogens are about 1 Å from an oxygen nucleus, and the hydrogen bond length comprises the remaining 1.76 Å. Generally, one hydrogen lies between adjacent oxygen atoms in the hydrogen bond found in ice. These structures form hexagonal plates where the top and bottom faces are the basal planes, consisting of the chair-form configuration. The six equivalent side faces are called the prism face and consist of the boat-form configuration. The I_h ice lattice unit is composed of four axes a_1, a_2, a_3, and c, and the surface of each unit has eight faces.[30-33] The structure of I_h is depicted in **Figure 1-1**. The basal faces are normal to the c-axis while the remaining six faces are the prism faces. At 0 °C and atmospheric pressure, ice growth is along the *a*-axis producing hexagonal shaped crystals which grow as sheets.[30-32, 34]

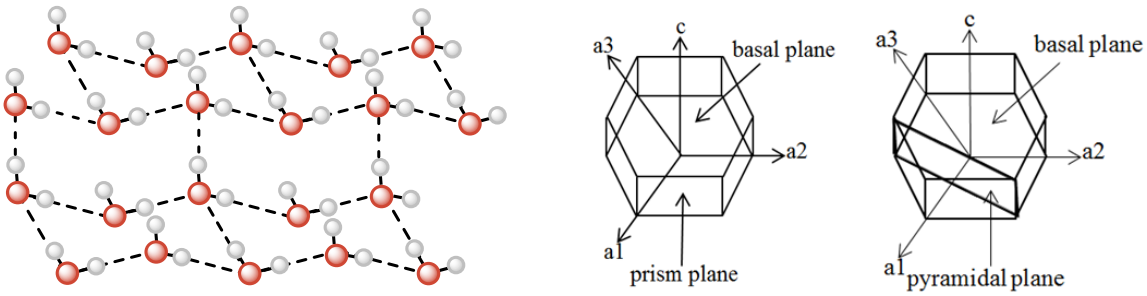

Figure 1-1. Structure of the hexagonal ice I_h lattice unit illustrating the three-dimensional hydrogen bonded network of water in which make up the different planes. Also illustrated are the different axes which are part of the lattice unit.[12]

The water surrounding newly formed ice crystals is not as dynamic as originally hypothesized.[35-39] It have been discovered that there is a semi-ordered layer of water at the interphase between solid ice and bulk water called the quasi-liquid layer (QLL).[33, 35, 40-44] **Figure 1-2** represents the QLL.

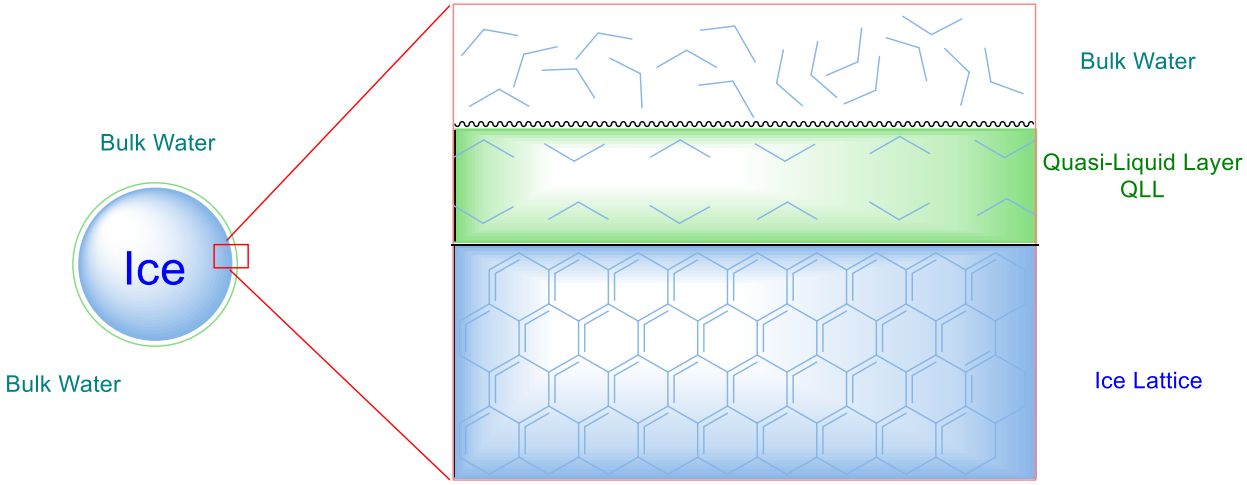

Figure 1-2. Schematic representation of the quasi-liquid layer (QLL) between bulk water and ice.

The thickness of the QLL is 10-15 Å thick but is highly temperature dependent.[35, 42, 45] Its thickness increases as the temperature approaches the melting point.[46] For example, the thickness of the QLL at -0.03 °C was measured to be 15 nm, or 40 monolayers of water. However, at -10 °C, less than a monolayer remains.[36] The exact molecular nature and thickness of the QLL interface has been debated throughout the literature and a wide variety of techniques have been used to study it, including atomic force microscopy, [47] X-ray diffraction, [48] infrared spectroscopy,[36] proton backscattering, [49] Raman spectroscopy, [50] quartz-crystal microbalance measurements,[51] light scattering techniques, [52-54] photoelectron spectroscopy,[55] optical

ellipsometry,[44, 56, 57] optical reflection[58] and mechanical measurements.[59] Ellipsometric studies, measuring the refractive index on the basal and prism faces of ice, have suggested that the interface is more water-like in nature, rather than ice-like.[43, 47, 55, 57, 60] In contrast, other studies have suggested that the orientation and motion of water molecules in the QLL closely resembles that of ice.[48, 49, 58] The exact nature of the QLL is still not understood indicating that the equilibrium between ice and water is complicated.

1.3 Mechanisms of Ice Recrystallization

The recrystallization of ice can be explained through two different mechanisms: grain boundary migration or Ostwald ripening. A grain of I_h ice (hexagonal ice) is the ordered arrangement of the water molecules in a crystalline structure (ice crystal). Grain boundaries represent the interface between differently oriented ice grains.[1, 61] At equilibrium, a grain of I_h would have six neighbouring I_h grains where the angle between the grain boundaries is 120° and all segments are straight. However, outside of equilibrium, some grains have more than six neighbours and some have fewer than six. Thus, the 120° angles require a grain boundary with curvature. A big grain (large ice crystal) tends to have more than six neighbors and thus, its grain boundary tends to be concave (bulge inwards). In contrast, a small grain (small ice crystal) tends to have fewer than six neighbours and thus, its grain boundary tends to be convex (bulge outwards).[1] During grain boundary migration, molecules of water transfer from an unfavourable orientation to a more favourable orientation within ice grains. Smaller ice grains have convex grain boundaries resulting in higher surface energy while in contrast, larger ice crystals have concave grain boundaries and thus lower surface energy.[1] Grain boundaries migrate to grow large ice crystals at the expense of smaller ice crystals to reduce the degree of curvature and thus reducing the overall energy in the system.[62, 63] Grain boundary migration is depicted in **Figure 1-3**.

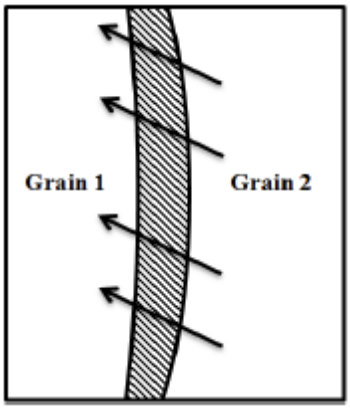

Figure 1-3 Representation of a liquid-layer (shaded) in a curved boundary between two ice grains. Large ice grains with concave boundaries (grain 2) grow larger while small grains with convex boundaries (grain 1) decrease in size to reduce the overall degree of grain boundary curvature. Arrows indicate the direction of boundary migration.[12]

The mechanism of grain boundary migration fails to discuss the interaction between ice, QLL and bulk water. In an ice crystal, water molecules on the surface are less stable than the water molecules in ice because the water molecules at the surface are unable to form the optimal amount of hydrogen bonds. Therefore, smaller ice crystals that have a higher surface area to volume ratio are thermodynamically less stable than large ice crystals which possess a greater volume to surface area ratio.[1] During Ostwald ripening, ice volume is assumed to remain constant.[64, 65] Therefore, Ostwald ripening suggests water molecules are transferred from the surface of smaller ice crystals to bulk water, and finally to larger ice crystals. This results in an overall reduction in the free energy of the system.[66]

Since the recrystallization of ice is detrimental to cells during the thaw process of cryopreservation,[67] there is an increasing interest in effective ice recrystallization inhibitors. Naturally occurring biological antifreezes are very effective inhibitors of ice recrystallization. These compounds protect certain organisms, such as fish, insects and amphibians, inhabiting in sub-zero climates from cryo injury.[32, 68-73]

1.4 Biological Antifreezes

There are two mains classes of biological antifreezes: antifreeze proteins (AFP) and antifreeze glycoproteins (AFGPs). AFPs were first discovered by Scholander and colleagues who observed the survival of telost fish in water temperatures of -1.9 °C (normal freezing point of the blood serum is -0.8 °C).[74, 75] DeVries and Wohlschlag later attributed their survival to proteins and glycoproteins.[76-78]

There are four different classes of AFPs found in fish and they differ significantly in their structures as shown in **Table 1-1**. AFPs have been found in many other organisms, such as the spruce budworm moth,[79, 80] the yellow mealworm beetle,[81, 82] the fire-coloured beetle[83] and the snow flea.[84] AFPs have also been found in plants,[85-92] fungi and bacteria.[93-98]

Table 1-1. Classification and structural differences between fish antifreeze proteins (AFPs) and antifreeze glycoproteins (AFGPs).[12]

Characteristic	AFGP	Type I AFP	Type II AFP	Type III AFP	Type IV AFP
Mass (kDa)	2.6-33	3.3-4.5	11-24	6.5	12
Key Properties	AAT repeat; disaccharide	Alanine-rich α-helix	Disulfide bonded	β-sandwich	Alanine rich; helical bundle
Representative Structure	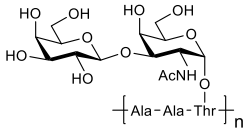				
Natural Source	Antarctic Notothenioids; northern cods	Right-eyed flounders; sculpins	Sea raven; smelt; herring	Ocean pout; wolfish; eel pout	Longhorn sculpin

AFGPs have homologous structures and are separated into eight classes based on their molecular weights. AFGP-1 has a molecular weight of 33.7 kDa while AFGP-8 has a molecular weight of 2.6 kDa.[99] A typical AFGP is shown in **Figure 1-4** and contains a repeating alanine-alanine-threonine tripeptide unit with the secondary oxygen of threonine glycosylated to β-D-galactosyl-(1,3)-α-*N*-acetyl-D-galactosamine.[78, 100] Some AFGP structures contain minor amino

acid variations, such as the alanine replaced by a proline or a threonine replaced by an arginine.[101-106]

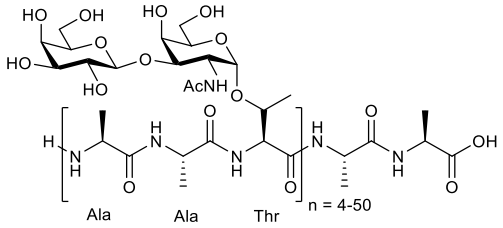

Figure 1-4. General structure of AFGPs.

1.5 Properties of Biological Antifreezes

There are two general properties of biological antifreezes: thermal hysteresis (TH) and ice recrystallization inhibition (IRI). TH activity of AF(G)Ps was the first property described in the literature. TH is defined as the selective depression of the freezing point of a solution relative to the melting point.[107-109] This activity is the direct result of AF(G)Ps binding to a seeded ice crystal which results in a localized freezing point depression.[110, 111] Pure water has a melting and freezing point of 0 °C. The introduction of salts into the system will result in a colligative depression the melting and freezing points by the same amount. Salts hinder the ability of water molecules to align properly to form an ice lattice. However, in the presence of AF(G)Ps, binding causes changes to the ice crystal habit and a difference between the melting point and freezing point is observed. The difference in temperature between these two properties is known as a TH gap (**Figure 1-6A**) and AF(G)Ps that cause this effect are referred to as possessing TH activity. Ice crystals formed within the TH gap are neither growing nor melting. This is significant because as long as the temperature is within the TH gap, large amounts of ice will not form therefore protecting organisms inhabiting sub-zero temperatures.

The mechanism of TH is attributed to an irreversible adsorption of AF(G)Ps to specific planes of a growing ice crystal. Binding occurs on the prism face of ice and thus ice growth occurs along the *c*-axis leading to spicule ice crystal shape. This change in the crystal shape is referred to as dynamic ice shaping and is illustrated in **Figure 1-5.**[99, 107, 112-115] As the temperature is cooled beyond the TH gap, ice crystals will continue to grow as sharp spicules and eventually cause complete freezing of the solution.

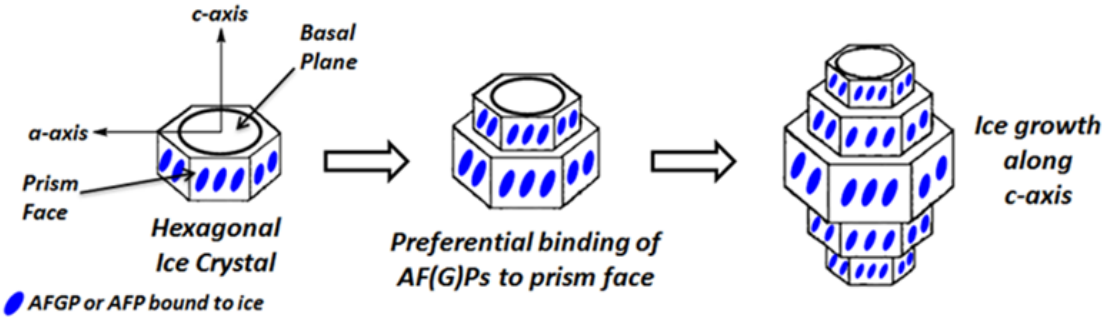

Figure 1-5. Change in an ice crystal habit during recrystallization in the presence of an AF(G)P.[12]

The irreversible adsorption of AF(G)Ps causing a localized freezing point depression can be rationalized using the Kelvin effect.[109, 113] In this effect, the AF(G)P adsorbs to an ice prism face and water molecules can only adsorb on the surface between the AF(G)P adsorption sites. As water molecules add to the surface, the radius of curvature increases. The increase of surface tension at the curved surface hinders the addition of subsequent water molecules and ice growth is stopped. However, if the temperature is decreased below the TH gap, the curvature increases to a point where the bound AF(G)P are frozen over, resulting in rapid expansion of the ice crystal, often forming spicules.[109] This radius threshold before the ice over-growth occurs is known as the Kelvin radius. This effect does not affect the energetics of the melting process and thus, only the freezing point is depressed.[72, 109, 115]

Two models have been developed to describe how AF(G)Ps inhibit ice growth within the TH gap: the Step-Pinning Model and the Mattress Model. In the Step-Pinning Model, ice growth is thought to occur in steps advancing across a plane and AF(G)Ps pin ice growth along these steps.[113] In the Mattress Model, AF(G)Ps inhibit ice growth perpendicular to the ice surface.[110] The TH gap and both of these models are presented in **Figure 1-6**.

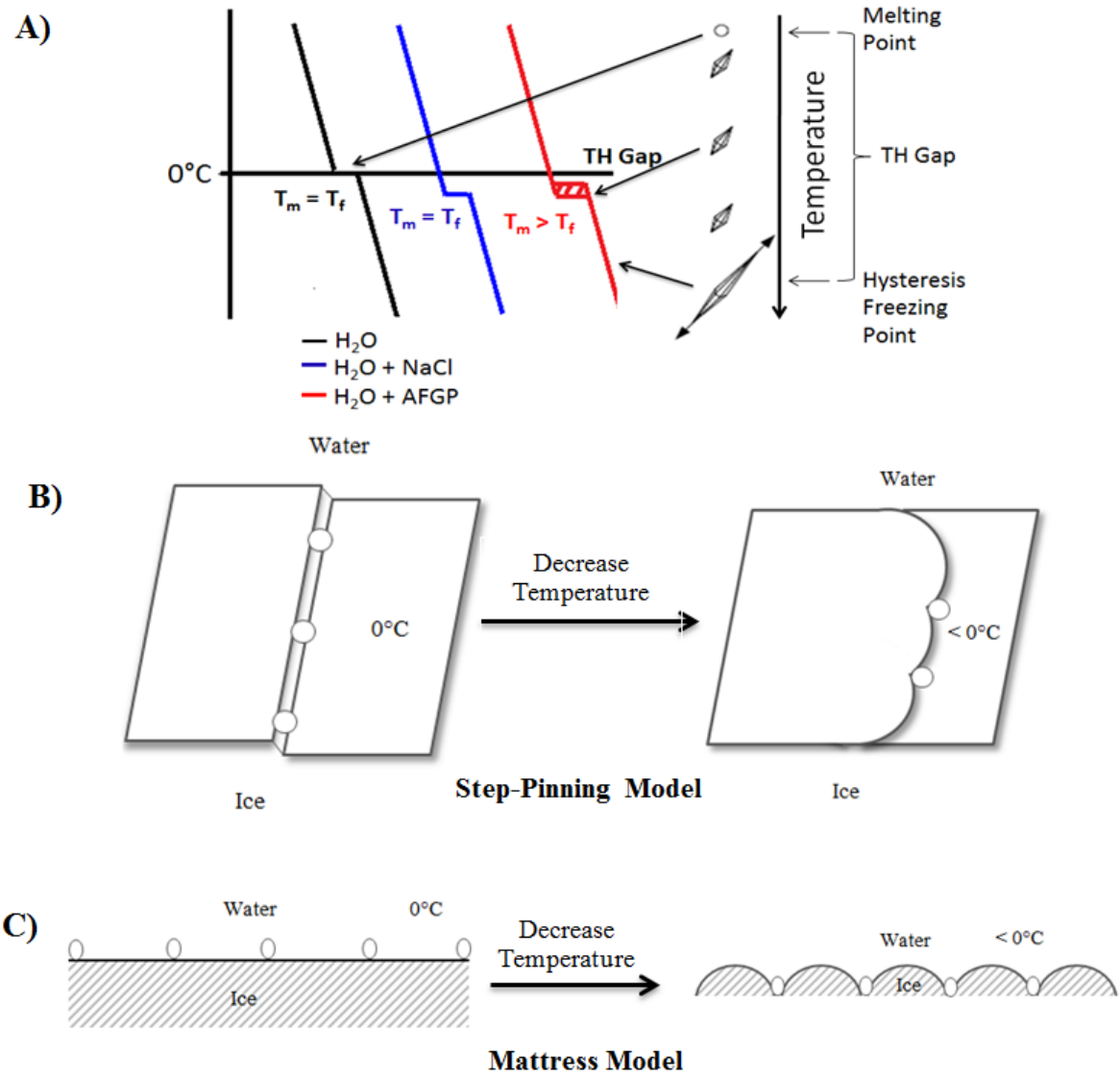

Figure 1-6. Illustrations of thermal hysteresis (TH) activity and two models of ice growth inhibition. A) An illustration of a TH gap resulting from the depression of a freezing point relative to the melting point. B) Step-Pinning Model and C) Mattress Model depicting the irreversible adsorption-inhibition mechanism of AF(G)Ps.[12]

The second property associated with biological antifreezes is ice recrystallization inhibition (IRI). IRI is the ability to maintain small ice crystals within a frozen solution. As described previously, while ice recrystallization can occur during freezing, it causes the most cellular damage during thawing in cryopreservation and thus, IRI is a highly desirable property.

While AF(G)Ps possess potent IRI activity, their use as cryoprotectants have yielded conflicting results. Cryopreservation studies utilizing AFGPs to cryopreserve pig oocytes, mouse embryos, carp spermatozoa and human platelet cells all displayed increases in cell viabilities post

cryopreservation. In contrast, high concentrations of AFGPs failed to protect an isolated rat heart during the freeze-thaw process.[116, 117] Overall, in the literature the use of AF(G)Ps as cryopreservatives is considered ineffective.[118] The lack of success as effective cryoprotectants is due to the formation of speculate ice crystals which form below the TH gap which damages cells. Temperatures employed during cryopreservation are well below the TH gap.[119] Therefore, an ideal cryoprotectant will possess the beneficial IRI activity without the damaging effects of TH.

1.6 Synthetic AFGP Analogues

The Ben laboratory was first to publish rationally designed and synthesized *C*-linked AFGP analogues **101-104** (**Figure 1-7**).

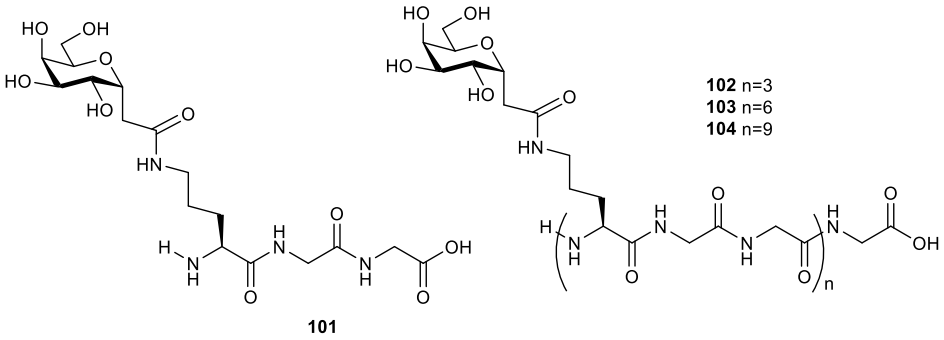

Figure 1-7. Structure of the first *C*-linked AFGP analogues.

These analogues possess potent IRI activity similar to AFGP-8 but do not possess the TH activity.[120] The lack of an *O*-glycosidic linkage, normally found in AFGPs, made these analogues less susceptible to hydrolysis under acidic or basic conditions. Comparing their structures to AFGPs, the disaccharide is replaced with D-galactose which is α-conjugated to lysine. Lysine was chosen to mimic arginine residues commonly found in AFGPs. Additionally, glycine was used to replace alanine to avoid racemization encountered during solid-phase synthesis. Only compounds **103** and **104** were moderately IRI active. Both compounds showed a TH gap of 0.06 °C and induced dynamic ice shaping.[120] However, a TH gap of 0.06 °C has been shown to be negligible during cryopreservation. [121]

In a follow-up study, the Ben laboratory published two more *C*-linked AFGP analogues exhibiting potent IRI activity. The structure of these compounds, **105** and **106** are shown in **Figure 1-8**.

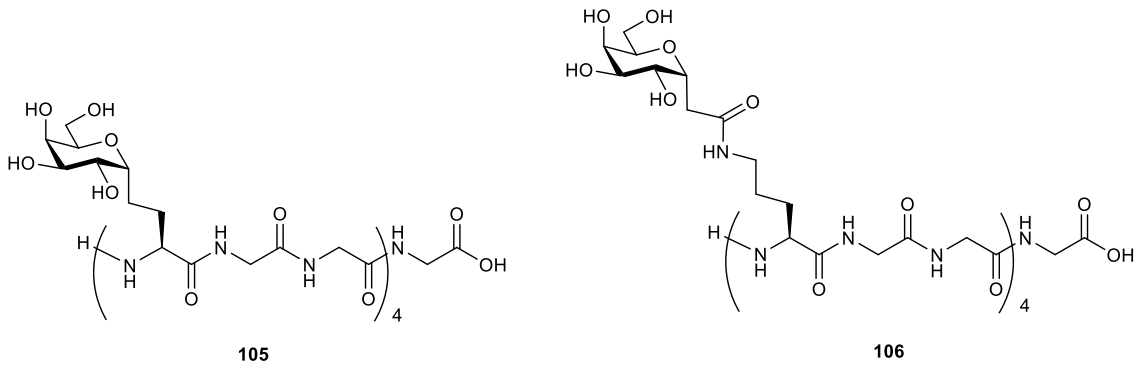

Figure 1-8. *C*-linked AFGP analogues containing "custom tailored" potent antifreeze activity.

Both compounds **105** and **106** contain a D-galactose unit which is *C*-linked to four tripeptide unit repeats. Compound **106** is structurally similar to lysine derivatives **102-104** but the D-galactose is now α-conjugated to an ornithine residue.[122] Compounds **105** and **106** both exhibited potent IRI activity at 5.5 μM and their activity was similar to that exhibited by AFGP-8 at 5.5 μM. Unlike AFGP-8, neither compound exhibited TH activity and compound **106** only exhibited very weak dynamic ice shaping.[122] These analogues were the first examples of compounds with "custom-tailored" antifreeze activity where the two properties of biological antifreezes, TH and IRI, were decoupled.

With these analogues in hand, the Ben laboratory performed structure-function work to determine the structural features necessary for potent IRI activity. Analogues of **106** were synthesized in which D-galactose was replaced with D-glucose (**107**), D-mannose (**108**) and D-talose (**109**) monosaccharide moieties (**Figure 1-9**).[38]

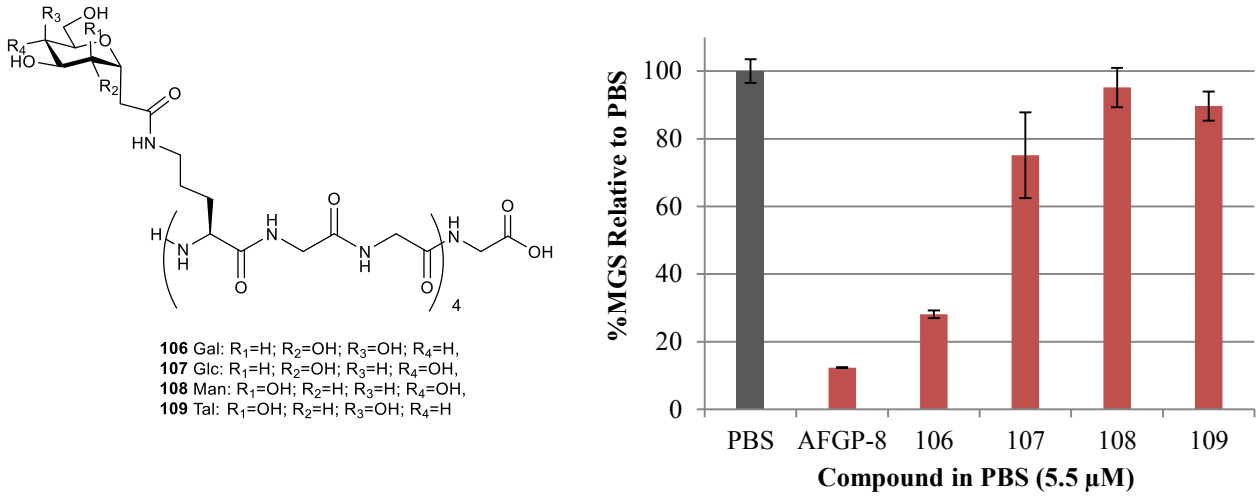

Figure 1-9. Structures of *C*-linked AFGP analogues containing various monosaccharide moieties.[38]

The IRI activity of **106-109** was measured using the splat-cooling assay.[123] In the splat-cooling assay, a 10 µL solution is dropped from 2 meters high onto a pre-cooled (-78 °C) aluminum block. This causes the solution to instantaneously freeze as a thin ice wafer forming many small ice crystals in the process. This ice wafer, measuring 1 cm wide and 20 µm thick, is then transferred to a glass cover slip and onto a Peltier unit. The wafer is then warmed to -6.4 °C and annealed for 30 minutes to allow for recrystallization to occur. The presence of small ice crystals after the annealing time indicates inhibition of recrystallization has occurred, whereas large ice crystals show no inhibition of ice recrystallization. The size of the ice crystals can be quantified using a Domain Recognition Software.[124] Commonly, analytes are assayed in a salt solution which negates non-specific IRI effects observed otherwise in pure water.[1] The Ben laboratory uses a phosphate buffered saline (PBS) solution, which is therefore a positive control for ice recrystallization. The IRI activity of **106-109** is presented in **Figure 1-9** where the *y*-axis of the graph represents the ice crystal mean grain size (MGS) relative to PBS. The D-galactose analogue, **106**, was the most potent derivative, while D-glucose analogue **107** exhibited moderate IRI activity. D-Mannose and D-talose analogues, **108** and **109**, exhibited weak IRI activity. The results illustrate the effect on IRI activity and thus the importance of the stereochemical relationship of the hydroxyl groups on the carbohydrate moiety of the glycopeptide.

A similar result was obtained when the monosaccharides were examined individually as reducing sugars. The IRI activity of the monosaccharides is shown in **Figure 1-10**.

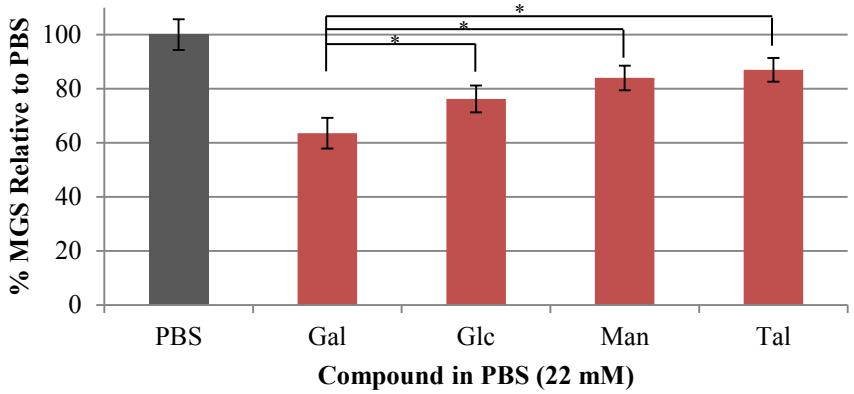

Figure 1-10. IRI activity of simple monosaccharides.[39] Asterisk indicates a statistical significant difference between samples and is defined by unpaired Student's *t*-test (*, $p < 0.05$). Statistical significant difference between the PBS control and samples is not shown. Samples have been run in triplicate (n = 3) and error bars indicate standard error of the mean (SEM).

D-Galactose was the most potent inhibitor while D-glucose exhibited only moderate IRI activity, and both D-mannose and D-talose possessed weak IRI activity. The stereochemistry of the hydroxyl group is also known to influence the hydration of the carbohydrate; and therefore, hydration of a compound is important when considering IRI activity.[39] A concentration scan of D-galactose revealed that concentration higher than 0.0022 M was required to generate IRI activity with 0.22 M being particularly effective. Although a 0.22 M concentration results in reasonable IRI activity, viscosity issues made it technically difficult to handle within the assay. However, a 0.022 M solution showed IRI activity nearly identical to that of a 0.044 M solution, but did not present viscosity issues[39] and thus, a 0.022 M concentration is generally utilized within this thesis. A recent study from the Ben laboratory examined the relationship between carbohydrate hydration and IRI activity, and found a strong linear relationship between the hydration number and IRI activity. The structures of the mono- and disaccharides studied along with their hydration numbers, isentropic molar compressibility, and partial molar volume values are shown in **Table 1-2**.[39]

Table 1-2 Isentropic molar compressibilities ($10^4K_2^o$(s), cm^3 mol^{-1} bar^{-1}) and hydration numbers of various monosaccharides and disaccharides. Errors of molar compressibility values and hydration numbers are shown in parentheses.[12]

Carbohydrate	Molar Compressibility (K_2^o(s)x10^4,cm^3 mol^{-1} bar^{-1})	Hydration Number	Carbohydrate	Molar Compressibility (K_2^o(s)x10^4,cm^3 mol^{-1} bar^{-1})	Hydration Number
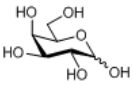 D-Galactose	-20.8 (0.5) -20.4 (0.4)	8.7 (0.2)	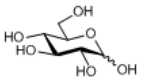 D-Glucose	-17.6 (0.3)	8.4 (0.2)
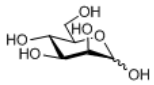 D-Mannose	-16.0 (0.5)	8.1 (0.2)	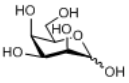 D-Talose	-11.9 (0.3)	7.7 (0.2)
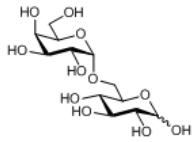 Melibiose	-31.2 (1.0)	15.5 (0.3)	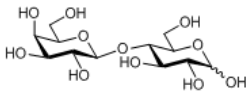 Lactose	-31.1 (0.2) -30.4 (1.0)	15.3 (0.3)
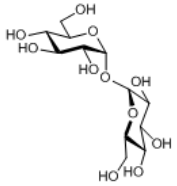 Trehalose	-30.2 (0.3)	15.3 (0.3)	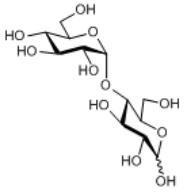 Maltose	-23.7 (1.0)	14.5 (0.3)
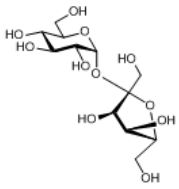 Sucrose	-17.8 (0.5)	13.9 (0.3)			

Hydration can be described as the number of water molecules that interact closely with a solute. In the 1990s, Galema *et al.* studied key parameters thought to dictate hydration characteristics and these were correlated to carbohydrate stereochemistry. The partial molar volumes, isentropic partial molar compressibilities and hydration numbers were determined for many commercially available mono- and disaccharides using kinetic experiments and density ultrasound measurements.[125-127] Using these values, Galema *et. al.* were able to quantify the "compatibility" of carbohydrates within the three-dimensional hydrogen bonded network of bulk water. The compatibility of the carbohydrate was directly related to the stereochemical relationship of the hydroxyl groups on the carbohydrate. For example, the presence of axial

hydroxyl groups on C2 and C4 of D-talose, had a higher isentropic molar compressibility value and a lower hydration number and thus fit well into the three-dimensional hydrogen bonded network of bulk water. However, with one axial hydroxyl group at C4, D-galactose, has a lower isentropic molar compressibility value and a higher hydration number. Therefore, D-galactose is a poor fit into the three-dimensional hydrogen bonded network of bulk water.[125-127] Highly hydrated carbohydrates with a poor fit into the three-dimensional hydrogen bonded network ultimately cause disorder in bulk water and the semi-ordered QLL since carbohydrates are thought to concentrate at the interface between bulk water and the semi-ordered QLL.[39] As stated in section 1.3, bulk water molecules transfer first to the QLL during ice recrystallization, and then from the QLL to the growing ice lattice. A carbohydrate with a poor fit in bulk water will cause a greater disturbance to its three-dimensional hydrogen bonded network, thus increasing the energy associated with the transfer of bulk water to the QLL. Therefore, IRI activity observed with carbohydrates occurred at the bulk water-QLL interface. Given that the thickness of the QLL is small and the entropy of the first hydration shell can extend out to the third hydration shell,[128] this energy difference would be significant. Highly hydrated carbohydrates, such as D-galactose, disrupted the pre-ordering of bulk water (increase the entropy of surrounding bulk water) making it energetically unfavorable for water molecules to transfer to the QLL thus causing inhibition of ice recrystallization.[39] The relationship between IRI activity and carbohydrate hydration is summarized in **Figure 1-11.**

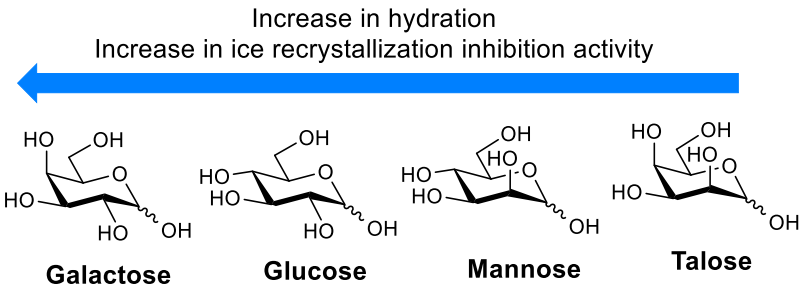

Figure 1-11. An illustration of the relationship between IRI activity and carbohydrate hydration.

1.7 Defining Potent IRI Activity

As described above, the effectiveness of IRIs has previously been accomplished using a splat-cooling assay. This generates mean grain size (MGS) of an analyte's ice crystals relative to a PBS positive control at a single time point.[124] However, this approach ignores two well-known aspects of recrystallization: time dependence of crystal growth and the heterogeneous nature of

crystal sizes obtained during recrystallization.[129] The MGS is not an accurate representation of a non-homogenous sample in which the distribution of ice crystal sizes is quite large, notably at increased time points. Recently, the Ben laboratory has developed a complimentary analysis ideally suited to measure a rate constant for the recrystallization process in the presence of IRIs when large ice volume fractions are present such as in the splat-cooling assay.[129] In this assay, ice crystals of each wafer were grouped into equally sized "bins", where the incremental bin size was determined by the smallest area into which all crystals could be fit at time zero. The summed area of all the crystal in each bin was then converted to a proportion of the area of the total sample, in order to emphasize the relative importance of each bin. It was observed that while most bins increased or decreased in population over time, the initial bin only decreased over time. Furthermore, this decrease could be described using a simple mono-exponential equation, providing a first order rate constant for the depopulation of the initial bin. Using previously discovered small molecule IRIs, the Ben laboratory were able to demonstrate that the rate constant varies as a function of the inhibitory concentration. A classic dose-response curve was utilized to characterize the concentration dependence on the rate-constant. Utilizing a four-parameter sigmoidal equation, parameters such as efficacy, potency (IC_{50}) and cooperativity (Hill slope) could be determined for each small molecule IRI. The small molecule IRIs utilized in the study proved to be full antagonists with low millimolar range IC_{50} values.[129] Additionally, the Hill slope was found to be greater than 1 and this suggested that cooperativity may be involved in the mechanism of action of these small molecule IRIs. It was suggested that these small molecules may for self-assembling structures within the QLL disfavouring the transfer of bulk water to the QLL and ultimately to ice during ice recrystallization.[129] While this assay provides further insight to the properties of the novel small molecule IRIs, many of the small molecules discussed within this thesis were analyzed using the traditional splat-cooling with a single time-point. Therefore, the MGS obtained from the traditional splat-cooling assay will be further defined in order to accurately discuss the effectiveness of the small molecule IRIs presented within this thesis.

Compounds producing a MGS of 25% or lower relative to PBS are referred to as possessing potent IRI activity. Compounds that have moderate IRI activity produce MGS of 25-80% relative to PBS. Finally, compounds that have weak to no IRI activity produce MGS of 80-100% relative to PBS.

1.8 Small Molecule Ice Recrystallization Inhibitors

Following the report that simple carbohydrates exhibit moderate IRI activity, the Ben laboratory developed various carbohydrate derivatives with the ability to inhibit ice recrystallization. Since *C*-linked AFGP analogues displayed potent IRI activity, α-*C*-linked allylated derivatives **110-113** of simple monosaccharides were assessed for IRI activity to investigate the effect of a carbon substituent at the anomeric carbon. Additionally, β-*C*-linked allylated derivatives **114-115** were also assessed.[39] The effect of fluorine was explored in **116** and its derivatives **117-118**.[130] Other D-galactose based analogues **119-121** have also been assessed for IRI activity.[130, 131] The structure of carbohydrate derivatives **110-121** are shown in **Figure 1-12**. At 22 mM, these analogues possessed only moderate IRI activity with activity not exceeding 60% MGS relative to PBS. It was concluded that simple groups at the anomeric carbon did not affect IRI activity.

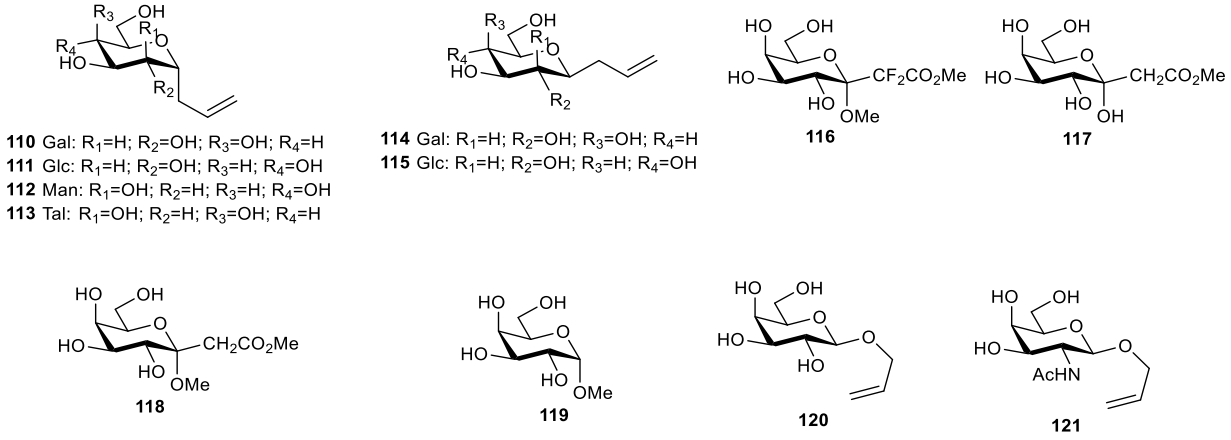

Figure 1-12. Structure of monosaccharide ice recrystallization inhibitors.

Along with monosaccharide analogues, structural analogues of the disaccharide found in native AFGPs were investigated for IRI activity. These included an analogue, **122**, of the native AFGPs (**Figure 1-13**), regioisomers of **122** where the terminal β-D-galactose moiety is linked to the C4-OH or C6-OH group of *N*-acetyl-D-galactosamine (**124** and **125** respectively), and disaccharide **123** in which the C2 *N*-acetyl group is replaced with a hydroxyl group. Disaccharides **122-125** exhibited similar IRI activity to D-galactose. The activities of **122** and **125** were statistically indistinguishable from D-galactose. This result indicated that the β-(1,3) and β-(1,6) linkages does not greatly affect IRI activity relative to D-galactose. However, the

most IRI active disaccharide was **124**, a disaccharide unlike the native AFGP.[131] This is interesting as the native disaccharide in AFGPs possess a β-(1,3) linkage whereas the most active disaccharide possess a β-(1,4) linkage. Most importantly, these disaccharides are not glycoconjugated to the native alanine-alanine-threonine peptide and thus, it is unknown whether a glycoconjugate of **124** would be more active than the native AFGP.[131]

As previously described, the Ben laboratory has generated compounds with "custom-tailored" antifreeze activity where the two properties of biological antifreezes, TH and IRI, were decoupled. It has been previously reported that the C2 acetamide in the native AFGP is crucial for TH activity.[132] However, removal of the C2 acetamide to generate **123** had no effect on IRI activity as **122** and **123** had indistinguishable IRI activity. It is very interesting that the C2 acetamide was deemed important for TH activity but not for IRI activity.

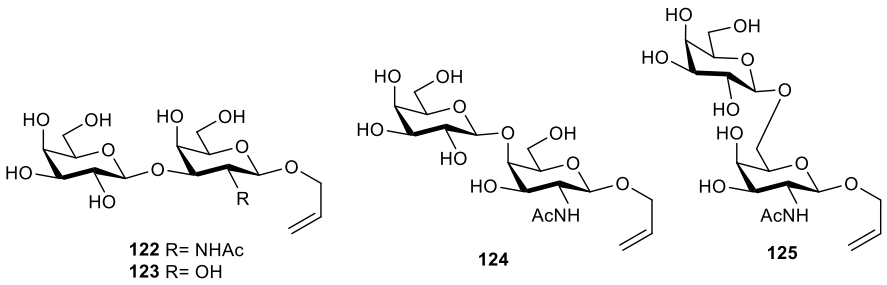

Figure 1-13. Structural disaccharide analogues of the native β-D-galactosyl-(1-3)-*N*-acetyl-D-galactosamine disaccharide found in native AFGPs.

Utilizing the structure-function worked described above, the Ben laboratory continued its efforts to generate potent small molecule IRIs which lack the detrimental TH activity. In 2012, the Ben laboratory demonstrated that small molecule carbohydrate-based surfactants and hydrogelators exhibit very potent IRI activity.[133] It was the first report of small molecules exhibiting very potent IRI activity.[133] Many of the compounds showed much more potent IRI activity than their parent reducing sugars. It was hypothesized that compounds such as surfactants and hydrogelators have the ability to disturb the structure of bulk water and therefore may also be effective IRIs. The structures of these compounds are shown in **Figure 1-14**.

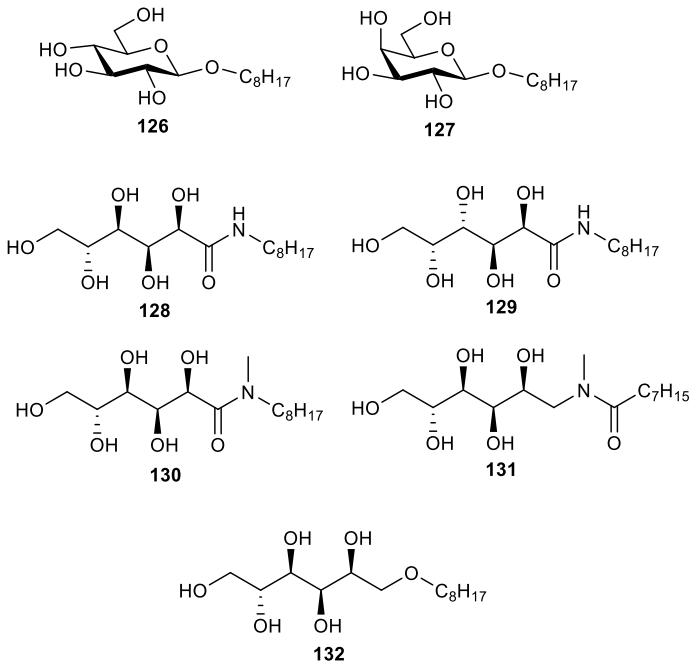

Figure 1-14. Structure of carbohydrate-based IRI active surfactants and hydrogelators.

After assessing non-ionic surfactants **126** and **127** for IRI activity, it was found that D-galactose based surfactant (**127**) exhibited potent IRI activity even at 11 mM. D-Glucose based surfactant (**126**) was only moderately IRI active. In addition to surfactants, hydrogelators of the *N*-octyl-D-aldoamides, **128** and **129**, were assessed for IRI activity. The D-glucose derivative was found to have unprecedented potent IRI activity at a low concentration of 0.5 mM (all other compounds were tested at 22 mM). To date, this is the most active small molecule IRI. Interestingly, the D-galactose derivative was found to be only weakly active at 0.5 mM. This trend is the opposite of that seen when testing D-glucose and D-galactose as reducing sugars. *N*-methylated analogues **130** and **131** exhibited weak activity which demonstrated the importance of the hydrogen linked to the amide nitrogen. Compound **132** exhibited weak IRI activity and highlighted the importance of the amide bond. None of these compounds were found to exhibit TH activity or dynamic ice shaping and thus were not binding to ice. This was later confirmed with solid-state NMR studies.[133] This was the first example of small molecules exhibiting "custom-tailored" antifreeze activity on par with AFGPs and their analogues.

Another class of surfactants possessing potent IRI activity developed by the Ben laboratory was based on low-molecular weight organogelators.[134-138] The structure of lysine based analogues is displayed in **Figure 1-15**. For surfactants **133-142**, the α- and ε-amino

terminals were acylated with alkyl chains of different lengths.[139] Additionally, the carboxylic acid was converted to a lithium, sodium or potassium carboxylate salt to improve solubility and thereby creating an anionic lysine surfactant.

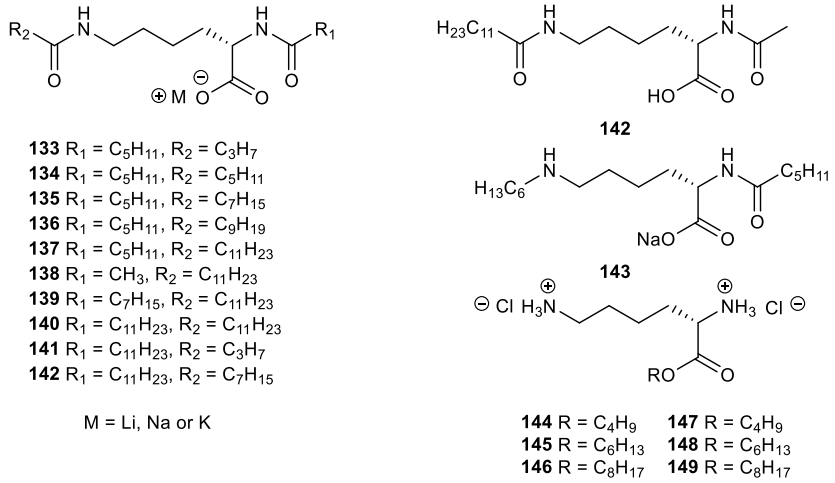

133 $R_1 = C_5H_{11}$, $R_2 = C_3H_7$
134 $R_1 = C_5H_{11}$, $R_2 = C_5H_{11}$
135 $R_1 = C_5H_{11}$, $R_2 = C_7H_{15}$
136 $R_1 = C_5H_{11}$, $R_2 = C_9H_{19}$
137 $R_1 = C_5H_{11}$, $R_2 = C_{11}H_{23}$
138 $R_1 = CH_3$, $R_2 = C_{11}H_{23}$
139 $R_1 = C_7H_{15}$, $R_2 = C_{11}H_{23}$
140 $R_1 = C_{11}H_{23}$, $R_2 = C_{11}H_{23}$
141 $R_1 = C_{11}H_{23}$, $R_2 = C_3H_7$
142 $R_1 = C_{11}H_{23}$, $R_2 = C_7H_{15}$

M = Li, Na or K

142

143

144 R = C_4H_9 **147** R = C_4H_9
145 R = C_6H_{13} **148** R = C_6H_{13}
146 R = C_8H_{17} **149** R = C_8H_{17}

Figure 1-15. Structure of lysine-based anionic and cationic surfactants.

Assessment of the lysine surfactants possessing a sodium carboxylate salt revealed that the most potent analogues had an eleven carbon alkyl chain at R_2 (**137-140**). These analogues were tested at 22 mM in a 0.5 mg/mL NaCl standard solution. Interestingly, the alkyl chain at R_1 did not significantly affect IRI activity.[139] The nature of the carboxylate salt had an impact on IRI activity, as the IRI activity of carboxylic acid **142** was lower than the activity of the carboxylate salt of direct analogue **138**. Conversion of **135-138** to either a lithium or potassium carboxylate salt affected IRI activity compared to their corresponding sodium carboxylate salts. During the study of carbohydrate-based surfactants, it was noticed that the presence of the amide bond was important to activity.[133] Similarly, removing the carbonyl group from the amide bond in **134** to generate **143**, resulted in a loss in IRI activity.[139]

Cationic lysine derivatives possessing alkyl esters of various lengths (**144-149**) were also assessed for their IRI activity. These derivatives possessed both amines as hydrochloride salts. At 22 mM in a 0.5 mg/mL NaCl solution, the most IRI active analogue contained a ten carbon chain (**147**).[139] Interestingly, increasing this alkyl chain to twelve or fourteen carbons (**148** and **145** respectively), resulted in a decrease in IRI activities.[139] An overall analysis of the studies utilizing compounds with long alkyl chains demonstrates the importance of hydrophobic moieties to IRI activity. Additionally, the position and size of these domains also affect IRI

activity. A delicate balance between hydrophobic and hydrophilic moieties is required for potent IRI activity.[100]

Of all the carbohydrate-based analogues discussed up to now, *C*-linked AFGP analogues **105** and **106** were one of the most potent IRI active compounds. Thus, the *C*-linked AFGP analogue **106** was truncated to determine the smallest sub-unit that can exhibit potent IRI activity.[140] The structures of truncated analogues of **106** are shown in **Figure 1-16**. Compounds **150-163** contain alkyl chains from one to sixteen carbons. Ionizable groups such as amine and carboxylic acid groups as well as alcohol groups were explored in **164-166**. Additionally, structurally diverse groups such as branched alkyl chains (**167-170**), rings (**171-172**), and various alkenes and alkynes (**173-177**) were also examined.

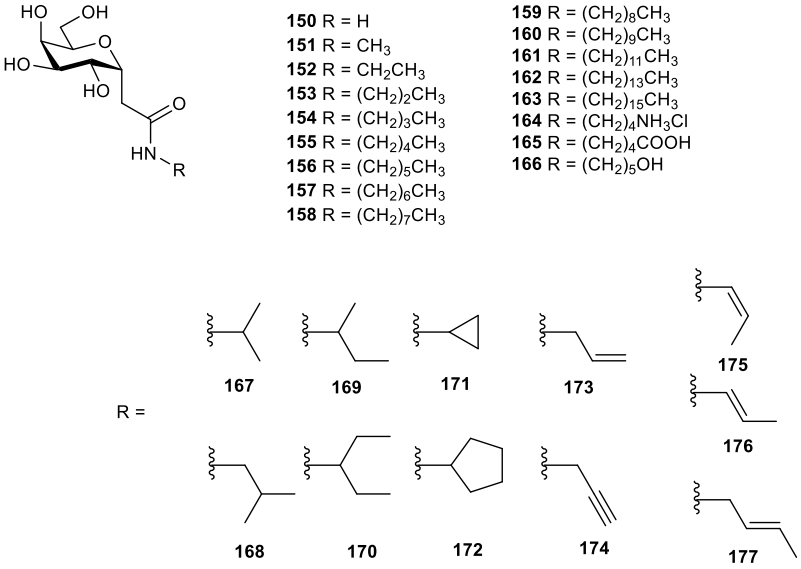

Figure 1-16. Structure of truncated *C*-linked AFGP analogues.

When derivatives containing alkyl chain analogues were assessed for IRI activity at 22 mM in PBS, compounds containing seven (**157**) and eight (**158**) carbons atoms, exhibited potent IRI activity. The analogues containing nine and ten carbon atoms (**159** and **160**) were tested at a lower concentration (5.5 mM) due to solubility problems and these were even more active than **157** and **158** at the same concentration. Even at 5.5 μM, the analogues with the longest alkyl chains, **162** and **163**, were as active as D-galactose at 22 mM while **157-161** had substantially decreased IRI activity at the 5.5 μM concentration. The ionizable groups did not improve IRI activity as **164** and **165** were only moderately active. However, a slight improvement in activity was observed in the presence of an alcohol (**166**). Compounds containing unsaturated alkyl

chains (**173**-**177**) were only moderately IRI active. Once again, it was concluded that hydrophobic moieties are beneficial for IRI activity and that small molecule ice recrystallization inhibitors with potent IRI activity can be developed.[140]

1.9 Chapter Summary

In summary, the utilization of cryopreservation as a process for the long term storage of many biological systems has great importance in many different industrial applications. Improvement of current cryopreservation has driven the search and use of novel cryoprotectants possessing high IRI activity. Thus far the use of highly IRI active compounds as cryoprotectants has been limited to AF(G)Ps, "custom-tailored" C-linked AFGP analogues and polymers. The use of small molecules during cryopreservation has been limited to simple carbohydrates possessing moderate IRI activity. Thus, there is continuous interest in the development of novel small molecules IRIs capable of acting as cryoprotectants in commercial applications. To date, small molecules possessing potent IRI activity is limited to carbohydrate-based molecules possessing large hydrophobic moieties which resemble organogelators or surfactants. Given that surfactants are likely detrimental to cell membranes, there is a need to further expand the variety of carbohydrate-based small molecule IRIs. As the application of novel IRI active molecules continues to expand, further development of small molecule IRIs will have a significant impact in many different commercial applications.

2.0 References

1. Knight, C. A.; Wen, D.; Laursen, R. A., *Cryobiology* **1995,** 32, 23-34.

2. Baust, J.; Van Buskirk, R., *In Vitro Cell. Dev. Biol. Animal* **2000,** 36, 262-270.

3. Baust, J. M., *Cell Preservation Technol.* **2002,** 1, 17-31.

4. Petzold, G.; Aguilera, J. M., *Food Biophys.* **2009,** 4, 378-396.

5. Mazur, P., *Science.* **1970,** 168, 939-949.

6. Hobbs, P. V., *Ice Physics*. 1st ed.; Oxford University Press, USA: Oxford, UK, 1975.

7. Lovelock, J. E., *Biochim. Biophys. Acta.* **1953,** 10, 414-426.

8. Lovelock, J. E., *Biochim. Biophys. Acta.* **1953,** 11, 28-36.

9. Meryman, H. T.; Williams, R. J.; Douglas, M. S. J., *Cryobiology* **1977,** 14, 287-302.

10. Meryman, H. T., *Cryobiology* **1971,** 8, 489-500.

11. Mazur, P., *Life in the Frozen State - Principles of Cryobiology*. CRC Press: Boca Baton, FL, 2004.

12. Capicciotti, C. J.; Doshi, M.; Ben, R. N., Ice Recrystallization Inhibitors: From Biological Antifreezes to Small Molecules. In *Recent Developments in the Study of Recrystallization*, Wilson, P., Ed. InTech: New York, 2013; pp 177-224.

13. Karlsson, J. O. M.; Cravalho, E. G.; Borel Rinkes, I. H.; Tompkins, R. G. Y., M. L.; Toner, M., *Biophys. J.* **1993,** 65, 2524-2536.

14. Mazur, P., *Cell Biophys.* **1990,** 17, 53-92.

15. Fowler, A.; Toner, M., *Ann. N.Y. Acad. Sci.* **2005,** 1066, 119-135.

16. Fowler, A.; Toner, M., *Ann. N.Y. Acad. Sci.* **1998,** 858, 245-252.

17. Farrant, J.; Molyneux, P.; Hasted, J. B.; Peares, P.; Echlin, P., *Phil. Trans. R. Soc. Lond. B* **1977,** 278, 191-205.

18. Acker, J. P.; McGann, L. E., *Cell Transplantation* **2002,** 11, 563-571.

19. Kingery, W. D., *J. Appl. Phys.* **1960,** 31, 833-838.

20. Broxmeyer, H. E.; Douglas, G. W.; Hangoc, G.; Cooper, S.; Bard, J.; English, D.; Arny, M.; Thomas, L.; Boyse, E. A., *Proc. Natl. Acad. Sci. U. S. A.* **1989,** 86, 3828-3832.

21. Mason, C.; Dunnill, P., *Regener. Med.* **2007,** 3, 1-5.

22. Saporta, S.; Kim, J.-J.; Willing, A. E.; Fu, E. S.; Davis, C. D.; Sanberg, P. R., *J. Hematother. Stem Cell Res.* **2003,** 12, 271-278.

23. Reimann, V.; Creutzig, U.; Kögler, G., *Deut. Arzt. Int.* **2009,** 106, 831-836.

24. Kalra, L.; Ratan, R. R., *Stroke* **2008,** 39, 273-275.

25. Moise, K. J. J., *Obstet. Gynecol.* **2005,** 106, 1393-1407.

26. Abrahamsen, J. F.; Wentzel-Larsen, T.; Bruserud, Ø., *Cytotherapy* **2004,** 6, 356-362.

27. Huige, N. J. J.; Thijssen, H. A. C., *J. Cryst. Growth* **1972,** 13–14, 483-487.

28. Pronk, P.; Infante Ferreira, C. A.; Witkamp, G. J., *J. Cryst. Growth* **2005,** 275, e1355-e1361.

29. Inada, T.; Modak, P. R., *Chem. Eng. Sci.* **2006,** 61, 3149-3158.

30. Fletcher, N. H., *The Chemical Physics of Ice*. 1st ed.; Cambridge University Press: London, 1970; p 271.

31. Devries, A. L.; Lin, Y., *Biochimica et Biophysica Acta (BBA) - Protein Structure* **1977,** 495, 388-392.

32. Harding, M. M.; Ward, L. G.; Haymet, A. D. J., *Eur. J. Biochem.* **1999,** 264, 653-665.

33. Hayward, J. A.; Haymet, A. D. J., *The Journal of Chemical Physics* **2001,** 114, 3713-3726.

34. Harding, M. M.; Anderberg, P. I.; Haymet, A. D. J., *Eur. J. Biochem.* **2003,** 270, 1381-1392.

35. Karim, O. A.; Haymet, A. D. J., *J. Chem. Phys.* **1988,** 89, 6889.

36. Sadtchenko, V.; Ewing, G. E., *J. Chem. Phys.* **2002,** 116, 4686-4697.

37. Haymet, A. D. J.; Ward, L. G.; Harding, M. M., *J. Am. Chem. Soc.* **1999,** 121, 941-948.

38. Czechura, P.; Tam, R. Y.; Dimitrijevic, E.; Murphy, A. V.; Ben, R. N., *J. Am. Chem. Soc.* **2008,** 130, 2928-2929.

39. Tam, R. Y.; Ferreira, S. S.; Czechura, P.; Chaytor, J. L.; Ben, R. N., *J. Am. Chem. Soc.* **2008,** 130, 17494-17501.

40. Fletcher, N. H., *Philos. Mag.* **1962,** 7, 255-269.

41. Fletcher, N. H., *Philos. Mag.* **1968,** 18, 1287 - 1300.

42. Karim, O. A.; Haymet, A. D. J., *Chem. Phys. Lett.* **1987,** 138, 531-534.

43. Furukawa, Y.; Ishikawa, I., *Journal of Crystal Growth* **1993,** 128, 1137-1142.

44. Beaglehole, D.; Nason, D., *Surf. Sci.* **1980,** 96, 357-363.

45. Karim, O. A.; Kay, P. A.; Haymet, A. D. J., *The Journal of Chemical Physics* **1990,** 92, 4634-4635.

46. Nenow, D., *Prog. Cryst. Growth Charact. Mater.* **1984,** 9, 185-225.

47. Döppenschmidt, A.; Butt, H.-J., *Langmuir.* **2000,** 16, 6709-6714.

48. Dosch, H.; Lied, A.; Bilgram, J. H., *Surf. Sci.* **1996,** 366, 43-50.

49. Golecki, I.; Jaccard, C., *J. Phys. C.* **1978,** 11, 4229.

50. Kahan, T. F.; Reid, J. P.; Donaldson, D. J., *J. Phys. Chem. A.* **2007,** 111, 11006-11012.

51. Kaverin, A.; Tsionsky, V.; Zagidulin, D.; Daikhin, L.; Alengoz, E.; Gileadi, E., *J. Phys. Chem. B.* **2004,** 108, 8759-8762.

52. Güttinger, H.; Bilgram, J. H.; Känzig, W., *J. Phys. Chem. Solids* **1979,** 40, 55-66.

53. Brown, R. A.; Keizer, J.; Steiger, U.; Yeh, Y., *J. Phys. Chem.* **1983,** 87, 4135-4138.

54. Bilgram, J. r. H., *Physics Reports* **1987,** 153, 1-89.

55. Bluhm, H.; Ogletree, D. F.; Fadley, C. S.; Hussain, Z.; Salmeron, M., *J. Phys.-Condens. Mat.* **2002,** 14, L227.

56. Beaglehole, D.; Wilson, P., *J. Phys. Chem.* **1993,** 97, 11053-11055.

57. Beaglehole, D.; Wilson, P., *J. Phys. Chem.* **1994,** 98, 8096-8100.

58. Elbaum, M.; Lipson, S. G.; Dash, J. G., *J. Cryst. Growth* **1993,** 129, 491-505.

59. Gilpin, R. R., *J. Colloid Interf. Sci.* **1980,** 77, 435-448.

60. Furukawa, Y.; Yamamoto, M.; Kuroda, T., *Journal of Crystal Growth* **1987,** 82, 665-677.

61. Knight, C. A., *J. Appl. Phys.* **1966,** 37, 568-574.

62. Alley, R. B.; Perepezko, J. H.; Bentley, C. R., *J. Glaciol.* **1986,** 32, 415-424.

63. Alley, R. B.; Perepezko, J. H.; Bentley, C. R., *J. Glaciol.* **1986,** 32, 425-433.

64. Sutton, R. L.; Lips, A.; Piccirillo, G.; Sztehlo, A., *J. Food Sci.* **1996,** 61, 741-745.

65. Hagiwara, T.; Hartel, R.; Matsukawa, S., *Food Biophys.* **2006,** 1, 74-82.

66. Budke, C.; Heggemann, C.; Koch, M.; Sewald, N.; Koop, T., *J. Phys. Chem. B.* **2009,** 113, 2865-2873.

67. Mazur, P., *Am. J. Physiol. Cell Physiol.* **1984,** 247, C125-C142.

68. Garner, J.; Harding, M. M., *ChemBioChem* **2010,** 11, 2489-2498.

69. Jia, Z.; Davies, P. L., *Trends Biochem. Sci.* **2002,** 27, 101-106.

70. Fletcher, G. L.; Hew, C. L.; Davies, P. L., *Annu. Rev. Physiol.* **2001,** 63, 359-390.

71. Davies, P. L.; Sykes, B. D., *Curr. Opin. Struc. Biol.* **1997,** 7, 828-834.

72. Yeh, Y.; Feeney, R. E., *Chem. Rev.* **1996,** 96, 601-618.

73. Venketesh, S.; Dayananda, C., *Crit. Rev. Biotech.* **2008,** 28, 57-82.

74. Scholander, P. F.; van Dam, L.; Kanwisher, J. W.; Hammel, H. T.; Gordon, M. S., *J. Cell. Comp. Physiol.* **1957,** 49, 5-24.

75. Gordon, M. S.; Amdur, B. H.; Scholander, P. F., *Biol. Bull.* **1962,** 122, 52-62.

76. DeVries, A. L.; Wohlschlag, D. E., *Science* **1969,** 163, 1073-1075.

77. DeVries, A. L.; Komatsu, S. K.; Feeney, R. E., *J. Biol. Chem.* **1970,** 245, 2901-2908.

78. DeVries, A. L., *Science* **1971,** 172, 1152-1155.

79. Tyshenko, M. G.; Doucet, D.; Davies, P. L.; Walker, V. K., *Nat. Biotech.* **1997,** 15, 887-890.

80. Hew, C. L.; Kao, M. H.; So, Y.-P.; Lim, K.-P., *Can. J. Zool.* **1983,** 61, 2324-2328.

81. Graham, L. A.; Liou, Y.-C.; Walker, V. K.; Davies, P. L., *Nature* **1997,** 388, 727-728.

82. Schneppenheim, R.; Theede, H., *Comp. Biochem. Physiol. B.* **1980,** 67, 561-568.

83. Duman, J. G.; Li, N.; Verleye, D.; Goetz, F. W.; Wu, D. W.; Andorfer, C. A.; Benjamin, T.; Parmelee, D. C., *J. Comp. Physiol. B.* **1998,** 168, 225-232.

84. Graham, L. A.; Davies, P. L., *Science* **2005,** 310, 461.

85. Smallwood, M.; Worrall, D.; Byass, L.; Elias, L.; Ashford, D.; Doucet, C. J.; Holt, C.; Telford, J.; Lillford, P.; Bowles, D. J., *Biochem. J.* **1999,** 340, 385-391.

86. Huang, T.; Nicodemus, J.; Zarka, D. G.; Thomashow, M. F.; Wisniewski, M.; Duman, J. G., *Plant Mol. Biol.* **2002,** 50, 333-344.

87. Sidebottom, C.; Buckley, S.; Pudney, P.; Twigg, S.; Jarman, C.; Holt, C.; Telford, J.; McArthur, A.; Worrall, D.; Hubbard, R.; Lillford, P., *Nature* **2000,** 406, 256-256.

88. Pudney, P. D. A.; Buckley, S. L.; Sidebottom, C. M.; Twigg, S. N.; Sevilla, M.-P.; Holt, C. B.; Roper, D.; Telford, J. H.; McArthur, A. J.; Lillford, P. J., *Arch. Biochem. Biophys.* **2003,** 410, 238-245.

89. Kumble, K. D.; Demmer, J.; Fish, S.; Hall, C.; Corrales, S.; DeAth, A.; Elton, C.; Prestidge, R.; Luxmanan, S.; Marshall, C. J.; Wharton, D. A., *Cryobiology.* **2008,** 57, 263-268.

90. John, U. P.; Polotnianka, R. M.; Sivakumaran, K. A.; Chew, O.; Mackin, L.; Kuiper, M. J.; Talbot, J. P.; Nugent, G. D.; Mautord, J.; Schrauf, G. E.; Spangenberg, G. C., *Plant, Cell Environ.* **2009,** 32, 336-348.

91. Griffith, M.; Ewart, K. V., *Biotech. Adv* **1995,** 13, 375-402.

92. Tremblay, K.; Ouellet, F. o.; Fournier, J.; Danyluk, J.; Sarhan, F., *Plant Cell Physiol.* **2005,** 46, 884-891.

93. Duman, J. G.; Olsen, T. M., *Cryobiology* **1993,** 30, 322-328.

94. Hoshino, T.; Kiriaki, M.; Nakajima, T., *Cryoletters* **2003,** 24, 135-142.

95. Gilbert, J. A.; Davies, P. L.; Laybourn-Parry, J., *FEMS Microbiol. Lett.* **2005,** 245, 67-72.

96. Sun, X.; Griffith, M.; Pasternak, J. J.; Glick, B. R., *Can. J. Microbiol.* **1995,** 41, 776-784.

97. Yamashita, Y.; Nakamura, N.; Omiya, K.; Nishikawa, J.; Kawahara, H.; Obata, H., *Biosci. Biotechnol. Biochem.* **2002,** 66, 239-247.

98. Kawahara, H.; Nakano, Y.; Omiya, K.; Muryoi, N.; Nishikawa, J.; Obata, H., *J. Biosci. Bioeng.* **2004,** 98, 220-223.

99. DeVries, A. L., *Comp. Biochem. Physiol. B.* **1988,** 90, 611-621.

100. Balcerzak, A. K.; Capicciotti, C. J.; Briard, J. G.; Ben, R. N., *RSC Adv.* **2014,** 4, 42682-42696.

101. Lin, Y.; Duman, J. G.; DeVries, A. L., *Biochem. Biophys. Res. Commun.* **1972,** 46, 87-92.

102. Hew, C. L.; Slaughter, D.; Fletcher, G. L.; Joshi, S. B., *Can. J. Zool.* **1981,** 59, 2186-2192.

103. Burcham, T. S.; Osuga, D. T.; Rao, B. N.; Bush, C. A.; Feeney, R. E., *J. Biol. Chem.* **1986,** 261, 6384-6389.

104. Geoghegan, K. F.; Osuga, D. T.; Ahmed, A. I.; Yeh, Y.; Feeney, R. E., *J. Biol. Chem.* **1980,** 255, 663-7.

105. O'Grady, S. M.; Schrag, J. D.; Raymond, J. A.; Devries, A. L., *J. Exper. Zool.* **1982,** 224, 177-185.

106. Fletcher, G. L.; Hew, C. L.; Joshi, S. B., *Can. J. Zool.* **1982,** 60, 348-355.

107. Raymond, J. A.; Wilson, P.; DeVries, A. L., *Proc. Natl. Acad. Sci. U.S.A.* **1989,** 86, 881-885.

108. Knight, C. A.; DeVries, A. L., *J. Cryst. Growth* **1994,** 143, 301-310.

109. Wilson, P. W., *Cryoletters* **1993,** 14, 31-36.

110. Knight, C. A.; Cheng, C. C.; DeVries, A. L., *Biophys. J.* **1991,** 59, 409-418.

111. Knight, C. A.; Driggers, E.; DeVries, A. L., *Biophys. J.* **1993,** 64, 252-259.

112. Feeney, R. E.; Burcham, T. S.; Yeh, Y., *Annu. Rev. Biophys. Biophys. Chem.* **1986,** 15, 59-78.

113. Raymond, J. A.; DeVries, A. L., *Proc. Natl. Acad. Sci. U.S.A.* **1977,** 74, 2589-2593.

114. Wilson, P. W.; Beaglehole, D.; DeVries, A. L., *Biophys. J.* **1993,** 64, 1878-1884.

115. Knight, C. A.; DeVries, A. L.; Oolman, L. D., *Nature* **1984,** 308, 295-296.

116. Mugano, J. A.; Wang, T.; Layne, J. R., Jr.,; DeVries, A. L.; E., L. R., *Cryobiology* **1995**, 556-557.

117. Wang, T.; Zhu, Q.; Yang, X.; Layne, J. R.; DeVries, A. L., *Cryobiology.* **1994,** 31, 185-192.

118. Wang, J.-H., *Cryobiology.* **2000,** 41, 1-9.

119. Pham, L.; Dahiya, R.; Rubinsky, B., *Cryobiology* **1999,** 38, 169-175.

120. Eniade, A.; Purushotham, M.; Ben, R. N.; Wang, J. B.; Horwath, K., *Cell. Biochem. Biophys.* **2003,** 38, 115-124.

121. Leclère, M.; Kwok, B. K.; Wu, L. K.; Allan, D. S.; Ben, R. N., *Bioconj. Chem.* **2011,** 22, 1804-1810.

122. Liu, S.; Ben, R. N., *Org. Lett.* **2005,** 7, 2385-2388.

123. Knight, C. A.; Hallett, J.; DeVries, A. L., *Cryobiology.* **1988,** 25, 55-60.

124. Jackman, J.; Noestheden, M.; Moffat, D.; Pezacki, J. P.; Findlay, S.; Ben, R. N., *Biochem. Biophys. Res. Commun.* **2007,** 354, 340-344.

125. Galema, S. A.; Hoeiland, H., *J. Phys. Chem.* **1991,** 95, 5321-5326.

126. Galema, S. A.; Engberts, J. B. F. N.; Hoeiland, H.; Foerland, G. M., *J. Phys. Chem.* **1993,** 97, 6885-6889.

127. Galema, S. A.; Howard, E.; Engberts, J. B. F. N.; Grigera, J. R., *Carbohydr. Res.* **1994,** 265, 215-225.

128. Heyden, M.; Bründermann, E.; Heugen, U.; Niehues, G.; Leitner, D. M.; Havenith, M., *Journal of the American Chemical Society* **2008,** 130, 5773-5779.

129. Abraham, S.; Keillor, K.; Capicciotti, C. J.; Perley-Robertson, G. E.; Keillor, J. W.; Ben, R. N., *Cryst. Growth Des.* **2015**.

130. Chaytor, J. L.; Ben, R. N., *Bioorg. Med. Chem. Lett.* **2010,** 20, 5251-5254.

131. Balcerzak, A. K.; Ferreira, S. S.; Trant, J. F.; Ben, R. N., *Bioorg. Med. Chem. Lett.* **2012,** 22, 1719-1721.

132. Tachibana, Y.; Fletcher, G. L.; Fujitani, N.; Tsuda, S.; Monde, K.; Nishimura, S.-I., *Angew. Chem. Intl. Ed.* **2004,** 43, 856-862.

133. Capicciotti, C. J.; Leclère, M.; Perras, F. A.; Bryce, D. L.; Paulin, H.; Harden, J.; Liu, Y.; Ben, R. N., *Chem. Sci.* **2012,** 3, 1408-1416.

134. Suzuki, M.; Abe, T.; Hanabusa, K., *J. Colloid Interf. Sci.* **2010,** 341, 69-74.

135. Suzuki, M.; Hanabusa, K., *Chem. Soc. Rev.* **2009,** 38, 967-975.

136. Suzuki, M.; Yumoto, M.; Kimura, M.; Shirai, H.; Hanabusa, K., *Chem. Eur. J.* **2003,** 9, 348-354.

137. Suzuki, M.; Yumoto, M.; Shirai, H.; Hanabusa, K., *Chem. Eur. J.* **2008,** 14, 2133-2144.

138. Suzuki, M.; Yumoto, M.; Shirai, H.; Hanabusa, K., *Tetrahedron* **2008,** 64, 10395-10400.

139. Balcerzak, A. K.; Febbraro, M.; Ben, R. N., *RSC Adv.* **2013,** 3, 3232-3236.

140. Trant, J. F.; Biggs, R. A.; Capicciotti, C. J.; Ben, R. N., *RSC Adv.* **2013,** 3, 26005-26009.

Chapter 2. Goals and Objectives

As previously discussed in section 1.1, cryostorage is a critical process in modern health care which is spawning the emergence of stem cell and regenerative therapies. The number of human specimens available for clinical use, however, is limited by a lack of ideal preservation methods.[1-4] Additionally, the lack of ideal preservation methods has also led to a loss in function of these stem cells post-thaw.[2, 4] Therefore, improved cryopreservation methods that maintain greater cell viabilities are very important. The most significant cause of decreased cell viability and impaired function during cryopreservation is direct mechanical damage due to ice recrystallization.[5, 6] While the use of cryoprotectants such as DMSO is effective to increase post-thaw viabilities, it has been shown that these cryoprotectants exhibit cytotoxicity.[7]

Consequently, the Ben laboratory is interested in the rational design and synthesis of novel non-cytotoxic small molecules as potent inhibitors of ice recrystallization. Another use of these small molecules is the inhibition of the formation of gas hydrates. A gas hydrate is defined as a highly ordered network of hydrogen bonded water molecules encompassing a gas molecule.[8] These hydrates cause blockages within oil and gas pipelines causing safety concerns and pipeline shutdown.[9] Many different types of gas hydrates can be formed (dependent on the gas molecule) yet they all consist of about 85% water on a molecular basis. Thus, many properties are shared between gas hydrates and ice. Given the similarities to ice, IRI active molecules such as AFPs have been utilized to inhibit the formation of problematic gas hydrates.[10] Unfortunately, difficulties associated with obtaining large quantities of these complex proteins have limited their use.

The design of small molecules IRIs is a relative new field and as such, work is required to determine the key structural features required for IRI activity. The following goals and objectives outline various nitrogen-containing carbohydrates as ice recrystallization inhibitors as well as their use in inhibiting problematic gas hydrates found in oil and gas pipelines.

2.1 Objective 1: Inhibiting Ice Recrystallization Utilizing Monosaccharides with an Endocyclic Ring Nitrogen

Previously, the Ben laboratory has demonstrated the relationship between hydration of carbohydrates and their ability to inhibit ice recrystallization.[11] A highly hydrated carbohydrate was found to be a poor fit into the three-dimensional hydrogen bonded network of bulk water and resulting in inhibition of ice recrystallization. Hydration was related to the relative

orientation of the hydroxyl groups within the pyranose ring. D-Galactose was found to be the most hydrated and thus the most IRI active monosaccharide tested by the Ben laboratory.[11] In addition, through an examination of mono-, di-, and trihydrates of simple carbohydrates, Simons *et. al.* have proposed that the hydration of a carbohydrate may be governed by the strength of the intramolecular hydrogen bond network within the pyranose ring. This hypothesis was based on the energy difference observed from the incorporation of a single water molecule within the intramolecular hydrogen bond network of the pyranose ring. It was found that the first water molecule incorporated between the weakest intramolecular hydrogen bond in order to limit the disruption of the intramolecular hydrogen bond network. In β-phenyl-D-glucose, water inserts between the C4-OH and C6-OH whereas in β-phenyl-D-galactose it inserts between C6-OH and the endocyclic ring oxygen (**Figure 2-1**). [12, 13]

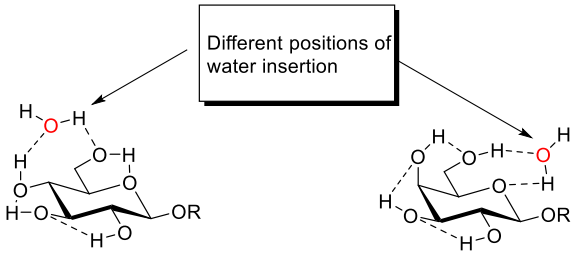

Figure 2-1. A schematic representation of the insertion of water within the intramolecular hydrogen bond network of the hydroxyl groups on the pyranose ring.

Therefore, individual hydroxyl groups maybe important positions for the addition of water molecules to the intramolecular hydrogen bond network of pyranose rings. Through MD simulations, Dashnau has also demonstrated that intramolecular hydrogen bond formation and hydrogen bonding cooperativity has a large effect on the structuring of water.[14] All of these studies clearly suggest that individual hydroxyl groups within the pyranose ring is important to this intramolecular hydrogen bond network and therefore, individual hydroxyl group may have a large impact on hydration and ultimately IRI activity. Based upon this precedent, the Ben laboratory prepared a number of derivatives of D-galactose by systematically replacing individual hydroxyl groups with an amine. At a pH of 7.4 (that used in the splat-cooling assay), an amine substituent maybe protonated and thus, the amine substituent could only act as a hydrogen bond donor. Previous structure-function work had suggested that the presence of a

hydrogen bond donor within the ring may be important to IRI activity. The structures of the synthesized amino derivatives are shown in **Figure 2-2**.

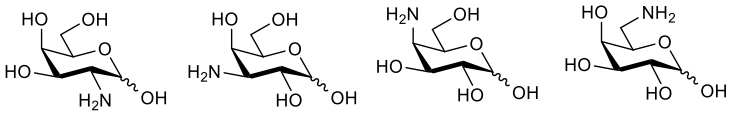

Figure 2-2. Structure of amino-deoxy-D-galactose derivatives.

It was found that the presence of an amine at C3 was the most beneficial to IRI activity (IRI activity of amino-deoxy-D-galactose derivatives will be further discussed in Chapter 3). This result demonstrated that simple structural modifications significantly affect IRI activity and further emphasis that individual hydroxyl groups can largely impact IRI activity. Thus, it is imperative to explore other simple modifications to the pyranose ring. All of the investigated amino-deoxy-D-galactose derivatives possess an endocyclic oxygen within the pyranose ring. Simons has shown that the ring oxygen plays a key role in hydrogen bonding to surrounding water molecules (**Figure 2-1**).[12, 13] With this in mind, it was imperative to replace the endocyclic oxygen to an amine within the pyranose ring. This simple structural modification may lead to highly IRI active compounds. Therefore, objective 1 involved the synthesis of azasugars (**Figure 2-3**) to further examine the role of the ring heteroatom in the interaction of carbohydrates with bulk water.

Figure 2-3. Structure of D-glucose and D-galactose based azasugars.

Compared to D-glucose and D-galactose, these azasugars possess a ring heteroatom bonded to hydrogen atom. The ring nitrogen can be utilized as a chemical handle for structural modifications which are not possible in a pyranose ring possessing a ring oxygen.

2.2 Objective 2: Inhibiting Gas Hydrate Formation Using Small Molecule Ice Recrystallization Inhibitors

Gas hydrates are ice-like solids containing gases within a highly-ordered network of water molecules.[8] Of the many different forms of gas hydrates, those containing a single molecule of methane are known as sI hydrates.[10] Hydrates pose a major problem in the

petroleum industry due to safety concerns and requirement of shutdown of the pipeline whilst the blockage is removed.[9, 10]

Gas hydrate formation is prevented using two classes of compounds: thermodynamic inhibitors (THI) and low-dosage hydrate inhibitors (LDHIs). THIs act as additives and induce a colligative freezing point depression. Generally, THIs are effective at 20-50 wt%. Such large concentrations impose significant financial implications, exacerbated by the difficulty in recovering or recycling the THIs post-addition.[10] Consequently, LDHIs are a cost-effective alternative. There are two classes of LDHIs: the kinetic gas hydrate inhibitors (KHIs) and anti-agglomeration agents (AAs). KHIs inhibit the nucleation and growth of gas hydrates while AAs reduce the propensity of small clusters of gas hydrates to aggregate and form blockages in pipelines.[9] While most KHIs are water-soluble polymers, recent work has shown that antifreeze proteins can inhibit the growth of gas hydrates.[15] Given the similarity between ice and gas hydrates, utility of AFPs as gas hydrate formation inhibitors is not surprising. As mentioned previously (section 1.5), AFPs possess two antifreeze properties: TH and IRI. The ability of AFPs to inhibit gas hydrate formation has been shown to be independent of their TH activity.[15] However, the difficulty associated with obtaining large quantities of these compounds prevents their use on industrial scale. Consequently, the goal was to investigate whether small molecule inhibitors of ice recrystallization could also inhibit the formation of gas hydrates. In contrast to AFPs, large scale synthesis of small molecule ice recrystallization inhibitors is facile. Investigation of the ability of small molecule IRIs to inhibit gas hydrate formation will give insight into the structural features required for inhibition and thus facilitate future development of these molecules.

2.3 Objective 3: Synthesis of Small Molecules Possessing Potent IRI Activity Using Essential Structural Features

Glycopeptides previously prepared by the Ben laboratory possessing potent IRI activity are not amendable to large-scale synthesis due to their size and complexity. The identification of simple small molecule ice recrystallization inhibitors with potent IRI activity has therefore been an important goal in the Ben laboratory. Recent work has led to the discovery of three classes of potent inhibitors of ice recrystallization: carbohydrate-based surfactants and hydrogelators, lysine-based surfactants/gelators and truncated *C*-linked glycopeptides.[16-18] Their general structures are shown in **Figure 2-4**.

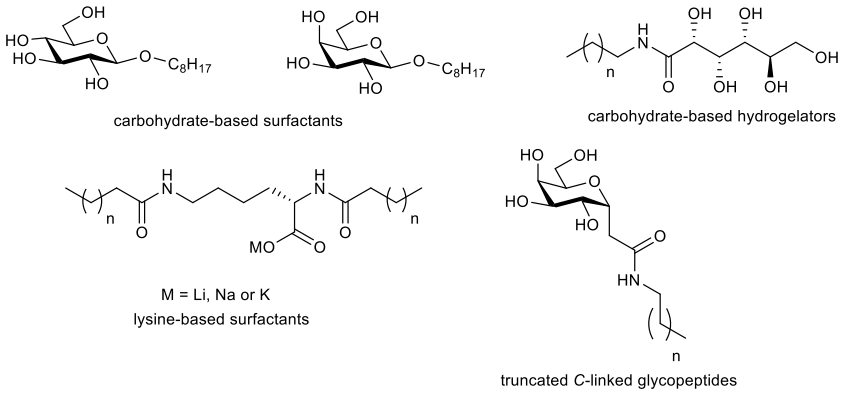

Figure 2-4. Structures of carbohydrate-based surfactants and hydrogelators, lysine-based surfactants/gelators and truncated *C*-linked glycopeptides.

Structure-function study of the small molecules presented in **Figure 2-4** revealed essential structural features which are important to IRI activity. These included: long alkyl chains, an amide linkage and an open-alditol chain. The surfactant nature of some of these compounds prevents their general use in cryopreservation because their surfactant-like properties can be detrimental to cells and solubilize cell membranes.[19-25] Additionally, the long alkyl chain has also been shown to reduce the solubility of these compounds in aqueous solutions.[16-18] As a surfactant, many of these compounds have the ability to form micelles in solution. However, it has been demonstrated that the ability to form micelles is independent of IRI activity.[16, 17] For example, carbohydrate-based non-ionic surfactant β-octyl-D-galactopyranoside was highly IRI active at a concentration well below its critical micelle concentration (CMC) where as β-octyl-D-glucopyranoside did not exhibit IRI activity well above its CMC value. Furthermore, it has been demonstrated that IRI activity is not correlated to the ability to form micelles for structurally different non-ionic and anionic surfactants and anti-ice nucleating agents.[16, 17] Therefore, removal of the surfactant nature of some of these compounds will not be detrimental to IRI activity and may help the cytotoxic profile of these types of compounds. Therefore, compounds lacking long alkyl chains were explored for their IRI activity.

2.3.1 Objective 3A: Combination of Essential Structural Features to Synthesize Novel Small Molecule IRIs

Recently, the Ben laboratory has utilized IRI-active phenoxyglycosides to reduce glycerol concentrations during the cryopreservation of red blood cells.[26] These results demonstrate that small molecules lacking long alkyl chains are capable of potent IRI activity and

have potential as novel cryoprotective agents. Based on this precedent, a number of small molecules have been generated which combine the essential features of phenoxyglycosides, D-galactose amino derivatives and carbohydrate-based hydrogelators to generate potentially highly IRI active compounds which lack a long alkyl chain (**Figure 2-5**). The goal of objective 3A is the synthesis and the complete IRI profiling of these small molecules. Their potential use as cryoprotectants will also be explored.

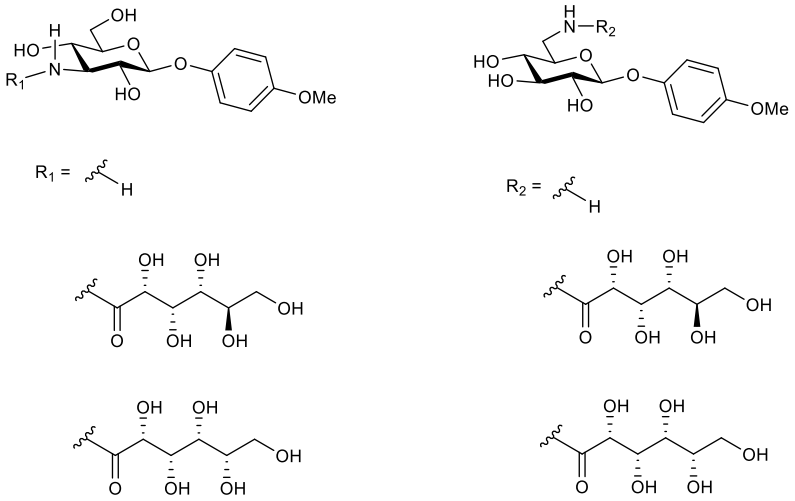

Figure 2-5. Structure of phenolic glycosides linked to open-alditol form of carbohydrates.

2.3.2 Objective 3B: Small Molecule IRIs with Hydrophobic Cycloalkyl Groups

While the presence of a long alkyl chain may be detrimental to solubility, the presence of a hydrophobic moiety is known to be important for IRI activity.[16-18] Other structure-function work has shown that an ideal balance between hydrophilicity and hydrophobicity is required for potent IRI activity. For example, modification to the alkyl chain length or modification of the carbohydrate head group in carbohydrate-based hydrogelators were shown to impact IRI activity.[17, 27] Thus, small molecules with varying hydrophobic and hydrophilic components were synthesized to elucidate the ideal structural features required for potent IRI activity. These compounds are shown in **Figure 2-6**. A hydroxyl group from the D-gluconamide analogues was either removed or replaced with an amine. It was hypothesized that modifications to the hydrophilic portion may affect hydrogen bond capability and hydration of these molecules. In order to circumvent the poor solubility and surfactant-like properties of previous small molecules possessing long alkyl chains, cyclic alkyl rings were chosen as the hydrophobic component. It was hypothesized that these cyclic rings will maintain the required hydrophobicity whilst their

cyclic nature will minimize their ability to act as surfactant-like molecules. The goal of objective 3B will be the synthesis and the complete IRI profiling of these small molecules. Their potential use as cryoprotectants will also be explored.

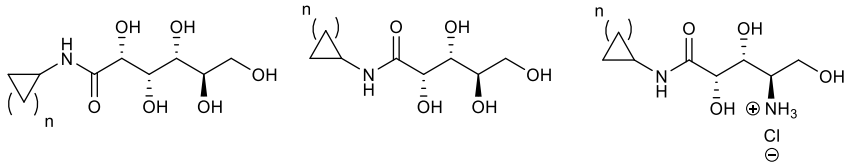

Figure 2-6. Structure of open-alditol carbohydrates containing cyclic alkyl rings.

2.4 References

1. Shimazu, T.; Mori, Y.; Takahashi, A.; Tsunoda, H.; Tojo, A.; Nagamura-Inoue, T., *Cytotherapy* **2015,** 17, 593-600.

2. Allan, D. S.; Keeney, M.; Howson-Jan, K.; Popma, J.; Weir, K.; Bhatia, M.; Sutherland, D. R.; Chin-Yee, I. H., *Bone Marrow Transplant* **2002,** 29, 967-972.

3. Abrahamsen, J. F.; Wentzel-Larsen, T.; Bruserud, Ø., *Cytotherapy* **2004,** 6, 356-362.

4. Pollock, K.; Sumstad, D.; Kadidlo, D.; McKenna, D. H.; Hubel, A., *Cytotherapy* **2015,** 17, 38-45.

5. Baust, J.; Van Buskirk, R., *In Vitro Cell. Dev. Biol. Animal* **2000,** 36, 262-270.

6. Baust, J. M., *Cell Preservation Technol.* **2002,** 1, 17-31.

7. Song, Y. C.; Khirabadi, B. S.; Lightfoot, F.; Brockbank, K. G. M.; Taylor, M. J., *Nat. Biotech.* **2000,** 18, 296-299.

8. Sloan, E. D.; Koh, C., *Clathrate Hydrates of Natural Gases*. Third ed.; CRC Press: Boca Raton, FL, 1997.

9. Kelland, M. A., *Energy Fuels* **2006,** 20, 825-847.

10. Perrin, A.; Musa, O. M.; Steed, J. W., *Chem. Soc. Rev.* **2013,** 42, 1996-2015.

11. Tam, R. Y.; Ferreira, S. S.; Czechura, P.; Chaytor, J. L.; Ben, R. N., *J. Am. Chem. Soc.* **2008,** 130, 17494-17501.

12. Stanca-Kaposta, E. C.; Gamblin, D. P.; Cocinero, E. J.; Frey, J.; Kroemer, R. T.; Fairbanks, A. J.; Davis, B. G.; Simons, J. P., *J. Am. Chem. Soc.* **2008,** 130, 10691-10696.

13. Simons, J. P.; Davis, B. G.; Cocinero, E. J.; Gamblin, D. P.; Stanca-Kaposta, E. C., *Tetrahedron: Asymmetry* **2009,** 20, 718-722.

14. Dashnau, J. L.; Sharp, K. A.; Vanderkooi, J. M., *J. Phys. Chem. B.* **2005,** 109, 24152-24159.

15. Ohno, H.; Susilo, R.; Gordienko, R.; Ripmeester, J.; Walker, V. K., *Chem. Eur. J.* **2010,** 16, 10409-10417.

16. Capicciotti, C. J.; Leclère, M.; Perras, F. A.; Bryce, D. L.; Paulin, H.; Harden, J.; Liu, Y.; Ben, R. N., *Chem. Sci.* **2012,** 3, 1408-1416.

17. Balcerzak, A. K.; Febbraro, M.; Ben, R. N., *RSC Adv.* **2013,** 3, 3232-3236.

18. Trant, J. F.; Biggs, R. A.; Capicciotti, C. J.; Ben, R. N., *RSC Adv.* **2013,** 3, 26005-26009.

19. de Almeida, M. V.; Hyaric, M. L., *Mini-Rev. Org. Chem.* **2005,** 2, 283-297.

20. Lorber, B.; Bishop, J. B.; DeLucas, L. J., *Biochim. Biophys. Acta* **1990,** 1023, 254-265.

21. Michel, H.; Oesterhelt, D., *Proc. Natl. Acad. Sci. U.S.A.* **1980,** 77, 1283-1285.

22. Harvie, P.; Wong, F. M. P.; Bally, M. B., *Biophys. J.* 75, 1040-1051.

23. Hildreth, J. E. K., *Biochem. J.* **1982,** 207, 363-366.

24. Baron, C.; Thompson, T. E., *Biochim. Biophys. Acta* **1975,** 382, 276-285.

25. Plusquellec, D.; Chevalier, G.; Talibart, R.; Wro´blewski, H., *Anal. Biochem.* **1989,** 179, 145-153.

26. Capicciotti, C. J.; Kurach, J. D.; Turner, T. R.; Mancini, R. S.; Acker, J. P.; Ben, R. N., *Sci. Rep.* **2015,** 5, 9692.

27. Capicciotti, C. J. The Rational Design of Potent Ice Recrystallization Inhibitors for Use as Novel Cryoprotectants. 2014, Ph. D. Dissertation, University of Ottawa.

Chapter 3. Inhibiting Ice Recrystallization Utilizing Monosaccharides with an Endocyclic Ring Nitrogen

3.1 Introduction

An important goal of the Ben laboratory is to rationally synthesize small molecules that function as ice recrystallization inhibitors. As mentioned in section 1.1, compounds with the ability to inhibit ice recrystallization have many industrial applications. Previous work by the Ben laboratory has shown that simple monosaccharides possess moderate ice recrystallization inhibition (IRI) activity and that this activity is linked to hydration.[1] In general, hydration is described as water molecules that interact closely with a solute. In the 1990s, Galema *et. al.* studied key parameters thought to dictate hydration characteristics and these were correlated to carbohydrate stereochemistry. The partial molar volumes, isentropic partial molar compressibilities and hydration numbers were determined for many commercially available mono- and disaccharides using kinetic experiments and density ultrasound measurements (**Table 1-2**).[2-4] The hydration number represents the number of water molecules that are hydrogen bonded and tightly bound to the solute.[1-4] These water molecules are part of the primary hydration shell or layer of the carbohydrate. They are generally referred to being non-compressible. As such, they are indicative of the number of water molecules that are interacting with the other hydration layers and bulk water. Partial molar compressibility is a measure of the ability of the water in the outer hydration layers to compress. For a hydrophobic compound, water in the hydration layer forms tighter hydrogen bonds with nearby water molecules. Thus, the hydration layer is more dense and less compressible, thereby decreasing the partial molar compressibility value of the compound. A lower partial molar compressibility means that the hydration layer of a solute does not resemble the bulk water. The total volume of a solute and its surrounding hydration shells that is able to displace a solution of bulk solvent is referred to as the partial molar volume.[1-4]

Using these measurements, Galema *et. al.* were able to quantify the "compatibility" of carbohydrates within the three-dimensional hydrogen bonded network of bulk water. The compatibility of the carbohydrate was directly related to the stereochemical relationship of the hydroxyl groups on the carbohydrate. For example, the presence of axial hydroxyl groups on C2 and C4 of D-talose, had a higher isentropic molar compressibility value and a lower hydration number and thus fit well into the three-dimensional hydrogen bonded network of bulk water.

However, with only one axial hydroxyl group at C4, D-galactose, has a lower isentropic molar compressibility value and a higher hydration number. Therefore, D-galactose is a poor fit into the three-dimensional hydrogen bonded network of bulk water.[2-4] This poor fit disrupts the ordering of bulk water molecules and decreases their ability to incorporate into the ice lattice and ultimately inhibiting ice recrystallization.[1] Tam *et. al.* discovered that the absolute hydration number of a carbohydrate does not accurately predict its IRI activity. Thus, a new parameter termed the hydration index was developed. The hydration index is the hydration number divided by the molar volume of the carbohydrate. The hydration index now takes into account the number of water molecules tightly bound to a carbohydrate and the volume of a particular solute and ultimately the concentration of hydrated water molecules.[1] The hydration index correlates well with IRI activity of many commercially available mono- and disaccharides. Furthermore, Tam *et. al.*, proposed that carbohydrates are able to disrupt the preordering of water by acting at the interface between bulk water and the quasi-liquid layer of water (the nature of the quasi-liquid layer has been described previously in section 1.2).

Dashnau has shown that intramolecular hydrogen bond formation and hydrogen bonding cooperativity has a large effect on the water structure in the first hydration shell.[5] Additionally, it has been proposed that a highly hydrated carbohydrate causes water in the surrounding hydration layers to become sequestered and less able to be integrated into the ordered hydrogen bond network of ice.[5] This suggests that the relative position of each hydroxyl group on a pyranose ring affects the ability of these groups to participate in intramolecular hydrogen bonding, and ultimately, impacts the interaction with bulk water. The C4-OH of a pyranose ring was shown to be particularly important because it is able to be involved in several different hydrogen bond networks. The formation of an intramolecular hydrogen bond between C2-OH and C4-OH in D-talose has been observed. This intramolecular hydrogen bond is suggested to account for the observation that D-talose is more hydrophobic and less hydrated than D-galactose or D-glucose. Given that the relative position of each hydroxyl group on a pyranose affects the ability of these groups to participate in intramolecular hydrogen bonding, one way to disrupt this effect is to prevent the various hydroxyl groups from participating in hydrogen bond formation by removing the ability to function as a hydrogen bond donor or acceptor. To this end, Chaytor systematically methylated individual hydroxyl groups on α-*C*-allyl-D-galactose and these derivatives were tested for IRI activity (**Figure 3-1**).[6]

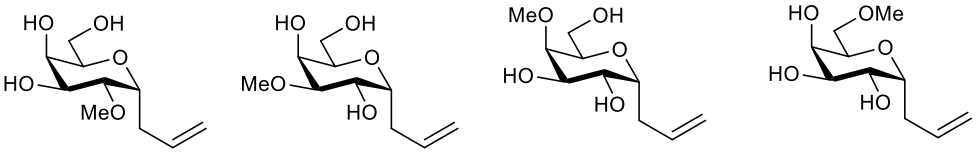

Figure 3-1. Structures of methoxy α-*C*-allyl-D-galactose regioisomers previously synthesized and tested for IRI activity.

It was hypothesized that methylation of the hydroxyl groups would ensure that the methylated hydroxyl group would function only as a hydrogen bond acceptor and not a donor[7] thus disrupting the intramolecular hydrogen bond network which is important for hydration of the molecule.[5] At 22 mM, all of the methylated α-*C*-allyl-D-galactose derivatives exhibited weak IRI activity. These results suggest that the presence of hydrogen bond donors within the pyranose ring is extremely important for IRI activity and possibly the hydration of the carbohydrates.[6] The hydration numbers of the methylated α-*C*-allyl-D-galactose derivatives is unknown and thus, a link between IRI activity and hydration could not be made. Since hydrogen bond donating groups maybe important to IRI activity, the Ben laboratory decided to explore replacement of the hydroxyl groups within the pyranose ring to hydrogen bond donors such as an amine. The PBS solution utilized in the splat-cooling assay is at a pH of 7.4. Carbohydrates possessing an amine such as D-galactosamine will be protonated at this pH and this protonation removes the lone pair (on the nitrogen) required for hydrogen bond acceptance. Therefore, an amine substituent is ideally suited to investigate the importance of hydrogen bond donation on IRI activity.

Previously structure-function work by the Ben laboratory had observed that replacement of the C2-OH on D-galactose to an amine resulted in a slight decrease in IRI activity as compared to D-galactose.[8] A similar observation has been made by Uedaira were the rotational correlation time, a measure of carbohydrate hydration, decreased for D-glucosamine relative to D-glucose.[9] Considering that carbohydrate hydration correlates to IRI activity, it may have been expected (from work done by Uedaria) that an amine at C2 of D-galactose would lead to decreased IRI activity. However, as Galema and Dashnau have both demonstrated the importance of the axial C4-OH on pyranose rings to hydration and intramolecular hydrogen bond network of a carbohydrate,[2, 5] it is important to replace the C4-OH on D-galactose with an amine. An amine at C4 may provide increased hydrogen bond donating to the pyranose ring and thus possibly

increase hydration impacting IRI activity. Given that individual hydroxyl groups may affect hydration, it is important to replace the other hydroxyl groups on D-galactose to amines. The structures of the amino derivatives **301-304** (synthesized by Leclère and Tonelli[10]) as well as the corresponding IRI activities are shown in **Figure 3-2**. The free reducing sugar was chosen to allow for direct comparison to D-galactose.

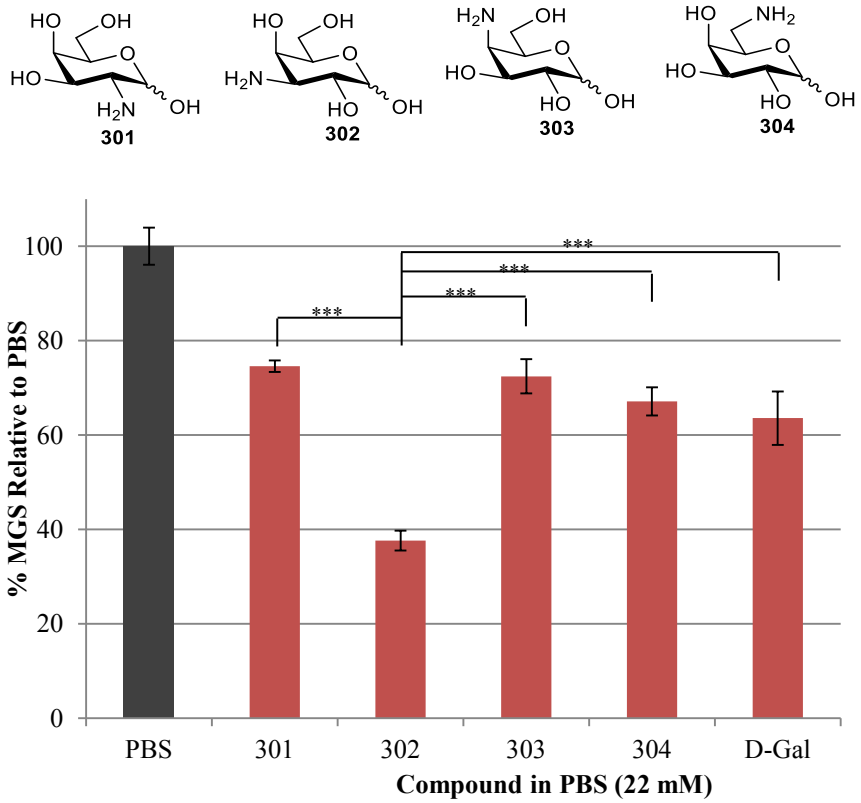

Figure 3-2 Structures of amino-deoxy-D-galactose derivatives and their IRI activity. Asterisk indicates a statistical significant difference between samples and is defined by unpaired Student's *t*-test (***, $p < 0.001$). Statistical significant difference between the PBS control and samples is not shown. Samples have been run in triplicate (n = 3) and error bars indicate standard error of the mean (SEM).

The IRI activities of amino derivatives **301**, **303** and **304** were all similar yet weaker than the activity of D-galactose. However, **302** containing an amino substitution at C3, was moderately IRI active and exhibited improved IRI activity over D-galactose. This suggests that the presence of an amine at C3 is beneficial to IRI activity. Additionally, this also suggests that the presence of hydrogen bond donors within the pyranose ring may also be beneficial to IRI activity. Interestingly, **303**, possessing an amine at C4 possessed decreased IRI activity than **302**. This was not expected as the importance of the C4-OH to hydration and thus IRI activity

has been previously demonstrated.[2-4] However, the hydration numbers or hydration characteristics are currently unknown for these series of compounds and thus, the impact of the amine on hydration cannot be determined at this time. In a PBS solution with pH equaling 7.4, compounds **301-304** will have a protonated amine (pKa is approximately 6.5-8.0 as measured in water[11]), although the nature of the negative counterion is not fully known. The negative counterion of the protonated amine may exchange with others found in PBS. The importance of the counterion to IRI activity has been previously studied by the Ben laboratory during the study of lysine-based surfactants.[12] Due to time restraints, the nature and effect of the negative counterion for amino D-galactose derivatives has not been fully assessed and should be examined in the future. Additionally, the presence of a compound possessing an amine may impact the pH of a PBS solution. However, given that the pKa of the protonated amine present on **301-304** is similar to a pH of 7.4, the addition **301-304** will minimally impact the pH of the PBS solution. A link or lack thereof between changes in the pH of the PBS solution and IRI activity has not been established and should be examined in the future.

The improved IRI activity exhibited by **302** demonstrates that strategic placement of an amine substituent on a pyranose ring can be beneficial to IRI activity. The only regioisomer of the amino-deoxy-D-galactose derivatives not been previously synthesized is the replacement of the ring oxygen with an amine. Through an examination of mono-, di-, and trihydrates of simple carbohydrates, Simons *et. al.* have proposed that the hydration of a carbohydrate may be governed by the strength of the intramolecular hydrogen bond network within the pyranose ring. This hypothesis was based on the energy difference observed from the incorporation of a single water molecule within the intramolecular hydrogen bond network of the pyranose ring (**Figure 3-3**).

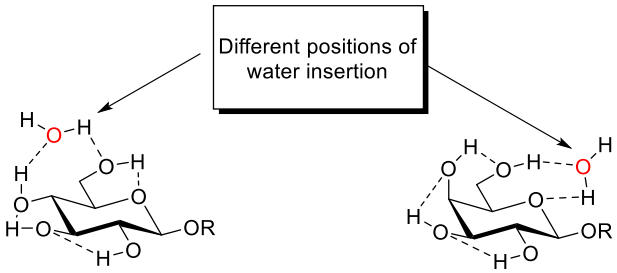

Figure 3-3. A schematic representation of water insertion into the weakest intramolecular hydrogen bonds of D-glucose and D-galactose.

It was found that the first water molecule incorporated between the weakest intramolecular hydrogen bond in order to limit the disruption of the intramolecular hydrogen bond network. In β-phenyl-D-glucose, water inserts between the C4-OH and C6-OH whereas in β-phenyl-D-galactose it inserts between C6-OH and the endocyclic ring oxygen (**Figure 3-3**).[11-15] This suggested that hydroxyl groups at C4 and C6 and the endocyclic ring oxygen on a pyranose ring are important in interacting with water. As mentioned previously, structure-function work has been carried out on the C4-OH with the 4-amino-4-deoxy-D-galactose and methylated α-*C*-allyl-D-galactose derivatives. To further explore the importance of the C6-OH, Capicciotti synthesized the 6-deoxy-heptogalactopyranose derivative **305** and the compound was assayed for IRI activity (**Figure 3-4**). The 6-deoxy-heptoglucopyranoside derivative **306** was prepared to compare to **305**.[16] These derivatives place the C6-OH (found in a traditional pyranose ring) spatially away from the rest of the hydroxyl groups and thus possibly disturbing the intramolecular hydrogen bond network of D-glucose and D-galactose. Much like the hypothesis governing the synthesis of the methylated α-*C*-allyl-D-galactose derivatives, it was initially expected that disturbing this intramolecular hydrogen bond network would lead to an increase in IRI activity.

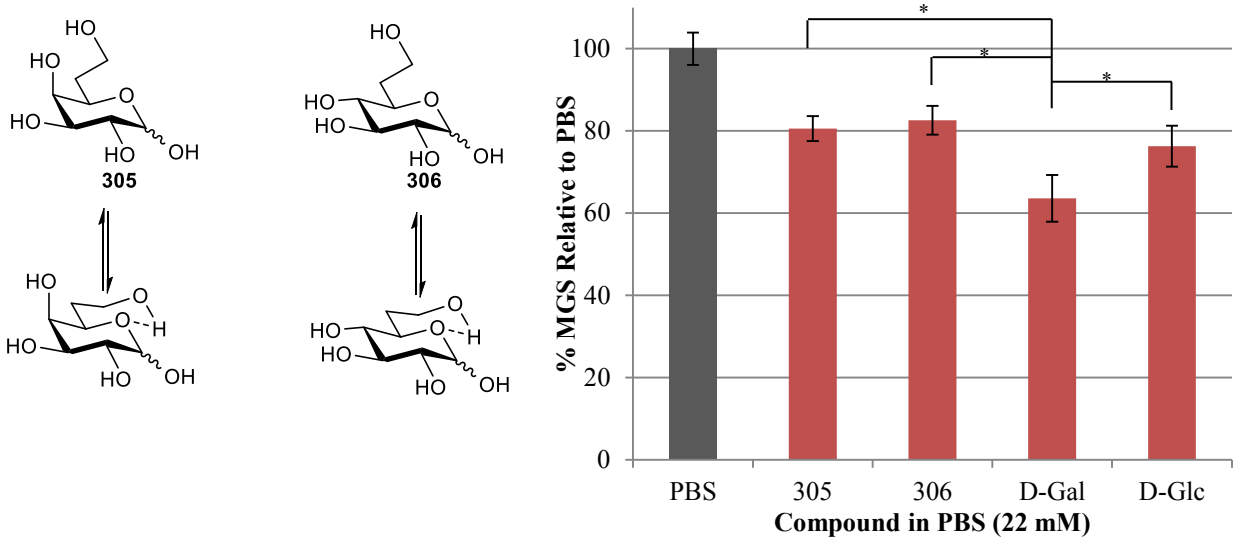

Figure 3-4. Structures of 6-deoxy-heptopyranose derivatives previously synthesized and tested for IRI activity.[18] Asterisk indicates a statistical significant difference between samples and is defined by unpaired Student's *t*-test (*, $p < 0.05$). Statistical significant difference between the PBS control and samples is not shown. Samples have been run in triplicate (n = 3) and error bars indicate standard error of the mean (SEM).

At 22 mM, 6-deoxy-heptose derivatives **305** and **306** exhibited weak IRI activity and were less potent IRIs than their parent monosaccharides. NMR studies were able to show that the solution conformations of **305** and **306** (**Figure 3-4**) blocked the site of water insertion present in the parent monosaccharides through intramolecular hydrogen bonding to the ring oxygen.[18] These results suggest that the ring heteroatom is crucial for IRI activity. In order to examine the importance of the ring oxygen, inositols **307-308** (generously provided by Dr. Mark Nitz from the University of Toronto) were tested for IRI activity (**Figure 3-5**). Lacking a ring oxygen, these inositols were hypothesized to be possess poor IRI activity.

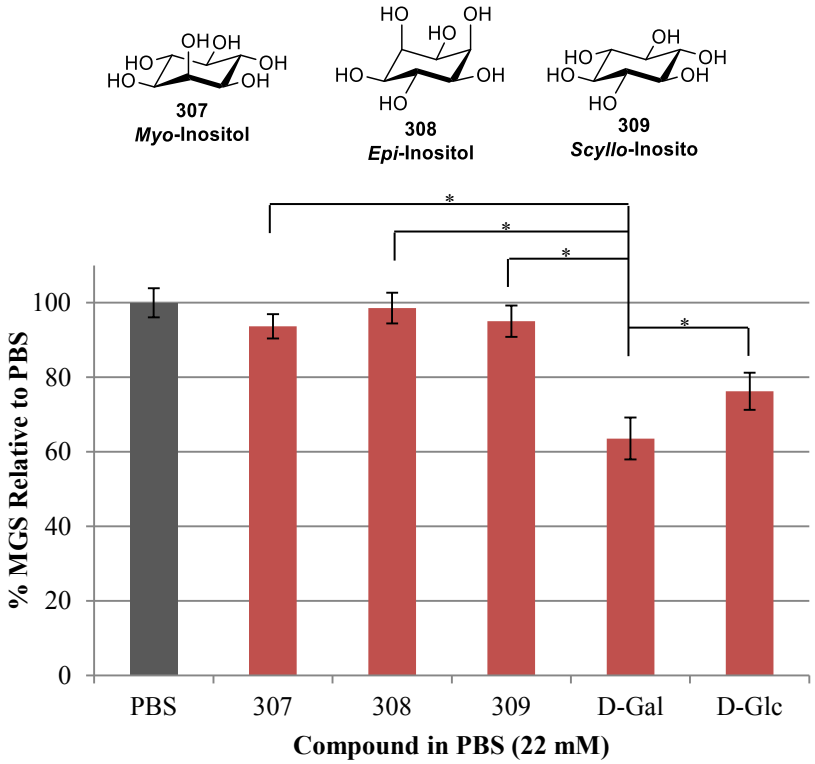

Figure 3-5. Structures of *Myo*-, *Epi*-, *Scyllo*-Inositol and the corresponding IRI activities.[18] Asterisk indicates a statistical significant difference between samples and is defined by unpaired Student's *t*-test (*, $p < 0.05$). Statistical significant difference between the PBS control and samples is not shown. Samples have been run in triplicate (n = 3) and error bars indicate standard error of the mean (SEM).

At 22 mM, all of the inositols exhibited similar IRI activity to PBS and thus reinforcing the idea that the ring heteroatom is necessary in the hydrogen bonding to water. Based on the IRI activity of 3-amino-3-deoxy-D-galactose, it was hypothesized that replacing the ring oxygen with

a secondary amine may result in better hydrogen bond donation resulting in improved IRI activity. Thus, azasugars **310** and **311** (**Figure 3-6**) were synthesized and assayed for IRI activity. Initial effort was placed toward the synthesis of D-galactose based azasugar (**310**) in order to compare its IRI activity to **301-304**. To compare differences between D-galactose and D-glucose, D-glucose based azasugar (**311**) was also synthesized and assayed for IRI activity.

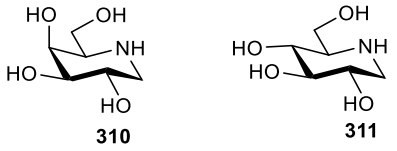

Figure 3-6. Structure of D-galactose (**310**) and D-glucose (**311**) based azasugars.

3.2 Retrosynthetic Analysis of Azasugars

Two synthetic approaches were envisioned for the preparation of azasugars **310** and **311**. The first strategy is presented in **Scheme 3-1** and the second in **Scheme 3-2**.

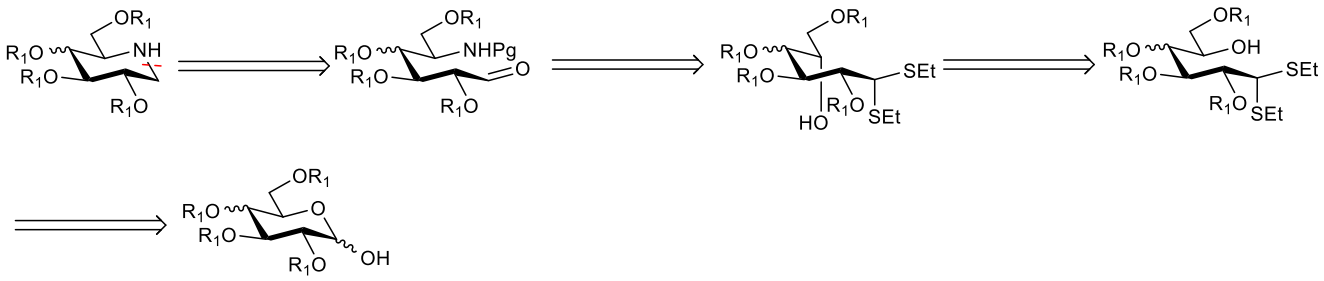

Scheme 3-1. Retrosynthetic analysis of the azasugars utilizing a series of stereoinversions followed by a ring closure.

The key sequence in **Scheme 3-1** involves two stereoinversions of the stereocenter at C5. These stereoinversions could be achieved through a series of Mitsunobu or S_N2 reactions. Once the desired stereocenter is set, a ring closure via a reductive amination would generate the corresponding azasugar. In the forward direction, the aldehyde will be protected utilizing a thioacetal. A similar approach was previously utilized by Martin during the synthesis of related azasugars.[19]

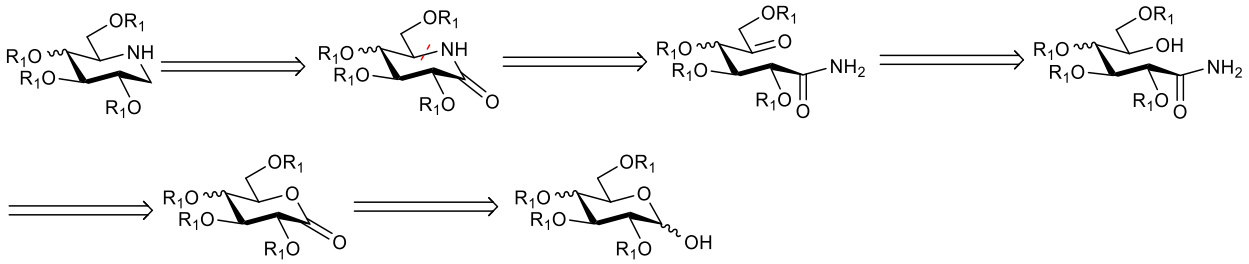

Scheme 3-2. Retrosynthetic analysis of the azasugars utilizing a key ring closure would generate the corresponding lactam which could then be reduced to generate the azasugars.

The second synthetic strategy involving with the lactam as a key intermediate to be generated from a ring closure by the amide nitrogen onto a C5 ketone. This strategy was previously utilized by Overkleeft during their synthesis of a family of azasugars.[20] The ketone could be formed through an oxidation of the C5 alcohol. The amide could be produced from a ring opening of the orthogonally protected lactone that would have been previously generated from an oxidation of the free reducing sugar.

3.3 Synthesis of the Azasugars

Initial efforts were placed towards the synthetic strategy shown in **Scheme 3-1**. To begin the synthesis, D-galactose was converted into its diethyldithioacetal derivative, **312**, in 47% yield upon treatment with HCl and ethanethiol (**Scheme 3-3**). C6-OH and C5-OH were protected as isopropylidenes using 2,2-dimethoxypropane and camphorsulfonic acid (CSA). The remaining hydroxyl groups were then acetylated using pyridine and acetic anhydride generating **313** in 42% yield over two steps. Deprotection of the isopropylidene under mild acidic or Lewis acidic conditions (pyridinium *p*-toluenesulfonate, oxalic acid or tin (II) chloride) led to a complex mixture of products resulting from acetate migration.

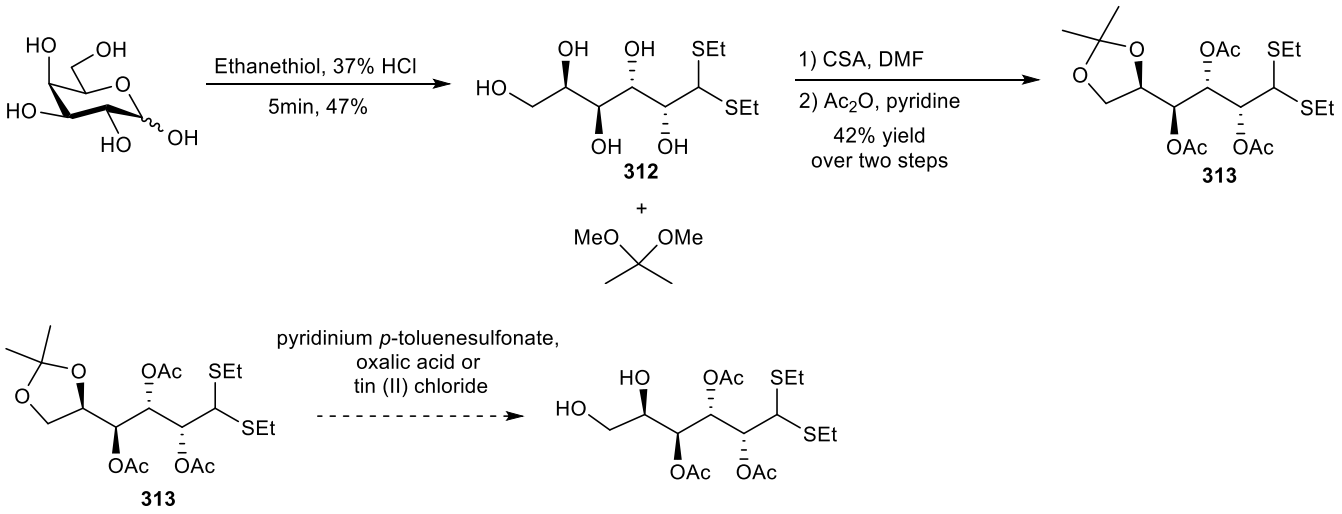

Scheme 3-3. Initial synthesis toward orthogonally protected D-galactose.

In an alternative synthetic route, benzoyl protecting groups were chosen (**Scheme 3-4**). Using standard benzoylation conditions, **314** was furnished in 44% yield over two steps. Deprotection of the isopropylidene using tin (II) chloride was also successful. Interestingly, during the deprotection of the isopropylidene, it was observed that products as result of protecting group migration had decreased as compared to **313**. While benzoyl groups are slightly more stable to basic conditions, the reason for decreased migration of the protecting group is unclear. Silylation of C6-OH was successful utilizing TBSOTf and 2,6-lutidine. However, subsequent triflation of C5-OH was unsuccessful and led to degradation. Upon successful triflation, a series of stereoinversions followed by deprotection would have generated the azasugars. However, due to the low yields and problematic steps of this synthetic pathway, this route was abandoned.

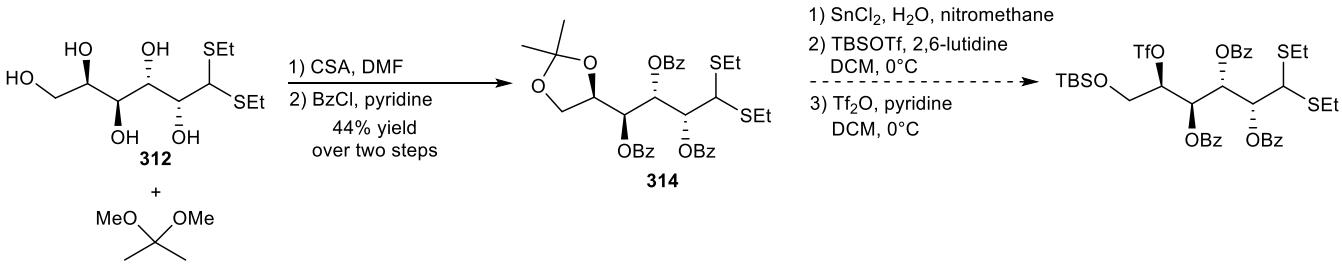

Scheme 3-4. Synthetic efforts toward orthogonal protection and subsequent activation of C5-OH.

A report by Martin demonstrated the use of sequential Mitsunobu reactions to successfully substitute C5-OH with a protected amine possessing the desired stereochemistry.[19] This approach was therefore chosen as the next synthetic route towards the azasugars (**Scheme 3-5**). The synthesis began with a Wittig methylenation of tetra-*O*-benzyl-D-galactopyranoside to give heptenitol **316** in 60% yield. Inversion of the C5 stereochemistry was achieved using *p*-nitrobenzoic acid under Mitsunobu conditions in 78% yield. Following transesterification under basic conditions, the desired stereochemistry at C5 was set using phthalimide as the nucleophile in a second Mitsunobu reaction in 75% yield. Deprotection of the thalamide using hydrazine and subsequent re-protection with a carboxybenzyl group generated **320** in 60% yield over two steps. However, intramolecular cyclization of **320** using mercury (II) trifluoroacetate followed by treatment with iodine was unsuccessful. It was expected that removal of the protecting groups followed by hydrolysis of the carbamate would generate the desired azasugar. Different modes of activation of the alkene in **320** were explored. Conversion of the alkene to an epoxide using mCPBA or iodonium (using iodine or *N*-iodosuccinimide) was unsuccessful and only starting material could be detected in the crude NMR. The lack of activation of the alkene cannot currently be accounted for.

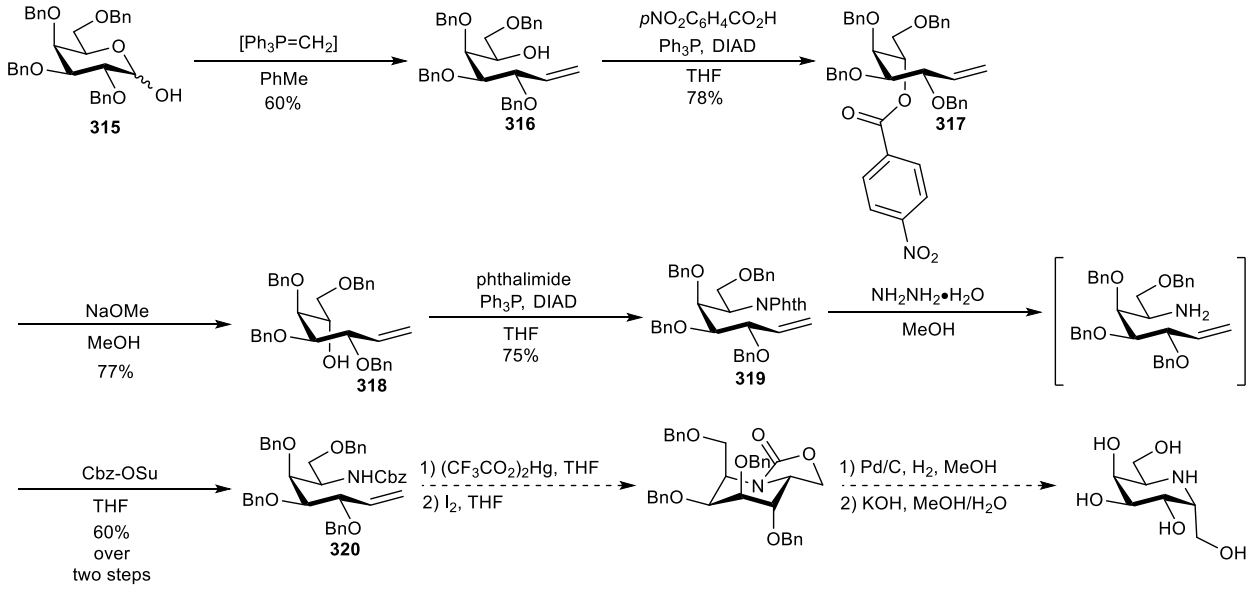

Scheme 3-5. Efforts toward the synthesis of azasugars utilizing a sequential Mitsunobu reaction followed by intramolecular cyclization.

A new route was necessary in order to achieve the intramolecular cyclization toward the synthesis of the azasugars. Pandit has demonstrated similar intramolecular cyclizations could be achieved through the condensation of a primary amide with a ketone.[20] Consequently, a new route was proposed towards the azasugars (**Scheme 3-6**) which involves the formation of lactam structures which could be interesting targets for testing the hydrogen bond capability of the ring nitrogen.

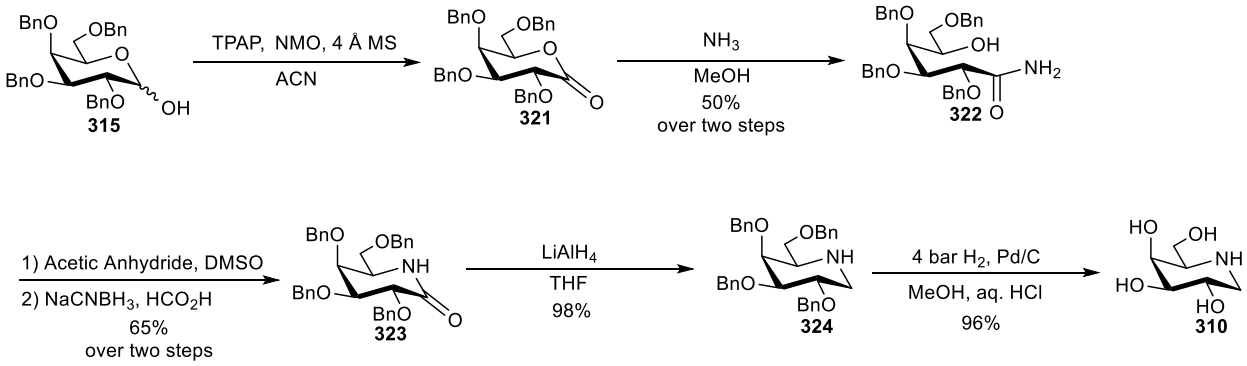

Scheme 3-6. Formation of azasugar **310** using an intramolecular cyclization involving the condensation of a primary amide onto a ketone. Compound 310 was isolated as the free amine with the use of ammonium hydroxide during flash chromatography (Chapter 6).

Oxidation of tetra-*O*-benzyl-D-galactopyranoside **315** using the Ley-Griffith oxidation[21] led to the corresponding lactone **321**. The lactone was then opened using ammonia to afford the amide **322** in 50% yield over two steps. Oxidation of the C5-OH by DMSO and acetic anhydride (Albright-Goldman conditions[22]) followed by reduction with sodium cyanoborohydride and formic acid led to lactam **323** in 65% yield over two steps. $LiAlH_4$ reduction of **323** led to the protected azasugar **324** in 98% yield. Finally, the D-galactose based azasugar **310** was formed in 96% yield by deprotection of the benzyl group using standard conditions. With the successful synthesis of the azasugar **310**, attention was turned toward the synthesis of D-glucose based azasugar **311**. While the synthetic route in **Scheme 3-6** was successful in the production of **310**, focus was placed on a more efficient synthesis that would generate suitable amounts of material required for IRI and cytotoxicity studies. Aerts and Overkleeft reported the synthesis of D-glucose based azasugar **311** in three steps from tetra-*O*-benzyl-D-gluconopyranoside.[23] To our knowledge, this was the shortest reported synthesis of **311** to date and thus was the chosen synthetic route (**Scheme 3-7**).

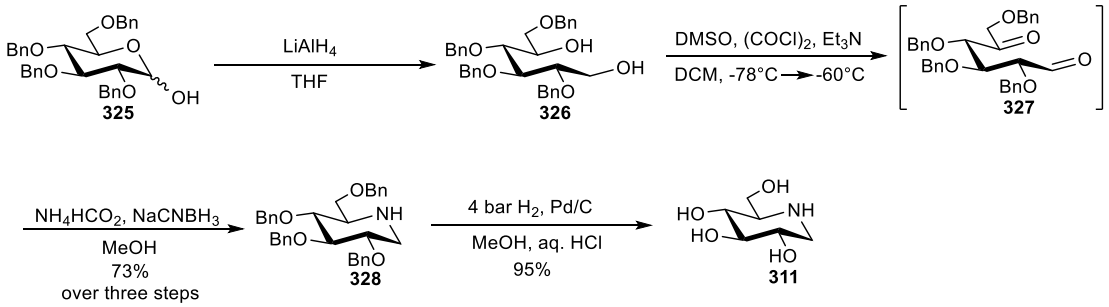

Scheme 3-7. Utilization of a Swern oxidation followed by double reductive amination to generate **311**. Compound 311 was isolated as the free amine with the use of ammonium hydroxide during flash chromatography (Chapter 6).

$LiAlH_4$ reduction of tetra-*O*-benzyl-D-glucopyranoside **325** led to glucitol **326**. Swern oxidation of **326** followed by reductive amination using sodium cyanoborohydride and ammonium formate efficiently led to protected D-glucose based azasugar **328** in 73% yield over three steps. Finally, deprotection of the benzyl groups using standard conditions led to the D-glucose based azasugar **311** in 95% yield.

3.4 IRI Activity of Azasugars

With the azsugars in hand, attention was turned toward their IRI activity. The IRI activities of azasugars **310** and **311** along with amino D-galactose regioisomers **301-304** are presented in **Figure 3-7**.

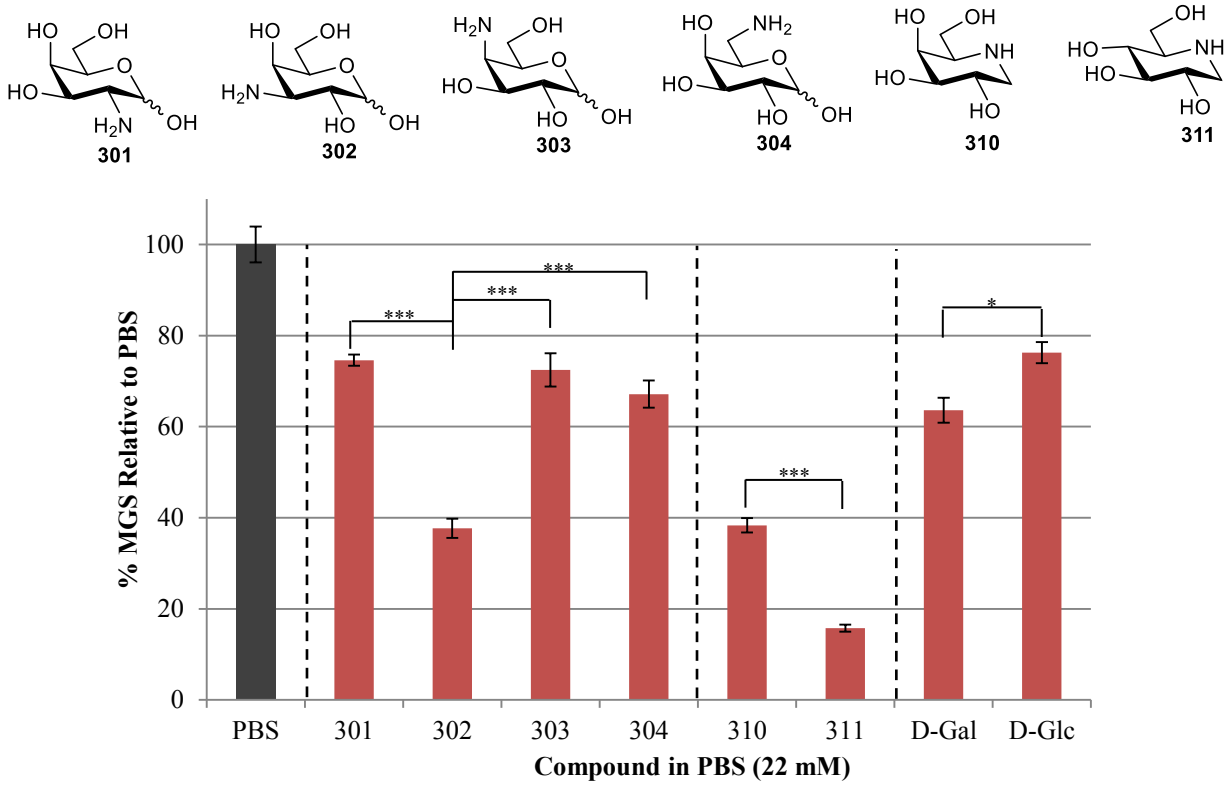

Figure 3-7. IRI activity of azasugars **310** and **311** and amino D-galactose regioisomers **301-304**. Asterisks indicates a statistical significant difference between samples (within each set) and is defined by unpaired Student's *t*-test (*, $p < 0.05$, ***, $p < 0.001$). Statistical significant difference between the PBS control and samples is not shown. Samples have been run in triplicate (n = 3) and error bars indicate standard error of the mean (SEM).

D-Galactose based azasugar **310** possessed moderate IRI activity; comparable to 3-amino-3-deoxy-D-galactose **302**. Compounds **302** and **310** possessed the highest IRI activity of all the amino-deoxy-D-galactose regioisomers tested. When comparing IRI activity of D-galactose and D-glucose based azasugars, **311** possesses potent IRI activity whereas **310** possesses only moderate activity. This is surprising since D-galactose possesses higher IRI activity than D-glucose.[1] However, the Ben laboratory has previously reported that D-glucose based small molecules can possess higher IRI activity than D-galactose based small molecules.[24] The reasoning behind this result is currently unclear.[24] At a pH of 7.4, endocyclic nitrogen in **310** and **311** will be protonated thus it will only be able to participate in hydrogen bond donation suggesting that hydrogen bond donors at the endocyclic position may be beneficial to IRI activity. Given the protonated state of the nitrogen in **310** and **311**, the nature of the negative counterion may also be important to IRI activity. As previously discussed with compounds **301**-

304, the nature of this counterion is currently unknown. Hydration characteristics of these azasugars are also unknown and thus the influence of hydration cannot be elucidated at this time. Considering the effect of replacing the counterion on IRI activity was previously examined for lysine-surfactants, the nature of the counterion in **301-304**, **310** and **311** and its hydration needs future examination in the future. Additionally, as mentioned previously with **301**-**304**, the presence of an amine may affect the pH of the PBS solution. However, the pKa of the protonated forms of **310** and **311** is approximately 6.7-8.0 as measured in water [25] and thus, should minimally affect the pH of the PBS solution. A link or lack thereof between changes in pH of the PBS solution and IRI activity is currently unknown and needs future exploration. Other future work should include synthesis of hemiaminal analogues of **310** and **311**. These structures would be interesting comparisons to **301**-**304** since those are present as the free reducing sugars. This will investigate if the presence of a hydroxyl group at the anomeric carbon is important to IRI activity. It has been previously demonstrated that compounds with substitutions at the anomeric carbon such as long alkyl chains[24] or various aryl groups[18] possess potent IRI activity and thus, anomeric substitutions may play a large role in IRI activity.

To further investigate the importance of the ring nitrogen to act as a hydrogen bond donor, lactams **329**, **330** and *N*-methylated analogue **331** were synthesized and assayed for IRI activity (**Figure 3-8**). Due to resonance, the ring nitrogen in lactams **329** and **330** were expected to remain unprotonated and thus is able to act as a hydrogen bond donor and acceptor. However, in solution, protonated forms of compounds **310** and **311** will possess two N-H bonds whereas the lactams **329** and **330** possess only one. Therefore, hydrogen bond donating ability was expected to be decreased in the lactam analogues. Therefore, the lactams should have decreased IRI activity as compared to azasugars **310** and **311**. The additional methyl group on **331** increases the steric bulk on the ring nitrogen. Given that protonation of the ring nitrogen must be accompanied by a negative counterion for stability, the additional steric bulk **331** will cause steric hindrance disfavouring the presence of the negative counterion. Additionally, the presence of the hydroxyl groups on the azasugars likely increase the acidity (through induction) of the protonated ring nitrogen. In combination with the additional steric bulk of the methyl groups, **331** may exist mostly in the unprotonated form. Therefore, *N*-methylated analog **331** was expected to only act as a hydrogen bond acceptor, much like the methylated α-*C*-allyl-D-galactose regioisomers tested by Chaytor, and thus also possess decreased IRI activity. Given

that the azasugars lack a substituent at the anomeric center, it is important to determine the impact of this on IRI activity. Thus, 1-deoxy-D-glucose (**335**) was synthesized and its activity was compared to D-glucose based azasugar **311**. Unfortunately, due to time restrictions, 1-deoxy-D-galactose was not synthesized.

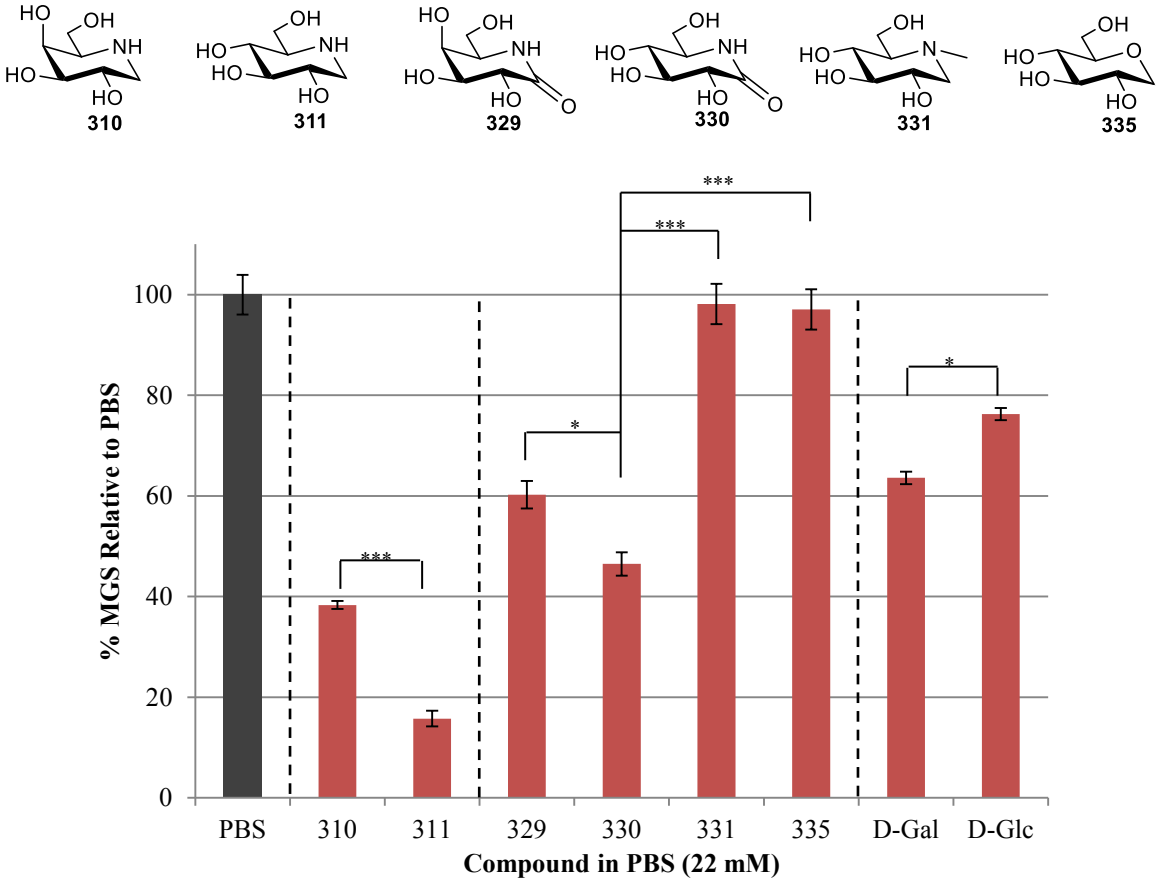

Figure 3-8. IRI activity of lactams **329** and **330** and *N*-methylated analog **331** compared to azasugars **310** and **311**. Additionally, 1-deoxy-D-glucose **335** is compared to azasugar **311**. Asterisks indicates a statistical significant difference between samples (within each set) and is defined by unpaired Student's *t*-test (*, $p < 0.05$, ***, $p < 0.001$). Statistical significant difference between the PBS control and samples is not shown. Samples have been run in triplicate (n = 3) and error bars indicate standard error of the mean (SEM).

Modifications made to the structure of the azasugars resulted in a loss of IRI activity. However, the improvement in activity (as compared to the *N*-methylated analogue) demonstrated by lactam **330** suggests that the hydrogen bond donating ability of the ring nitrogen in **311** plays a larger role than the hydrogen bond accepting ability. As the ability for the endocyclic ring nitrogen to act as a hydrogen bond donor increases, this causes the IRI activity to increase. Finally, 1-deoxy-D-glucose **335**, possessed little to no IRI activity suggesting that the lack of a

substituent is likely not important and maybe detrimental to IRI activity. This further supports that the endocyclic ring amine may be crucial for IRI activity.

Since **310** and **311** possess moderate to potent IRI activity, it is important to explore whether these azasugars were binding to ice in a similar manner to AF(G)Ps. The TH activity of the most IRI active azasugars, **310** and **311**, was examined using nanolitre osmometry.[26] The ice crystal habit of **310** and **311** is shown in **Figure 3-9**. Neither **310** nor **311** displayed changes to ice crystal habit suggesting that these compounds do not interact with ice. This is consistent with the lack of TH activity for the potently IRI active carbohydrate-based and lysine-based surfactants and hydrogelators.[12, 24] Additionally, this result is also consistent with *C*-linked AFGP analogues which possessed potent IRI activity but do not possess TH activity.[27-29] Thus, these azasugars exhibit "custom-tailored" antifreeze activity and may be ideally suited for future application in cryopreservation.

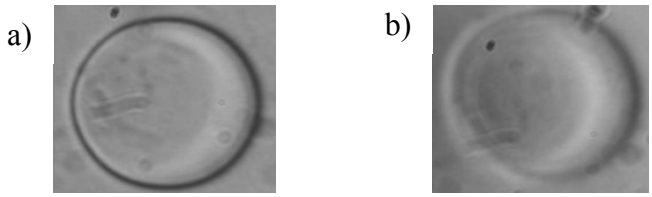

Figure 3-9. Ice crystal habit in the presence of a) **310** (10 mg/mL) and b) **311** (10 mg/mL).

3.5 Cytotoxicity of Azasugars

The cytotoxicity of **310** and **311** was examined. Cytotoxicity is an important property to consider for any small molecules which may be used in cryopreservation studies.[30] Cytotoxicity of azasugars was determined using an MTT assay using Hep G2 cells (human liver carcinoma).[30-32] Hep G2 cells were chosen due to their use as models for cryopreservation using monosaccharides.[30 26] In an MTT assay, Hep G2 cells are grown to confluency in a 96 well plate. Next, the compounds are incubated with Hep G2 cells at different concentrations for 24 hours. The MTT reagent (3-(4,5-dimethylthiazol-2-yl)-2,5-diphenyltetrazolium bromide) is added to the solutions and only living cells are able to reduce the MTT to a purple-coloured formazan dye which precipitates out of solution (**Figure 3-10**).[31] This assay screens for mitochondrial function since the reduction of the MTT reagent is accomplished by mitochondrial and cytosolic enzymes which use cellular reducing equivalents such as NADH. Solubilisation of

the formazan using isoproponal allows for the absorbance of the dissolved formazan to be measure and thus, the concentration at which the compound is toxic can be deduced.

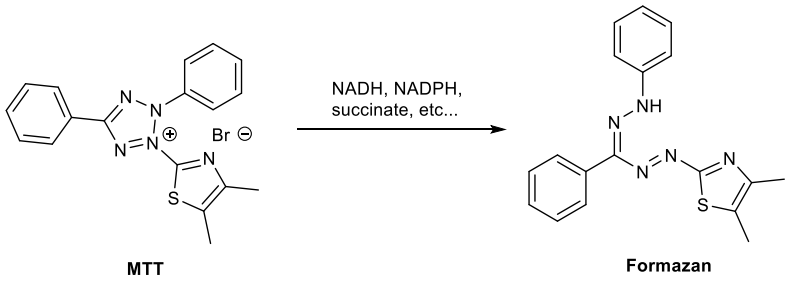

Figure 3-10. Reduction of MTT (3-(4,5-dimethylthiazol-2-yl)-2,5-diphenyltetrazolium bromide) in the cytotoxicity cell viability colorimetric assay.

The MTT assay has a few disadvantages which have limited its use. One major disadvantage is that the reduction of tetrazolium reflects cell metabolism and not cell number. The rate of MTT reduction can change with culture conditions and physiological state of the cell.[27] Additionally, cells growing rapidly as a monolayer will have a different metabolic rate that those that have undergone differentiation, grown into a confluent monolayer.[29] The factors need consideration during the use of this assay. Another disadvantage is that assay conditions that affect the reduction of MTT reagent result in increased background absorbance and assay artifacts. A variety of chemical compounds are known to interfere with the assay. These are generally reducing compounds leading to non-enzymatic reduction of MTT to formazan. Examples include ascorbic acid, glutathione, coenzyme A and dithioreitol.[30-33] Chemicals that uncouple the electron transport from oxidative phosphorylation of ATP are also known to interfere with the assay.[34] Finally, long-term exposure to the MTT reagent to light and elevated pH of culture medium may also result in production of formazan.[27] This interference is mitigated by using appropriate control such as wells containing the MTT reagent and test compound in cell medium with cells present. Lastly, the MTT reagent itself is also known to be somewhat cytotoxic to cells. It has been shown to be cytotoxic to eukaryote cells and cause a dramatic change in cell morphology. This cytotoxicity has been associated with the diversion of important reducing equivalents such as NADH. NADH is required in many critical cellular functions.[29] Additionally, the formazan crystals have also been associated with causing damage to cell membranes.[35] While many disadvantages are present, the broad application of this assay is based on its simplicity of the homogenous protocol, which utilises adding two reagents to the assay well and does not require additional steps such was cell washing. This assay is also ideally suited

for a 96 well plate format and thus has found application in high-throughput screening studies.[29] Cytotoxicity results of **310** and **311** at 0.5 mM-22 mM are presented in **Figure 3-11**.

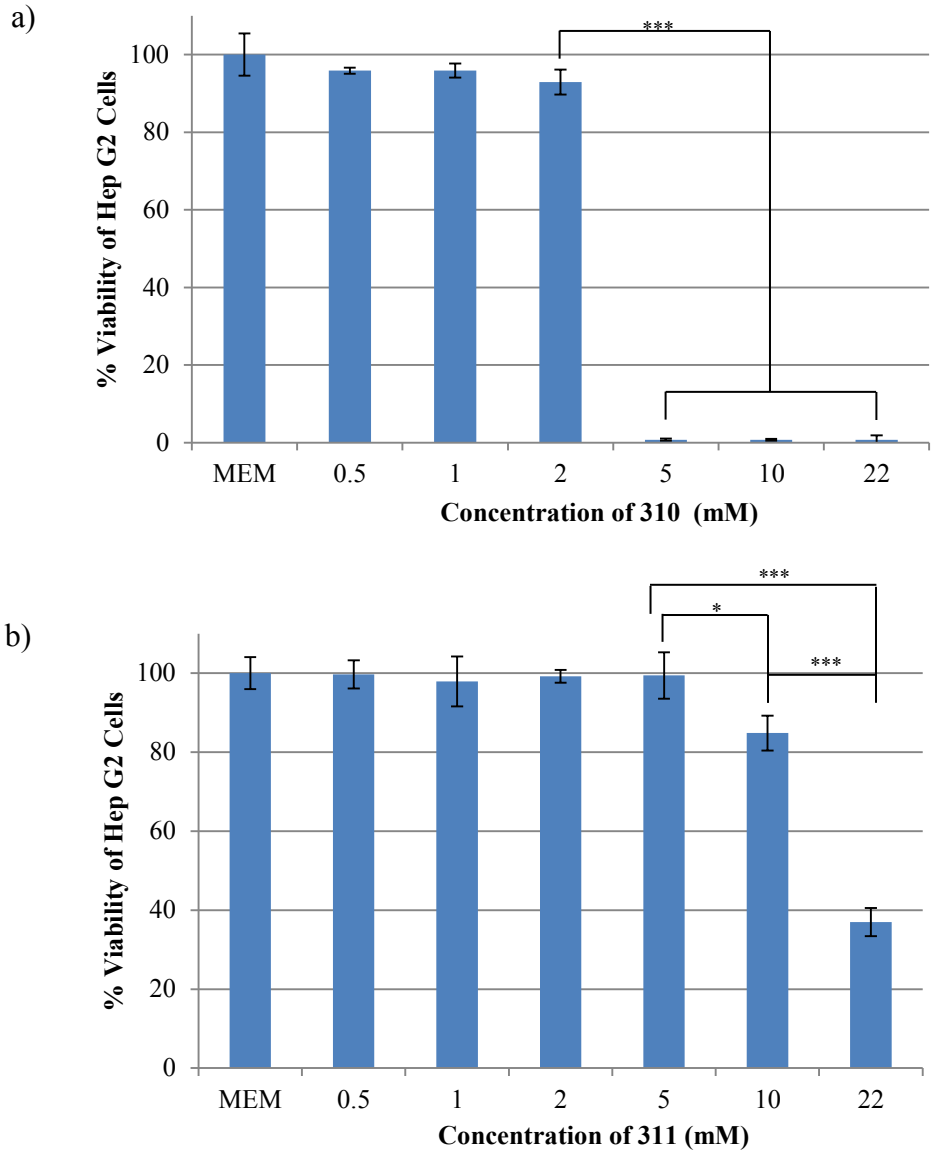

Figure 3-11. Percent cell viability of Hep G2 cells incubated with azasugars a) **310** and b) **311** in a MTT assay. Asterisks indicates a statistical significant difference between samples and is defined by unpaired Student's *t*-test (*, $p < 0.05$, ***, $p < 0.001$). Statistical significant difference between the MEM control and samples is not shown. Samples have been run in triplicate (n = 3) and error bars indicate standard error of the mean (SEM).

Compound **310** was highly toxic at concentrations as low as 5 mM whereas **311** was non-toxic at higher concentrations. Only at 22 mM of **311** did cell viabilities decrease to 40% for **311**. The difference in cyctotoxicity between **310** and **311** is not surprising since **311** is used to treat a number of diseases.[40] Interestingly, with only one structural change (an axial C4-OH) **310**

possess a drastically different cytotoxicity profile than **311**. The Ben laboratory has previously shown that the cytotoxicity profiles of D-glucose and D-glactose were very similar and neither compound was highly cyctotoxic even up to high concentrations such as 500 mM.[41] Therefore, the cytotoxicity of **310** is specific to pyranose azasugars. This is not surprising as **310**, **311** as well as other structurally similar azasugars are well known inhibitors (transition state mimics) of the highly important glycosidase family of enzymes. These enzymes play a crucial role in the breakdown of complex carbohydrates.[42] With its low cytotoxicity and potent IRI activity, **311** should be further explored as a cryoprotective agent.

3.6 Chapter Summary

In summary, the work described in this chapter described the impact of simple structural modifications to monosaccharides have on hydrogen bond capability and IRI activity. Specifically, systematic amino substitutions on D-galactose were explored for their IRI activity and an amino substitution of the C3-OH (**302**) was found to be the most potent. Amino groups were chosen because at a physiological pH, this group would be protonated and thus only be able to act as a hydrogen bond donor. Previous structure-function work had suggested that hydrogen bond donation may be an important feature for IRI activity. Further structure-function work suggested that replacement of the ring oxygen by an amine in D-galactose and D-glucose (azasugars) may generate potent IRI active small molecules. The synthesis of azasugars was efficiently accomplished through a reductive intramolecular cyclization. The moderate to potent IRI activity of the synthesized azasugars suggested the hydrogen bond donating capability of the ring heteroatom is important to IRI activity with D-glucose based azasugar **311** being the most potent azasugar. Given the likely protonated state of **310** and **311** at a pH of 7.4, the nature of the negative counterion needs future investigation. The importance of the counterion to IRI activity has been established by the Ben laboratory with lysine-based surfactants. Additionally, the relationship between changes in pH and IRI activity requires addressing. Modification to the endocyclic ring nitrogen such as methylation or modification to the electronics (lactams **329** and **330**) resulted in a decrease in IRI activity as compared to the parent azasugar. Finally, cytotoxicity studies using Hep G2 cells suggested that the glucose based azasugar should be further explored as a cryoprotective agent due to its low toxicity.

3.7 References

1. Tam, R. Y.; Ferreira, S. S.; Czechura, P.; Chaytor, J. L.; Ben, R. N., *J. Am. Chem. Soc.* **2008,** 130, 17494-17501.

2. Galema, S. A.; Hoeiland, H., *J. Phys. Chem.* **1991,** 95, 5321-5326.

3. Galema, S. A.; Engberts, J. B. F. N.; Hoeiland, H.; Foerland, G. M., *J. Phys. Chem.* **1993,** 97, 6885-6889.

4. Galema, S. A.; Howard, E.; Engberts, J. B. F. N.; Grigera, J. R., *Carbohydr. Res.* **1994,** 265, 215-225.

5. Dashnau, J. L.; Sharp, K. A.; Vanderkooi, J. M., *J. Phys. Chem. B* **2005,** 109, 24152-24159.

6. Chaytor, J. L. Examining the Role of Carbohydrate Hydration and Structure in Preventing Ice Recrystallization. 2010, Ph. D. Dissertation, University of Ottawa.

7. Palusiak, M.; Grabowski, S. J., *J. Mol. Struct.* **2002,** 642, 97-104.

8. Ferreira, S. S. Improving the rational design of antifreeze glycoproteins through identification of the parameters that influence ice recrystallization inhibition. 2009, University of Ottawa.

9. Uedaira, H.; Okouchi, S.; Tsuda, S.; Uedaira, H., *Bull. Chem. Soc. Jpn.* **2001,** 74, 1857-1861.

10. Tonelli, D. L. Small Molecule Ice Recrystallization Inhibitors and Their Use in Methane Clathrate Inhibition. 2012, M. Sc. Dissertation, University of Ottawa.

11. Pedersen, C. M.; Olsen, J.; Brka, A. B.; Bols, M., *Chem. Eur. J.* **2011,** 17, 7080-7086.

12. Balcerzak, A. K.; Febbraro, M.; Ben, R. N., *RSC Adv.* **2013,** 3, 3232-3236.

13. Çarçabal, P.; Jockusch, R. A.; Hünig, I.; Snoek, L. C.; Kroemer, R. T.; Davis, B. G.; Gamblin, D. P.; Compagnon, I.; Oomens, J.; Simons, J. P., *J. Am. Chem. Soc.* **2005,** 127, 11414-11425.

14. Cocinero, E. J.; Stanca-Kaposta, E. C.; Scanlan, E. M.; Gamblin, D. P.; Davis, B. G.; Simons, J. P., *Chem. Eur. J.* **2008,** 14, 8947-8955.

15. Hünig, I.; Painter, A. J.; Jockusch, R. A.; Carcabal, P.; Marzluff, E. M.; Snoek, L. C.; Gamblin, D. P.; Davis, B. G.; Simons, J. P., *Phys. Chem. Chem. Phys.* **2005,** 7, 2474-2480.

16. Simons, J. P.; Jockusch, R. A.; ÇarÇabal, P.; Hünig, I.; Kroemer, R. T.; Macleod, N. A.; Snoek, L. C., *Int. Rev. Phys. Chem.* **2005,** 24, 489-531.

17. Simons, J. P.; Davis, B. G.; Cocinero, E. J.; Gamblin, D. P.; Stanca-Kaposta, E. C., *Tetrahedron: Asymmetry* **2009,** 20, 718-722.

18. Capicciotti, C. J. The Rational Design of Potent Ice Recrystallization Inhibitors for Use as Novel Cryoprotectants. 2014, Ph. D. Dissertation, University of Ottawa.

19. Martin, O. R.; Saavedra, O. M.; Xie, F.; Liu, L.; Picasso, S.; Vogel, P.; Kizu, H.; Asano, N., *Bioorg. Med. Chem.* **2001,** 9, 1269-1278.

20. Overkleeft, H. S.; van Wiltenburg, J.; Pandit, U. K., *Tetrahedron* **1994,** 50, 4215-4224.
21. Griffith, W. P.; Ley, S. V.; Whitcombe, G. P.; White, A. D., *J. Chem. Soc., Chem. Commun.* **1987**, 1625-1627.

22. Albright, J. D.; Goldman, L., *J. Am. Chem. Soc.* **1965,** 87, 4214-4216.

23. Wennekes, T.; van den Berg, R. J. B. H. N.; Donker, W.; van der Marel, G. A.; Strijland, A.; Aerts, J. M. F. G.; Overkleeft, H. S., *J. Org. Chem.* **2007,** 72, 1088-1097.

24. Capicciotti, C. J.; Leclère, M.; Perras, F. A.; Bryce, D. L.; Paulin, H.; Harden, J.; Liu, Y.; Ben, R. N., *Chem. Sci.* **2012,** 3, 1408-1416.

25. Lopez, O.; Bols, M., Isofagomine, Noeuromycin and other 1-Azasugars, Iminosugar-Related Glycosidase Inhibitors. In *Iminosugars*, John Wiley & Sons, Ltd: 2008; pp 131-151.

26. Chakrabartty, A.; Hew, C. L., *Eur. J. Biochem.* **1991,** 202, 1057-1063.

27. Eniade, A.; Ben, R. N., *Biomacromol.* **2001,** 2, 557-561.

28. Liu, S.; Ben, R. N., *Org. Lett.* **2005,** 7, 2385-2388.

29. Czechura, P.; Tam, R. Y.; Dimitrijevic, E.; Murphy, A. V.; Ben, R. N., *J. Am. Chem. Soc.* **2008,** 130, 2928-2929.

30. Chaytor, J. L.; Tokarew, J. M.; Wu, L. K.; Leclère, M.; Tam, R. Y.; Capicciotti, C. J.; Guolla, L.; von Moos, E.; Findlay, C. S.; Allan, D. S.; Ben, R. N., *Glycobiology* **2012,** 22, 123-133.

31. Mosmann, T., *J. Immunol. Methods* **1983,** 65, 55-63.

32. Liu, S.; Wang, W.; von Moos, E.; Jackman, J.; Mealing, G.; Monette, R.; Ben, R. N., *Biomacromol.* **2007,** 8, 1456-1462.

33. Riss, T.; Moravec, R.; Niles, A.; Benink, H.; Worzella, T.; Minor, L., *Cell viability assays*. Bethesda (MD): Eli Lilly & Company and the National Center for Advancing Translational Sciences: 2013.

34. Ulukaya, E.; Colakogullari, M.; Wood, E. J., *Chemotherapy* **2004,** 50, 43-50.

35. Chakrabarti, R.; Kundu, S.; Kumar, S.; Chakrabarti, R., *J. Cell. Biochem.* **2001,** 80, 133-138.

36. Bernas, T.; Dobrucki, J., *Cytometry* **2002,** 47, 236-242.

37. Pagliacci, M. C.; Spinozzi, F.; Migliorati, G.; Fumi, G.; Smacchia, M.; Grignani, F.; Riccardi, C.; Nicoletti, I., *Eur. J. Cancer* **1993,** 29, 1573-1577.

38. Collier, A. C.; Pritsos, C. A., *Biochem. Pharmacol.* **2003,** 66, 281-287.

39. Lü, L.; Zhang, L.; Wai, M. S. M.; Yew, D. T. W.; Xu, J., *Toxicol. In Vitro* **2012,** 26, 636-644.

40. Compain, P.; Martin, O. R., Iminosugars: from synthesis to therapeutic applications. In *Iminosugars: from synthesis to therapeutic application*, Compain, P.; Martin, O. R., Eds. John Wiley & Sons: Chichester, 2007.

41. Chaytor, J. L.; Tokarew, J. M.; Wu, L. K.; Leclère, M.; Tam, R. Y.; Capicciotti, C. J.; Guolla, L.; von Moos, E.; Findlay, C. S.; Allan, D. S.; Ben, R. N., *Glycobiology* **2012,** 22, 123-133.

42. Compain, P.; Martin, O. R., *Iminosugars: Past, Present and Future*. John Wiley & Sons, Ltd: 2008.

Chapter 4. Inhibiting Gas Hydrate Formation Using Small Molecule Ice Recrystallization Inhibitors

4.1 Introduction

Gas hydrates are ice-like solids containing gases within a highly ordered network of water molecules.[1] The similarity of gas hydrates to ice becomes evident considering that a gas hydrate consists of about 85% water on a molecular basis. Thus, many of the hydrate structural properties resemble those of ice I_h.[1] For example, hydrate hydrogen bonds average only 1% longer than those in ice and the O-O-O angles differ from ice tetrahedral angles by 3.0-3.7° in two common gas hydrate structures.[1] However, the reorganization of water molecules is drastically different between gas hydrates and ice. For example, the diffusion rates of water molecules in gas hydrates are much higher than those found in ice I_h. This difference in diffusion rates has been linked to an increase in mechanical strength for gas hydrates. The biggest difference between these two solids is that ice is a pure component and gas hydrates will not form without the proper gas molecules.[1 1] Furthermore, gas hydrates are supported by the repulsion forces imparted on the water molecules by the guest gas molecule.[2]

These hydrates can form at ambient temperatures (less than 27 °C) and moderate pressures (> 0.6 MPa or 87 psi); conditions frequently found in oil and gas pipelines.[3] These materials were initially discovered by Sir Humphrey Davy in 1811 through the crystallization of a cold aqueous solution of chlorine.[4] Hydrates are problematic in the petroleum industry as they can produce pipeline blockages causing safety concerns and shutdowns of the pipeline during the removal of the blockage.[5, 6] **Figure 4-1** shows a pipeline blockage caused by gas hydrates. Decomposition of the natural occurring gas hydrates due to drilling through hydrate zones has also caused major concerns. Drilling through hydrate zones is generally performed for gas production from there naturally occurring hydrates or for oil and gas production from reservoirs located below the *in-situ* hydrates. This drilling has caused uncontrolled gas release, blowouts and fires through and outside the drilling columns.[1, 7, 8] Thus, gas hydrates are highly problematic.

Figure 4-1. Pipeline blockage caused by gas hydrates.[9]

Three structures of gas hydrates have been discovered: sI (cubic), sII (cubic) and sH (hexagonal), and the size of the gas molecule determines which structure is formed.[10] The structures of sI and sII hydrates were first elucidated by von Stackelberg and coworkers through crystal diffraction studies.[11-14] Following this work, Mak, McMullan and Jeffrey completed additional diffraction studies and provided more conclusive evidence for the structures.[15, 16] The structure of sH was discovered by Ripmeester using solid state NMR studies.[17] The different structures of a unit cell of gas hydrates are represented in **Figure 4-2**.

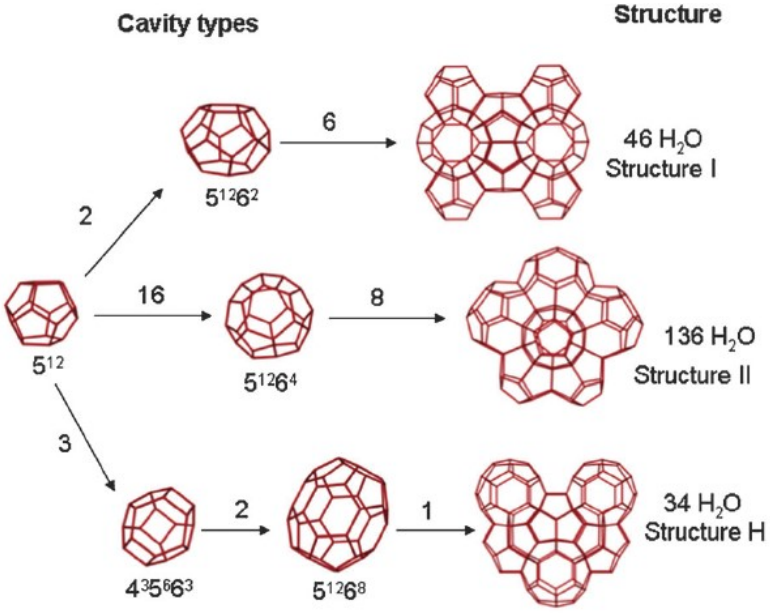

Figure 4-2. Cavity composition of sI, sII, sH.[2]

The formalism A^B is used to describe the structure of a cavity where A represents the number of hydrogen bonded edges of the face and B represents the number of faces with A sides.[18] Thus, the cavity 5^{12}, a common cavity found in each gas hydrate structure, results from the combination of 12 pentagonal units. A sI hydrate comprises of two 5^{12} cavities and six $5^{12}6^2$ to form a unit cell comprised of 46 water molecules. A sII hydrate is made from sixteen 5^{12} and eight $5^{12}6^4$ cavities to form a unit cell with 136 water molecules. Finally, sH comprises of three 5^{12}, two $4^35^66^3$ and one $5^{12}6^8$ cavity to form a unit cell containing 34 water molecules. sI can accommodate small gases such as methane whereas sII and sH can accommodate larger guest molecules.[1, 19, 20] In order to fully understand the different forms of gas hydrates, an explanation of the mechanism of gas hydrate formation is required.

Gas hydrate formation is known to be stochastic in nature making the study of gas hydrates difficult.[1] Gas hydrate nucleation is thought to occur at the interface of water and gas in the presence of high concentrations of both, gas and water.[1, 21] The site of nucleation has been confirmed by Ohmura using videographs to study nucleation of crystals in a water-gas system. A water droplet was placed onto a Teflon stage inside a test cell and the atmosphere within the cell was replaced with methane, ethane or propane. Finally, the temperature was reduced to induce nucleation of gas hydrates (**Figure 4-3**).[22]

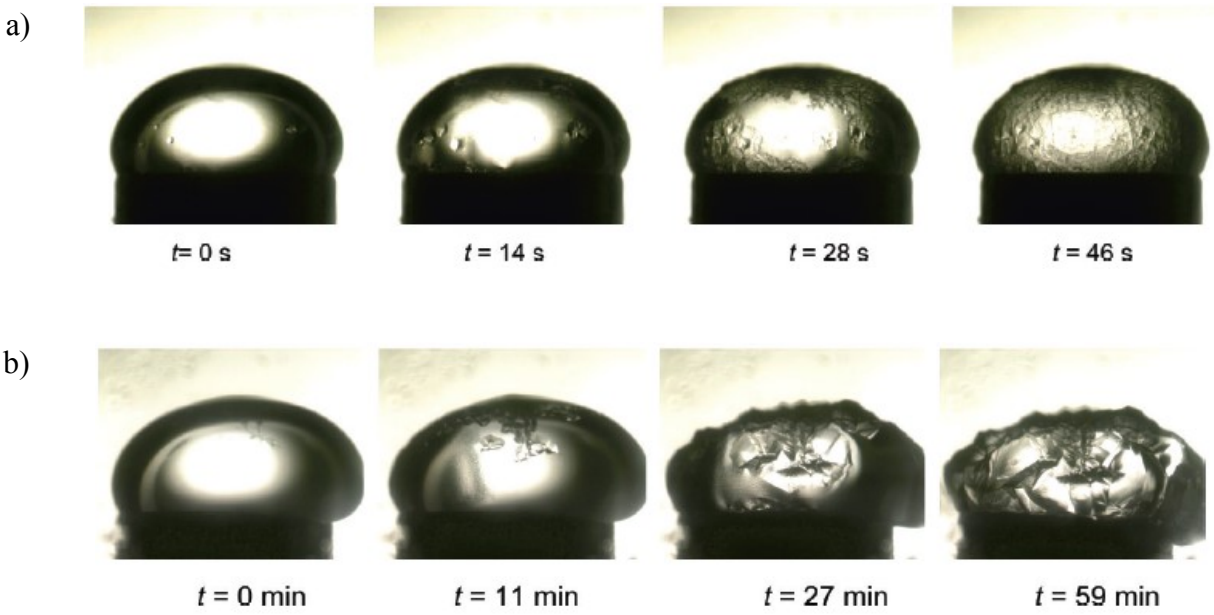

Figure 4-3. Videographs of the nucleation and growth of a methane hydrate at the surface of a water droplet under high subcooling (a) and low subcooling (b).[22]

It was demonstrated that nucleation occurs at random points along the surface of the water droplet and critical sized nucleation was followed by polycrystalline growth.[22] Three different mechanisms have been suggested to describe gas hydrate nucleation: the labile cluster hypothesis,[23] interfacial nucleation[24, 25] and local structuring.[2] The labile cluster hypothesis was first proposed by Sloan and Christiansen[23] (**Figure 4-4**).

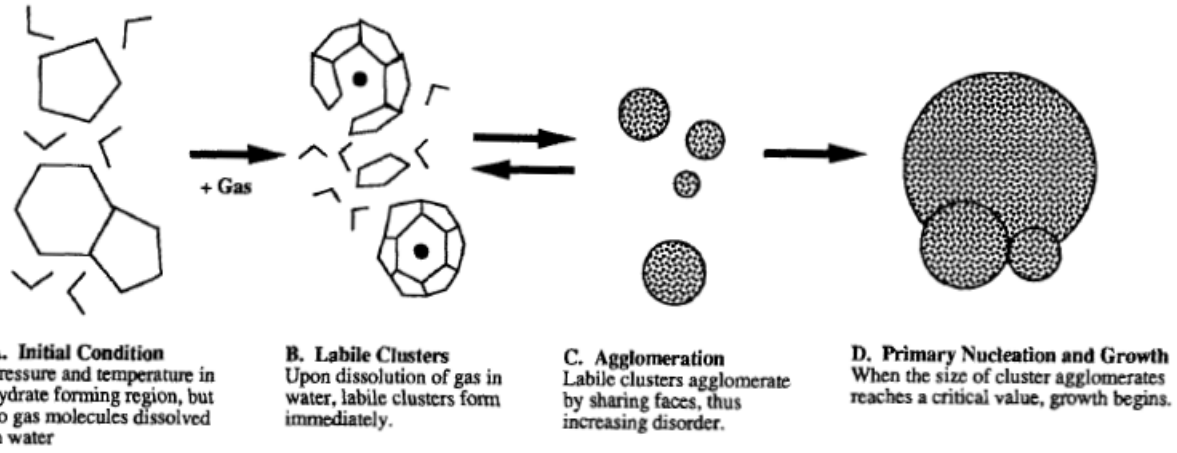

Figure 4-4. Schematic representation of the labile cluster hypothesis.[23]

Guest gas molecules are dissolved in water where metastable (below critical size) labile clusters form. These structures can dissipate or agglomerate to attain a critical size where growth of gas hydrates can occur. [23] In the interfacial nucleation hypothesis (proposed by Long and Kvamme), gas molecules are transported to water cages through surface diffusion where gas hydrates can undergo nucleation.[1] Finally, the local structuring nucleation hypothesis suggests that gas molecules assemble (through thermal fluctuation) in a configuration required for gas hydrate formation. This arrangement of gas molecules results in a disturbance of bulk water thereby generating a critical nucleus upon which growth can occur.[26]

4.2 Inhibiting Gas Hydrate Formation

Given the disruptive nature of gas hydrates, the petroleum industry continues to research inhibitor species to prevent or delay large-scale gas hydrate formation. In general, prevention of gas hydrates is accomplished with two general types of compounds: thermodynamic hydrate inhibitors (THI) and low-dosage hydrate inhibitors (LDHI). In the presence of a THI, gas hydrate formation requires higher pressures and lower temperatures. Methanol is a common THI;

however, 20-50 wt% is generally required to be effective.[6] In addition to the large volumes, difficulties in recovering or recycling the methanol post-addition brings significant financial implications.[27] Consequently, LDHIs are a cost-effective alternative as they are effective at low concentrations (0.01-5 wt%).[6] There are two classes of LDHI: anti-agglomeration agents (AAs) and kinetic gas hydrate inhibitors (KHIs). AAs prevent the aggregation of small clusters of gas hydrates into forming a blockage while KHIs inhibit the rate of nucleation and growth of gas hydrates. The structure and properties will now be discussed.

4.2.1 Structure and Properties of Anti-Agglomeration Agents

Two types of AAs are known: 1) The French Petroleum Institute (IFP) type that provides a special kind of water-in-oil emulsion which does not agglomerate upon gas hydrate formation, and 2) The Shell type that have a hydrate-philic head and a long hydrophobic tail. [1] The IFP have discovered amphiphilic compounds that form a water-in-oil emulsion, which confine the gas hydrate to water droplets. This confinement effectively prevents their agglomeration.[6] However, the AAs developed by the IFP still await field trial (structure of AAs developed by IFP is not released within the patent[28]).[1] The AAs developed by Shell are also amphiphilic compounds where the hydrate-philic end of the AA is dissolved within the gas hydrate while the hydrophobic end is dissolved in the hydrocarbon liquid (oil). The chemical spacer between the two ends of the AA provides separation of the gas hydrate and prevents agglomeration from occurring.[1] The structures of two types of AAs developed by Shell are shown in **Figure 4-5**.

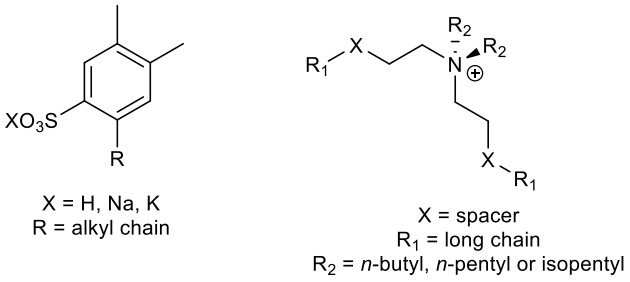

Figure 4-5. Structures of anti-agglomeration agents developed by Shell.

4.2.2 Structure and Properties of Kinetic Hydrate Inhibitors

One major drawback of AAs is the requirement for continual agitation for optimal effectiveness.[29] Additionally, within the context of gas pipelines, the application of AAs is not possible since they require a liquid hydrocarbon phase (gas pipelines contain little to no liquid

hydrocarbon phase).[6] Based on these setbacks, the development of novel KHIs is essential. The majority of KHIs are water-soluble polymers. Polyvinylpyrrolidone (PVP, **Figure 4-6**) is an example of a KHI developed by Shell in conjunction with the Colorado School of Mines.[6, 30]

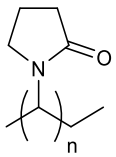

Figure 4-6. Structure of Polyvinylpyrrolidone.

Testing of PVP by Shell was completed using a ball-stop rig with a THF hydrate as a model system.[30] A ball-stop rig measures the time required for a metal ball to cease movement through a cooled cell containing a hydrate-forming liquid containing an inhibitor.[6] The formation of a hydrate blockage causes ball movement to cease. While high molecular weights of PVP were effective at inhibiting the ball movement for 6 hours, low molecular weight PVP 10 (10,000 g/mol) was also an effective inhibitor. It has been shown that the PVP with a lower molecular weight such as PVP 10, had a pronounced effect on disturbing the structure of bulk water and thus had a greater inhibition of gas hydrate nucleation.[31] Along with PVP, recent work has led to the discovery that polyvinylcaprolactam and various branched polyester amides can also function as KHIs.[2, 6]

4.2.3 Inhibition of Gas Hydrates Using Ice Recrystallization Inhibitors

Whilst LDHIs offer economic benefits in comparison to THIs, further development is required to improve biodegradability as well as performance under extreme conditions. It has been reported that deeper sea gas and oil fields will be exploited in the near future and thus, there is a need for high performance gas hydrate inhibitors.[8, 32] Recently, Walker and Ripmeester demonstrated the use of antifreeze proteins as gas hydrate formation inhibitors.[33-35] Given the structural similarity between ice and gas hydrates[1], the use of AFPs is not surprising. As stated in section 1.5, AFPs possess two antifreeze activities: IRI and TH. It has been demonstrated that TH activity was not necessary for inhibition of gas hydrates.[19] While IRI active AFPs are inhibitors of gas hydrates, the difficulty associated with obtaining them on large scale has prevented their use in the industry. Consequently, it was hypothesized that small molecules recently developed by our laboratory possessing potent IRI activity and lacking TH activity may

be effective inhibitors of gas hydrate formation. Their low molecular weight (< 300 g/mol) makes them ideal candidates since a lower weight percent concentration may be needed to achieve potent inhibition of gas hydrates. Additionally, the small molecule IRIs are easy to synthesize on large scale. Therefore, initial efforts were placed toward using these compounds to inhibit methane gas hydrates (sI); as these tend to be problematic in the petroleum industry.[5]

4.3 Quantifying Gas Hydrate Nucleation and its Inhibition

The driving force for gas hydrate nucleation increases as temperature decreases. As a gas hydrate undergoes nucleation, heat is released and a differential scanning calorimeter (DSC) is used to track this evolution of heat .[34, 36-39] This approach has been shown by Walker and Ripmeester to be an effective method for quantifying gas hydrate nucleation.[19] **Figure 4-7** is a representative of an isothermal analysis using PVP 10 at 1 mM.

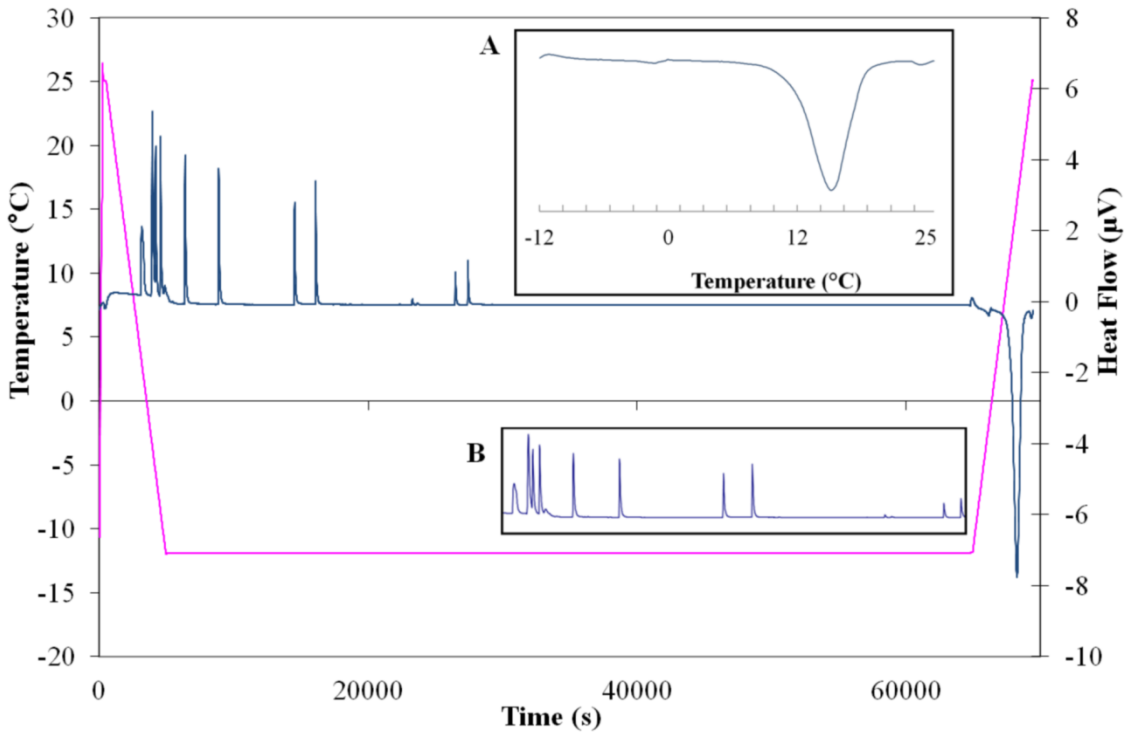

Figure 4-7. DSC curve (blue line) representing of a test run for an isothermal temperature experiment (-12 °C, pink line) with 1 mM PVP 10. **Inset A** magnifies the observed melting event with temperature (°C) on the x-axis while heat flow (µV) is on the y-axis and **Inset B** magnifies the observed nucleation events with the remperature (°C) and heat flow (µV) on the y-axis while time (s) is on the axis.

Twelve solutions of PVP 10 were prepared by dissolving PVP 10 in distilled water at 1 mM. The solutions are then confined in silica gel and placed in twelve borosilicate tubes. Silica gel was chosen because it increases the water-gas interface and thus facilitates gas hydrate nucleation.[40] These samples were then placed under 100 bar of methane gas and allowed to stand; saturating the liquid phase with methane. Based on literature precedent, a sI gas hydrate was assumed under an atmosphere of methane gas.[34, 41] Upon cooling, sharp exothermic peaks (represented by the blue line) represent nucleation events. The sharp profiles of the exothermic peaks indicates that crystal nucleation was followed by rapid growth due to large surface area of the sample, small sample volume and high driving force for hydrate formation. Therefore, the position of the peaks represents nucleation events while the area under the curve represents growth. The pink line represents the temperature profile of the experiment. As multiple nucleation events are possible in a single sample, the number of exothermic peaks is often larger than twelve. Trials containing fewer than twelve exothermic peaks represent instances where nucleation did not occur in some samples. During the warming phase, a single negative peak corresponding to the warming event is observed (**Figure 4-7**, **Inset A**). This negative peak is representative of a single gas hydrate and under an atmosphere of methane, it is a sI gas hydrate. It is important to note that no warming peak corresponding to ice was observed. This suggests that the hydrate formation is a homogenous process forming only a sI gas hydrate.[34, 37, 42 41] Each experiment is repeated three times with a total of 36 trials for each sample. The integrated average of the area under the exothermic peaks was used to generate a total cumulative heat of reaction. This cumulative heat of reaction directly correlates to gas hydrate growth. The time to the first nucleation event (first positive value for the cumulative heat of reaction) represents the induction time and thus indicates the degree to which initial gas hydrate nucleation is delayed.[34] Therefore, the use and analysis of this assay determines two properties of a KHI: the ability to delay the first nucleation event and its ability to inhibit gas hydrate formation.

4.4 Inhibiting Formation of Gas Hydrates Using *n*-octyl-β-D-pyranosides

n-Octyl-β-D-pyranosides **126** and **127** are known inhibitors of gas hydrates[43] in addition to the potent IRI activity of *n*-octyl-β-D-galactopyranoside **127**. [44] As stated in section 4.2.3, AFPs are potent inhibitors of ice recrystallization and effective inhibitors of gas hydrate formation. Their ability to inhibit gas hydrate formation is independent of their TH activity.[34] *n*-

Octyl-β-D-pyranosides **126** and **127** (as well as other small molecules developed by our laboratory) do not possess TH activity;[44] suggesting that some of the structural properties necessary for IRI activity may also be important for inhibiting gas hydrate formation (initial nucleation followed growth). Thus, small molecules IRIs developed by our laboratory are ideal molecules to investigate the possibility of a correlation between IRI activity and performance as inhibitors of gas hydrate formation. Inhibition of gas hydrate formation was measured for both **126** and **127**. PVP 10 and water are utilized as negative and positive controls respectively for gas hydrate formation. Initial experiments utilized a sample concentration of 1 mM.[34] The cumulative heat of reaction in Joules generated by **126** and **127** is presented in **Figure 4-8**.

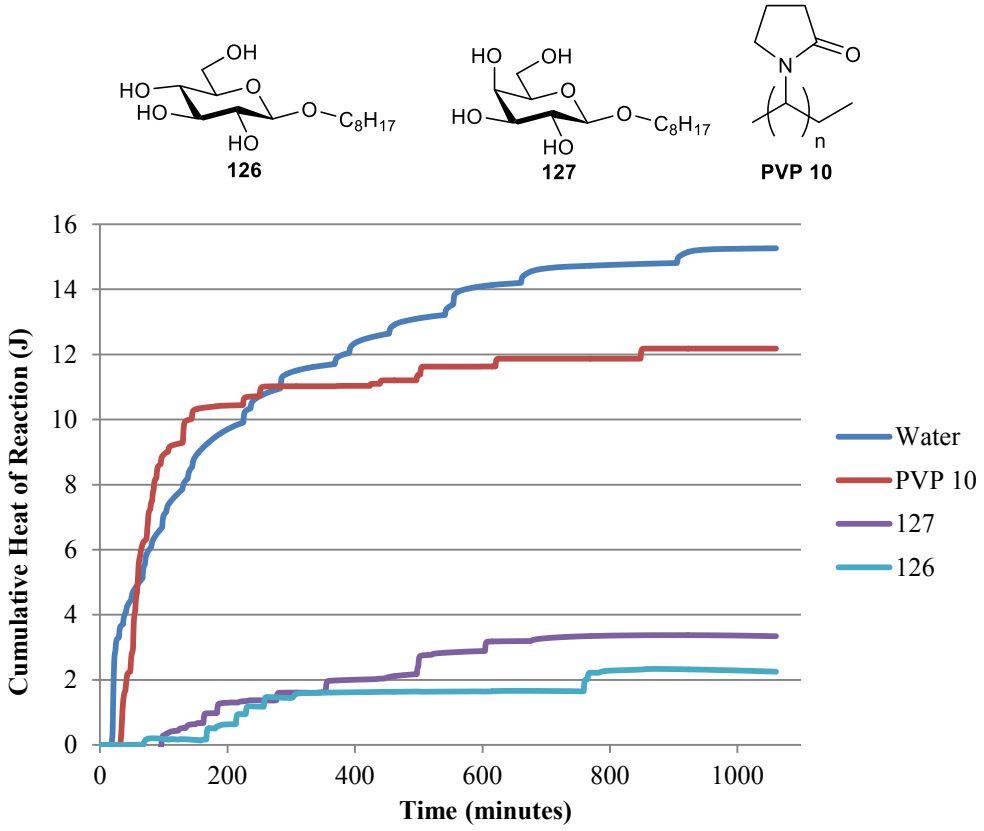

Figure 4-8. Cumulative heat of reaction of gas hydrate inhibitor PVP 10 and anti-agglomeration agents **126** and **127** at 1 mM. The result for each compound is based on the integrated average of 36 trials at -12 °C. Time = 0 minutes represents the start of the cooling phase.

126 and **127** are significantly better inhibitors of gas hydrate formation than PVP 10. Based upon the relative areas under each curve, the inhibition by **126** and **127** is approximately ten times greater than the commercial inhibitor PVP 10. It should be noted that t = 0 minutes represents the start of the cooling phase. Thus, the time to the first positive value for the heat of reaction represents the onset time for nucleation. A key measure for KHI performance is the delay of the first nucleation event.[6] **126** and **127** are both able to delay the first nucleation event for significantly longer time than PVP 10. This degree of inhibition of gas hydrate formation is very impressive when considering the lower molecular weights of **126** and **127**. **126** and **127** have molecular weights of roughly 300 g/mol, which are significantly less than 10,000 g/mol for PVP 10. A 1 mM solution of PVP 10 corresponds to a 1% w/v solution (10 mg/mL), whereas a 1 mM solution of **126** and **127** corresponds to a 0.03% w/v solution (0.29 mg/mL). The lower weight percent concentration makes **126** and **127** ideal candidates for commercial use. Interestingly, little difference is observed between the inhibition of gas hydrate formation activity of **126** (a D-glucose analogue) and **127** (a D-galactose analogue). This is surprising as the Ben laboratory has previously demonstrated that D-galactose analogue **127** is a significantly better inhibitor of ice recrystallization than the D-glucose analogue **126**.[44] This suggests that the structural requirements for IRI may not be the same as those for gas hydrate formation inhibition. The differences in structural requirements may be expected considering the lack of bulk water within pipelines.

4.5 Small Molecule IRIs as Inhibitors of Gas Hydrate Formation

Given the gas hydrate inhibition activity of **126** and **127**, other IRI active small molecules were investigated for their ability to inhibit gas hydrate formation. Previous work investing the IRI activity of *n*-octyl-β-D-pyranosides has demonstrated the importance of long alkyl chains to IRI activity. Within this study, other compounds possessing long alky chains such as *N*-octyl-D-gluconamide (**128**) were found to be highly IRI active. This was the first report of small molecules exhibiting "custom-tailored" antifreeze activity on par with AFGPs and their analogues.[44] The importance of long alkyl chains to IRI activity has been demonstrated with truncated *C*-linked D-galactose derivatives and lysine-based surfactants.[45, 46] The IRI activity of the *C*-linked D-galactose derivatives and lysine-based surfactants has been previously discussed in Chapter 1. Along with compounds possessing long alkyl chains, azasugars **310** and **311** have

also been shown to be IRI active molecules with **311** possessing potent activity. In contrast to compounds **126-128**, these azasugars lack the long alkyl chains yet still possess moderate to potent IRI activity. Consequently, the following were investigated: a) the relationship between hydrophobic alkyl chains of different lengths and IRI activity and b) whether small molecule IRIs would also inhibit the nucleation of gas hydrates. This will help elucidate if the important structural feature present in small molecule IRIs are necessary for inhibition of gas hydrate formation. Specifically, the presence of long alkyl chains, an open-aliditol chain, pyranose rings possessing either an endocyclic oxygen or nitrogen will be examined.

The IRI activity of compounds **128**, **401**, **402**, **310**, **311** and **331** is shown in **Figure 4-9**. While the activity of **128**, **310**, **311** and **331** has been presented previously (in independent publications and within this thesis), it is presented again to facilitate an accurate discussion of the relationship between IRI activity of these small molecules and their ability to inhibit gas hydrate formation.

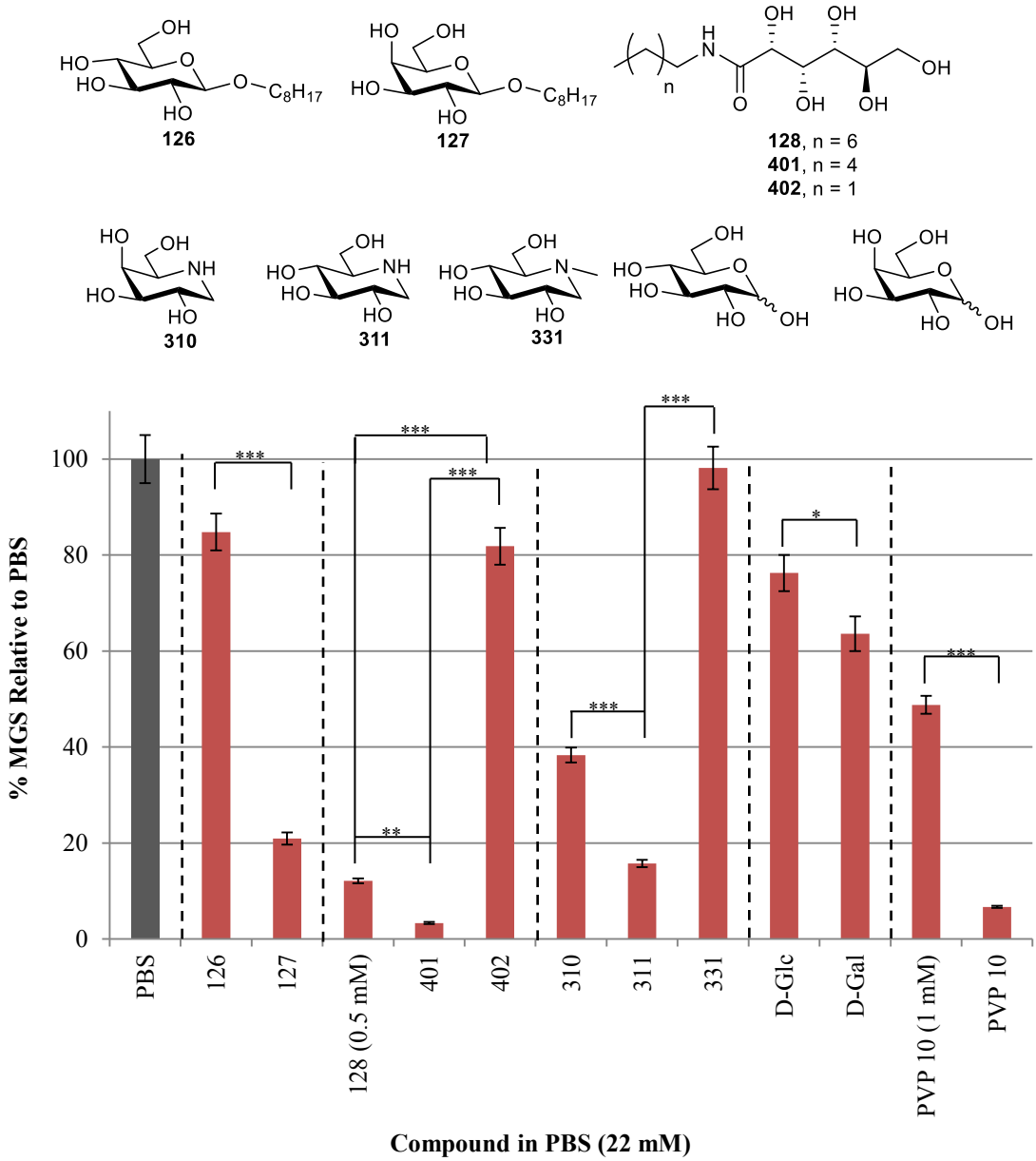

Figure 4-9. IRI activity of compounds **126-128**, **401**, **402**, **310**, **311** and **331** is shown and compared to PVP 10. Asterisks indicates a statistical significant difference between samples (within each set) and is defined by unpaired Student's *t*-test (*, $p < 0.05$, **, $p < 0.01$, ***, $p < 0.001$). Statistical significant difference between the PBS control and samples is not shown. Samples have been run in triplicate (n = 3) and error bars indicate standard error of the mean (SEM).

Compounds **128** and **401** exhibited very potent IRI activity at concentrations as low as 0.5 mM. Both of these compounds are significantly more IRI active than PVP 10 at 1 mM and possess comparable IRI activity to PVP 10 at 22 mM. Compound **128** could only be tested at 0.5

mM due to poor solubility. The benefit of long alkyl chains on IRI activity is apparent when comparing compounds **128** to **402**. Compound **128**, containing an eight carbon chain, possesses potent IRI activity whereas **402**, with a three carbon chain, has poor IRI activity. As discussed in Chapter 3, azasugars containing an endocyclic nitrogen within the pyranose ring possess moderate to potent IRI activity. Azasugars **310** and **311** exhibited more potent IRI activity than a 1 mM solution of PVP and **311** possessed potent IRI activity similar to a 22 mM solution of PVP 10. Azasugars **310** and **311** also exhibited similar IRI activity to the known gas hydrate formation inhibitors **126** and **127** as well as to the potent inhibitors of ice recrystallization, **128** and **401**. With these azasugars and alditol derivatives demonstrating potent IRI activity, their performance as inhibitors of gas hydrate formation was investigated. First the alditol derivatives containing different alkyl chain lengths were examined and compared to water, PVP 10 and **126**.

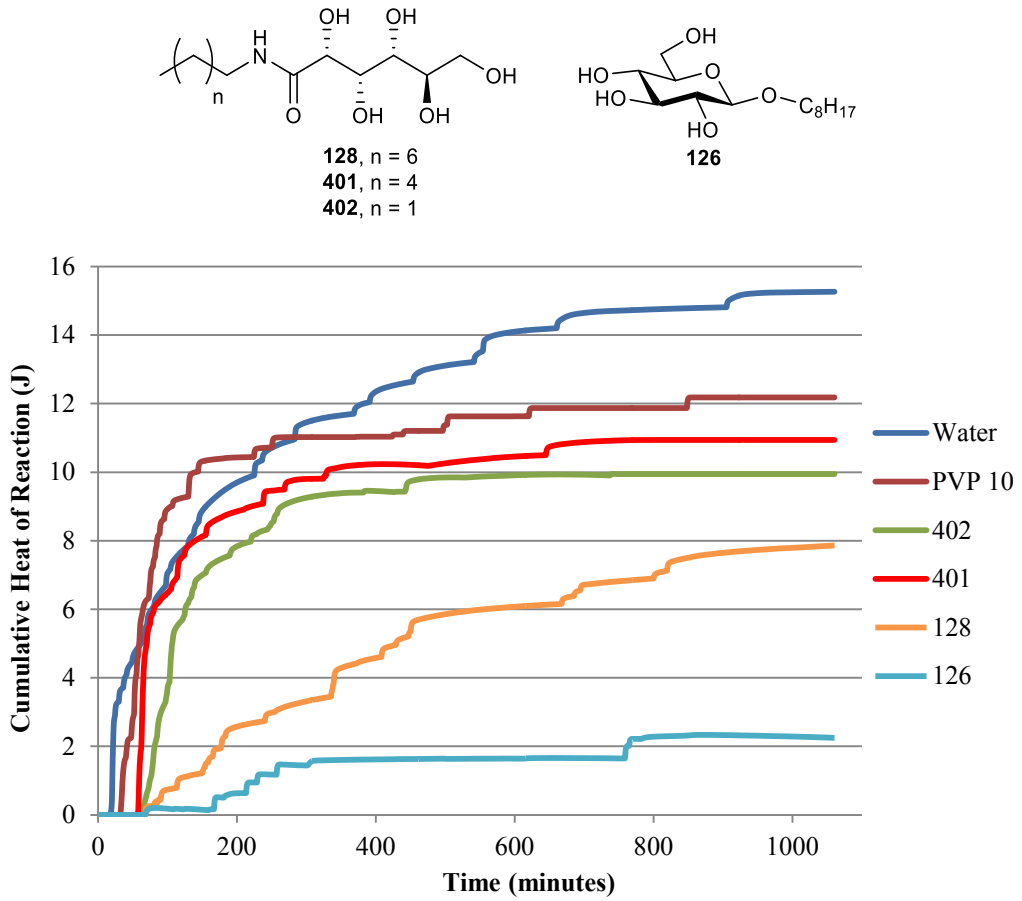

Figure 4-10. Cumulative heat of reaction of compounds **126**, **128**, **401** and **402** at 1 mM. Water and PVP 10 (1 mM) are included as representative controls. The result for each compound is based on the integrated average of 36 trials at -12 °C. Time = 0 minutes represents the start of the cooling phase.

Compounds **128**, **401** and **402** all exhibit similar onset time (time to the first nucleation event) as known gas hydrate formation inhibitor **126**. Compounds containing six and three carbon chains (**401** and **402** respectively) exhibited comparable gas hydrate formation ability to the commercial inhibitor PVP 10. Compound **128** with an eight carbon chain showed an improvement in its ability to inhibit gas hydrate formation relative to **401** and **402**. However **126**, also containing an eight carbon chain, is a much better inhibitor of gas hydrate formation than **128**. This shows that the presence of a pyranose ring is important in determining a good inhibitor of gas hydrate formation. Replacement of the pyranose ring in *n*-octyl-β-D-glucopyranoside to an open-alditol chain in *N*-octyl-D-gluconamide (**126** versus **128**) led to a decrease in gas hydrate formation inhibition activity. Thus, it is imperative to assay small molecule IRIs possessing a pyranose ring and lacking a long alkyl chain to examine if the activity can be retained. Therefore,

azasugars **310** and **311** were assayed for their ability to inhibit gas hydrate formation. Additionally, as discussed previously, simple monosaccharide reducing sugars such as D-glucose and D-galactose also posses IRI activity.[47] Thus, D-glucose and D-galactose will also be assayed for their ability to inhibit gas hydrate formation (**Figure 4-11**).

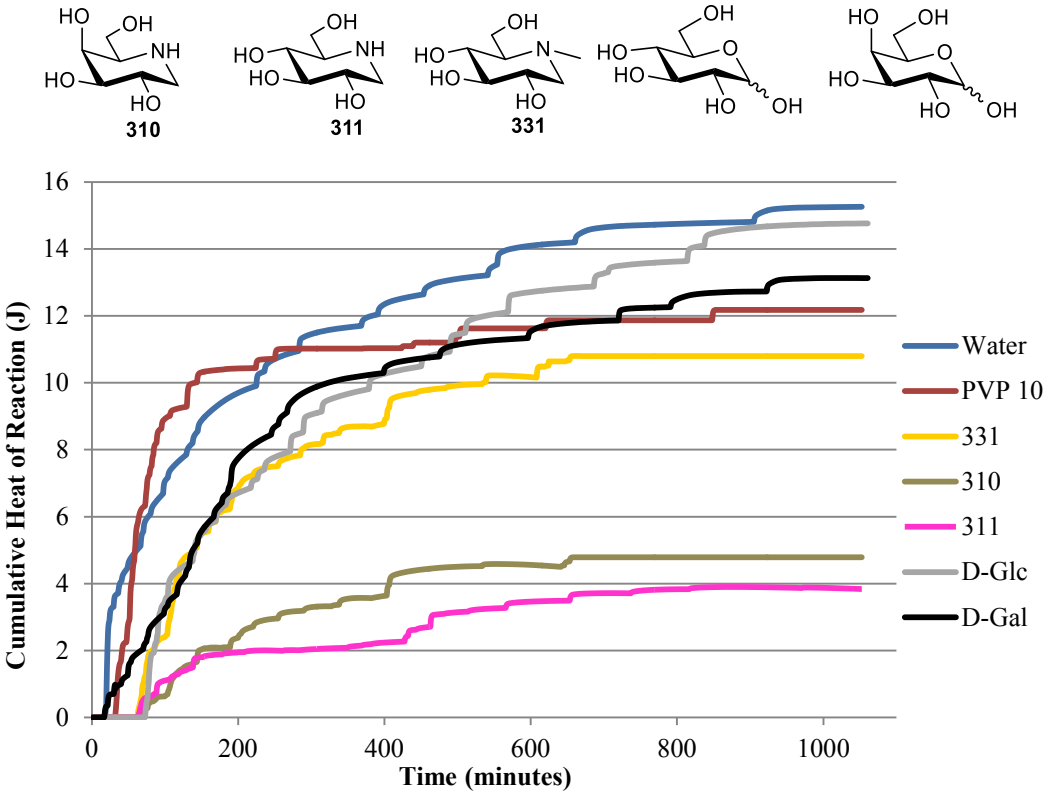

Figure 4-11. Cumulative heat of reaction of **310**, **311**, **331**, D-glc and D-gal at 1 mM. Water and PVP 10 (1 mM) are shown as representative controls. The result for each compound is based on the integrated average of 36 trials at -12 °C. Time = 0 minutes represents the start of the cooling phase.

D-Glucose and D-galactose failed to delay the initial nucleation event (onset time was similar to water and PVP 10). Additionally, D-glucose and D-galactose also failed inhibit gas hydrate formation and exhibited similar activity to water which was a positive control for gas hydrate formation. Azasugars **310** and **311** were very effective inhibitors of gas hydrate formation and their activity is comparable to **126** and **127**. The azasugars also possessed similar onset times to **126** and **127**. Interestingly, the *N*-methylated version (**331**) of **311** is only marginally more effective at inhibiting gas hydrate formation than PVP 10. However, **331** was able to delay the first nucleation event to the same degree as **311** and **126**. As previously demonstrated, **331** possessed worse IRI activity than **311** and the same trend is observed in

inhibiting gas hydrate formation. Most of the small molecule IRIs examined for gas hydrate formation inhibition also inhibited ice recrystallization to some degree. However, given that not all potent inhibitors of ice recrystallization were able to act as potent inhibitors of gas hydrate formation, IRI activity was correlated to the ability to inhibit gas hydrate formation. **Figure 4-12** shows the IRI activity as percent mean grain size as well as the maximum heat of reaction for formation of gas hydrates for all of the compounds assayed. As stated in section 1.7, potent IRI activity is defined as < 25% mean grain size and an effective inhibitor of gas hydrate formation is defined as compounds which exhibit more potent activity than PVP 10 (commercial inhibitor). These strict definitions generate four unique quadrants.

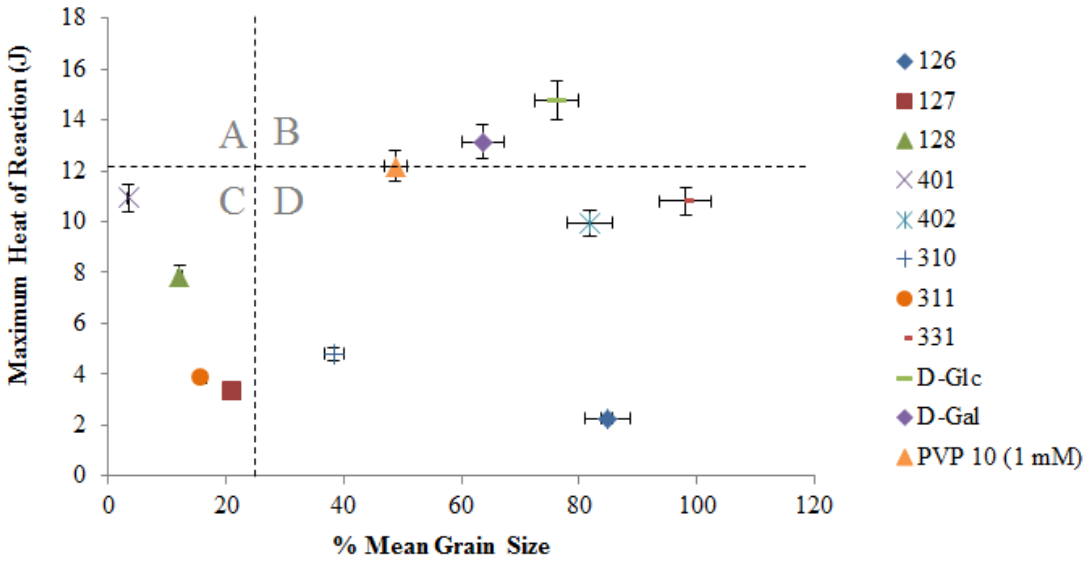

Figure 4-12. Correlating IRI activity (%MGS relative to PBS) with the ability to inhibit gas hydrate formation (maximum heat of reaction).

Quadrant C is the most important as it represents compounds with ideal structural features required for potent IRI activity and very effective inhibition of gas hydrate formation. Four of the ten small molecules tested belong to this quadrant. These include alditol derivatives **128** and **401**, pyranose derivative **127** and azasugar **311**. An overall analysis of **Figure 4-12** clearly demonstrates that a compound with potent IRI activity may not necessarily have the ability to inhibit gas hydrate formation. For example, compounds **126** (*n*-octyl-β-D-glucose) and **127** (*n*-octyl-β-D-galactose) are equally effective at inhibiting gas hydrate formation (< 4 J) but only **127** is a very effective inhibitor of ice recrystallization. Similarly, alditol derivative **402** possessing a three hydrocarbon chain and azasugar derivative **331** (the *N*-methyl version of **311**)

are poor inhibitors of ice recrystallization but are just as effective at inhibiting gas hydrate formation as PVP 10. Finally, the IRI activities of alditol **402** and *n*-octyl-β-D-pyranoside **126** are approximately the same (80% MGS relative to PBS). While both compounds inhibit gas hydrate formation, **126** is as effective as **127** yet the IRI activities of **126** and **127** are very different. Out of the ten compounds tested for IRI activity and inhibition of gas hydrate formation, only four of the ten are effective inhibitors of both processes (quadrant C), eight of the ten are effective inhibitors of gas hydrate formation but only four of these ten are potent inhibitors of ice recrystallization.

4.6 Thermal Hysteresis and Gas Hydrate Nucleation Inhibition

Three mechanisms have been proposed for KHIs and their inhibition of gas hydrates: 1) adsorption onto the surface of the growing crystal structure, 2) binding to a pre-critical nucleus preventing it from reaching critical size and 3) structuring of water molecules to prevent nucleation from occurring. Adsorption onto the gas hydrate surface for PVP 10 is thought to occur through hydrogen bonding between the amide of PVP 10 and the gas hydrate surface.[48] The adsorption hypothesis was tested using an ethylene oxide hydrate (sI hydrate structure). Uninhibited ethylene oxide hydrate crystals are dodecahedral with rhombic {110} faces. In the presence of low concentrations of the inhibitor (< 0.1 wt%), the octahedral shape changes to a 2-dimensional hexagonal morphology. Use of higher concentrations of the inhibitors led to complete inhibition of crystal growth.[48] In this study, ethylene oxide hydrate was used as a model for a sI gas hydrate (such as a methane hydrate) in order to avoid the use of high pressures. While an ethylene oxide hydrate is not a true gas hydrate, this study suggests that adsorption of PVP 10 to a sI gas hydrate surface may lead to a change in crystal morphology. This type of change in crystal morphology as a result of adsorption onto the surface of gas hydrates is similar to the dynamic ice shaping commonly observed with the adsorption onto the surface of ice with AFPs. Previous work has shown that the TH activity of AFPs does not correlate well to the ability to inhibit gas hydrate formation.[34] Given the similarity between ice and gas hydrates, the compounds exhibiting potent ability to inhibit gas hydrate formation (**126**, **127**, **310**, **311**) were tested for their TH activity using a nanoliter osmometer.[49] Single ice crystals grown in the presence of molecules that do not interact with the ice crystal surface are "disk-like". TH measurements and single ice morphologies are shown in **Table 4-1**.

Table 4-1. Ice crystal habit in the presence of **126** and **127** at 1 mg/mL and **310** and **311** at 10 mg/mL.

Compound	Melting Point (°C)	Freezing Point (°C)	Ice Crystal Habit
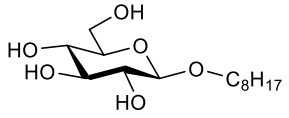 **126**	-0.09	-0.09	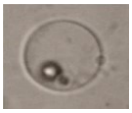
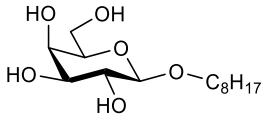 **127**	-0.05	-0.05	
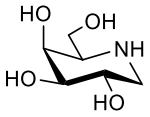 **310**	-0.33	-0.33	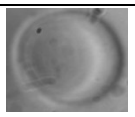
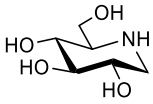 **311**	-0.24	-0.24	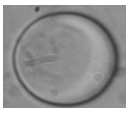

The TH activity and dynamic ice shaping capabilities of **126** and **127** have been previously reported.[44] As seen in **Table 4-1**, none of the compounds interact with the ice surface. Based on this, it is unlikely that these compounds are capable of directly interacting with the surface of gas hydrates. Unfortunately, the current DSC based assay utilized in studying the gas hydrate formation inhibition ability of small molecule IRIs, does not give insight into their exact mode of action. The Ben laboratory has previously demonstrated that the IRI activity of D-galactose and D-glucose results from their ability to disrupt the structure of bulk water through hydration. Therefore, future work investigating the mode of action of these small molecule IRIs towards inhibiting gas hydrate formation should be focused towards the disruption of water molecules surrounding a sI gas hydrate.

4.7 Chapter Summary

The use of small, carbohydrate-based molecules to inhibit gas hydrate formation was demonstrated. This may have potential applications in the petroleum industry since a few of these small molecules are significantly better inhibitors of gas hydrate formation than the commercial inhibitor PVP 10. The low molecular weights, facile synthesis and potency of these compounds make them ideal candidates for commercial use. Certain structural features of these compounds, such as a six membered ring especially one containing a nitrogen heteroatom, appear to be crucial in the inhibition of gas hydrate formation. Unlike molecules with IRI activity, the presence of an alkyl chain was not necessary for the inhibition of gas hydrate formation. In conclusion, while some of the structural features within these molecules may be amenable to both activities; it seems that the ability to inhibit ice recrystallization is not a good indicator of a compound's ability to inhibit gas hydrate formation. Overall, further studies are required to elucidate the mechanism of action of gas hydrate formation inhibition of these small molecules.

4.8 References

1. Sloan, E. D.; Koh, C., *Clathrate Hydrates of Natural Gases*. Third ed.; CRC Press: Boca Raton, FL, 1997.

2. Perrin, A.; Musa, O. M.; Steed, J. W., *Chem. Soc. Rev.* **2013,** 42, 1996-2015.

3. Sloan, E. D., *Ind. Eng. Chem. Res.* **2000,** 39, 3123-3129.

4. Davy, H., *Philos. Trans. R. Soc. London* **1811,** 101, 1-35.

5. Hammerschmidt, E. G., *Ind. Eng. Chem.* **1934,** 26, 851-855.

6. Kelland, M. A., *Energy Fuels* **2006,** 20, 825-847.

7. Barker, J. W.; Gomez, R. K., *J. Petrol. Technol.* **1989,** 41, 297-301.

8. Koh, C. A.; Sloan, E. D., *AIChE Journal* **2007,** 53, 1636-1643.

9. Rojas, Y.; Lou, X., *Asia-Pac. J. Chem. Eng.* **2010,** 5, 310-323.

10. Strobel, T. A.; Hester, K. C.; Koh, C. A.; Sum, A. K.; Sloan Jr, E. D., *Chem. Phys. Lett.* **2009,** 478, 97-109.

11. Stackelberg, M. v., *Naturwissenschaften* **1949,** 36, 327-333.

12. Stackelberg, M. v.; Müller, H. R., *J. Chem. Phys.* **1951,** 19, 1319-1320.

13. Claussen, W. F., *J. Chem. Phys.* **1951,** 19, 662-662.

14. Pauling, L.; Marsh, R. E., *Proc. Natl Acad. Sci. U. S. A.* **1952,** 38, 112-118.

15. Mak, T. C. W.; McMullan, R. K., *J. Chem. Phys.* **1965,** 42, 2732-2737.

16. McMullan, R. K.; Jeffrey, G. A., *J. Chem. Phys.* **1965,** 42, 2725-2732.

17. Ripmeester, J. A.; Tse, J. S.; Ratcliffe, C. I.; Powell, B. M., *Nature* **1987,** 325, 135-136.

18. Koh, C. A., *Chem. Soc. Rev.* **2002,** 31, 157-167.

19. Ohno, H.; Strobel, T. A.; Dec, S. F.; Sloan, J. E. D.; Koh, C. A., *J. Phys. Chem. A* **2009,** 113, 1711-1716.

20. Mehta, A. P.; Sloan, E. D., *SPE Journal, SPE 53450* **1999,** 4, 3-8.

21. Ribeiro Jr, C. P.; Lage, P. L. C., *Chem. Eng. Sci.* **2008,** 63, 2007-2034.

22. Tanaka, R.; Sakemoto, R.; Ohmura, R., *Cryst. Growth Des.* **2009,** 9, 2529-2536.

23. Christiansen, R. L.; Sloan, E. D., *Ann. N. Y. Acad. Sci.* **1994,** 715, 283-305.

24. Long, J. Gas Hydrate Formation Mechanism and Its Kinetic Inhibtion. 1994, Colorado School of Mines.

25. Kvamme, B. Proceedings of the Second International Confrence on Gas Hydrates, Toulouse, France, June 2-6, 1996.

26. Radhakrishnan, R.; Trout, B. L., *J. Chem. Phys.* **2002,** 117, 1786-1796.

27. Mitchell, G. F.; Talley, L. D., Application of Kinetic Hydrate Inhibitor in Black-Oil Flowlines. In *SPE Annual Technical Confrence and Exhibition SPE 56770*, Society of Petroleum Engineers: Houston, Texas, 1999.

28. Sugier, A.; Bourgmayer, P.; Behar, E.; Freund, E. *US4915176*, 1990.

29. Kelland, M. A.; Svartås, T. M.; Andersen, L. D., *J. Pet. Sci. Eng.* **2009,** 64, 1-10.

30. Sloan, E. D. *US5420370*, 1995.

31. O'Reilly, R.; Ieong, N. S.; Chua, P. C.; Kelland, M. A., *Chem. Eng. Sci.* **2011,** 66, 6555-6560.

32. Sloan, E. D., *Energy Fuels* **1998,** 12, 191-196.

33. Zeng, H.; Walker, V. K.; Ripmeester, J. A., *Angew. Chem. Int. Ed.* **2007,** 46, 5402-5404.

34. Ohno, H.; Susilo, R.; Gordienko, R.; Ripmeester, J.; Walker, V. K., *Chem. Eur. J.* **2010,** 16, 10409-10417.

35. Gordienko, R.; Ohno, H.; Singh, V. K.; Jia, Z.; Ripmeester, J. A.; Walker, V. K., *PLoS ONE* **2010,** 5, e8953.

36. Zeng, H.; Wilson, L. D.; Walker, V. K.; Ripmeester, J. A., *J. Am. Chem. Soc.* **2006,** 128, 2844-2850.

37. Lachance, J. W.; Dendy Sloan, E.; Koh, C. A., *Chemical Engineering Science* **2008,** 63, 3942-3947.

38. Lachance, J. W.; Sloan, E. D.; Koh, C. A., *Chemical Engineering Science* **2009,** 64, 180-184.

39. Daraboina, N.; Ripmeester, J.; Walker, V. K.; Englezos, P., *Energy Fuels* **2011,** 25, 4392-4397.

40. Seo, Y.-T.; Moudrakovski, I. L.; Ripmeester, J. A.; Lee, J.-w.; Lee, H., *Environ. Sci. Techol.* **2005,** 39, 2315-2319.

41. Circone, S.; Kirby, S. H.; Stern, L. A., *J. Phys. Chem. B* **2005,** 109, 9468-9475.

42. Semenov, M. E.; Manakov, A. Y.; Shitz, E. Y.; Stoporev, A. S.; Altunina, L. K.; Strelets, L. A.; Misyura, S. Y.; Nakoryakov, V. E., *J Therm Anal Calorim* **2015,** 119, 757-767.

43. Reynhout, M. J.; Kind, C. E.; Klomp, U. C. DE *92202095.3*, 1992.

44. Capicciotti, C. J.; Leclère, M.; Perras, F. A.; Bryce, D. L.; Paulin, H.; Harden, J.; Liu, Y.; Ben, R. N., *Chem. Sci.* **2012,** 3, 1408-1416.

45. Trant, J. F.; Biggs, R. A.; Capicciotti, C. J.; Ben, R. N., *RSC Adv.* **2013,** 3, 26005-26009.

46. Balcerzak, A. K.; Febbraro, M.; Ben, R. N., *RSC Adv.* **2013,** 3, 3232-3236.

47. Tam, R. Y.; Ferreira, S. S.; Czechura, P.; Chaytor, J. L.; Ben, R. N., *J. Am. Chem. Soc.* **2008,** 130, 17494-17501.

48. Larsen, R.; Knight, C. A.; Sloan Jr, E. D., *Fluid Phase Equilib.* **1998,** 150–151, 353-360.

49. Chakrabartty, A.; Hew, C. L., *Eur. J. Biochem.* **1991,** 202, 1057-1063.

Chapter 5. Synthesis of Small Molecules Possessing Potent IRI Activity Using Key Structural Features.

5.1 Structural Features of Small Molecules Exhibiting "Custom-tailored" IRI Activity

An important goal for the Ben laboratory is the development of novel small molecule IRIs. As previously discussed, compounds possessing potent IRI activity is very important in industrial applications such as cryopreservation of precious cells. Recent work has led to the discovery of three classes of small molecule potent inhibitors of ice recrystallization: carbohydrate-based surfactants and hydrogelators, lysine-based surfactants and truncated *C*-linked glycopeptides.[1-4] Their general structures are shown in **Figure 5-1**.

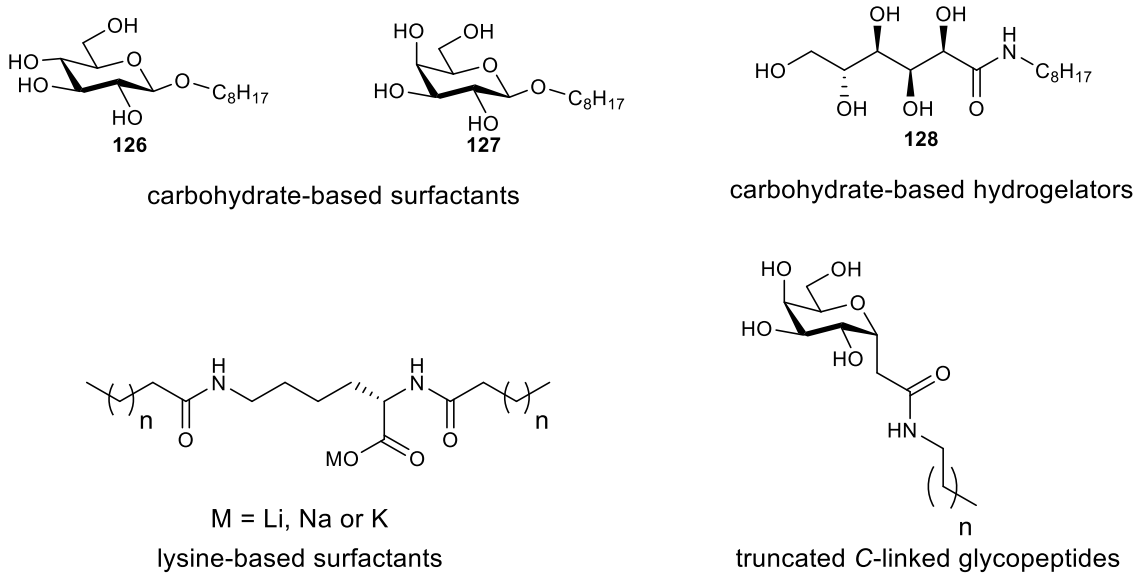

Figure 5-1. Structure of carbohydrate-based surfactants and hydrogelators, lysine-based surfactants/gelators and truncated *C*-linked glycopeptides.

As previously discussed in chapter 1, highly hydrated carbohydrates generally exhibited moderate IRI activity. Hydration was attributed to the ability of these molecules to disrupt the structure of bulk water.[5] Based on this precedent, it was hypothesized that other molecules with the ability to alter the structure of bulk water, such as surfactants, hydrogelators and organogelators may also be effective inhibitors of ice recrystallization.[1, 2] Initially, the carbohydrate-based surfactants, *n*-octyl-β-D-pyranosides **126** and **127** were assayed for IRI their activity.[1] It was found that *n*-octyl-β-D-glucopyranoside **126** exhibited weak IRI activity comparable to D-glucose. However, *n*-octyl-β-D-galactopyranoside **127** was highly IRI active

even at 11 mM (normally the splat-cooling assay utilizes a concentration of 22 mM).[1] Replacement of the pyranose ring found in *n*-octyl-β-D-pyranosides **126** and **127** to an open-alditol chain while maintaining the eight carbon alkyl chain led to *N*-octyl-D-aldonamide **128**. This hydrogelator was found to exhibit unprecedented potent IRI activity at a low concentration of 0.5 mM. To date, this is the most active small molecule IRI. Methylation of the amide nitrogen led to compounds possessing weak IRI activity. Additionally, replacement of the amide linkage with an ether linkage also led to a decrease in IRI activity. This demonstrated that the amide linkage is important to IRI activity.[1] Neither of the carbohydrate-based surfactants or hydrogelators displayed thermal hysteresis activity or dynamic ice shaping capabilities as a result of binding to ice and thus, these compounds were the first example of small molecules exhibiting "custom-tailored" antifreeze activity on par with AFGPs and their analogues.[1] Overall, along with long alkyl chains, this work has highlighted the importance of an open-alditol chain and an amide linkage.

The importance of alkyl chains has been demonstrated by the lysine-based surfactants and truncated *C*-linked glycopeptides.[2, 4] The presence of long alkyl chains (longer than nine carbons) to the ε-amino group of the lysine-based surfactants resulted in potent IRI activity. The presence of seven carbon chains or longer conjugated to the amide bond resulted in potent IRI activity for the truncated *C*-linked glycopeptides.[3] Once again, both of these compounds utilize an amide linkage and thus, it is clearly important to IRI activity. Additionally, these studies have demonstrated the importance of a hydrophobic moiety such a long alkyl chain to IRI activity.

While these compounds exhibit potent IRI activity, the presence of the long alkyl chains gives them a surfactant-like nature. This surfactant-like nature can be detrimental to cells and solubilize cell membranes.[6-12] Furthermore, as a surfactant, many of these compounds have the ability to form micelles in solution. However, it has been demonstrated that the ability to form micelles is independent of IRI activity.[1, 2] For example, carbohydrate-based non-ionic surfactant *n*-octyl-β-D-galactopyranoside was highly IRI active at a concentration well below its critical micelle concentration (CMC) whereas *n*-octyl-β-D-glucopyranoside did not exhibit IRI activity well above its CMC value.[1] Additionally, it has been demonstrated that IRI activity is not correlated to the ability to form micelles for structurally different non-ionic and anionic surfactants and anti-ice nucleating agents.[1, 2] Therefore, removal of the surfactant-like nature of

some of these compounds will not be detrimental to IRI activity and may help the cytotoxicity profile of these types of compounds.

Based on this precedent, other hydrophobic moieties were explored by the Ben laboratory to generate small molecules with potent IRI activity. An aryl ring was chosen as the hydrophobic moiety and phenoxyglycosides were synthesized and assayed for their IRI activity (**Figure 5-2**).[13] These aryl rings will maintain the necessary hydrophobic moiety required for IRI activity whilst removing the long alkyl chains which facilitated the surfactant-like properties of previous small molecule IRIs.

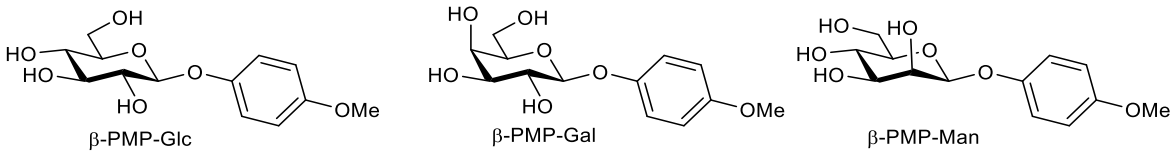

Figure 5-2. Structure of D-glucose, D-galactose and D-mannose based phenoxyglycosides.

β-PMP-Gal and β-PMP-Man both exhibited weak IRI activity. However, β-PMP-Glc exhibited potent IRI activity and was significantly more active than β-PMP-Gal and β-PMP-Man.[13] β-PMP-Glc exhibited IRI activity (at equimolar concentrations) to previously reported carbohydrate-based surfactant, *n*-octyl-β-D-galactopyranoside **127**.[1] As previously discussed, our laboratory has correlated IRI activity to carbohydrate hydration where an increase in carbohydrate hydration leads to an increase in IRI activity. This trend was used to explain the difference in IRI activity of D-glucose and D-galactose based surfactants **126** and **127** respectively.[1] D-Galactose exhibits higher IRI activity than D-glucose due increased hydration.[5] Based on this precedent, it is surprising that β-PMP-Glc is more active that β-PMP-Gal. It was also surprising that β-PMP-Gal and β-PMP-Man both possessed identical IRI activity despite the difference in hydration between the parent reducing sugars.[5, 14] Unfortunately, hydration number or molar compressibilities of these phenoxyglycosides is unavailable and a correlation between IRI activity of these compounds and their hydration characteristics is not presently possible. However, a plausible explanation is that hydration characteristics of the molecules are altered by the aryl ring.[13] These results demonstrated that the presence of a methoxyphenyl group at the anomeric carbon is beneficial to IRI activity and compounds lacking long alkyl chains can also possess potent IRI activity. These IRI active phenoxyglycosides have been successfully utilized

to reduce glycerol concentrations during the cryopreservation of red blood cells.[13] This further demonstrates the utility of small molecule IRIs lacking long alkyl chains in cryopreservation.

Another class of small molecule IRIs lacking long alkyl chains has been discussed within this thesis. This includes the carbohydrates possessing an amine such as the amino D-galactose derivatives and pyranose azasugars.

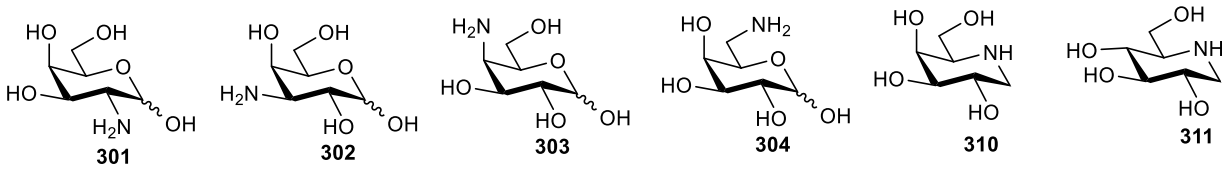

Figure 5-3. Structure of amino-deoxy-D-galactose regioisomers and D-glucose and D-galactose based azasugars.

The amine present in these molecules was thought to be protonated at pH of 7.4 in the PBS solution utilized in the splat-cooling assay and thus, would be able to function as hydrogen donors rather than acceptors. The importance of hydrogen bond donation to interacting with bulk water and affecting hydration and IRI was suggested with previously weak IRI activity of α-*C*-allyl-D-galactose derivatives (chapter 3).[15] Additionally, the presence of a compound possessing an amine may impact the pH of a PBS solution. However, given that the pKa of the protonated amine (approximately 6.5-8.0 as measured in water[16]) present on **301**-**304** is similar to a pH of 7.4, the addition **301**-**304** will minimally impact the pH of the PBS solution. A link or lack thereof between changes in the pH of the PBS solution and IRI activity has not been established.

IRI activity of **301**-**304** and azasugars **310** and **311** revealed that the presence of an amine at C3 on D-galactose and the presence of an endocyclic ring nitrogen (**310** and **311**) were important to IRI activity. Compounds **302**, **310** and **311** exhibited moderate to potent IRI activity and thus demonstrate that small molecule IRIs can be developed without the need for long alkyl chains and a surfactant-like nature.

5.2 Combination of Essential Structural Features to Synthesize Novel Small Molecule IRIs

An overall analysis of these studies reveals that the following structural features (aside from long alkyl chains) are important to IRI activity: an amide linkage, the presence of an open-alditol chain, pyranose rings possessing a *p*-methoxylphenyl moiety at the anomeric carbon and

pyranose rings possessing an amine either at the C3 position or at the endocyclic position. In an effort to develop other novel small molecule IRIs, these structural features were combined to generate potentially highly IRI active compounds (**Figure 5-4**).

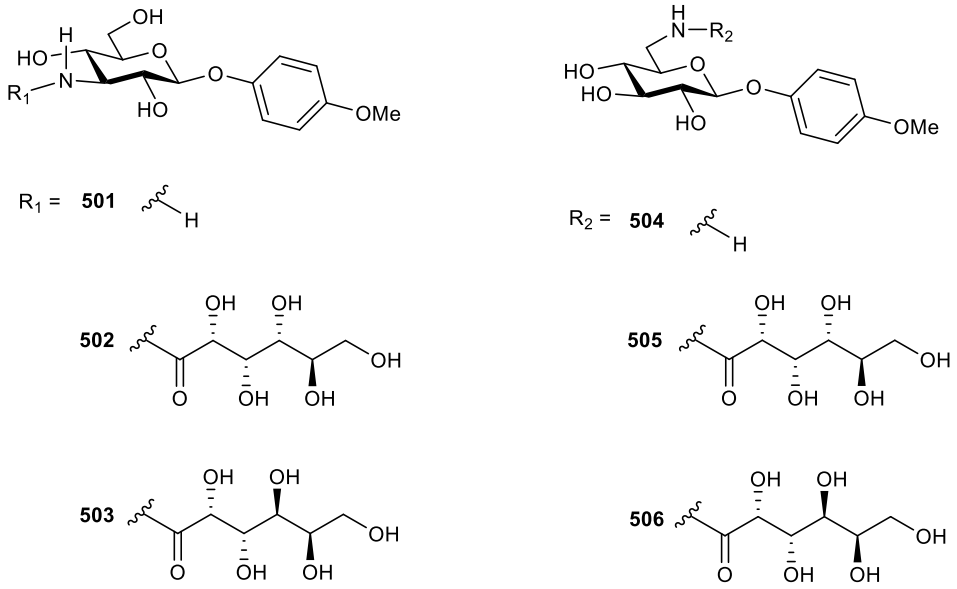

Figure 5-4. Structure of phenoxyglycosides linked via an amide at C3 and C6 to open-alditol chain of D-glucose and D-galactose.

The small molecules presented in **Figure 5-4** contain the *p*-methoxylphenyl moiety at the anomeric carbon found in β-PMP-Glc. The C3-OH was replaced for an amine in compounds **501-503** due the moderate IRI activity exhibited by 3-amino-3-deoxy-D-galactose (**302**). The IRI activity of **302** was identical to D-galactose based azasugar **310**. The C6-OH was substituted for an amine in compounds **504-506** due to synthetic accessibility. Amine **501** and **504** were coupled to open-alditol chain of D-glucose (**502** and **505**) due to the potent IRI exhibited by the *N*-octyl-D-gluconamide hydrogelators **128.** Compounds **503** and **506** possess the open-alditol chain of D-galactose. Previous work has demonstrated that the D-galactose based hydrogelator, *N*-octyl-D-galactonamide, exhibited weak IRI activity whereas *N*-octyl-D-gluconamide possessed potent IRI activity at equimolar concentrations. However, the structural targets presented in **Figure 5-4** are drastically different than the carbohydrate-based hydrogelators previously examined for IRI activity. Additionally, D-galactose and its derivative *n*-octyl-β-D-galactopyranoside possess higher IRI activity than D-glucose and its derivative *n*-octyl-D-glucopyranoside. Thus, the open-alditol chain of D-galactose requires further investigation. These open-alditol chains have been

linked via an amide because an amide linkage has been previously demonstrated to be important to IRI activity. The synthesis of these small molecules was envisioned according to the retrosynthetic analysis presented in **Scheme 5-1** and **Scheme 5-2**.

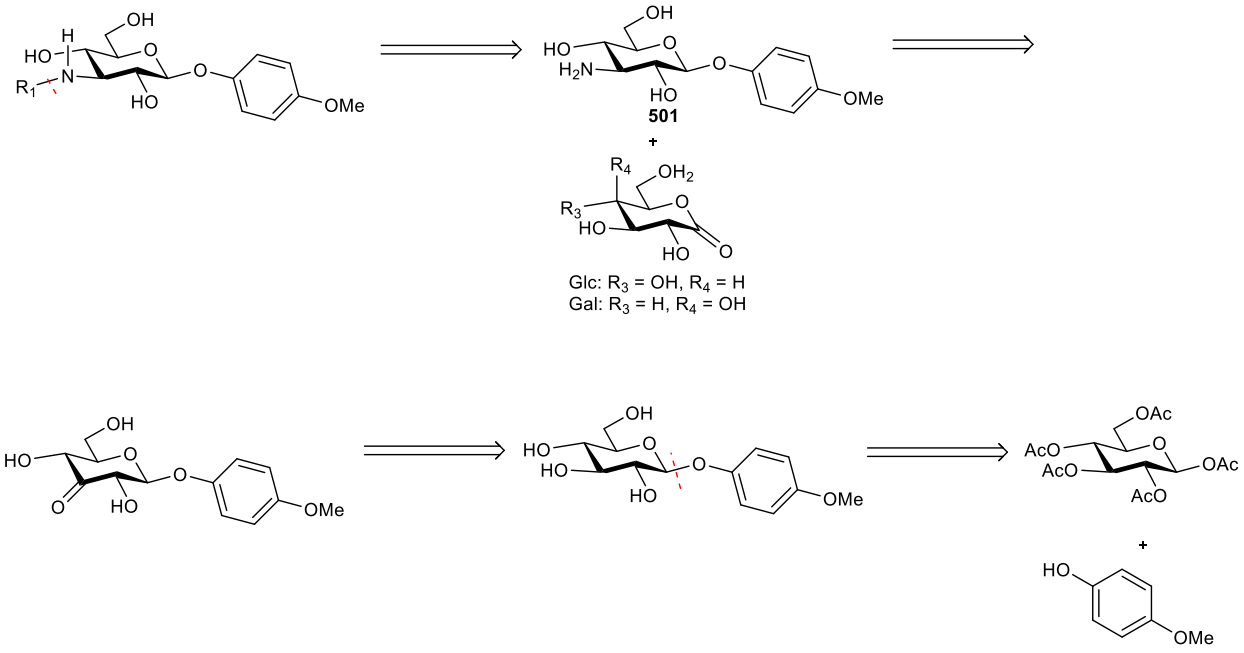

Scheme 5-1. Retrosynthetic analysis of the synthesis of compounds **501-503**.

Disaccharides **502** and **503** were thought to arise from nucleophilic attack of amine **501** onto the appropriate lactone. Amine **501** was thought to be furnished from a reductive amination of a ketone at C3. Following a report on selective oxidation of unprotected glycosides using a palladium catalyst,[17] this ketone was envisioned to arise from a selective oxidation of β-PMP-Glc. β-PMP-Glc was thought to be furnished from a glycosidation of β-D-glucose pentacetate.

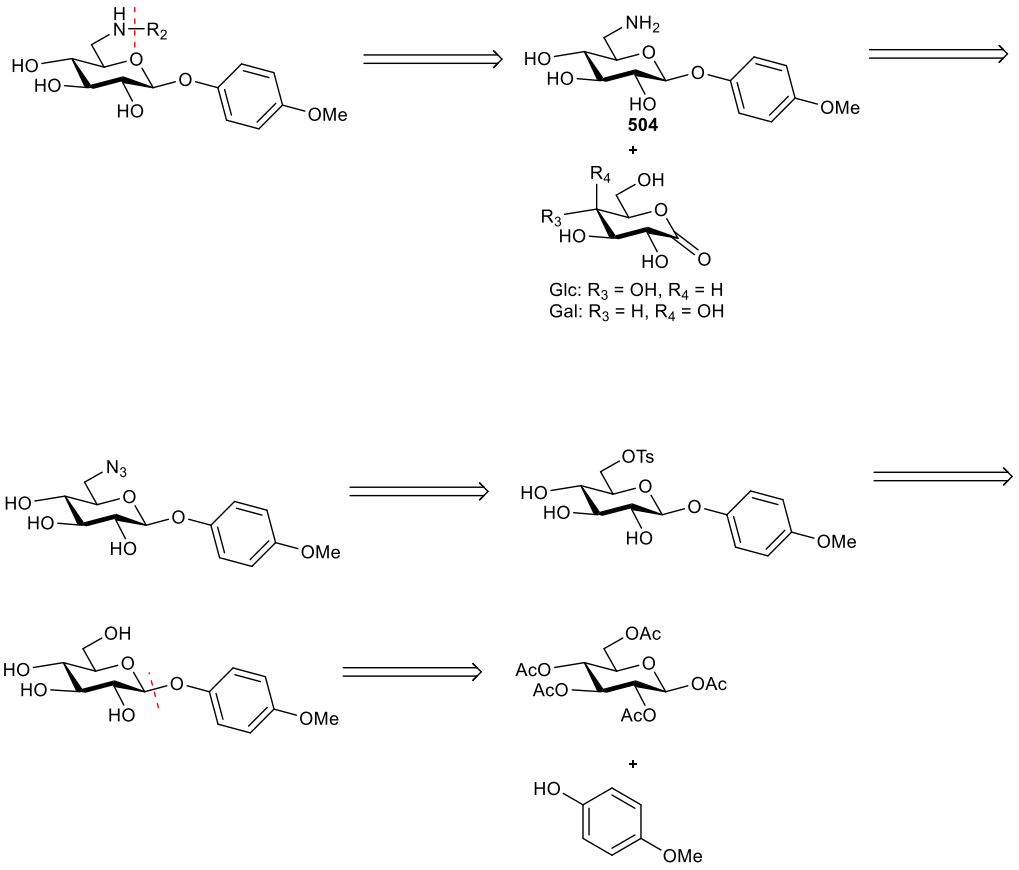

Scheme 5-2. Retrosynthetic analysis of the synthesis of compounds **504-506**.

Similar to **502** and **503**, disaccharides **505** and **506** were thought to arise from nucleophilic attack of amine **504** onto the appropriate lactone. Amine **504** could be generated from an azide at C6 using a Staudinger reduction. The azide can be generated from an S_N2 displacement of a tosylate at C6 of β-PMP-Glc. Once again, β-PMP-Glc can be furnished from a glycosidation of β-D-glucose pentaacetate.

The synthesis began by generating β-PMP-Glc through the glycosidation of β-D-glucose pentacetate using boron trifluoride diethyl etherate as a Lewis acid and *p*-methoxyphenol as the nucleophile to afford the glycosidated product. Deprotection of the acetate groups was carried out in basic methanol to form β-PMP-Glc (**507**) in 74% yield over two steps (**Scheme 5-3**).

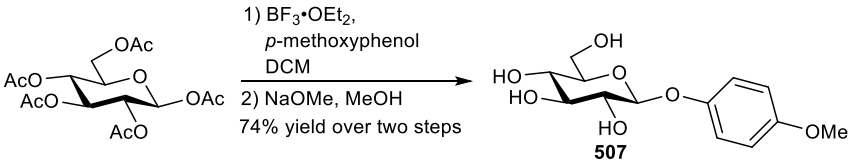

Scheme 5-3. Synthesis of β-PMP-Glc utilizing a boron trifluoride diethyl etherate promoted glycosidation.

With β-PMP-Glc in hand, initial efforts were towards the synthesis of amine **504** and disaccharides **505** and **506** because of what should be an efficient synthesis (**Scheme 5-2**).

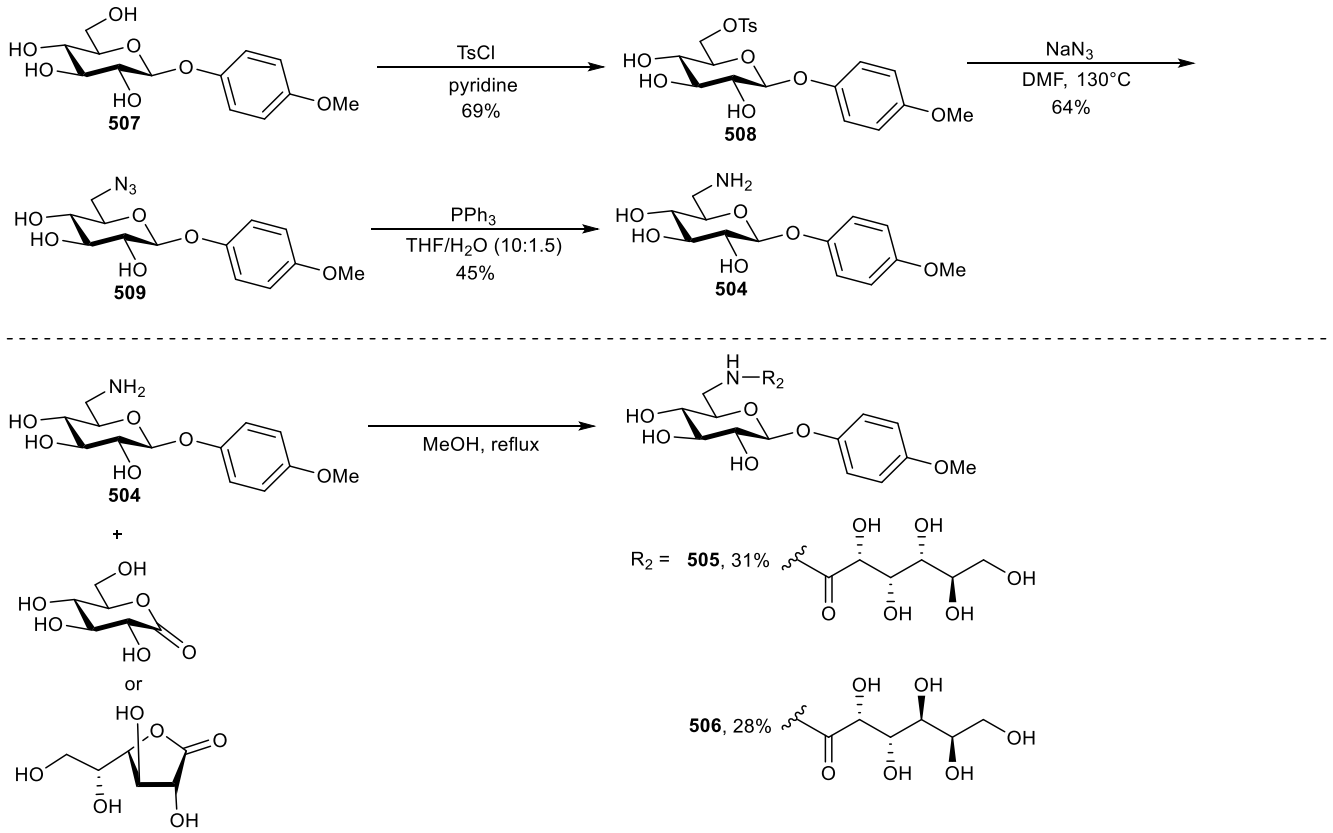

Scheme 5-4. Synthesis of amine **504** and subsequent coupling to afford disaccharides **505** and **506**.

As shown in **Scheme 5-4**, conversion of β-PMP-Glc to tosylate **508** was accomplished using *p*-toulenesulfonyl chloride and pyridine in 69% yield. Subsequent conversion of the tosylate to the azide is achieved using sodium azide in DMF in 64% yield. Staudinger reduction of the azide furnishes amine **504** in 45% yield. Coupling of amine **504** with the appropriate lactone in

refluxing methanol gave disaccharides **505** and **506** in 31% and 28% yields respectively. With compounds **504-506** in hand, attention was turned towards the synthesis of the amine **501** and disaccharides **502** and **503**.

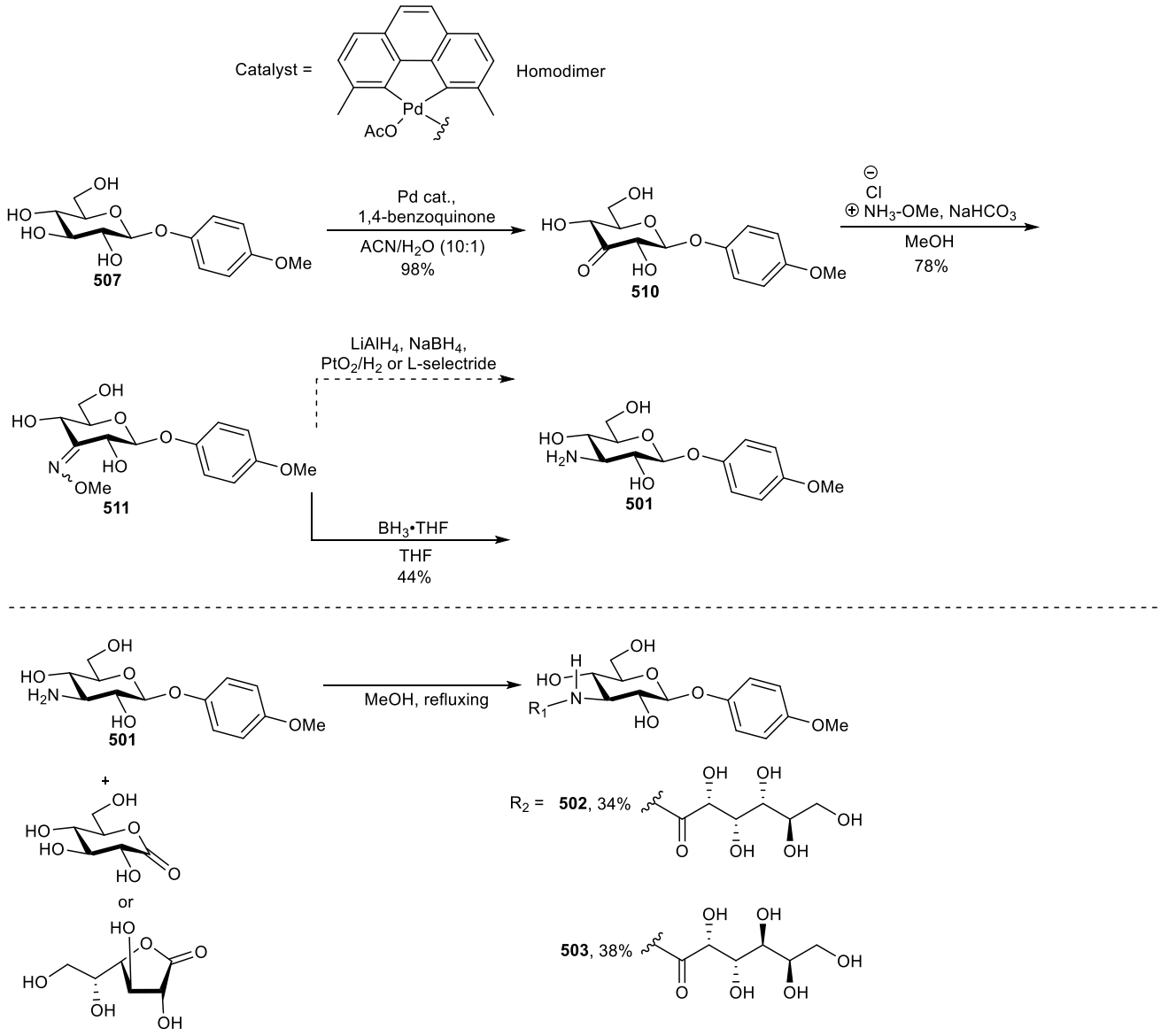

Scheme 5-5. Synthesis of amine **501** and subsequent coupling to afford disaccharides **502** and **503**.

To begin the synthesis of **501**, C3-OH of β-PMP-Glc was oxidized using the catalytic selective oxidation developed by de Vries and Minnaard in 98% yield.[17] The oxidation of the C3-OH was the only product observed using [(2,9-dimethyl-1,10-phenanthroline)-Pd(μ-OAc)]$_2$(OTf)$_2$ (**Scheme 5-5**) as the catalyst. This catalyst was synthesized according to

Waymouth.[18] This selectivity is remarkable considering the lack of protecting groups on C2-C6. An explanation for the regioselectivity is currently unavailable but a plausible explanation is a kinetically controlled coordination of the catalyst to the C3-OH group, followed by deprotonation and subsequent hydride abstraction. Simultaneous coordination to the C4-OH group could also possibly assist with the regioselectivity.[17] The ketone was then converted to the oxime using methoxyamine hydrochloride and sodium bicarbonate in 78% yield. Reduction of the oxime using the following conditions: lithium aluminium hydride, sodium borohydride, platinum (IV) oxide and hydrogen gas or L-selectride were all unsuccessful. Fortunately, using the borane-THF complex as the reducing agent successfully gave amine **501** in 44% yield. Coupling of amine **501** with the appropriate lactone in refluxing methanol gave disaccharides **502** and **503** in 34% and 38% yields respectively. With successful synthesis of **501-506** in hand, attention was turned toward their IRI activities, which are presented in **Figure 5-5**.

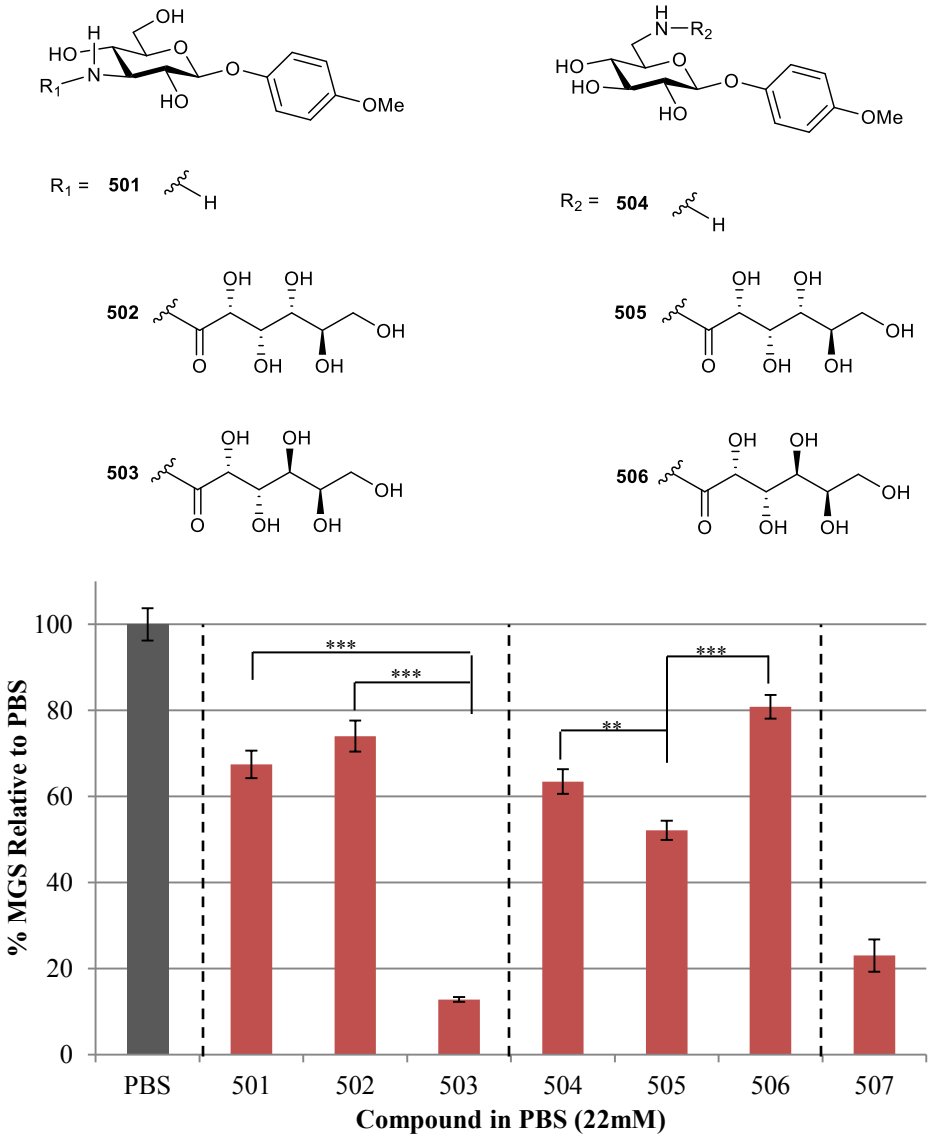

Figure 5-5. IRI activities of amines **501** and **504**, disaccharides **502**, **503**, **505** and **506** and β-PMP-Glc (**507**). Asterisks indicate a statistical significant difference between samples and is defined by unpaired Student's *t*-test (*, $p < 0.05$, **, $p < 0.01$, ***, $p < 0.001$). Statistical significant difference between the PBS control and samples is not shown. Samples have been run in triplicate (n = 3) and error bars indicate standard error of the mean (SEM).

Amines **501** and **504** exhibited moderate IRI activity; however, they were significantly less potent than β-PMP-Glc (**507**). This is surprising as an amine at C3 on D-galactose possessed increased IRI activity as compared to the other amino-deoxy-D-galactose derivatives **301**, **303** and **304** (amines at C2, C4 and C6 respectively). Thus, it was hypothesized that the presence of an amine at C3 on β-PMP-Glc may increase the IRI activity of β-PMP-Glc. Disaccharides **502**, **505** and **506** all possessed moderate to weak IRI activity while **503** exhibited potent activity.

Additionally, **503** exhibits increased IRI activity over β-PMP-Glc (**507**). Disaccharides **502** and **505** both possess similar IRI activity to amines **501** and **504**. This suggests that the presence of the open-alditol chain of D-glucose is not beneficial to IRI activity for these series of compounds regardless of substitution. This is highly surprising given that the hydrogelators *N*-octyl-D-gluconamide was one the potent inhibitors of ice recrystallization known to date. The drastic difference in IRI activity between **503** and **506** and the improvement in activity over β-PMP-Glc clearly suggests that the presence on an open-alditol chain of D-galactose at C3 on the structure of β-PMP-Glc is highly beneficial to IRI activity.

Overall, these specific hydrophilic modifications to the structure of β-PMP-Glc generally led to a decrease in IRI activity. Unfortunately, hydration number or molar compressibility of β-PMP-Glc or compounds **501**-**506** is unavailable and thus, a correlation between the IRI activities of these compounds and their hydration characteristics is not presently possible. The mode of action β-PMP-Glc and **503** utilize towards inhibiting ice recrystallization requires future investigation. Along with changes to hydration, the addition of carbohydrates possessing an amine to the PBS solution may affect the pH of the solution. In chapter 3, it was reasoned that the pKa of the prtonotaed amine present in amino-deoxy-D-galactose derivatives and azasugars was similar to a pH of 7.4 and thus should minimally affect the pH of the solution. However, amines **501** and **504** have a dramatically different structure (due to the aryl group at C1) than those discussed in chapter 3 and therefore, may possess a different pKa. Unfortunately, the pKa of the protonated amine present in **501** and **504** is unknown and thus, their impact on pH of the PBS solution and consequently, IRI activity, cannot be presently discussed.

5.3 Synthesis and IRI Activity of *N*-cycloalkyl-D-aldonamides

To date, carbohydrate-based hydrogelators such as *N*-octyl-D-gluconamide (**128**), has demonstrated to be one of the most potent small molecule IRIs. From this study, the presence of a long alkyl chain, an amide linkage and an open-alditol chain were all demonstrated to be important to IRI activity.[1] Within this study, *N*-octyl-D-galactonamide was also investigated for IRI activity and it was found that it exhibited only moderate IRI activity. Interestingly, *N*-octyl-D-gluconamide and *N*-octyl-D-galactonamide only differ by a single stereocenter. This suggested that the carbohydrate head group is influential on IRI activity. Considering this drastic difference in activity, Capicciotti synthesized analogues of *N*-octyl-D-gluconamide utilizing different head

groups including L-mannose and D-gulose as the head groups.[19] Additionally, given the importance of long alkyl chains, analogues of *N*-octyl-D-gluconamide were synthesized in which the length of the alky chain was shortened to either a hexyl or propyl alkyl chains. The IRI activity of *N*-hexyl- and *N*-propyl-D-gluconamide at 22 mM has been presented within chapter 4 and has been compared to *N*-octyl-D-gluconamide at 0.5 mM. During the study, Capicciotti observed that the length of the alkyl chain affected the IRI activity. The propyl derivative exhibited weak IRI activity at 22 mM whereas the IRI activity of the hexyl derivative significantly increased at 22 mM. However, at 11 mM the hexyl derivative exhibited a drastic loss in activity. Increasing the alkyl length from six to eight led to the highly IRI active *N*-octyl-D-gluconamide.[19] These results clearly suggest that there is a balance between hydrophilicity (carbohydrate moiety) and hydrophobicity (alkyl chain). A similar effect was observed when the carbohydrate head group of *N*-octyl-D-gluconamide was replaced with either the open-alditol chain of D-galactose, L-mannose or D-gulose. These head group modify the stereochemistry of the carbohydrate moiety of *N*-octyl-D-gluconamide. Replacement of the carbohydrate head group generally led to a significant loss in IRI activity (all were tested at 0.5 mM).[19] Again, these results suggested that a balance is required between hydrophilicity and hydrophobicity. Similar observations have also been made with lysine-based surfactants and truncated *C*-linked AFGP analogues. IRI activity was dependent on factors such as length of alkyl chains and position and mode of attachment of alkyl chains.[2-4]

While many of the small molecules discussed till now possess potent IRI activity, they also possess structures resembling surfactants. As previously discussed, this surfactant nature can be detrimental to cells and solubilize cell membranes.[6-12] Given the cytotoxic nature of surfactant-like molecules, the goal was to design small molecules possessing potent IRI activity, high solubility in an aqueous solution and a non-surfactant type structure. With these properties in mind, *N*-cycloalkyl-D-aldonamide type small molecules (**Figure 5-6**) were explored for IRI activity.

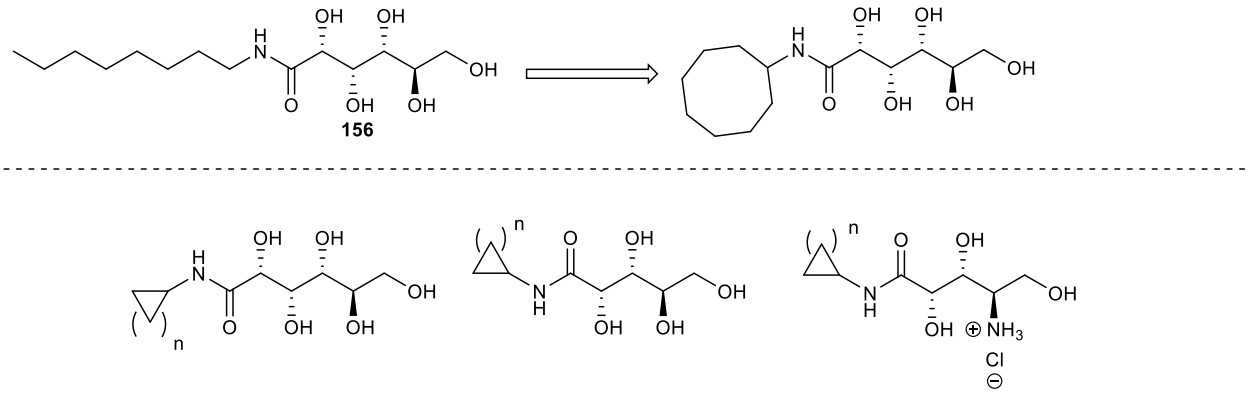

Figure 5-6. Structure of *N*-cycloalkyl-D-aldonamides with varying hydrophilic and hydrophobic moieties.

Aldonamides in **Figure 5-6** were chosen as the importance of an open-alditol chain to IRI activity has already been established.[1] Cycloalkyl rings were utilized as they were would maintain the required hydrophobicity whilst removing the surfactant-like nature associated with the hydrogelators. The ring size and the number of hydroxyl groups were varied for each aldonamide to in order to determine the ideal balance of hydrophilicity and hydrophobicity required for potent IRI activity. The synthesis of the *N*-cycloalkyl-D-aldonamides is outlined in **Scheme 5-6**.

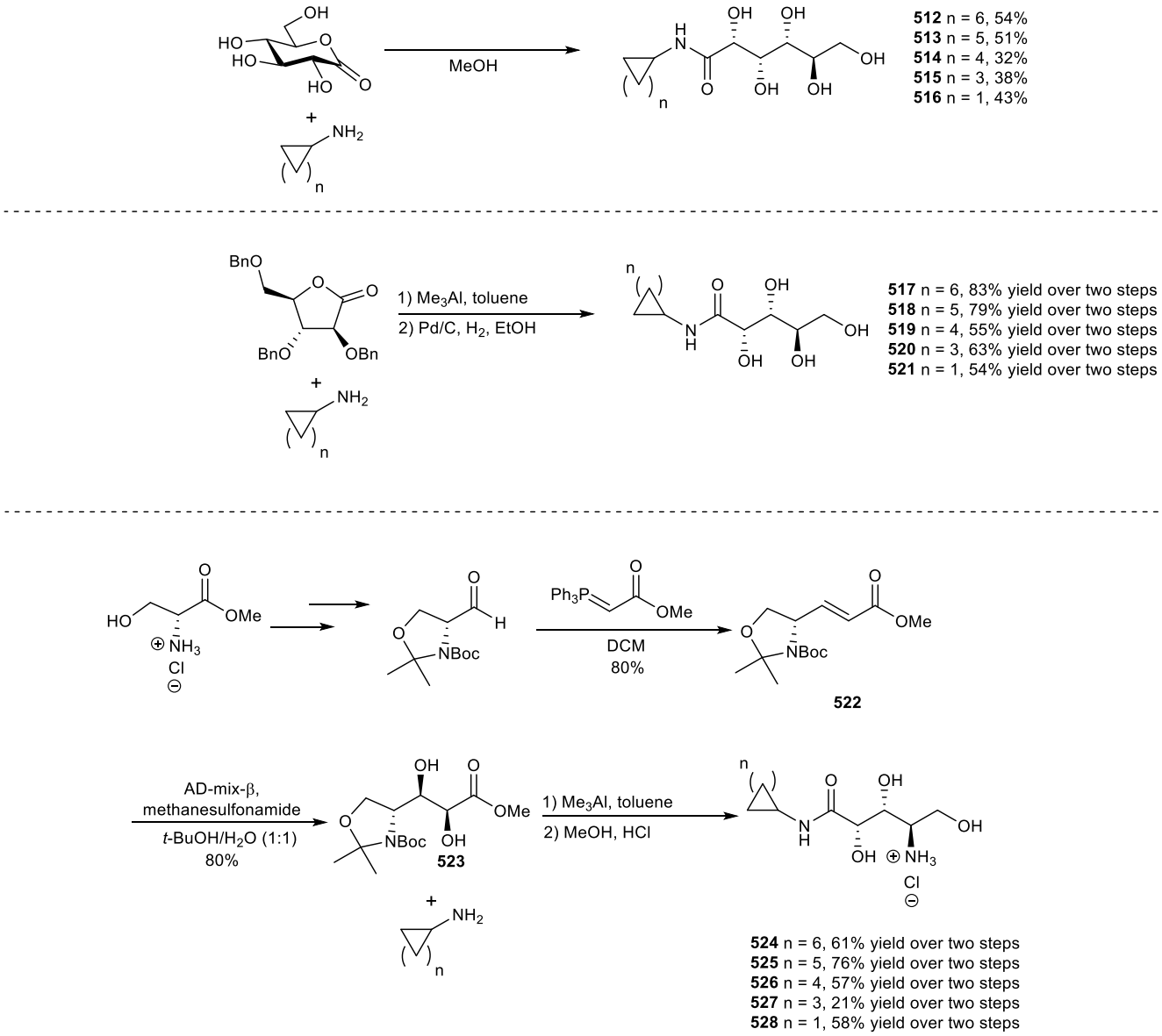

Scheme 5-6. Synthesis of *N*-cycloalkyl-D-aldonamides.

The synthesis of **512-516** occurs through the opening of δ-gluconolactone with the appropriate cycloalkylamine in 32-54% yield. **517-521** were generated in a two-step manner. 2,3,5-tri-*O*-benzyl-D-arabino-1,4-lactone was activated using trimethylaluminium and nucleophilic attack with the appropriate cycoalkylamine formed the benzylated amide. The benzyl groups were then removed under standard conditions generating the product in 54-83% yield over two steps. Formation of **524-528** required the production of ester **522**. The synthesis of **522** began with a stabilized wittig of the Garner aldehyde to form α,β-unsaturated ester **522** in

80% yield. Sharpless dihydroxylation of **522** generated diol **523** in 80% yield. The Sharpless dihydroxylation was performed in the presence of methanesulfonamide as it is known to facilitate the hydrolysis of the key osmate ester (formed during the reaction).[20] The ester moiety in **523** was activated using trimethylaluminium and nucleophilic attack with the appropriate cycloalkylamine furnished the protected amide. The isopropylidene and Boc groups were deprotected using acidic methanol to form **524-528** in 21-76% yield over two steps. With successful synthesis of the *N*-cycloalkyl-D-aldonamides in hand, attention was turned towards their IRI activity. *N*-Cycloalkyl-D-gluconamides **512-516** were first assayed for IRI activity (**Figure 5-7**).

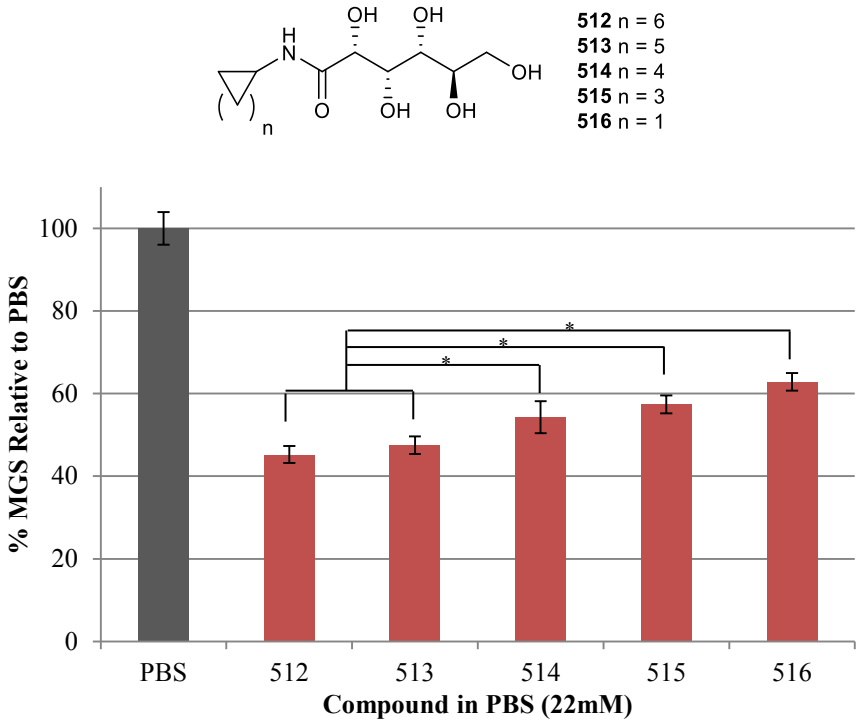

Figure 5-7. IRI activity of *N*-cycloalkyl-D-gluconamides **512-516**. Asterisks indicate significant different defined by unpaired Student's *t*-test (*, $p < 0.05$). Asterisks indicate a statistical significant difference between samples and is defined by unpaired Student's *t*-test ($p < 0.05$). Statistical significant difference between the PBS control and samples is not shown. Samples have been run in triplicate (n = 3) and error bars indicate standard error of the mean (SEM).

All *N*-cycloalkyl-D-gluconamides exhibited moderate activity. With a cyclooctyl ring and cycloheptyl ring, **512** and **513** exhibited the highest IRI activity of all *N*-cycloalkyl-D-gluconamides. **512** and **513** exhibited only a marginal improvement in activity over **516**, which possesses a cyclopropyl ring. This is very surprising as it has been previously been demonstrated

that *N*-octyl-D-gluconamide is a potent inhibitor of ice recrystallization while *N*-propyl-D-gluconamide is a significantly weak inhibitor. This suggested that the presence of a large hydrophobic moiety is beneficial to IRI activity. With changes in ring size only marginally impacting IRI activity, attention was turned toward the influence of the hydrophilic group on IRI activity. Thus, a single hydroxyl group was removed from compounds **512-516** to generate D-arabinose derivatives **517-521**. The IRI activities of D-arabinose and its derivatives **517-521** are presented in **Figure 5-8**.

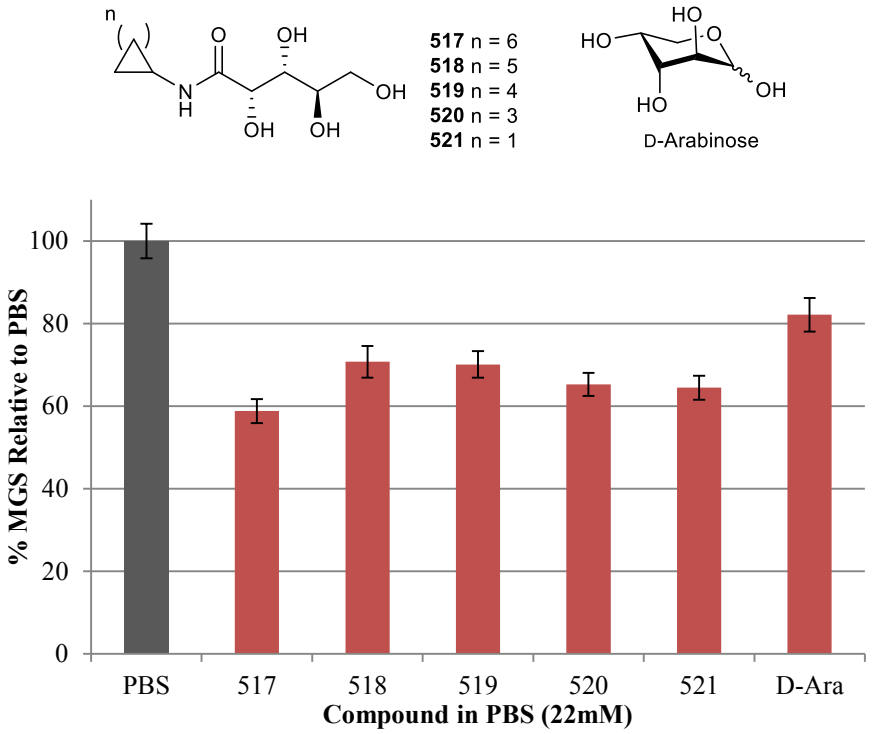

Figure 5-8. IRI activities of *N*-cycloalkyl-D-arabonamides **517-521** and D-arabinose. No statistical difference between the samples could be defined by unpaired Student's *t*-test ($p < 0.05$). Statistical significant difference between the PBS control and samples is not shown. Samples have been run in triplicate (n = 3) and error bars indicate standard error of the mean (SEM).

All of the *N*-cycloalkyl-D-arabonamides exhibited moderate yet decreased activity as compared to *N*-cycloalkyl-D-gluconamide. No statically relevant difference between the IRI activity of these derivatives could be determined. The loss of a hydroxyl may have impacted the hydration of these *N*-cycloalkyl-D-arabonamides by impacting their hydrogen bond ability. Unfortunately, hydration characteristics of these small molecules are not known. In order to further study the importance of the carbohydrate head group, a single hydroxyl group in *N*-

cycloalkyl-D-arabonamides was replaced with an amine to generate compounds **524-528**. As previously demonstrated with amino D-galactose derivatives and azasugars, the presence of an amine is beneficial to IRI activity possibly due to the improved ability to participate in hydrogen bond donation with bulk water. Compounds **524-528** were assayed for IRI activity and the results are presented in **Figure 5-9**.

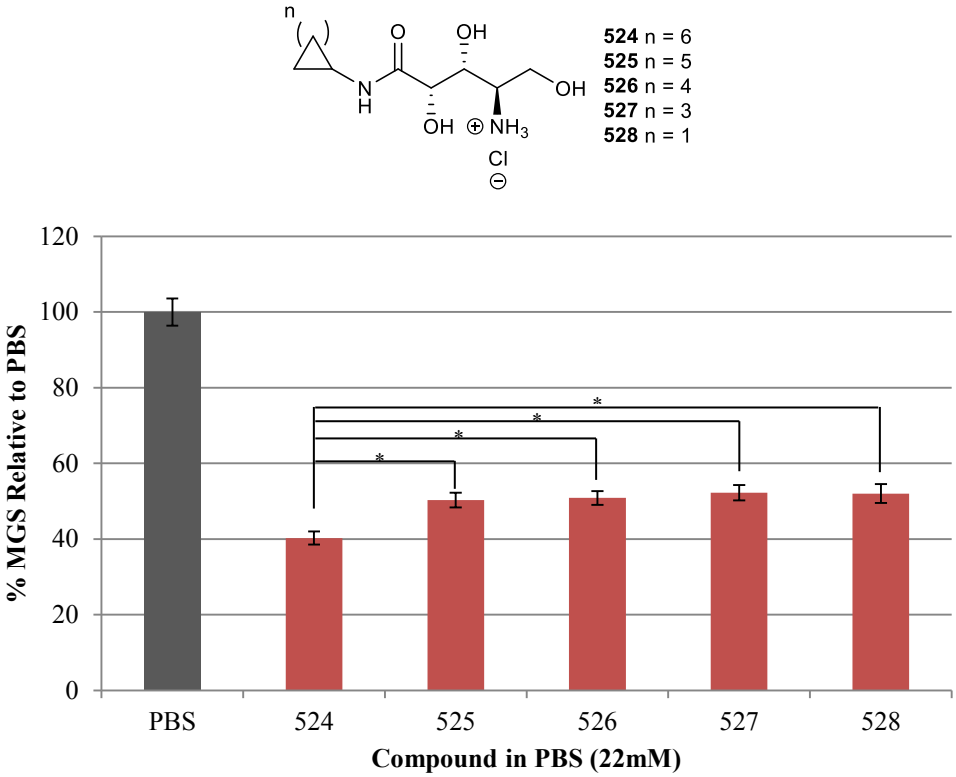

Figure 5-9. IRI activities of **512-516**. Asterisk indicates a statistical significant difference between samples and is defined by unpaired Student's *t*-test (*, $p < 0.05$). Statistical significant difference between the PBS control and samples is not shown. Samples have been run in triplicate (n = 3) and error bars indicate standard error of the mean (SEM).

Compounds **524-528** exhibited moderate IRI activity. Similar to the previously assayed *N*-cycloalkyl-D-aldonamides, the substitution of different cycloalkyl groups does not cause a drastic change in IRI activities of **524-528**. Interestingly, **524**, possessing the cyclooctyl ring exhibited the highest IRI activity out of **524-528**. Additionally, **524-528** exhibited improved activities as compared to the *N*-cycloalkyl-D-arabonamides. The presence of an amine may have helped the hydrogen bond donation ability of the hydrophilic group thus possibly disturbing bulk water and ultimately affecting hydration and IRI. However, hydration characteristics for these

compounds need future investigation in order to correlate to IRI activity. The addition of a protonated amine may also impact the pH of the PBS solution and consequently impact IRI activity. However, the pKa of **524**-**528** is currently unavailable. Additionally, the impact of pH on IRI activity is also unknown. Thus, the change in pH as a result of the addition of **524**-**528** and subsequent impact on IRI activity cannot be presently discussed. In order to further explore the benefits of an amine substitution to *N*-cycloalkyl-D-aldonamides, a hydroxyl group on *N*-cyclooctyl-D-gluconamide was replaced with an amine to generate *N*-cyclooctyl-5-amino-5-deoxy-D-gluconamides **533** and **534**. The amino substitution in **533** and **534** is a similar to the amine substitution found in the IRI active azasugars. Additionally, a cyclooctyl ring was chosen as this hydrophobic moiety generated the most IRI active compounds within the *N*-cycloalkyl-D-aldonamides assayed for IRI activity. Therefore, these structural features in **533** and **534** may lead to potent inhibitors of ice recrystallization. The synthesis is shown in **Scheme 5-7**.

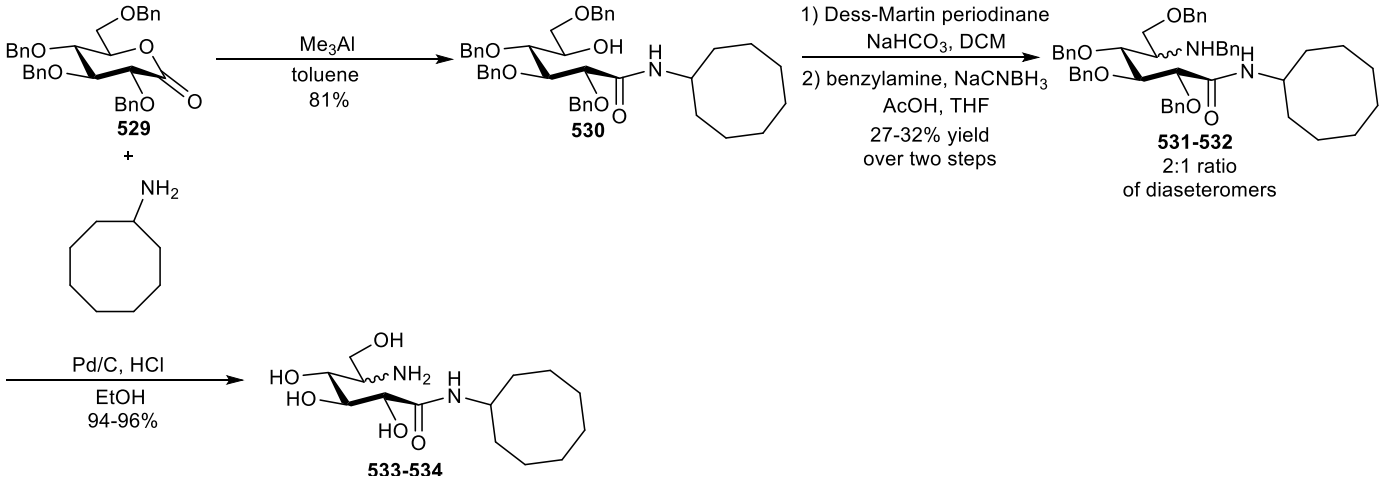

Scheme 5-7. Synthesis of *N*-cyclooctyl-5-amino-5-deoxy-D-gluconamide **533** and **534** utilizing a reductive amination key step.

Nucleophilic attack by cyclooctylamine onto activated lactone **529** affords amide **530** in 81% yield. The free alcohol in **530** is oxidized using a Dess-Martin oxidation followed by a reductive amination using benzylamine and sodium cyanoborohydride to generate a separable mixture of diastereomers **531** and **532** in 27-32% yield over two steps. Unfortunately, the stereochemical assignment of the reductive amination was not possible through NMR studies. Both diastereomers were deprotected using standard debenzylation conditions to form **533** and

534 in 94-96% yield. Both diastereomers were assayed for IRI activity which is presented in **Figure 5-10**.

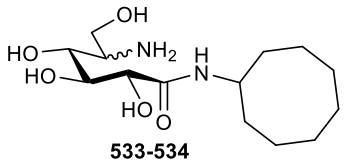

533-534

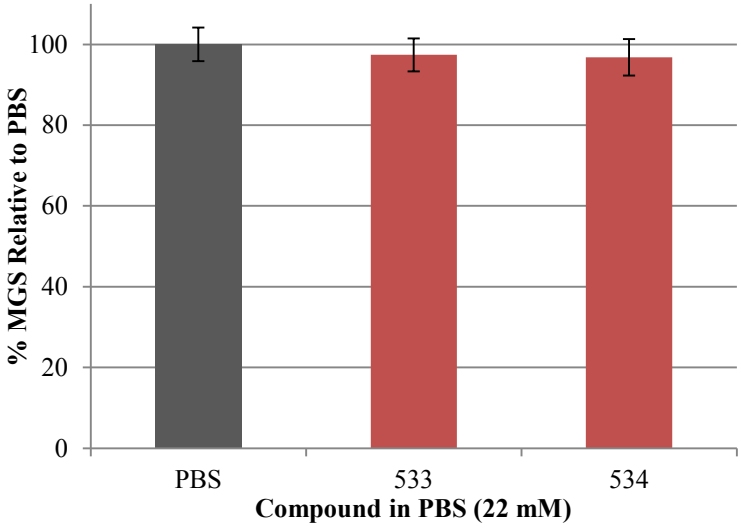

Figure 5-10. IRI activity of *N*-cyclooctyl-5-amino-5-deoxy-D-gluconamides **533** and **534**. No statistical significant difference between samples could be defined by unpaired Student's *t*-test ($p < 0.05$). Statistical significant difference between the PBS control and samples is not shown. Samples have been run in triplicate (n = 3) and error bars indicate standard error of the mean (SEM).

The IRI activity of both diastereomers is similar to that of PBS. This is very surprising as the amine substitution is at the C5 position is a similar substitution found in the IRI active azasugars previously discussed. Both diasetereomers are significantly less active than *N*-cyclooctyl-D-gluconamide **512**. An amino substitution was beneficial to the IRI activity of *N*-cycloalkyl-D-arabonamides **517-521** but was detrimental to the IRI activity of *N*-cyclooctyl-D-gluconamide **512**. While the influence of hydration or changes to pH of PBS (as a result of the addition of **533-534**) on IRI activity is unclear for these *N*-cycloalkyl-D-aldonamides, these results clearly demonstrate that small structural changes can have a large influence on IRI activity. Further work is required to determine the influence these substitutions have on the three-dimensional hydrogen bonded network of bulk water.

5.3.1 Summary of the IRI Activity of *N*-cycloalkyl-D-aldonamides

While our laboratory has reported that compounds containing hydrophobic moieties conjugated to an aldonamide possess potent IRI activity, the utilization of cycloalkyl groups as the hydrophobic portion failed to produce small molecules with potent IRI activity. Changes to the hydrophilic portion of the aldonamides such as removal of a hydroxyl group or substitution of a hydroxyl group with an amine, had a larger impact on IRI activity. Removal of a hydroxyl group generally led to a loss in IRI activity. An amine substitution resulted in a marginal improvement in IRI activity with the *N*-cycloalkyl-D-arabonamides but was detrimental to the activity of *N*-cyclooctyl-D-gluconamide. Overall, the utilization of cycloalkyl groups as the hydrophobic moiety conjugated to aldonamides failed to generate small molecules with potent IRI activity.

5.4 Synthesis and IRI Activity of *N*-aryl-D-aldonamides

With compounds **503** and β-PMP-Glc exhibiting potent IRI activity, the utilization of an aryl moiety as the hydrophobic component required further exploration. Our laboratory has previously demonstrated *N*-aryl-D-aldonamides as potent inhibitors of ice recrystallization.[21] Based on this precedent, *N*-aryl-D-aldonamides **535-537** were synthesized and assayed for IRI activity (**Figure 5-11**). Initially, a phenyl ring was chosen as the aryl ring because it is the simplest aryl ring and allows for direct comparison to the cyclohexyl ring previously utilized.

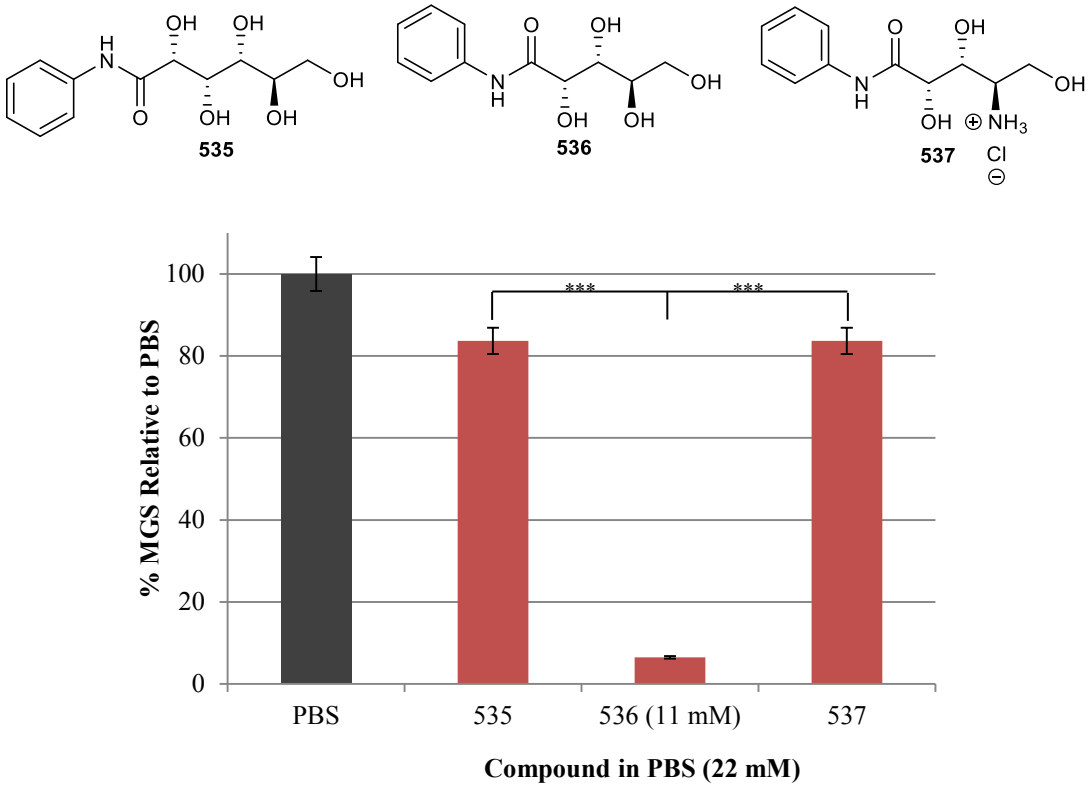

Figure 5-11. IRI activity of *N*-aryl-D-aldonamides **535-537**. **536** was tested at 11 mM due to insolubility. Asterisk indicates a statistical significant difference between samples and is defined by unpaired Student's *t*-test (***, $p < 0.05$). Statistical significant difference between the PBS control and samples is not shown. Samples have been run in triplicate (n = 3) and error bars indicate standard error of the mean (SEM).

While **533** and **537** exhibited weak IRI activity, arabonamide, **536**, exhibited potent IRI activity. **536** possesses similar IRI activity to *N*-alkyl-D-gluconamides **156** and **401** (known hydrogelators) and phenolic-glycoside, β-PMP-Glc (**507**). With 6.5% MGS relative to PBS, it is one of the most potent inhibitors of ice recrystallization assayed throughout this thesis. **536** possesses one less hydroxyl group than **535** and also possesses one of the simplest hydrophobic moieties. The activity of **536** suggests that a fine balance of hydrophobicity and hydrophilicity is required for potent IRI activity. With potent IRI activity, further investigation of this compound's activity is required.

5.5 Kinetic Profile of the IRI Activity of *N*-phenyl-D-arabonamide

Given the importance of ice recrystallization inhibition to many commercial and medical applications, it is not surprising that many methods have been developed to assess this process. These include the capillary method, wide-angle X-ray scattering (WAXS), differential scanning calorimetry (DSC) and the splat-cooling assay.[22-27] During the capillary method, many samples can be run simultaneously and thus, direct comparison of samples can be performed whilst running the assay. However, this method does not provide any quantification of IRI activity. Instead, it only indicates the presence of IRI activity.[23, 24] WAXS and DSC methods provide evidence of freezing point depression in the presence of antifreezes, as well as the morphology of ice crystals. Again, these are qualitative assessments and not a quantitative assessment of IRI activity.[25, 27] The splat-cooling assay is the most commonly utilized method for assessing IRI and is currently used by the Ben laboratory.[28] In this assay, recrystallization is observed by monitoring the change in ice crystal size where the presence of smaller ice crystals indicates a greater degree of activity.[28-30] The details of this assay have been presented in chapter 1. Commonly, analytes are assayed in a salt solution which negates non-specific IRI effects observed otherwise in pure water.[31] The Ben laboratory uses a phosphate buffered saline (PBS) solution, which is therefore a positive control for ice recrystallization.[28] The presence of other solutes ensures that the solution is liquid at the annealing temperature and that the eutectic point is below this temperature. Liquid is therefore present between ice crystal boundaries and liquid inclusions can be formed, where inhibitors become concentrated.[31] Ice crystal size in the splat-cooling assay is quantified by measuring the mean largest ice grain dimension along any axis or by measuring mean ice grain area.[28-30, 32] This generates mean grain size (MGS) of an analyte's ice crystals relative to a PBS positive control at a single time point.[28] However, this approach ignores two well-known aspects of recrystallization: time dependence of crystal growth and the heterogeneous nature of crystal sizes obtained during recrystallization.[33] The MGS is not an accurate representation of a non-homogenous sample in which the distribution of ice crystal sizes is quite large, notably at increased time points. Given these limitations, interest has grown in developing a method for studying the kinetics and rate of ice recrystallization and its inhibition. Recently, Koop and coworkers have investigated the kinetics associated with IRI using AF(G)Ps. They were able to generate "dose-response" curves to better quantify activity.[29, 34, 35] Utilizing a time-dependence on the measurement of IRI activity takes into account the time dependence of

crystal growth and heterogeneity in crystal sizes during recrystallization. However, in their approach, the ratio of ice to unfrozen fraction is small and thus it is not an accurate representation of a frozen sample commonly found during cryopreservation.[36] Thus, the Ben laboratory has developed a complimentary analysis ideally suited to measure a rate constant for the recrystallization process in the presence of IRIs when large ice volume fractions are present such as in the splat-cooling assay.[33]

In this assay, ice crystals of each wafer were grouped into equally sized "bins", where the incremental bin size was determined by the smallest area into which all crystals could be fit at time zero. The summed area of all the crystal in each bin was then converted to a proportion of the area of the total sample, in order to emphasize the relative importance of each bin.[33] It was observed that while most bins increased or decreased in population over time, the initial bin only decreased over time. Furthermore, this decrease could be described using a simple mono-exponential equation, providing a first order rate constant for the depopulation of the initial bin.[33] Using previously discovered small molecule IRIs, such as β-PMP-Glc and β-*p*BrPh-Glc, the Ben laboratory were able to demonstrate that the rate constants vary as a function of the inhibitory concentration. A classic dose-response curve was utilized to characterize the concentration dependence on the rate-constant. Utilizing a four-parameter sigmoidal equation, parameters such as efficacy, potency (IC_{50}) and cooperativity (slope) could be determined for each small molecule IRI. It was observed that at low concentration of the small molecule, the rate for the depletion of the initial bin was indistinguishable from that of PBS. Thus the rate constants were normalized by dividing the PBS rate constant and the top plateau was set to $k_{norm} = 100$. At high concentrations of the small molecule IRIs, complete suppression for the depletion on the initial bin was observed and thus, these compounds were acting as full antagonists and thus possessed excellent efficacy. These observations simplified the fitting of the small molecule IRIs. The sigmoidal dose response curves of β-PMP-Glc and β-*p*BrPh-Glc are shown in **Figure 5-12**.

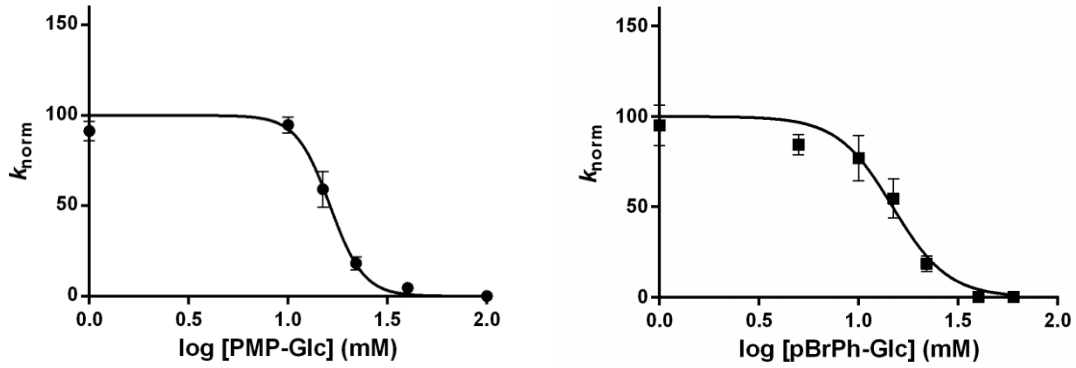

Figure 5-12. Dose-response curves of β-PMP-Glc and β-*p*BrPh-Glc. Normalized rate constants were measured in triplicate and error bars represent SEM. A two-parameter sigmoidal curve was used to fit the data.[33]

Analysis of the dose-response curves generated IC_{50} values for β-PMP-Glc and β-*p*BrPh-Glc. β-PMP-Glc has an IC_{50} value of 16.3 ± 1.4 mM while the IC_{50} value for β-*p*BrPh-Glc is 14.8 ± 2.2 mM. In contrast, a complete sigmoidal curve could not be defined for D-galactose, a moderate inhibitor of ice recrystallization, even at concentration up to 100 mM. Finally, the slope between the plateaus was also determined for β-PMP-Glc (5.1 ± 0.8) and β-*p*BrPh-Glc (3.1 ± 0.6). This slope is referred to a Hill slope and because its value for both inhibitors was greater than 1, it suggests possible cooperativity in their inhibition mechanism.[33] In contrast, D-galactose, did not show significant cooperativity. The cooperativity for β-PMP-Glc and β-*p*BrPh-Glc was possibly attributed to their ability to form self-assembling structures in solution.[1, 33] As previously discussed, the IRI activity of simple carbohydrates is attributed to their ability hydration as a result of their ability to disrupt bulk water within the QLL between bulk water and ice.[5] Therefore, the cooperativity in β-PMP-Glc and β-*p*BrPh-Glc possibly results in the formation of self-assembling structures within the QLL.[33] These structures are known to increase the ordering of bulk water. Given that diffusion of water molecules of an ordered crystal to less ordered water is favoured, the relative ordering of bulk water via cooperativity between small molecules would result in the diffusion process being less favored overall.[33]

Using the new method developed by the Ben laboratory, the dose-response curve of *N*-phenyl-D-arabonamide **536** was generated and is displayed in **Figure 5-13**.

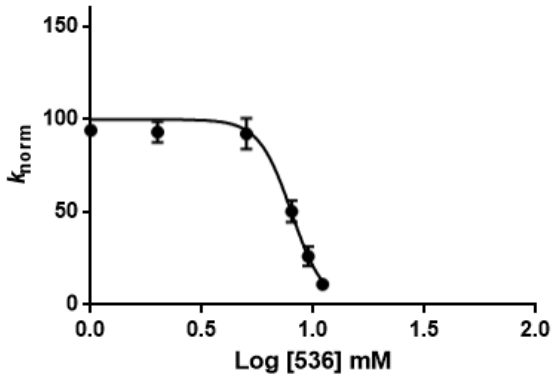

Figure 5-13. Dose-response curve of *N*-phenyl-D-arabonamide **536**. Normalized rate constant were measured in triplicate and error bars represent SEM. A two-parameter sigmoidal curve was used to fit the data.

A complete sigmodial curve could not be fit to the data due to insolubility of **536** past 11 mM. As evidence from the dose-response curve, **536** exhibits excellent efficacy (k_{norm} is close to zero at the bottom plateau of the sigmoidal curve). It is possible that **536** may exhibit full antagonism however; additional data points would be required to support this claim. The excellent efficacy is similar to that displayed by β-PMP-Glc and β-*p*BrPh-Glc.[33] **536** also exhibited an IC_{50} value of 8.3 mM and a Hill slope of 6.0 ± 0.7. The IC_{50} value is similar to the IC_{50} of β-PMP-Glc and β-*p*BrPh-Glc which are 16.3 ± 1.4 mM and 14.8 ± 2.2 mM respectively. While other small molecules developed by our laboratory must be assayed using this new method, this demonstrates that **536** is one of the more potent IRI active compounds discovered by our laboratory. The large Hill slope of **536** also suggests that the mechanism of action towards inhibiting ice recrystallization may involve an element of cooperativity. Much like β-PMP-Glc and β-*p*BrPh-Glc, it is possible that **536** may form self-assembling structures in solution. However, the nature of these structures is unknown and future work is required towards uncovering the exact mechanism of action of **536**.

Given, the utility in developing a kinetic profile of IRI active compounds, future work must be devoted to the kinetic profiling of other potent inhibitors of ice recrystallization including D-galactose based azasugar **310**, D-glucose based azasugar **311** and disaccharide **503**. Along with providing a detailed description of the IRI activity exhibited by these compounds, utilizing this novel kinetic approach may also provide insight into their mechanism of action.

5.6 Cryopreservation of Human Umbilical Cord Blood

As discussed in Chapter 1, cryopreservation is an important, simple and economic solution for long-term storage of biological materials. A major drawback of this process is the presence of cell death during the freeze-thaw cycle. This decreased viability is the result of either cell necrosis due to intracellular ice formation, mechanical damage to external cell membranes by either ice or osmotic flux, or cold-induced apoptosis.[37-39] Umbilical cord blood (UCB) banking has become a common practice in the past decade due to two applications. First, stem cells from cord blood are regarded as a practical alternative to autologous bone marrow stem cells[40] and second, the success of new stem cell-based regenerative therapies has increased in the past decade. However, decreased cell viabilities post-thaw is a current issue in regenerative therapies.[41, 42] Lower cell viabilities post-thaw result in a lower proportion of viable cells prior to transplant.[41, 42] Therefore, improved cryopreservation protocols are required. Currently, clinical protocols for UCB cryopreservation utilize a 10% dimethyl sulfoxide (DMSO) cryoprotectant solution. In clinical settings, however, DMSO is found to be highly cytotoxic.[43-45] Simple mono- and disaccharides have been investigated as potential UCB cryoprotectants.[46-48] These studies have explored the use of carbohydrate alone or in combination with DMSO. The novel small molecule IRIs identified in this chapter were investigated for their use as cryoprotectants of UCB using decreased amounts of DMSO was explored.

The cryopreservation experiments were carried out according to the protocols utilized commonly within clinics. This work was completed with the assistance of a fellow doctoral student, Jennie Briard. The procedure is based on the previous method developed by Rubinstein.[49] Whole UCB units were obtained and processed to obtain volume reduced leukocyte concentrates (LCs). Red-blood cells were sedimented by rouleaux formation using a sedimentation agent such as pentastarch (Pentaspan) or hydroxyethylstarch.[49, 50] A leukocyte rich buffy coat supernatant (separated using centrifugation) is removed and centrifuged to pellet the leukocyte from plasma. The leukocytes are then resuspended in plasma to provide the LC for the cryopreservation experiments. The processed LC that are hematopoietic stem cells ranges from 0.1-1% of total leukocytes present.[49-52] Following re-suspension, the LCs were then cryopreserved utilizing a cryprotectant solution containing the small molecule IRIs with or without DMSO. A standard freezing rate of 1°C/min to -80 °C is employed followed by storage in liquid nitrogen at -196 °C.[49, 50] They are then thawed using a fast-thaw (37 °C) protocol. These

are the optimal freezing and taw rates for HSCs and have been previously determined by the Ben laboratory.[19] As previously discussed, an optimal cooling and thawing rates for each cell type are necessary to mitigate cryo injury. The mechanism by which this cryo injury occurs has been discussed in detail in chapter 1. Post-thaw HSC viability was determined using flow cytometry using ISHAGE guidelines.[53] In flow cytometry, cells are passed through a laser in a fluid stream and when the cells pass through the laser intercept, they scatter light. Any fluorescent molecules present on the cell undergo fluorescence and the scattered and fluorescent light is collected by appropriately positioned lenses. A combination of beam splitters and filters steer the light to the detector. The detector produces electronic signals proportional to the optical signals striking them.[54] All human leukocytes and HSCs express the leukocyte common antigen, CD45, on their cell surfaces. HSCs also express the CD34 antigen and this antigen is not present on mature leukocytes. Thus, fluorescently tagged antibodies for both CD45 and CD34 can be employed to identify the cell population within the leukocytes that are HSCs using a specific gating strategy with flow cytometry.[53] HSCs are identified as $CD45^+$ and $CD34^+$ cells, whereas remaining leukocytes (or total mononuclear cells) are $CD45^+$ but $CD34^-$. By also employing 7-aminoactinomycin D (7-AAD) in the flow cytometric analysis, post-thaw cell viabilities of both of the HSCs present in the LC can be quantified. 7-AAD intercalates in double-stranded DNA. Although 7-AAD does not readily pass through cell membranes, cell can be marked as 7-AAD-positive if their membranes have been compromised or damaged due to cryo injury. It is assumed that a compromised or damaged cell membrane is an indicator of non-viable cells.[54]

Of the compounds exhibiting moderate to potent IRI activity in this chapter, only those possessing IRI activity of 0-50% MGS relative to PBS were explored for their ability to act as cryoprotectants during the cryopreservation of UCB. The first small molecule explored was disaccharide **503** which exhibited potent IRI activity with 12.8% MGS relative to PBS. **Figure 5-14** displays post-thaw viability of $CD34^+$ cells (HSCs). Statistically significant differences within the control and samples (for all compounds assayed) results were determined using an unpaired Student's *t*-test ($p < 0.05$). Additionally, statistically significant difference between the control and sample results were also determined using the same test.

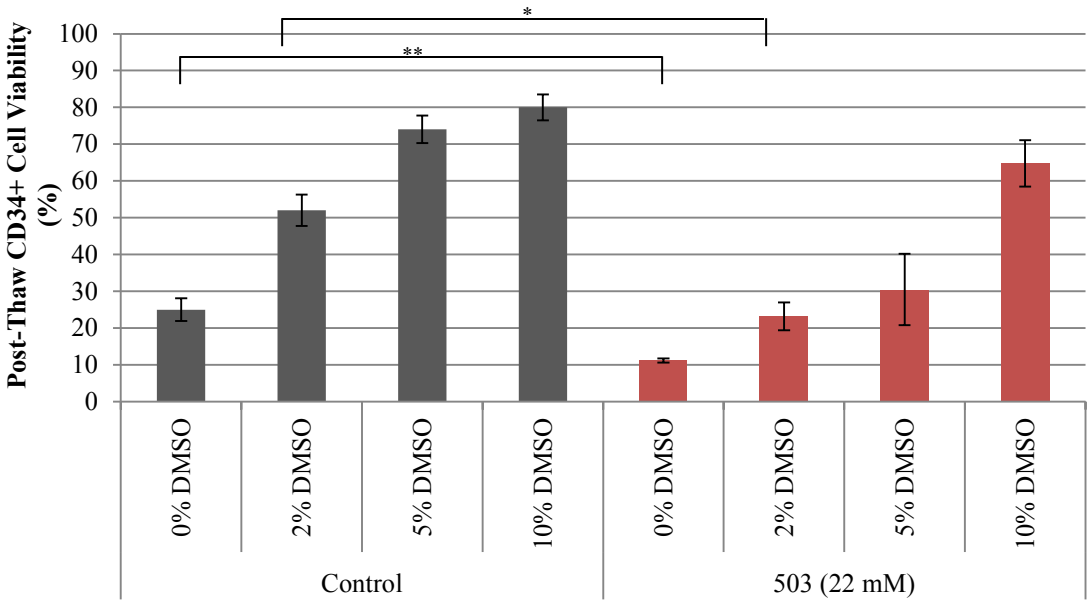

Figure 5-14. Post-thaw % cell viability of HSCs ($CD34^+$ cells) cryopreserved with 22 mM **503** in varying amounts of DMSO cryoprotectant solution. Samples were run in duplicate (n = 2). Asterisks indicate a statistical difference between the sample and its respective control DMSO solution. Control solution containing 0% and 2% DMSO concentrations were statistically different from the rest of the control solution. Statistically significant difference is defined by unpaired Student's *t*-test (*, $p < 0.05$, **, $p < 0.01$).

The post-thaw percent viabilities with the addition of **503** decreased overall as compared to the control DMSO cryoprotectant solution lacking **503**. The post-thaw percent viabilities for **503** utilizing 0 and 2% DMSO were statistically lower than the respective control solutions lacking **503**. Additionally, the post-thaw viabilities with **503** utilizing 5 and 10% DMSO were statistically similar to the control 5 and 10% DMSO solutions lacking **503**. Therefore, the addition of **503** offered no additional improvement to the cryoprotective ability of DMSO. In certain cases, the addition of **503** led to decreased post-thaw cell viabilities suggesting that **503** is possibly detrimental to cell membranes and thus cytotoxic to cells. While a small molecule may be generally damaging to cell membrane, this damage can occur during the freezing process as well. During the slow cooling (1 °C/min), ice will prefer to form in the extracellular medium.[55] The formation extracellular ice causes an osmotic pressure across the cell membrane. All solutes including small molecules are excluded from the ice lattice of extracellular ice and concentrated in the extracellular medium.[56-59] This concentration of small molecule increase outside the cell membrane may cause damage to cell membranes. Unfortunately, the exact nature of the

cytotoxicity of **503** is currently unclear and requires future studies. Next, the *N*-cycloalkyl-D-aldonamides were explored for their cryopreservation ability (**Figure 5-15**).

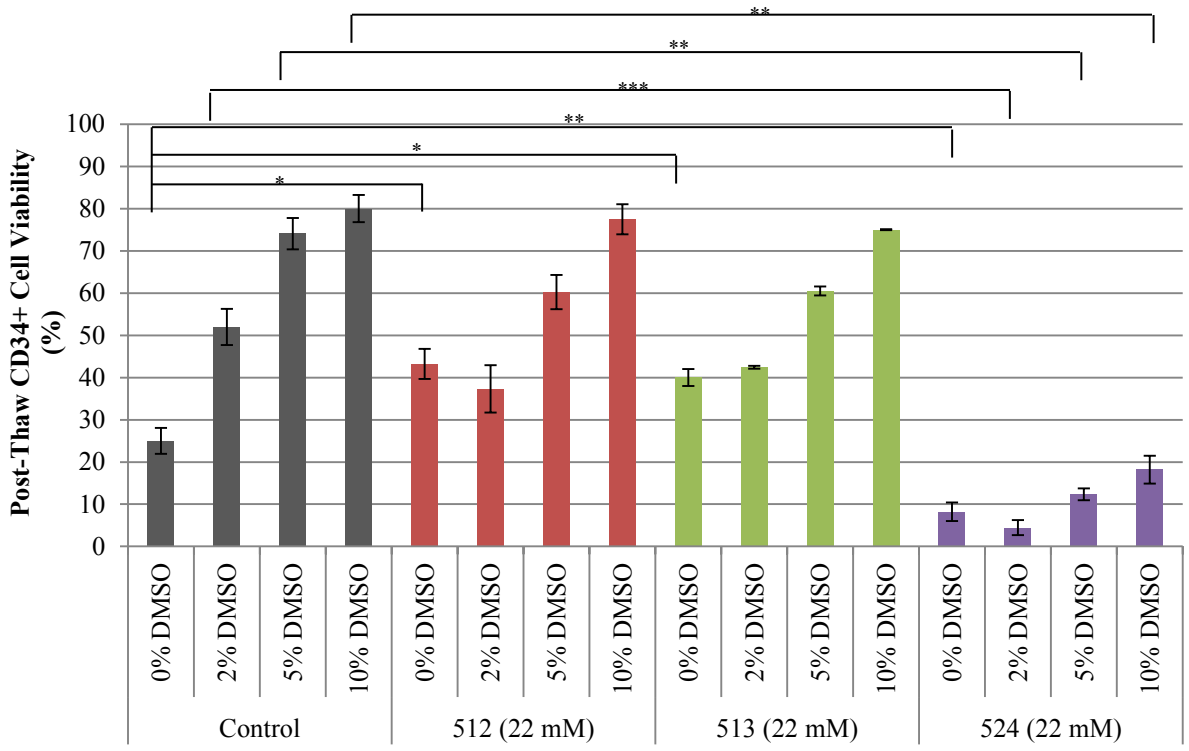

Figure 5-15. Post-thaw % cell viability of HSCs ($CD34^+$ cells) cryopreserved with 22 mM **512**, **513** and **524** in varying amounts of DMSO cryoprotectant solution. Samples were run in duplicate (n = 2). Asterisks indicate a statistical difference between the sample and its respective control DMSO solution. Control solution containing 0% and 2% DMSO concentrations were statistically different from the rest of the control solution. Statistically significant difference is defined by unpaired Student's *t*-test ((*, $p < 0.05$, **, $p < 0.01$, ***, $p < 0.001$).

Compounds **512** and **513** exhibited similar post-thaw cell viabilities to each other. No statistically significant difference in post-thaw cell viabilities was observed between the control, **512** and **513** samples using the various DMSO concentrations. Compound **524** exhibited exceptionally poor post-thaw cell viabilities. All viabilities were statistically decreased as compared to their respective control using DMSO at different concentrations lacking **524**. The exceptionally poor post-thaw percent viabilities of **524** suggests that this compound may be particularly cytotoxic. Much like **503**, compound **524** may be damaging the cell membrane and thus causing cytotoxicity to cells. However, the nature of this cytotoxicity requires future experiments for example the use of the MTT assay. The MTT assay will determine if the

cytotoxicity is the potential result of a loss in mitochondrial function. Finally, the quite potent *N*-phenyl-D-arabonamide **536** was assessed for its cryoprotective ability (**Figure 5-16**).

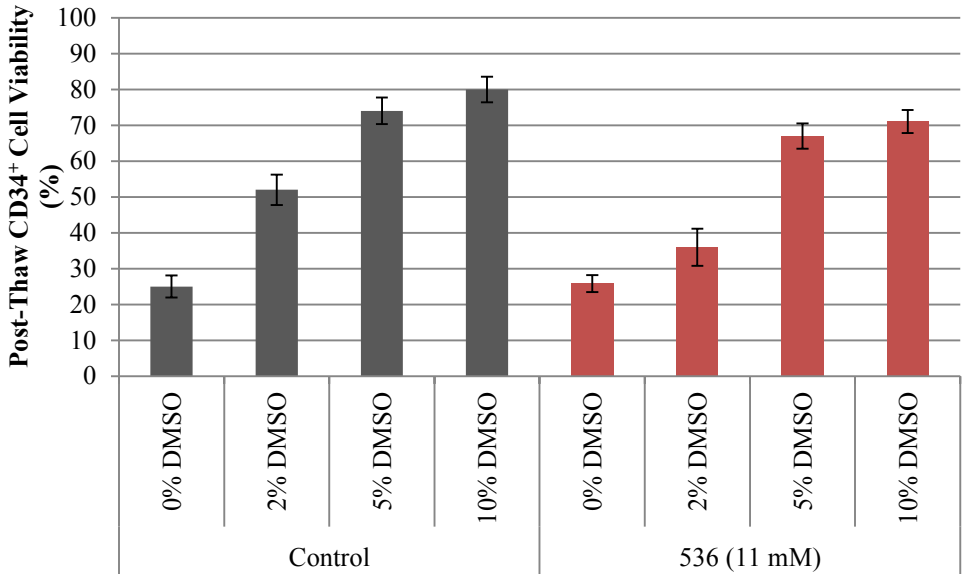

Figure 5-16. Post-thaw % cell viability of HSCs ($CD34^+$ cells) cryopreserved with 11 mM **536** in varying amounts of DMSO cryoprotectant solution. Samples were run in duplicate (n = 2). No statistically significant difference between the sample and its respective control DMSO solution could be defined using an unpaired Student's *t*-test ($p < 0.05$).

With potent IRI activity, **536** was hypothesized to be a beneficial cryoprotectant and display higher post-thaw percent viabilities compared to the control DMSO cyroprotectant solution lacking **536**. Unfortunately, no statistically significant difference in the post-thaw cell viabilities was observed between the control lacking **536** and the sample with **536** at the various DMSO concentrations. This is surprising as the Ben laboratory has previously demonstrated the use of "custom-tailored" IRI active *C*-linked AFGP analogues to increase post-thaw cell viabilities of embryonic liver cells (over a DMSO control). Embryonic liver cells were chosen as they can model stem cells.[60] Additionally, it has been demonstrated that IRI active mono- and disaccharides exhibiting minimal cytotoxicity significantly increased post-thaw cell viabilities of $CD34^+$ hematopoietic progenitor cells and human embryonic liver cells compared to less IRI active carbohydrates. Both of these studies demonstrate the correlation of IRI activity to increases in post-thaw cell viabilities.[61, 62] Due to a lack of significant improvement in post-thaw cell viability using **536**, the role of **536** during cryopreservation and its possible cytotoxicity to the cell membrane requires further investigation in future work.

5.7 Chapter Summary

A goal of the Ben laboratory is the development of novel small molecules with potent IRI activity. Given the inherent surfactant-like nature of previously developed small molecules, attention was placed toward the synthesis of small molecule IRIs not resembling surfactants in structure whilst possessing hydrophobic and hydrophilic groups. Previous work with phenoxyglycosides, such as β-PMP-Glc, led to the design and synthesis of disaccharides containing a *p*-methoxyphenyl group at the anomeric center. The C3-OH and C6-OH were substituted for amines (based on work discussed in Chapter 3) and these amines were conjugated to open-alditol chains of D-glucose and D-galactose. The presence of an amine and the additional hydroxyl groups were thought to improve the overall hydration of the molecule. Unfortunately, only one potent IRI was found. Thus, attention was shifted to *N*-cycloalkyl-D-aldonamide compounds. The cycloalkyl ring was chosen to maintain the hydrophobic nature of the long alkyl chains found in the previously IRI active *N*-alkyl-D-aldonamides whilst lacking their surfactant-like nature. Varying the ring size and hydrophilicity of the *N*-cycloalkyl-D-aldonamide resulted in moderate inhibitors of ice recrystallization but no potent activity was observed. Fortunately, replacing the cycloalkyl ring with a phenyl ring generated *N*-phenyl-D-arabonamide as one of the most IRI active molecules synthesized in this thesis. Kinetic analysis using a new method developed by our laboratory revealed an IC_{50} value of 8.3 mM for *N*-phenyl-D-arabonamide. This was one of the lowest IC_{50} values measured. Additionally, it was demonstrated that *N*-phenyl-D-arabonamide was a full antagonist (excellent efficacy) of the ice recrystallization process. Its IRI activity was also attributed to cooperativity and it was speculated that *N*-phenyl-D-arabonamide may for self-assembling structures capable to disrupting the bulk water around it and ultimately leading to potent IRI activity. With the generation of many moderate and a few potent inhibitors of ice recrystallization, their ability to act as cryoprotective agents during the cryopreservation of umbilical cord blood was explored. Unfortunately, none of the small molecules were able to improve the cryoprotective ability of a DMSO cryoprotectant solution. Future work requires the investigation of the further development of small molecules containing aryl groups as novel cryoprotectants.

5.6 References

1. Capicciotti, C. J.; Leclère, M.; Perras, F. A.; Bryce, D. L.; Paulin, H.; Harden, J.; Liu, Y.; Ben, R. N., *Chem. Sci.* **2012,** 3, 1408-1416.

2. Balcerzak, A. K.; Febbraro, M.; Ben, R. N., *RSC Adv.* **2013,** 3, 3232-3236.

3. Balcerzak, A. K.; Capicciotti, C. J.; Briard, J. G.; Ben, R. N., *RSC Adv.* **2014,** 4, 42682-42696.

4. Trant, J. F.; Biggs, R. A.; Capicciotti, C. J.; Ben, R. N., *RSC Adv.* **2013,** 3, 26005-26009.

5. Tam, R. Y.; Ferreira, S. S.; Czechura, P.; Chaytor, J. L.; Ben, R. N., *J. Am. Chem. Soc.* **2008,** 130, 17494-17501.

6. de Almeida, M. V.; Hyaric, M. L., *Mini-Rev. Org. Chem.* **2005,** 2, 283-297.

7. Lorber, B.; Bishop, J. B.; DeLucas, L. J., *Biochim. Biophys. Acta* **1990,** 1023, 254-265.

8. Michel, H.; Oesterhelt, D., *Proc. Natl. Acad. Sci. U.S.A.* **1980,** 77, 1283-1285.

9. Harvie, P.; Wong, F. M. P.; Bally, M. B., *Biophys. J.* 75, 1040-1051.

10. Hildreth, J. E. K., *Biochem. J.* **1982,** 207, 363-366.

11. Baron, C.; Thompson, T. E., *Biochim. Biophys. Acta* **1975,** 382, 276-285.

12. Plusquellec, D.; Chevalier, G.; Talibart, R.; Wro´blewski, H., *Anal. Biochem.* **1989,** 179, 145-153.

13. Capicciotti, C. J.; Kurach, J. D. R.; Turner, T. R.; Mancini, R. S.; Acker, J. P.; Ben, R. N., *Sci. Rep.* **2015,** 5.

14. Czechura, P.; Tam, R. Y.; Dimitrijevic, E.; Murphy, A. V.; Ben, R. N., *J. Am. Chem. Soc.* **2008,** 130, 2928-2929.

15. Chaytor, J. L. Examining the Role of Carbohydrate Hydration and Structure in Preventing Ice Recrystallization. 2010, Ph. D. Dissertation, University of Ottawa.

16. Pedersen, C. M.; Olsen, J.; Brka, A. B.; Bols, M., *Chem. Eur. J.* **2011,** 17, 7080-7086.

17. Jäger, M.; Hartmann, M.; de Vries, J. G.; Minnaard, A. J., *Angew. Chem. Int. Ed.* **2013,** 52, 7809-7812.

18. Painter, R. M.; Pearson, D. M.; Waymouth, R. M., *Angew. Chem.* **2010,** 122, 9646-9649.

19. Capicciotti, C. J. The Rational Design of Potent Ice Recrystallization Inhibitors for Use as Novel Cryoprotectants. 2014, Ph. D. Dissertation, University of Ottawa.

20. Kolb, H. C.; VanNieuwenhze, M. S.; Sharpless, K. B., *Chem. Rev.* **1994,** 94, 2483-2547.

21. Ben, R.; Capicciotti, C. J. *US20150157010*, 2013.

22. Knight, C. A.; Hallett, J.; DeVries, A. L., *Cryobiology.* **1988,** 25, 55-60.

23. Tomczak, M. M.; Marshall, C. B.; Gilbert, J. A.; Davies, P. L., *Biochem. Biophys. Res. Commun.* **2003,** 311, 1041-1046.

24. Yu, S. O.; Brown, A.; Middleton, A. J.; Tomczak, M. M.; Walker, V. K.; Davies, P. L., *Cryobiology.* **2010,** 61, 327-334.

25. Yagci, Y. E.; Antonietti, M.; Börner, H. G., *Macromol. Rapid Commun.* **2006,** 27, 1660-1664.

26. Mastai, Y.; Rudloff, J.; Cölfen, H.; Antonietti, M., *ChemPhysChem.* **2002,** 3, 119-123.

27. Baruch, E.; Mastai, Y., *Macromol. Rapid Commun.* **2007,** 28, 2256-2261.

28. Jackman, J.; Noestheden, M.; Moffat, D.; Pezacki, J. P.; Findlay, S.; Ben, R. N., *Biochem. Biophys. Res. Commun.* **2007,** 354, 340-344.

29. Budke, C.; Heggemann, C.; Koch, M.; Sewald, N.; Koop, T., *J. Phys. Chem. B.* **2009,** 113, 2865-2873.

30. Inada, T.; Lu, S.-S., *Cryst. Growth Des.* **2003,** 3, 747-752.

31. Knight, C. A.; Wen, D.; Laursen, R. A., *Cryobiology* **1995,** 32, 23-34.

32. Gibson, M. I.; Barker, C. A.; Spain, S. G.; Albertin, L.; Cameron, N. R., *Biomacromolecules* **2009,** 10, 328-333.

33. Abraham, S.; Keillor, K.; Capicciotti, C. J.; Perley-Robertson, G. E.; Keillor, J. W.; Ben, R. N., *Cryst. Growth Des.* **2015**.

34. Budke, C.; Dreyer, A.; Jaeger, J.; Gimpel, K.; Berkemeier, T.; Bonin, A. S.; Nagel, L.; Plattner, C.; DeVries, A. L.; Sewald, N.; Koop, T., *Cryst. Growth Des.* **2014,** 14, 4285-4294.

35. Nagel, L.; Budke, C.; Erdmann, R. S.; Dreyer, A.; Wennemers, H.; Koop, T.; Sewald, N., *Chem. Eur. J.* **2012,** 18, 12783-12793.

36. Rajashekar, C. B.; Burke, M. J., *Plant Physiol.* **1996,** 111, 597-603.

37. Mazur, P., *Am. J. Physiol. Cell Physiol.* **1984,** 247, C125-C142.

38. Karlsson, J. O. M.; Toner, M., *Biomaterials* **1996,** 17, 243-256.

39. Farrant, J.; Walter, C. A.; Lee, H.; McGann, L. E., *Cryobiology* **1977,** 14, 273-286.

40. Broxmeyer, H. E., *Cell Stem Cell* 6, 21-24.

41. Allan, D. S.; Keeney, M.; Howson-Jan, K.; Popma, J.; Weir, K.; Bhatia, M.; Sutherland, D. R.; Chin-Yee, I. H., *Bone Marrow Transplant* **2002,** 29, 967-972.

42. Abrahamsen, J. F.; Wentzel-Larsen, T.; Bruserud, Ø., *Cytotherapy* **2004,** 6, 356-362.

43. Davis, J. M.; Rowley, S. D.; Braine, H. G.; Piantadosi, S.; Santos, G. W., *Blood* **1990,** 75, 781-786.

44. Berz, D.; McCormack, E. M.; Winer, E. S.; Colvin, G. A.; Quesenberry, P. J., *Am. J. Hematol.* **2007,** 82, 463-472.

45. Galmes, A.; Gutiérrez, A.; Sampol, A.; Canaro, M.; Morey, M.; Iglesias, J.; Matamoros, N.; Duran, M. A.; Novo, A.; Bea, M. D., *Haematologica* **2007,** 92, 986-989.

46. Chaytor, J. L.; Tokarew, J. M.; Wu, L. K.; Leclère, M.; Tam, R. Y.; Capicciotti, C. J.; Guolla, L.; von Moos, E.; Findlay, C. S.; Allan, D. S.; Ben, R. N., *Glycobiology* **2012,** 22, 123-133.

47. Rodrigues, J. P.; Paraguassú-Braga, F. H.; Carvalho, L.; Abdelhay, E.; Bouzas, L. F.; Porto, L. C., *Cryobiology* **2008,** 56, 144-151.

48. Buchanan, S. S.; Gross, S. A.; Acker, J. P.; Toner, M.; Carpenter, J. F.; Pyatt, D. W., *Stem Cells Dev.* **2004,** 13, 295-305.

49. Rubinstein, P.; Dobrila, L.; Rosenfield, R. E.; Adamson, J. W.; Migliaccio, G.; Migliaccio, A. R.; Taylor, P. E.; Stevens, C. E., *Proc. Natl Acad. Sci. U. S. A.* **1995,** 92, 10119-10122.

50. Yang, H.; Acker, J.; Abley, D.; McGann, L.; Akabutu, J., *Bone marrow transplantation* **2001,** 27, 457-461.

51. Yang, H.; Loutfy, M. R.; Mayerhofer, S.; Shuen, P., *Transfusion* **2011,** 51, 284-292.

52. Yang, H.; Acker, J. P.; Hannon, J.; Miszta-Lane, H.; Akabutu, J. J.; McGann, L. E., *Cytotherapy* **2001,** 3, 377-386.

53. Sutherland, D. R.; Anderson, L.; Keeney, M.; Nayar, R.; Chin-Yee, I. A. N., *J. Hematother. Stem Cell Res.* **1996,** 5, 213-226.

54. Biosciences, B., In San Jose, California, 2000; Vol. 11-11032-01.

55. Mazur, P., *Science.* **1970,** 168, 939-949.

56. Hobbs, P. V., *Ice Physics*. 1st ed.; Oxford University Press, USA: Oxford, UK, 1975.

57. Lovelock, J. E., *Biochim. Biophys. Acta.* **1953,** 10, 414-426.

58. Lovelock, J. E., *Biochim. Biophys. Acta.* **1953,** 11, 28-36.

59. Meryman, H. T.; Williams, R. J.; Douglas, M. S. J., *Cryobiology* **1977,** 14, 287-302.

60. Leclère, M.; Kwok, B. K.; Wu, L. K.; Allan, D. S.; Ben, R. N., *Bioconj. Chem.* **2011,** 22, 1804-1810.

61. Wu, L. K.; Tokarew, J. M.; Chaytor, J. L.; von Moos, E.; Li, Y.; Palii, C.; Ben, R. N.; Allan, D. S., *Carb. Res.* **2011,** 346, 86-93.

62. Chaytor, J. L.; Tokarew, J. M.; Wu, L. K.; Leclère, M.; Tam, R. Y.; Capicciotti, C. J.; Guolla, L.; von Moos, E.; Findlay, C. S.; Allan, D. S.; Ben, R. N., *Glycobiology* **2012,** 22, 123-133.

Chapter 6. Experimental Procedures and Characterization Data

6.1 General Experimental Conditions

All anhydrous reactions were performed in flame-dried glassware under a positive pressure of dry argon. Air or moisture-sensitive reagents and anhydrous solvents were transferred with oven-dried syringes or cannulae. All flash chromatography was performed with E. Merck silica gel 60 (230-400 mesh). All solution phase reactions were monitored using analytical thin layer chromatography (TLC) with 0.2 mm pre-coated silica gel aluminum plates 60 F254 (E. Merck). Components were visualized by illumination with a short-wavelength (254 nm) ultra-violet light and/or staining (ceric ammonium molybdate, ninhydrin stain, potassium permanganate, or phosphomolybdate stain solution).

All solvents used for anhydrous reactions were distilled. Tetrahydrofuran (THF) and diethyl ether were distilled from sodium/benzophenone under nitrogen. Dichloromethane and acetonitrile were distilled from calcium hydride. *N,N*-dimethylformamide (DMF) was stored over activated 4Å molecular sieves under argon.

^{1}H (300, 400 or 500 MHz) and ^{13}C NMR (76 or 100 or 125 MHz) spectra were recorded at ambient temperature on a Bruker Avance 300, Bruker Avance 400, Bruker Avance 500, or Varian Inova 500 spectrometer. Deuterated chloroform ($CDCl_3$), methanol (CD_3OD), DMSO (DMSO-d_6) or water (D_2O) were used as NMR solvents, unless otherwise stated. Chemical shifts are reported in ppm downfield from trimethylsilane (TMS) or the solvent residual peak as an internal standard. Splitting patterns are designated as follows: s, singlet; d, doublet; t, triplet; q, quartet; quint, quintet; m, multiplet and br, broad. Low resolution mass spectrometry (LRMS) was performed on a Micromass Quatro-LC Electrospray spectrometer with a pump rate of 20 μL/min using electrospray ionization (ESI).

6.2 Ice Recrystallization Inhibition (IRI) Assay

Sample analysis for IRI activity was performed using the "splat-cooling" method as previously described.[1] In this method, the analyte was dissolved in phosphate buffered saline (PBS) solution and a10 μL droplet of this solution was dropped from a micropipette through a two meter high plastic tube (10cm in diameter) onto a block of polished aluminum precooled to approximately -80 °C. The droplet froze instantly on the polished aluminum block and was

approximately 1 cm in diameter and 20 μm thick. This wafer was then carefully removed from the surface of the block and transferred to a cryostage held at -6.4 °C for annealing. After a period of 30 min, the wafer was photographed between crossed polarizing filters using a digital camera (Nikon CoolPix 5000) fitted to the microscope. A total of three images were taken from each wafer. During flash freezing, ice crystals spontaneously nucleated from the supercooled solution. These initial crystals were relatively homogeneous in size and quite small. During the annealing cycle, recrystallization occurred, resulting in a dramatic increase in ice crystal size. A quantitative measure of the difference in recrystallization inhibition of two compounds X and Y is the difference in the dynamics of the ice crystal size distribution. Image analysis of the ice wafers was performed using a novel domain recognition software (DRS) program.[2] This processing employed the Microsoft Windows Graphical User Interface to allow a user to visually demarcate and store the vertices of ice domains in a digital micrograph. The data was then used to calculate the domain areas. All data was plotted and analyzed using Microsoft Excel. The mean grain (or ice crystal) size (MGS) of the sample was compared to the MGS of the control PBS solution for that same day of testing. IRI activity is reported as the percentage of the MGS (% MGS) relative to the PBS control, and the % MGS for each sample was plotted along with its standard error of the mean. Large percentages represent a large MGS, which is indicative of poor IRI activity.

6.2.1 Kinetic Measurement of IRI Activity

The "splat-cooling" assay is run as in section 6.2. However, the anneal time is reduced from 30 min to 5 min. The rate constants / initial rates were determined for 6-8 concentrations of ice recrystallization inhibitors in PBS buffer, two log units or the highest possible concentration in the case of solubility issues. For each sample concentration, triplicate wafers were prepared and single image was obtained for each wafer. The images recorded at each time point was analyzed using ImageJ. Specifically, all crystals within the field of view were circled, excluding those only partially visible at the image boundary. The area of each circled crystal was calculated using ImageJ and corrected for the appropriate magnification factor of the objective lens. These crystals were then sorted into discrete bins using a programmed Excel spreadsheet designed by Professor Jeffrey Keillor. Bin sizes were assigned in increments of 0.001 mm^2, as it was observed that at time zero, all ice crystals could be just contained within this bin. In this way, subsequent crystal growth would result in larger crystals moving out of Bin 1 and into higher bins. The relative importance of each bin

was determined by summing the area of each crystal within that bin, and dividing by the sum of the areas of all crystals within the field of view. In this way, the proportionate area of each bin was calculated for every sample wafer. The average rate constant measured in triplicate at zero inhibitor concentration (i.e. in PBS buffer alone) was used to normalize the rate constants measured in the presence of inhibitor. This provided, for each inhibitor, a set of normalized rate constants, k_{norm}, versus inhibitor concentration, [I], whose log values were used in dose-response fitting according to the following equation:

$$k_{\text{norm}} = \frac{100}{1 + n \text{ x } 10^{\text{ logIC50-log[I]}}}$$

This sigmoidal equation was fitted with 2 parameters in GraphPad.In this two-parameter sigmodial equation, IC_{50} is the concentration of the inhibitor that gives 50% antagonism and *n* is the Hill slope.

6.3 Thermal Hysteresis (TH) Assay

Nanoliter osmometry was performed using a Clifton nanoliter osmometer (Clifton Technical Physics,Hartford, NY), as described by Chakrabartty and Hew.[3] All of the measurements were performed in doubly distilled water. Ice crystal morphology was observed through a Leitz compound microscope equipped with an Olympus 20× (infinity-corrected) objective, a Leitz Periplan 32X photo eyepiece, and a Hitachi KPM2U CCD camera connected to a Toshiba MV13K1 TV/VCR system. Still images were captured directly using a Nikon CoolPix digital camera.

6.4 Gas Hydrate Formation Inhibition DSC Measurements

Through differential scanning calorimetery (Setaram Inc, m-DSC VII) methane hydrate nucleation was observed. Samples were prepared by injecting 1 μL of test solution into approximately 1.8 mg of silica gel isolated in a 1 mm diameter borosilicate capillary tube. 12 capillaries containing identical samples were then loaded into a DSC cell and pressurized to 100 Barr under methane. Starting at 20 °C the DSC was cooled to -12 °C at -0.0085 °C/sec. The cell was then kept at -12 °C for 20 hours before being heated to 20 °C 0.0085 °C/sec. This trial is repeated three times sequentially, resulting in 36 trials for each test solution. Test solutions are prepared from 5 mM stock solutions and are tested at all desired concentrations. *n*-Octyl-β-D-pyranosides **126** and **127** and *N*-alkyl-D-gluconamides **128**, **401** and **402** were previously

synthesized by fellow doctoral student Chantelle Capicciotti. Experimental procedures and full characterization of **126-128**, **401** and **402** can be found within her Ph.D thesis.[4]

6.5 Hep G2 Cell Culture

Hep G2 cells (human liver hepatocellular carcinoma cells, ATCC, HB-8065) were cultured in Eagle's minimum essential media (MEM) supplemented with 10% FBS (fetal bovine serum), 1% non-essential amino acids, 1 mM sodium pyruvate and 1% penicillin-streptomycin in 75cm^2 Corning® flasks. Cells were incubated in a 37°C incubator supplied with 5% CO_2. Passages 5-18 were used in this study. No evidence of overgrowth or morphological changes consistent with apoptosis was observed. All cells were removed from the plates using 3 mL Accutase solution for use in experiments. The media was changed every two days and the cells were split every seven days. The splitting involved removing media solution from flasks, adding 3 mL of Accutase solution and incubating at 37°C for 5 min. The detached cells were transferred to a 50 mL falcon tube and pelleted at 1000 rpm for 5 min. The media was discarded from falcon tubes and the pellet was resuspend in 5 mL of MEM and agitated to disperse cells. A 1/8 dilution of the cell solution was counted with a hemocytometer with trypan blue as a dye. The cell solution was transferred to a new flask and 20 mL of RPM1 was added.

6.6 MTT assay with HepG2 Cells

The MTT assay was performed as described previously.[5] Hep G2 cells were plated in 96-well plates and treated with 100 µL of compound MEM solution and incubated at 37°C for 16 h with 5% CO_2. Cells incubated with MEM without compound were used as a negative control, and cells supplemented with 1% Triton-X were used as a positive control. Following incubation, the supplemented media was removed and 200 µL of fresh media and 50 µL of MTT solution (5 mg/mL) in HBSS (Hank's balanced salt solution) were added and the plates were incubated at 37°C with 5% CO_2 for 3 h. The plates were then centrifuged, the media aspirated and 200 µL of MTT solubilization solution (10% Triton X-100, 0.1 N HCl in isopropanol) was added to each well. The plates were incubated at room temperature in the dark for 2-4 h and the absorbance of each well was then read at a wavelength of 570 nm with a multiwell plate reader (AD 34°C Absorbance Detector, Beckman Coulter, Inc., Mississauga, ON). Viability was reported as a percentage of the control. All experiments were repeated at least three times in 10 consecutive wells for each condition.

6.7 Collection and Processing of Cord Blood

Umbilical cord blood was collected following healthy term delivery and informed consent from mothers, in accordance with institutional approval from the Research Ethics Board of The Ottawa Hospital. Cord Blood was processed as according to Rubinstein's method to obtain leukocyte concentrates (LCs).[6] 10% pentastarch (Pentaspan) was added to the cord blood aliquoted into 50 mL Falcon tubes in the collection bag to obtain a final concentration of 2% and was incubated at room temperature for 10 min. The cord blood was then centrifuged at 52 g at 10°C for 15-20 min depending upon the volume of cord blood. The buffy coat aliquoted into 50 mL Falcon tubes to removes this layer from the packed RBCs and this buffy coat layer was then centrifuged at 400 g for 10 min at 10°C. The plasma was removed and stored in a separate Falcon tube and the packed leukocytes were resuspended in 20 mL of plasma resulting in the leukocyte concentrate (LC). Total mononuclear cell counts and $CD34^+$ cell concentrations and viability were then determined by flow cytometry.

6.8 Cryopreservation of UBC, Thawing and Flow Cytometry

Cryopreservation of the LCs obtained from processed UCB was performed similarly to protocols described previously.[6] Aliquots of LCs containing 4×10^6 total mononuclear cells were added to 1.5 mL Eppendorf tubes and cells were pelleted by centrifugation for 10 min at 400 g and 10 °C. The supernatant was removed and the cells were resuspended in 80 μL plasma. To this, 20 μL of cryo-solution supplemented with 5% (w/v) Dextran were added to afford a final concentration of cryo-solution as indicated in the text supplemented with 1% (w/v) Dextran. The cryo-solutions added (20 μL) were at 5 times the desired concentration as they were diluted to the appropriate amount when added to the mononuclear cells suspended in plasma (80 μL). Cell suspensions were transferred to 2 mL cryogenic vials and placed in a "Mr. Frosty" freezing container. The container was placed in a -80°C freezer for 16 h to provide a cooling rate of 1°C/min. Samples were then stored in the vapor phase of liquid nitrogen (−196°C) for a minimum of 24 hours. Following storage, samples were either rapidly thawed in a 37°C water bath with gentle agitation or thawed slowly at room temperature for flow cytometry analysis.

Flow cytometric analysis of UCB was conducted as according to the ISHAGE guidelines.[7,8]After cryopreservation and thawing, cell suspensions were diluted with 900 μL of DPBS and 200 μL were transferred to polypropylene flow cytometry tubes. 8 μL of CD45-FITC

and 8 μL of CD34-PE were added and the samples were vortexed and incubated in the dark for 10 min. 8 μL of 7-AAD was then added and the samples were vortexed and incubated in the dark for 5 min. Following incubation, 20 μL of CountBright counting beads were added and samples were diluted to 1 mL with 1X RBC lysing buffer. Flow cytometry analysis was carried out on a Beckman Coulter FC500 flow cytometer. Data analysis and gating strategies were carried out as according to the ISHAGE guidelines.[7,8] Viability of $CD34^+$ cells was determined by the total number $CD45^+/CD34^+$ cells that were 7-AAD-. Time between thawing and analysis by flow cytometry was less than 1 h. All samples were tested in duplicates.

6.9 Characterization Data and Spectra

D-galactose diethyldithioacetal (312)

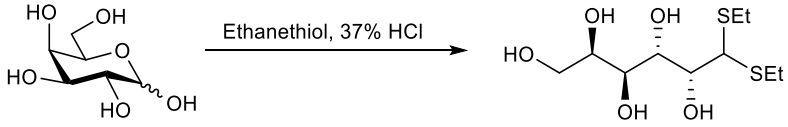

312

D-galactose (20.1 g, 112 mmol) was dissolved in a 37% (v/v) solution of aq. HCl (30 mL) and ethanethiol (20 mL, 277 mmol) was added to the mixture. After 5 min, ice-water is added to the reaction till a precipitate formed. The precipitate was then filtered and rinsed with EtOH. The remaining solid is then recrystallized from EtOH to give a **312** brown solid (14.8 g, 46% yield). ^{1}H NMR (300 MHz, CD_3OD): δ 4.00 (d, J = 9.2 Hz, 1H), 3.85 (m, 3H), 3.68 (dd, J = 13.2, 9.2 Hz 2H), 3.43-3.41 (m, 1H), 2.64-2.55 (m, 4H), 1.16 (t, J = 7.4 Hz, 6H).^{13}C NMR (125 MHz, CD_3OD): δ 72.3, 70.6, 70.2, 70.0, 63.8, 55.3, 24.9, 24.3, 15.1, 15.1. LRMS (ESI): *m/z* calcd. for $C_{10}H_{26}NO_5S_2$ $[M+NH_4]^+$ 304.4, found 304.8. All spectral data was consistent with that reported in the literature.[9]

5,6-*O*-isopropylidene-2,3,4-acetyl-D-galactose diethyl dithioacetal (313)

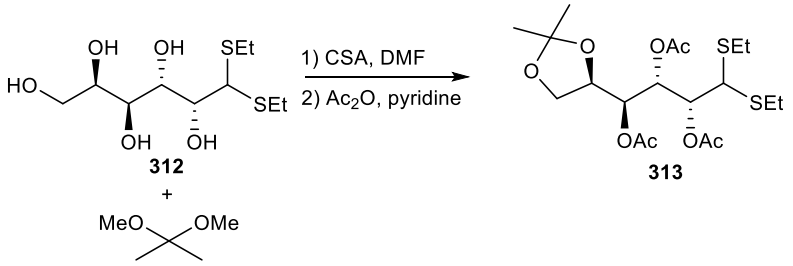

312 (3.93 g, 13.7 mmol) was dissolved in DMF (50 mL) and 2,2-dimethoxypropane (1.8 mL, 14.3 mmol) and camphorsulfonic acid (13.9 mg, 0.06 mmol) were added to the mixture. The reaction was monitored by TLC till starting material was consumed. The reaction is then quenched with trimethylamine and concentrated in *vacuo.* The mixture is then dissolved in pyridine (30 mL) and acetic anhydride (10 mL) and the mixture was stirred overnight. The mixture is the concentrated in *vacuo.* and purified by flash chromatography to give **313** as a clear oil (2.61 g, 42% yield over two steps). ^{1}H NMR (300 MHz, $CDCl_3$): δ 5.75 (dd, *J* = 7.8, 2.1 Hz, 1H), 5.29 (dd, *J* = 7.8, 2.1 Hz, 1H), 5.02 (dd, *J* = 7.7, 3.8 Hz 1H), 4.17-4.11 (m, 1H), 3.95 (dd, *J* = 8.7, 6.7 Hz, 1H), 3.87 (d, *J* = 8.1 Hz, 1H), 3.73 (dd, *J* = 8.7, 5.7, 1H), 2.75-2.55 (m, 4H), 2.11 (s, 3H), 2.10 (s, 3H), 2.06 (s, 3H), 1.38 (s, 3H), 1.29 (s, 3H), 1.24-1.18 (m, 6H).^{13}C NMR (125 MHz, $CDCl_3$): δ 170.3, 170.0, 169.5, 109.7, 74.1, 70.8, 70.4, 70.2, 65.8, 52.0, 26.0, 25.4, 25.1, 24.9, 21.1, 20.9, 20.8, 14.3, 14.1. LRMS (ESI): *m/z* calcd. for $C_{19}H_{32}NaO_8S_2$ $[M+Na]^+$ 457.6, found 457.8.

5,6-*O*-isopropylidene-2,3,4-benzoyl-D-galactose diethyl dithioacetal (314)

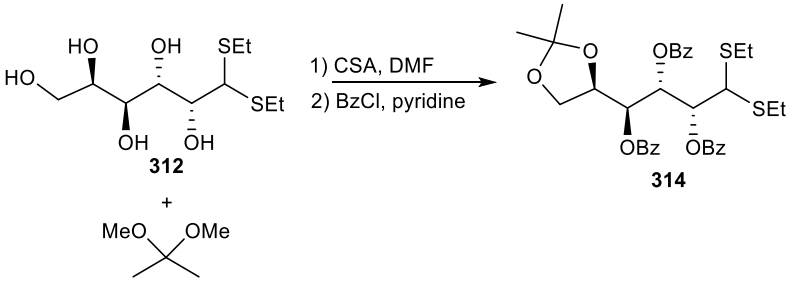

312 (3.90 g, 13.6 mmol) was dissolved in DMF (50 mL) and 2,2-dimethoxypropane (1.8 mL, 14.3 mmol) and camphorsulfonic acid (13.9 mg, 0.06 mmol) were added to the mixture. The reaction was monitored by TLC till starting material was consumed. The reaction is then quenched with trimethylamine and concentrated in *vacuo.* The mixture is then dissolved in pyridine (4.2 mL) and benzoyl chloride (3.1 mL, 40.2 mmol) was added. The reaction was stirred overnight and toluene was added and the mixture was concentrated in *vacuo.* The resulting syrup was dissolved in EtOAc, washed H_2O (2x), the organic layer was dried with $MgSO_4$, filtered and concentrated in *vacuo.* The resulting oil is then purified by flash chromatography to give a **314** as a clear oil (3.83 g, 44% yield over two steps). ^{1}H NMR (400 MHz, $CDCl_3$): δ 8.11-8.07 (m, 2H), 7.96-7.88 (m, 4H),7.60-7.50 (m, 1H), 7.50-7.40 (m, 4H), 7.34-7.23 (m, 4H), 6.25 (dd, *J* = 5.32, 2.5 Hz, 1H), 5.91 (dd, *J* = 7.1, 2.5 Hz, 1H), 5.60 (dd, *J* = 5.2, 4.0 Hz, 1H), 4.50 (td, *J* = 6.54, 6.53, 4.01 Hz, 1H), 4.18 (d, *J* = 7.10 Hz, 1H), 4.05 (dd, *J* = 8.7, 6.7 Hz, 1H), 3.83 (dd, *J* = 8.7, 6.7, 1H), 2.75-2.55 (m, 4H), 1.40 (s, 3H), 1.30 (s, 3H), 1.16 (td, *J* = 7.4, 2.4 Hz, 6H).^{13}C NMR (100 MHz, $CDCl_3$): δ 165.7, 165.4, 165.4, 133.4, 133.1, 133.0, 130.0, 129.9, 129.8, 129.7, 129.6,

129.3, 128.5, 128.3, 128.2, 109.9, 74.8, 72.1, 71.8, 71.6, 65.9, 52.4, 26.2, 25.5, 25.4, 25.1, 14.3, 14.2. LRMS (ESI): *m/z* calcd. for $C_{34}H_{38}NaO_8S_2$ $[M+Na]^+$ 638.8, found 638.5.

3,4,5,7-tetra-*O*-benzyl-1,2-dideoxy-D-galacto-hept-1-enitol (316)

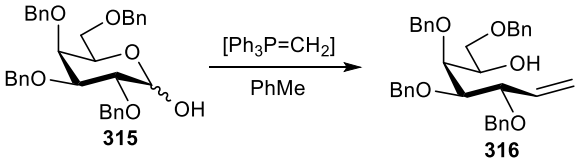

Methyltriphenylphosphonium bromide (3.97 g, 11.1 mmol) was suspended in toluene (60 mL) and cooled to 0 °C and 2.5 M butyllithium in hexanes (4.5 mL, 11.1 mmol) was added dropwise. A solution of **315** (1.99 g, 3.70 mmol) in toluene (16 mL) was cannulated to the reaction and this mixture was then stirred for 48h at rt. The reaction was quenched with acetone (20 mL), the mixture is diluted with ether and extracted with water. The aqueous layer is extracted with ether (2x), the organic layers were combined, dried with $MgSO_4$, filtered and concentrated in *vacuo.* The residue was purified by flash chromatography to give **316** as a syrup (1.19 g, 60% yield). ^{1}H NMR (300 MHz, $CDCl_3$): δ 7.34-7.14 (m, 20H), 5.86 (ddd, *J* = 17.9, 10.1, 7.9 Hz, 1H), 5.39-5.23 (m, 2H), 4.76-4.72 (m, 2H), 4.63 (d, *J* = 11.8 Hz, 1H), 4.50-4.29 (m, 5H), 4.15-4.05 (m, 2H), 3.83-3.76 (m, 2H), 3.49 (ddd, *J* = 17.6, 9.4, 6.3 Hz, 2H), 3.00 (d, *J* = 5.4 Hz, 1H).^{13}C NMR (75 MHz, $CDCl_3$): δ138.3, 138.2, 138.2, 138.1, 135.8, 128.4, 128.2, 128.1, 127.8, 127.8, 127.7, 127.6, 119.3, 82.1, 80.8, 76.6, 75.3, 73.2, 73.2, 71.3, 70.3, 69.7. LRMS (ESI): *m/z* calcd. for $C_{35}H_{38}KO_5$ $[M+K]^+$ 577.8, found 577.4. All spectral data was consistent with that reported in the literature.[10]

3,4,5,7-tetra-*O*-benzyl-1,2-dideoxy-6-*O*-(4-nitrobenzoyl)-L-altro-hept-1-enitol (317)

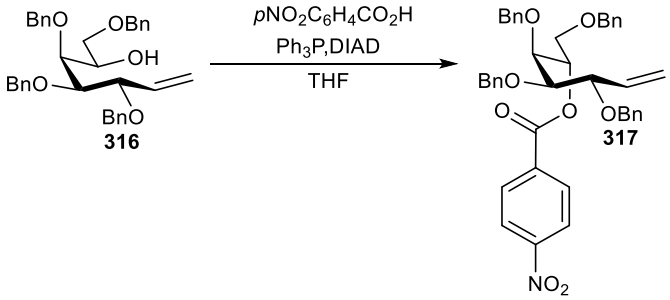

316 (129 mg, 0.239 mmol), triphenylphosphine (188 mg, 0.717 mmol) and 4-nitrobenzoic acid (159 mg, 0.956 mmol) were dissolved in THF (20 mL) at 0°C. DIAD (0.2 mL, 0.956 mmol) was added dropwise and the reaction was stirred overnight. The reaction was then concentrated in *vacuo.* and purified by flash chromatography to give **317** as a syrup (128 mg, 78% yield). ^{1}H NMR (300 MHz, $CDCl_3$): δ 8.28 (d, *J* = 8.9 Hz, 2H), 8.15 (d, *J* = 8.9 Hz, 2H), 7.50-7.30 (m, 20H), 6.08 (ddd, *J* = 17.9, 10.1, 7.9 Hz, 1H), 5.97 (dd, *J* = 7.4, 2.8 Hz, 1H), 5.56-5.45 (m, 2H), 4.96-4.44 (m, 8H), 4.30-4.22 (m, 2H), 4.07-4.05 (m, 2H) 3.90 (t, *J* = 5.2 Hz, 1H). ^{13}C NMR (75 MHz, $CDCl_3$): δ163.9, 150.5, 138.3, 138.3, 138.2, 138.1, 135.8, 135.7, 130.8, 128.4, 128.4, 128.4, 128.3, 128.0, 127.9, 127.9, 127.8, 127.7, 127.7, 127.6, 127.6, 123.5, 119.3, 81.7, 80.7, 78.8, 74.7, 74.6, 73.2, 73.0, 70.6, 68.8. LRMS (ESI): *m/z* calcd. for $C_{42}H_{41}NaO_5$ $[M+Na]^+$ 710.8, found 710.3. All spectral data was consistent with that reported in the literature.[10]

3,4,5,7-tetra-*O*-benzyl-1,2-dideoxy-L-altro-hept-1-enitol (318)

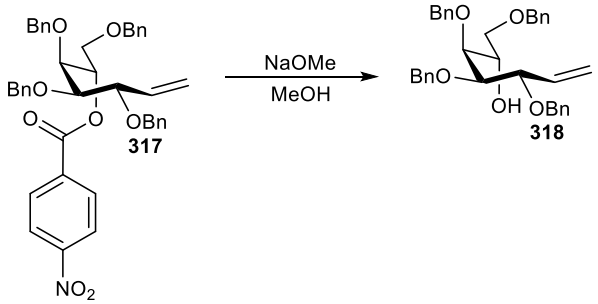

317 (358 mg, 0.521 mmol) was dissolved in MeOH (20 mL) and a few drops of a solution NaOMe in MeOH (1 M) till pH = 9. Once the starting material is consumed as seen by TLC, Amberlite® IR-120 (H^+) ion exchange resin is added till pH = 7. The resin is removed by filtration and washed with MeOH and the filtrate was concentrated in *vacuo.* to give **318** as a clear oil. This compound was used without further purification.

3,4,5,7-tetra-*O*-benzyl-1,2,6-trideoxy-6-phthalimido-D-galacto-hept-1-enitol (319)

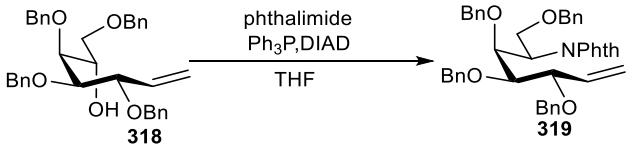

318 (855 mg, 1.24 mmol), triphenylphosphine (1.30 g, 4.97 mmol) and phthalimide (732 mg, 4.97 mmol) was dissolved THF (170 mL). DIAD (1 mL, 4.97 mmol) was added dropwise to the mixture and the reaction was stirred overnight. The mixture was then concentrated under *vacuo.* and the resulting residue was triturated with ether. The precipitate was removed by filtration and the filtrate was concentrated under *vacuo.* and the resulting residue was purified by flash chromatography to give **319** as a syrup (605 mg, 73% yield. ^{1}H NMR (300 MHz, $CDCl_3$): δ 7.71-7.62 (m, 4H), 7.39-6.98 (m, 20H), 5.92 (ddd, J = 17.9, 10.1, 7.9 Hz, 1H), 5.40-5.34 (m, 2H), 4.92 (dt, J = 9.3, 5.1 Hz, 1H), 4.81 (s, 2H), 4.63 (d, J = 11.8 Hz, 1H), 4.54 (d, J = 11.8 Hz, 1H), 4.41-4.26 (m, 4H), 4.21 (dd, J = 8.3, 2.8 Hz, 1H) 4.09-4.00 (m, 2H), 3.79-3.73 (m, 2H). ^{13}C NMR (75 MHz, $CDCl_3$): δ 168.7,138.5, 138.5, 138.0, 138.0, 135.5, 133.5, 132.1, 128.3, 128.2, 128.2, 128.0, 127.8, 127.7, 127.6, 127.4, 127.2, 123.0, 119.5, 83.0, 81.4, 74.7, 73.1, 72.4, 70.7, 67.0, 52.2. LRMS (ESI): *m/z* calcd. for $C_{43}H_{42}O_6$ $[M+H]^+$ 667.8, found 667.7. All spectral data was consistent with that reported in the literature.[10]

3,4,5,7-tetra-*O*-benzyl-1,2-dideoxy-6-[(benzyloxycarbonyl)amino]-1,2,6-trideoxy-D-galacto-1-enitol (320)

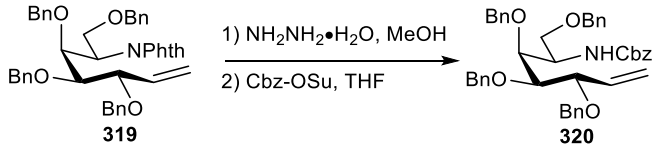

319 (623 mg, 0.931 mmol) and hydrazine hydrate (2.5 mL) are dissolved in MeOH (60 mL) and heated to 67°C for 1h. The reaction is then concentrated in *vacuo.* and dissolved in THF (120 mL) and saturated $NaHCO_3$ (2.5 mL) was added and the reaction is stirred for 5min. *N*-(benzyloxycarbonyloxy)succinimide (349 mg, 1.40 mmol) was added in one portion at 0°C and the reaction is stirred for 3h at 0°C. The reaction was then concentrated in *vacuo.* and purified by flash chromatography to give **320** as a yellow oil (300 mg, 48% yield over two steps). ^{1}H NMR (300 MHz, $CDCl_3$): δ 7.43-7.24 (m, 23H), 7.15-7.13 (m, 2H), 6.02 (ddd, *J* = 17.9, 10.1, 7.9 Hz, 1H), 5.15-5.06 (m, 3H), 5.15-5.06 (m, 2H), 4.71-4.35 (m, 8H) 4.18-4.14 (m, 1H), 4.10-4.08 (m, 1H), 3.66-3.58 (m, 2H), 3.54-3.48 (m, 1H). ^{13}C NMR (75 MHz, $CDCl_3$): 156.1, 138.4, 138.4, 138.1, 136.6, 136.2,128.5, 128.4, 128.3, 128.3, 128.1, 128.1, 128.0, 127.8, 127.8, 127.7, 127.6, 127.6, 127.5, 118.9, 81.4, 80.5, 75.9, 75.1, 73.6, 72.9, 70.2, 69.6, 66.7. LRMS (ESI): *m/z* calcd. for $C_{43}H_{46}O_6$ $[M+H]^+$ 671.8, found 671.3. All spectral data was consistent with that reported in the literature.[10]

2,3,4,6-tetra-*O*-benzyl-D-galactono-δ-lactone (321)

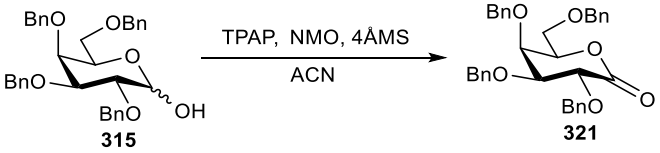

315 (5.03 g, 9.30 mmol) in 50 mL acetonitrile was added tetrapropylammonium perruthenate (176 mg, 0.501 mmol) and *N*-methylmorpholine-*N*-oxide (1.63 g, 13.9 mmol). This solution was stirred till TLC indicated complete consumption of the starting material. The crude mixture was filtered over Celite® and concentrated under *vacuo*. The resulting crude mixture was diluted with ethyl acetate and washed 2x with a saturated solution of sodium thiosulfate. Afterwards, it was washed with brine, dried over magnesium sulfate and concentrated in *vacuo.* The product was used for further reactions without further purification.

2,3,4,6-tetra-*O*-benzyl-D-galactonamide (322)

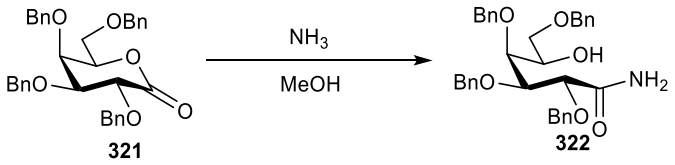

Compound **321** (3.12 g, 5.79 mmol) was dissolved in 40 mL solution of methanol saturated with ammonia. The resulting mixture was stirred at room temperature for 1.5 h under argon atmosphere. The reaction mixture was then concentrated in *vacuo.* Recrystallization of the resulting white solid from ethyl acetate and petroleum ether afforded **322** as a white powder (2.56 g, 50% yield over two steps). ^{1}H NMR (300 MHz, $CDCl_3$): δ 7.33-7.17 (m, 20H), 6.62 (bs, 1H), 5.54 (bs, 1H), 4.71-4.32 (m, 8H), 4.19-4.14 (m, 3H), 3.90 (dd, *J* = 8.3, 1.4 Hz, 1H), 3.59 (dd, *J* = 9.3, 6.6 Hz, 1H), 3.51 (dd, J = 9.4, 6.5 Hz, 1H), 2.49 (bs, 1H). ^{13}C NMR (100 MHz, $CDCl_3$): δ 174.8, 137.9, 137.9, 137.7, 136.7, 128.6, 128.4, 128.4, 128.2, 128.2, 128.0, 127.8, 127.7, 127.4, 79.7, 79.3, 77.2, 75.0, 73.7, 73.3, 73.2, 71.3, 69.2. LRMS ESI-MS *m*/*z* calcd for $C_{34}H_{37}NO_6$ $[M + H]^+$: 556.3, found 557.3. All spectral data was consistent with that reported in the literature.[11]

2,3,4,6-tetra-*O*-benzyl-D-galactono-δ-lactam (323)

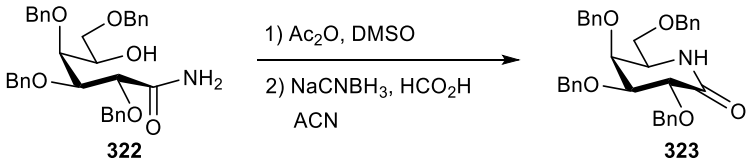

322 (2.56 g, 4.61 mmol) was dissolved in 19 mL of dimethyl sulfoxide and 11 mL of acetic anhydride. The mixture was stirred overnight. After, 60 mL of water was added and the mixture is stirred for 15 more minutes during which a yellow oil precipitated. The water layer was removed and the residue was extracted with water 3x. The residue was dissolved in dichloromethane and extracted with brine 2x. The organic fractions were combined and dried over $MgSO_4$ and concentrated in *vacuo*. The product (2.11 g, 83% yield) was used for further reactions without further purification. This mixture was dissolved in 60 mL of acetonitrile and 15 mL of formic acid. To this mixture, sodium cyanoborohydride (1.19 g, 18.9) was added and the reaction was refluxed for two hours. The mixture was then cooled in ice and the reaction was quenched by adding aq. HCl-solution (0.1 M). After stirring for 15 minutes, the mixture was poured into a mixture of ethyl acetate/ saturated aqueous $NaHCO_3$ solution (1:1, 200 mL). The water layer was separated and extracted with ethyl acetate; the combined organic fractions were then washed with brine and dried over $MgSO_4$ and concentrated in *vacuo*. Flash chromatography gave **323** as a yellow syrup (1.61 g, 65% yield over two steps). ^{1}H NMR ($CDCl_3$, 300MHz): δ 7.48-7.26 (m, 20H), 5.30 (br s, 1H), 5.26 (d, J = 11.3 Hz, 1H), 4.96-4.44 (m, 8H), 4.03 (br s, 1H), 3.86 (dd, J = 9.2 Hz, 1.4 Hz, 1H), 3.61-3.58 (m, 2H) 3.51-3.49 (m, 1H). ^{13}C NMR (100 MHz, $CDCl_3$): δ 171.1, 138.4, 138.2, 138.0, 137.5, 128.6, 128.5, 128.4, 128.4, 128.3, 128.1, 128.1, 128.0, 127.9, 127.8, 127.7, 127.6, 80.7, 77.5, 77.5, 77.2, 76.9, 75.4, 74.2, 73.6, 73.1 53.6. LRMS ESI-MS *m*/*z* calcd for $C_{34}H_{36}NO_5$ $[M + H]^+$: 538.7, found 538.2. All spectral data was consistent with that reported in the literature.[11]

2,3,4,6-tetra-*O*-benzyl-1,5-dideoxy-1,5-imino-D-galactiol (324)

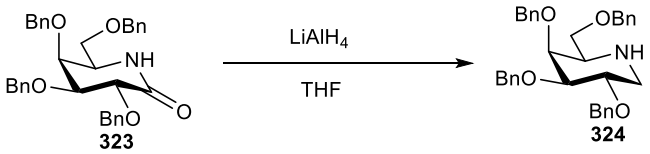

323 (210 mg, 0.391 mmol), was dissolved in 10 mL THF. Then, lithium aluminiumhydride (53.6 mg, 1.41) was added and the reaction mixture was stirred for 3 hours at 70°C under argon atmosphere. The reaction mixture was then poured into a stirred mixture of 50 mL ice water and 50 mL diethyl ether. After stirring for 10 minutes 75 mL sodium hydroxide solution (0.5 M) was added and the mixture was stirred for another 10 minutes. The water layer was then removed and extracted with 25 mL of diethyl ether (2x); the combined organic fractions were washed with brine and water. Flash chromatography gave **324** as a light yellow oil (198 mg, 98% yield).[1]H NMR ($CDCl_3$, 300MHz): δ 7.40-7.25 (m, 20H), 4.90 (d, *J* = 11.4 Hz, 1H), 4.78 (d, *J* = 12.0 Hz, 1H), 4.73 (d, *J* = 9.7 Hz, 1H), 4.64 (d, *J* = 11.6 Hz, 1H), 4.55 (d, *J* = 11.5 Hz, 1H), 4.47 (d, *J* = 11.8 Hz, 1H), 4.46 (d, *J* = 11.8 Hz, 1H), 4.00-3.95 (m, 1H), 3.90 (ddd, *J* = 9.8, 9.8, 5.3 Hz, 1H), 3.53 (dd, *J* = 8.9, 6.7 Hz, 1H), 3.47 (dd, *J* = 9.2, 2.6 Hz, 1H), 3.34-3.41 (m, 1H), 3.31 (dd, *J* = 13.3, 4.6 Hz, 1H), 2.86 (t, *J* = 7 Hz, 1H), 2.52 (dd, *J* = 10.4, 2.4 Hz, 1H). ^{13}C NMR (100 MHz, $CDCl_3$): δ 138.6, 138.6, 138.5, 137.8, 128.4, 128.4, 128.3, 128.2, 128.2, 128.0, 127.8, 127.5, 74.4, 74.1, 73.4, 73.2, 72.8 58.2. LRMS ESI-MS *m*/*z* calcd for $C_{34}H_{37}NNaO_4$ $[M + Na]^+$: 546.7, found 546.5. All spectral data was consistent with that reported in the literature.[11]

D-galacto-1-deoxynojirimycin (310)

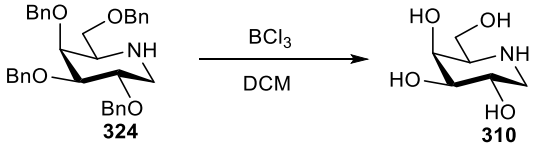

Boron trichloride (2.5 mL, 1M in CH_2Cl_2) was added to a cooled (0 °C) solution of compound **324** (198 mg, 0.378 mmol) in CH_2Cl_2 (4 mL). The reaction mixture was stirred for 20 hours at 0 °C after which MeOH (0.5 mL) was carefully added. The reaction mixture was concentrated and co-evaporated with toluene. Flash column purification of the residue over aluminumoxide (with ammonium hydroxide added to the solvent system) provided **310** as a colorless oil (59.2 mg, 96% yield). ^{1}H NMR (300 MHz, D_2O): δ 3.87 (d, *J* = 2.6 Hz, 1H), 3.62 (dt, *J* = 10.6, 5.2 Hz, 1H), 3.43-3.55 (m, 2H), 3.30 (dd, *J* = 9.9, 3.3 Hz, 1H), 3.00 (dd, *J* = 12.9, 5.6, 1H), 2.68 (t, *J* = 6.8 Hz, 1H), 2.29 (dd, *J* = 10.9, 1.5 Hz, 1H). ^{13}C NMR (100 MHz, D_2O): δ 74.8, 69.0, 67.8, 61.1, 58.8, 48.8. LRMS ESI-MS *m*/*z* calcd for $C_6H_{14}NO_4$ $[M + H]^+$: 164.2, found 164.2, 186.1. All spectral data was consistent with that reported in the literature.[11]

2,3,4,6-tetra-O-benzyl-1,5-dideoxy-1,5-imino-D-glucitiol (326)

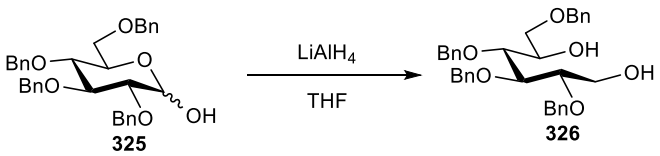

325 (1.21 g, 2.24 mmol) was dissolved in THF (15 mL) and $LiAlH_4$ (297 mg, 7.83 mmol) was added in small portions at 0°C.The reaction mixture was stirred overnight, allowing it to warm to rt. The excess $LiAlH_4$ was quenched via Fieser quench. The mixture was diluted with EtOAc and washed with sat. aq. NH_4Cl (3x). The organic phase was dried with $MgSO_4$ and concentrated in *vacuo.* The crude was not purified and carried onto the next step.

2,3,4,6-tetra-O-benzyl-1,5-dideoxy-1,5-imino-D-glucitiol (328)

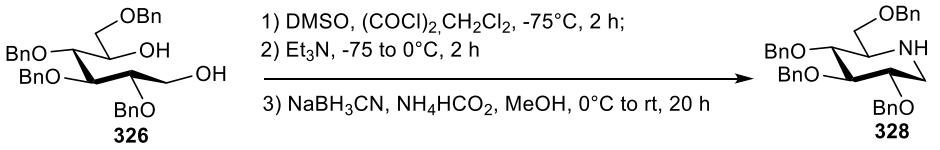

A solution of oxalylchloride (0.6 mL) in DCM (7.4 mL) was cooled to -78°C. After dropwise addition of a solution of DMSO (0.7 mL) in DCM (4.6 mL) over 10 minutes, the reaction mixture was stirred for 40 minutes while being kept below -70 °C. Next, a dry solution of the glucitol intermediate **326** (1.21 g, 2.24 mmol) in DCM (3.7 mL) was added dropwise to the reaction mixture over a 15 minute period, while keeping the reaction mixture below -70°C. After stirring the reaction mixture for 2 hours below -65°C, Et_3N (3 mL) was added dropwise over a 10 minute period, while keeping the reaction mixture below -65 °C. After addition, the reaction mixture was allowed to warm to -5 °C over 2 hours. The Swern reaction mixture was concentrated at a moderate temperature (~30 °C) with simultaneous co-evaporation of toluene (3x). The residue was dissolved in MeOH (37 mL) and NH_4HCO_2 (2.32 g, 36.8 mmol) was added. The mixture was cooled to 0 °C and stirred until all NH_4HCO_2 had dissolved. Activated 3Å molsieves (10 g/mmol) were added and reaction mixture was stirred for 20 minutes, after which $NaBH_3CN$ (463 mg, 7.36 mmol) was added. The reaction mixture was kept at 0 °C for one hour after which the cooling source was removed and the reaction was stirred for an additional 20 hours. After removal of the mol. sieves by filtering over Celite®, the filtrate was concentrated, dissolved in EtOAc and washed with sat. aq. $NaHCO_3$. The aqueous phase was back-extracted with EtOAc (3x) and the combined organic layers were dried with $MgSO_4$ and concentrated in *vacuo.* and purified by flash chromatography giving **328** as a light yellow crystalline solid (856 mg, 73% yield over three steps). ^{1}H NMR (300 MHz, $CDCl_3$): δ 7.35-7.14 (m, 20H), 4.97 (d, J = 12.9 Hz, 1H), 4.87-4.82 (m, 2H), 4.68 (d, J = 11.7 Hz, 1H), 4.64 (d, J = 11.7 Hz, 1H), 4.48 (d, J = 11.0 Hz, 1H), 4.45 (d, J = 11.8 Hz, 1H), 4.40 (d, J = 11.8 Hz, 1H), 3.65 (dd, J = 9.0 Hz, 2.6 Hz, 1H), 3.57-3.45 (m, 3H), 3.34 (dd, J = 8.8 Hz, 1H), 3.22 (dd, J = 12.2 Hz, 4.9 Hz, 1H), 2.53 (ddd, J = 9.8, 5.9 Hz, 2.6 Hz, 1H), 2.49 (dd, J = 12.2 Hz, 10.3 Hz, 1H). ^{13}C NMR (100 MHz, $CDCl_3$): δ 138.9, 138.5, 138.4, 138.0, 128.4, 128.4, 128.3, 128.0, 127.9, 127.8, 127.8, 127.7, 127.6, 127.5, 87.3, 80.5, 80.1, 75.6, 75.2, 73.4, 72.8, 70.2, 59.7, 48.1. LRMS ESI-MS *m*/*z* calcd for $C_{37}H_{34}NNaO_4$ $[M+Na]^+$: 546.7, found 546.5. All spectral data was consistent with that reported in the literature.[12]

D-gluco-1-deoxynojirimycin (311)

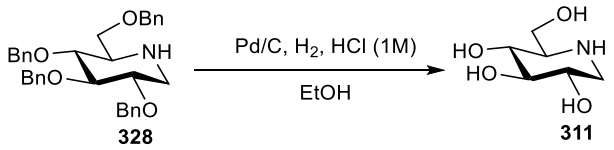

A solution of **328** (150 mg, 0.285 mmol) in EtOH (10 mL) was acidified to pH ~2 with 1M aq HCl. Pd/C (10 wt%, 30.3 mg) was added and the mixture was exposed to 4 bar of hydrogen for 20 hours. The reaction mixture was filtered over Celite® and the filter cake was rinsed successively with MeOH (4×20 mL) and H_2O (2×20 mL). The combined filtrate was concentrated and co-evaporated with MeOH (3×50 mL). The residue was purified by flash column chromatography with aluminum oxide (ammonium hydroxide added to the solvent) to provide **311** as a colorless oil (46.7 mg, 98% yield). ^{1}H NMR (300 MHz, D_2O) δ 3.77 (dd, J = 12.7, 3.2 Hz, 1H), 3.70 (dd, J = 12.8, 5.3 Hz, 1H), 3.60 (ddd, J = 10.5, 5.2, 3.1 Hz, 1H), 3.44-3.39 (m,1H), 3.36-3.30 (m,2H), 3.04-2.99 (m, 1H), 2.82-2.76 (m,1H). ^{13}C NMR (100 MHz, D_2O) δ 76.1, 67.8, 67.0, 60.0, 57.7, 45.9. LRMS ESI-MS m/z calcd for $C_6H_{14}NO_4$ m/z $[M+H]^+$ 164.2, found 164.1. All spectral data was consistent with that reported in the literature.[12]

D-galactono-δ-lactam (329)

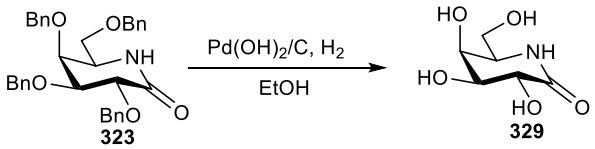

323 (206 mg, 0.383 mmol) was dissolved in EtOH (6 mL). $Pd(OH)_2/C$ (20.3 mg) was added to the mixture and exposed to 20 bar of hydrogen overnight. The reaction mixture was filtered over Celite® and the filter cake was rinsed successively with MeOH (4×20 mL) and H_2O (2×20 mL). The combined filtrate was concentrated in *vacuo.* to provide **329** as a brown solid (41.4 mg, 61% yield). ^{1}H NMR (300 MHz, D_2O) δ 4.12-4.07 (m, 2H), 3.82 (dd, J = 10.1, 2.5 Hz, 1H), 3.70-3.62 (m, 1H), 3.58-3.53 (m, 2H). ^{13}C NMR (125 MHz, D_2O): δ 173.5, 72.1, 69.2, 67.7, 60.8, 54.7. LRMS ESI-MS m/z calcd for $C_{34}H_{36}NO_5$ $[M + H]^+$: 538.7, found 538.3. All spectral data was consistent with that reported in the literature.[11]

2,3,4,6,-tetra-*O*-benzyl-D-glucono-δ-lactone (332)

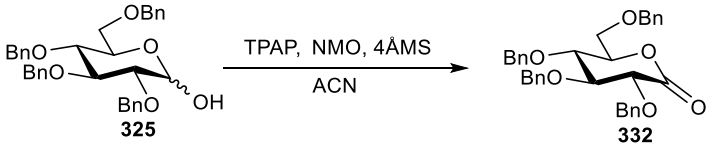

325 (3.04 g, 5.62 mmol) and 4-methylmorpholine-*N*-oxide (975 mg, 8.32 mmol) was dissolved in acetonitrile (30 mL) containing activated 4Å molecular sieves. This mixture was stirred for 1h and tetrapropylammoniumperruthenate (98.8 mg, 0.281 mmol) was added and this solution was stirred till TLC indicated complete consumption of the starting material. The crude mixture was filtered over Celite® and concentrated under *vacuo.* The resulting crude mixture was diluted with ethyl acetate and washed (2x) with a saturated solution of sodium thiosulfate. Afterwards, it was washed with brine, dried over MgSO, filtered and concentrated in *vacuo.* This gave **332** as a clear oil (1.33g, 44% yield). The crude product was not purified at this stage and carried forward to the next reaction.

2,3,4,6 tetra-*O*-benzyl-D-gluconamide (333)

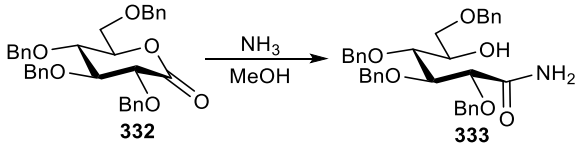

332 **333**

332 (1.33 g, 2.47 mmol) was dissolved in 50 mL of an 8N ammonia in MeOH. After stirring for 1.5 hour under nitrogen atmosphere the reaction mixture was concentrated in *vacuo.* Recrystallization of the resulting white solid from ethyl acetate and petroleum ether afforded **333** as white crystals (1.33 g, 97% yield). ^{1}H NMR (500 MHz, $CDCl_3$) δ 7.36-7.24 (m, 20H), 6.62 (br s, 1H), 5.45 (br s, 1H), 4.75-4.49 (m, 8H), 4.26 (d, J = 3.4 Hz, 1H), 4.15-4.07 (m, 1H), 3.92-3.88 (m, 2H), 3.65 (dd, J = 9.5, 2.9 Hz, 1H), 3.61 (dd, J = 9.5, 5.3 Hz, 1H), 2.82 (br s, 1H).^{13}C NMR (125 MHz, $CDCl_3$): δ 173.9, 138.1, 138.0, 137.7, 136.7, 129.0, 128.6, 128.4, 128.3, 128.2, 128.2, 128.0, 127.8, 127.7, 127.7, 125.3, 80.6, 79.6, 77.6, 75.2, 74.1, 73.7, 73.4, 71.3, 71.0. LRMS ESI-MS *m/z* calcd for $C_{34}H_{38}NO_6$ $[M + H]^+$: 556.7, found 556.6. All spectral data was consistent with that reported in the literature.[11]

2,3,4,6-tetra-*O*-benzyl-D-glucono-δ-lactam (334)

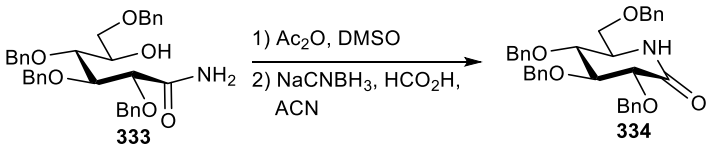

333 **334**

333 (1.33 g, 2.39 mmol) was dissolved in 10 mL dimethyl sulfoxide and 5 mL acetic anhydride and stirred under a nitrogen atmosphere for 12 hours. 40 mL water was added and the mixture was stirred for another 15 minutes during which yellow oil precipitated. The water layer was then removed and the residue was dissolved in dichloromethane and extracted with brine. The organic fractions were dried with $MgSO_4$ and concentrated in *vacuo*. to give 1.21 g of a yellow syrup. The crude product was not purified at this stage and carried forward to the next reaction. The product were dissolved in 20 mL acetonitrile and 5.3 mL formic acid was added. Sodium cyanoborohydride (227 mg, 3.61 mmol) was added and the reaction mixture was refluxed for 2h. The mixture was then cooled in ice and the reaction was quenched by adding aq. HCl (0.1 M). After stirring for 15 minutes, the mixture was poured into a mixture of ethyl acetate / saturated aqueous $NaHCO_3$, solution (1:1. 100 mL). The aqueous layer was separated and extracted with ethyl acetate. The combined organic fractions were then washed with brine and dried over $MgSO_4$, filtered and concentrated in *vacuo.* the resulting white solid was recrystallized from ethyl acetate and petroleum ether to give **334** as white powder (861 mg, 67% yield over three steps). ^{1}H NMR (500 MHz, $CDCl_3$) δ 7.41-7.15 (m, 20H), 5.95 (br s, 1H), 5.14 (d, J = 11.3 Hz, 1H), 4.86-4.69(m, 4H), 4.48-4.42 (m, 3H), 3.98 (d, J = 8.0 Hz, 1H), 3.89 (t, J = 7.8 Hz, 1H), 3.56-3.48 (m, 3H), 3.27-3.23 (m, 1H). ^{13}C NMR (125 MHz, $CDCl_3$): δ 170.4, 138.0, 137.8, 137.5, 137.2, 128.5, 128.4, 128.4, 128.3, 128.1, 128.0, 128.0, 127.9, 127.8, 82.3, 78.7, 77.1, 74.7, 74.6, 74.6, 73.3, 70.0, 53.7. LRMS ESI-MS *m/z* calcd for $C_{34}H_{36}NO_5$ $[M + H]^+$: 538.7, found 538.3. All spectral data was consistent with that reported in the literature.[11]

D-glucono-δ-lactam (330)

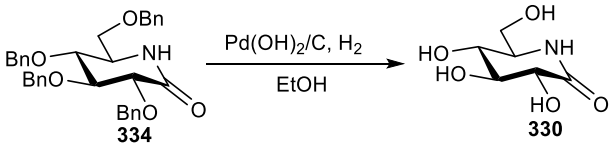

334 (84.8 mg, 0.158 mmol) was dissolved in EtOH (3 mL). $Pd(OH)_2/C$ (10.4 mg) was added to the mixture and exposed to 20 bar of hydrogen overnight. The reaction mixture was filtered over Celite® and the filter cake was rinsed successively with MeOH (4×10 mL) and H_2O (2×10 mL). The combined filtrate was concentrated in *vacuo.* to give **330** as a brown solid (19.9 mg, 71% yield). ^{1}H NMR (300 MHz, D_2O) δ 3.87-3.79 (m, 2H), 3.65-3.57 (m, 4H), 3.23-3.19 (m, 1H). ^{13}C NMR (125 MHz, D_2O): δ173.3, 73.2, 70.5, 67.4, 60.1, 56.8. LRMS ESI-MS *m/z* calcd for $C_{34}H_{36}NO_5$ $[M + H]^+$: 538.7, found 538.3. All spectral data was consistent with that reported in the literature.[11]

***N*-methyl-D-gluco-1-deoxynojirimycin (331)**

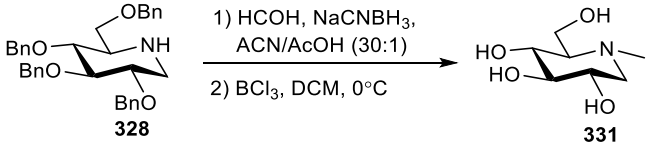

Formaldehyde (43.1 mg, 0.12 mL of a 35 wt% solution in water 1.43 mmol) and $NaCNBH_3$ (54.1 mg, 0.861 mmol) were successively added to a solution of **328** (150 mg, 0.287 mmol) in CH_3CN/AcOH (3 mL, 30:1, v/v). The reaction mixture was stirred for 20 hours after which sat. aq. $NaHCO_3$ (10 mL) was added and the resulting mixture was extracted with Et_2O (3×10 mL). The combined organic phases were dried (Na_2SO_4) and concentrated to provide the crude *N*-methylated intermediate. The crude intermediate was co-evaporated with dichloroethane and dissolved in CH_2Cl_2 (3.6 mL). The solution was cooled to 0 °C and BCl_3 (3.9 mL, 1 M in CH_2Cl_2) was added. After stirring for 20 hours at 0 °C MeOH (5 mL) was carefully added. The mixture was concentrated and co-evaporated with toluene. The residue was purified by flash chromatography (containing ammonium hydroxide in the solvent) to produce **331** as a colorless oil (16.1 mg, 10.7% yield over two steps). ^{1}H NMR (300 MHz, D_2O) δ 3.95-3.83 (m, 2H), 3.69-3.60 (m, 1H), 3.53-3.50 (m, 1H), 3.40-3.33 (m, 2H), 2.94-2.84 (m, 2H), 2.79 (s, 3H). ^{13}C NMR (100 MHz, D_2O) δ 72.6, 69.8, 66.1, 64.3, 59.0, 57.1, 40.8. LRMS ESI-MS *m/z* calcd for $C_7H_{15}NNaO_4$ *m/z* $[M+Na]^+$ 200.2 , found 200.5. All spectral data was consistent with that reported in the literature.[13]

1-deoxy-D-glucose (335)

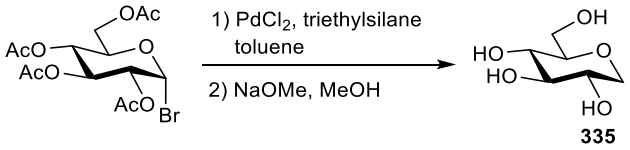

335

2,3,4,6-tetra-*O*-acetyl-α-D-glucopyranosyl bromide (498 mg, 1.21 mmol) was dissolved in toluene (15 mL). Triethylsilane (1.8 mL, 11.1 mmol) and palladium chloride (71.1 mg, 0.402 mmol) were then added and the reaction was stirred till the starting materials were fully consumed. The reaction was then concentrated in *vacuo.* and filtered over a pad of silica gel and ceoncentrated in *vacuo.* and dissolved in MeOH (20 mL). A 1 M NaOMe/MeOH solution is then added till pH = 9 and the reaction is left to stir overnight. The reaction is quenched using Amberlite® IR-120 acidic resin till pH = 7. The solution is then filtered and concentrated in *vacuo*. to give **335** as a white solid (198 mg, 64% yield over two steps). ^{1}H NMR (300 MHz, $CDCl_3$): δ 3.85 (dd, *J* = 11.1, 5.6 Hz, 1H), 3.75 (dd, *J* = 12.1, 1.7 Hz, 1H), 3.56-3.42 (m, 2H), 3.33-3.20 (m, 3H), 3.18-3.11 (m, 1H). ^{13}C NMR (100 MHz, $CDCl_3$): δ 80.2, 77.4, 69.7, 69.3, 68.8, 60.9. LRMS (ESI): *m/z* calcd. for $C_6H_{12}NaO_5$ $[M+Na]^+$ 187.2, found, 187.4.

4-methoxyphenyl-β-D-gluconopyranoside (507)

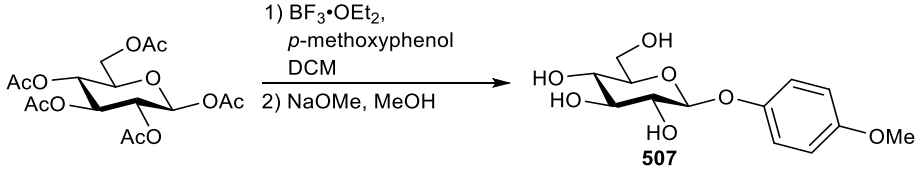

507

β-D-glucose pentacetate (5.14 g, 13.2 mmol) was dissolved in DCM (50 mL) and Boron trilfluoride diethyl etherate (3.2 mL, 25.6 mmol) was added to the mixture. The solution was stirred overnight. The reaction is the quenched with saturated $NaHCO_3$ and the mixture is diluted with DCM and extracted with saturated $NaHCO_3$ (2x). The organic layers were combined and dried with $MgSO_4$, filtered and concentrated under *vacuo.* The syrup is then dissolved in a minimum about of EtOAc and heptanes are added till a white solid formed. This white solid was removed through filtration and dissolved in MeOH (50 mL). A 1 M NaOMe/MeOH solution is then added till pH = 9 and the reaction is left to stir overnight. The reaction is quenched using Amberlite® IR-120 acidic resin till pH = 7. The solution is then filtered and concentrated in *vacuo*. to give **507** as a white solid (2.79 g, 74% yield over two steps). ^{1}H NMR (300 MHz, $CDCl_3$): δ 6.98 (d, *J* = 8.8 Hz, 2H), 6.84 (d, *J* = 8.8 Hz, 2H), 4.87 (d , *J* = 7.6 Hz, 1H), 3.79 (dd, *J* = 12.4, 2.1, 1H), 3.67 (s, 3H), 3.60 (dd, *J* = 12.4, 5.8, 1H), 3.49-3.31 (m, 4H). ^{13}C NMR (100 MHz, $CDCl_3$): δ 155.0, 150.8, 118.1, 115.0, 101.1, 76.0, 75.5, 72.9, 69.4, 60.5, 55.7. LRMS (ESI): *m/z* calcd. for $C_{13}H_{18}NaO_6$ $[M+Na]^+$ 293.2, found, 293.1.

6-tosyl-4-methoxyphenyl-β-D-gluconopyranoside (508)

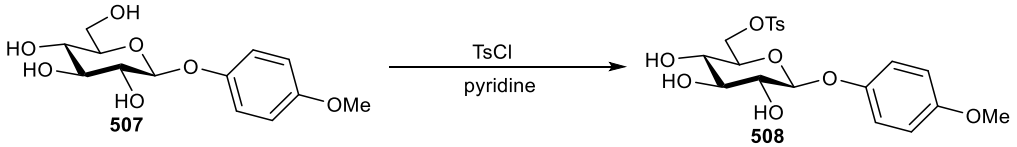

507 (986 mg, 3.44 mmol) was dissolved in pyridine (50 mL). The resulting solution was left to stir at 0 ^{o}C for 20 minutes. *p*-Toluenesulfonyl chloride (1.33 g, 6.98 mmol) was added to the solution and was left to stir overnight. The resulting mixture was diluted with DCM and extracted twice with saturated $NaHCO_3$. The organic layer was dried with $MgSO_4$, filtered, and concentrated in *vacuo*. The resulting oil is then purified by flash chromatography to give a **508** as a white solid (1.05 g, 69% yield).^{1}H NMR (300MHz, $CDCl_3$): δ 7.76 (d, *J* = 8.4 Hz, 2H), 7.25-7.22 (m, 2H), 6.92 (d, *J* = 9.1 Hz, 2H), 6.78 (d, *J* = 9.1 Hz, 2H), 4.69 (d , *J* = 7.1 Hz, 1H), 4.34-4.26 (m, 2H), 3.75 (s, 3H), 3.59-3.58 (m, 4H), 2.38 (s, 3H). ^{13}C NMR (100MHz, $CDCl_3$): δ 155.6, 150.8, 145.0, 132.5, 129.8, 128.0, 118.5, 114.5, 101.7, 75.9, 73.6, 73.3, 69.3, 68.4, 55.6, 21.6. LRMS (ESI): *m/z* calcd. for $C_{20}H_{25}O_7$ $[M+H]^+$ 441.5, found, 441.

6-azido-6-deoxy-4-methoxyphenyl-β-D-gluconopyranoside (509)

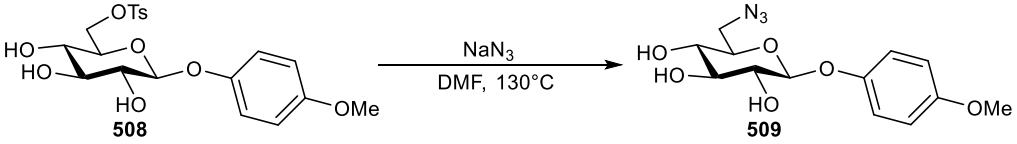

508 (2.58 g, 5.85 mmol) was dissolved in dry N,N-dimethylformamide (50 mL) and sodium azide (1.33 g, 20.5 mmol) was added. The reaction was then refluxed at 130 ^{o}C overnight. The resulting mixture was then concentrated in *vacuo*. The resulting brown syrup is then purified by flash chromatography to give a **509** as a clear oil (1.16 g, 64% yield). ^{1}H NMR (300MHz, $CDCl_3$): δ 7.05 (d, *J* = 9.1 Hz, 2H), 6.84 (d, *J* = 9.1 Hz, 2H), 4.78 (d, *J* = 7.7 Hz, 1H), 3.76 (s, 3H), 3.60-3.55 (m, 1H), 3.53-3.49 (m, 1H), 3.46-3.40 (m, 3H). ^{13}C NMR (100MHz, $CDCl_3$): δ 155.4, 151.6, 118.2, 114.0, 102.2, 76.2, 75.3, 73.5, 70.8, 54.5, 51.4. LRMS (ESI): *m/z* calcd. for $C_{13}H_{17}KN_3O_6$ $[M+K]^+$ 350.4, found, 350.6.

6-amino-6-deoxy-4-methoxyphenyl-β-D-gluconopyranoside (504)

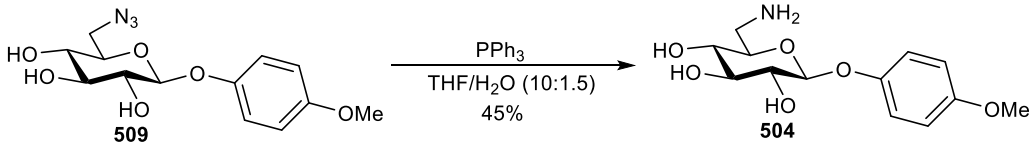

509 (411 mg, 1.32 mmol) was dissolved in a solution of THF/water (10 mL, 10:1.5), the resulting solution was stirred for 20 minutes. triphenylphosphine (691 mg, 2.63 mmol) was added and the reaction was stirred overnight. The solution was then concentrated in *vacuo.* and the resulting yellow oil is then purified by flash chromatography to give a **504** as a yellow solid (169 mg, 45% yield). ^{1}H NMR (300MHz, D_2O): δ 7.01 (d, *J* = 9.1 Hz, 2H), 6.88 (d, *J* = 9.1 Hz, 2H), 4.96 (d, *J* = 7.4 Hz, 1H), 3.70 (s, 3H), 3.47 (t, *J* = 8.1 Hz, 2H), 3.41-3.28 (m, 3H), 3.07 (dd, *J* = 13.6, 8.8 Hz, 1H). ^{13}C NMR (75MHz, D_2O): δ 154.8, 150.4, 118.2, 115.0, 101.0, 74.9, 72.6, 71.7, 71.0, 55.7, 40.2. LRMS (ESI): *m/z* calcd. for $C_{13}H_{20}O_6$ $[M+H]^+$ 286.3, found, 286.9.

***N*-gluconoamide-6-amino-6-deoxy-4-methoxyphenyl-β-D-gluconopyranoside (505)**

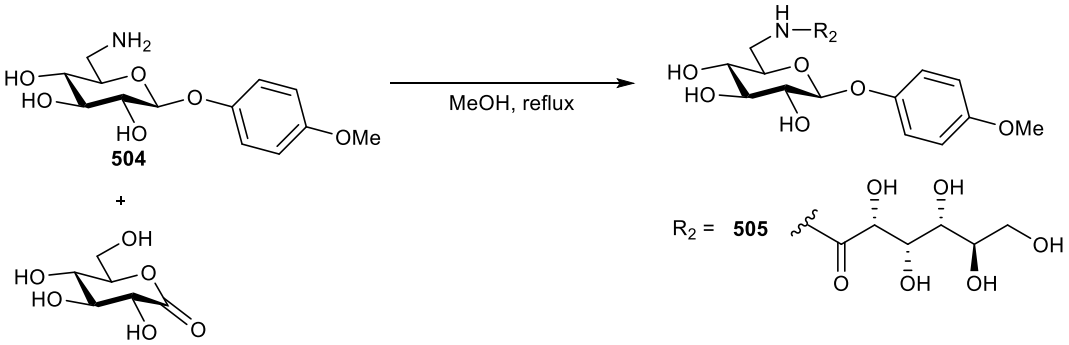

504 (112 mg, 0.386 mmol) and δ-gluconolactone (82.5 mg, 0.463 mmol) were dissolved in MeOH (10 mL) and the mixture is then refluxed overnight. The mixture is then concentrated in *vacuo.* and the resulting solid was recrystallized from boiling EtOH to give **505** as a white solid (55.5 mg, 31% yield). ^{1}H NMR (300MHz, D_2O): δ 6.97 (d, *J* = 9.0 Hz, 2H), 6.85 (d, *J* = 9.0 Hz, 2H), 4.87 (d, *J* = 7.6 Hz, 1H), 4.20 (d, *J* = 3.7 Hz, 1H), 3.93 (t, *J* = 2.9 Hz, 1H), 3.68 (s, 3H), 3.64-3.50 (m, 6H), 3.46-3.37 (m, 3H), 3.27 (t, *J* = 8.9 Hz, 1H) . ^{13}C NMR (75MHz, D_2O): δ 174.6, 154.7, 150.6, 118.2, 114.9, 101.0, 75.0, 74.0, 73.2, 72.8, 71.9, 71.0, 70.6, 70.3, 62.5, 55.7, 39.5. LRMS (ESI): *m/z* calcd. for $C_{19}H_{29}NNaO_{12}$ $[M+Na]^+$ 486.4, found, 486.8.

***N*-galactonoamide-6-amino-6-deoxy-4-methoxyphenyl-β-D-gluconopyranoside (506)**

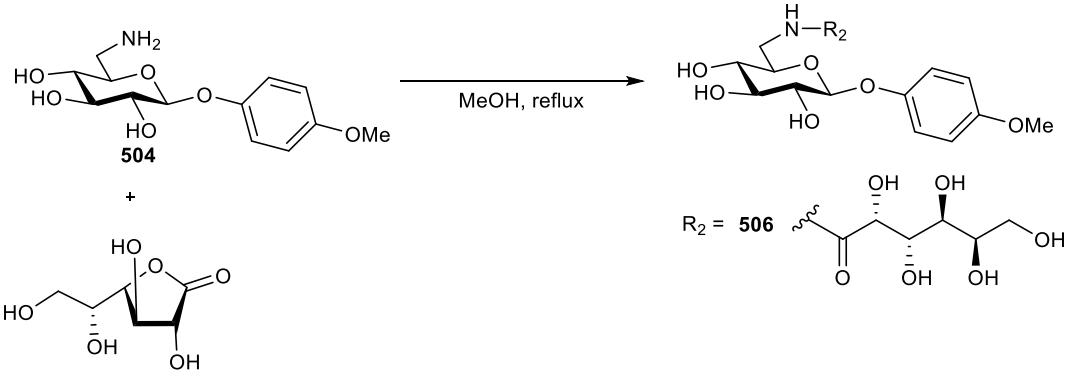

504 (112 mg, 0.386 mmol) and D-galactono-1,4-lactone (82.5 mg, 0.463 mmol) were dissolved in MeOH (10 mL) and the mixture is then refluxed overnight. The mixture is then concentrated in *vacuo.* and the resulting solid was recrystallized from boiling EtOH to give **506** as a white solid (50.1 mg, 28% yield). ^{1}H NMR (300MHz, D_2O): δ 7.10 (d, *J* = 9.0 Hz, 2H), 6.96 (d, *J* = 9.0 Hz, 2H), 5.06 (d, *J* = 7.6 Hz, 1H), 4.30 (d, *J* = 3.7 Hz, 1H), 4.02-3.89 (m, 1H), 3.78 (s, 3H), 3.75-3.63 (m, 4H), 3.60-3.54 (m, 2H), 3.44-3.38 (m, 3H) 3.15 (dd, *J* = 13.4, 9.2 Hz, 1H) . ^{13}C NMR (75MHz, D_2O): δ 176.5, 154.6, 150.7, 118.1, 114.9, 101.6, 77.0, 70.9, 70.7, 70.5, 69.8, 69.0, 67.7, 63.1, 60.4, 57.0, 55.7. LRMS (ESI): *m/z* calcd. for $C_{19}H_{29}NNaO_{12}$ $[M+Na]^+$ 486.4, found, 486.5.

4-methoxyphenyl-β-D-ribo-hexapyranoside-3-ulose (510)

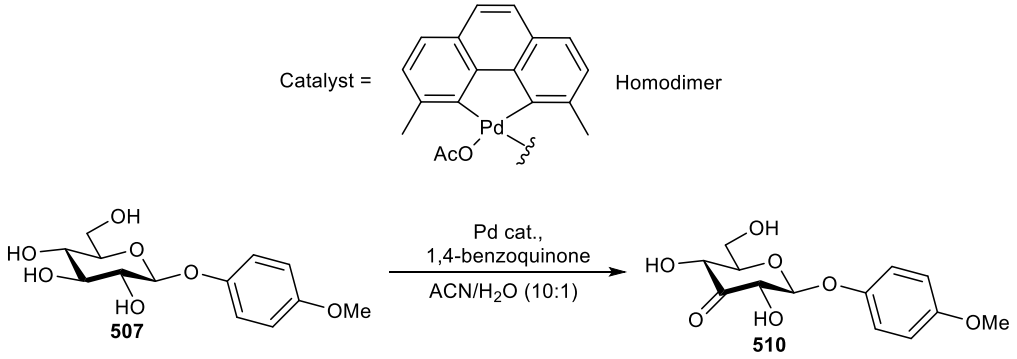

507 (99.9 mg, 0.349 mmol) and benzoquinone (113.5 mg, 1.05 mmol) were dissolved in a mixture of ACN/H_2O (11 mL, 10:1). [(2,9-dimethyl-1,10-phenanthroline)-Pd(μ-OAc)]$_2$(OTf)$_2$ (1.83 mg, 0.00175 mmol) is then added to the reaction and it was stirring overnight. Toluene (5 mL) is then added to the reaction and the mixture is extracted with water (2x). The combined aqueous layers were washed with diethyl ether and the aqueous layer is then filtered and concentrated in *vacuo.* the resulting brown solid is then purified by flash chromatography to give a **510** as a white solid (97.2 mg, 98% yield). ^{1}H NMR (300MHz, CD_3OD): δ 7.10 (d, J = 9.2 Hz, 2H), 6.86 (d, J = 9.2 Hz, 2H), 4.85 (d, J = 7.6 Hz, 1H), 4.39 (dd, J = 7.8, 1.7 Hz, 1H), 4.33 (d, J = 10.1, 1.7 Hz, 1H), 3.97 (dd, J = 12.1, 2.2, 1H), 3.83 (dd, J = 12.1, 4.8 Hz, 1H), 3.76 (s, 3H), 3.49-3.44 (m, 1H). ^{13}C NMR (75MHz, D_2O): δ205.1, 118.1, 114.1, 103.4, 76.9, 76.7, 72.1, 60.9, 54.6. LRMS (ESI): *m/z* calcd. for $C_{13}H_{17}O_7$ $[M+H]^+$ 285.3, found, 285.6.

***E/Z*-methyl-3-*O*-methyloxime-4-methoxylphenyl-β-D-gluconopyranoside (511)**

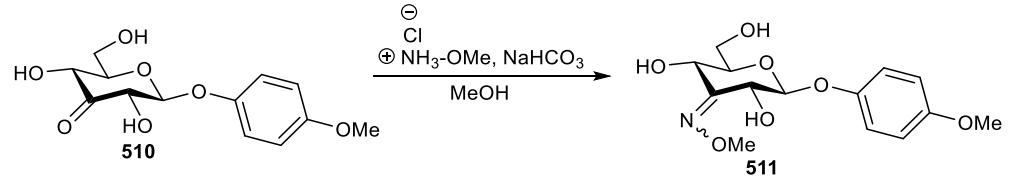

510 (1.06 g, 3.73 mmol) and $NaHCO_3$ (1.25 g, 14.9 mmol) was dissolved in MeOH (50 mL). *O*-methylhydroxylamine hydrochloride (1.25 g, 14.9 mmol) was added and the reaction was refluxed for 2h. The salts were then filtered and the filtrate was concentrated in *vacuo.* the resulting residue was extracted with hot ethyl acetate and concentrated in *vacuo.* the resulting yellow solid is then purified by flash chromatography to give **511** as a white solid (913 mg, 78% yield). ^{1}H NMR (300MHz, D_2O): δ 6.99-6.96 (m, 4H), 6.88-6.85 (m, 4H), 5.43 (d, J = 5.1 Hz, 1H), 5.40 (d, J = 3.8 Hz, 1H), 4.73 (d, J = 5.1 Hz, 1H), 4.41 (d, J = 5.6 Hz, 1H), 4.28 (d, J = 3.8 Hz, 1H), 3.94-3.91 (m, 2H), 3.83 (s, 3H), 3.82 (s, 3H), 3.69-3.68 (m, 8H), 3.62 (dd, J = 12.1, 4.2 Hz, 1H), 3.56-3.51 (m, 2H). ^{13}C NMR (75MHz, D_2O): δ 183.7, 155.1, 154.6, 154.1, 150.1, 149.9, 118.4, 118.1, 116.3, 115.0, 115.0, 110.6, 99.1, 78.5, 76.4, 69.6, 66.2, 64.9, 62.2, 62.1, 62.0, 61.4, 61.1, 55.7. LRMS (ESI): *m/z* calcd. for $C_{19}H_{20}NO_7$ $[M+H]^+$ 314.3, found, 314.7.

3-amino-3-deoxy-4-methoxyphenyl-β-D-gluconopyranoside (501)

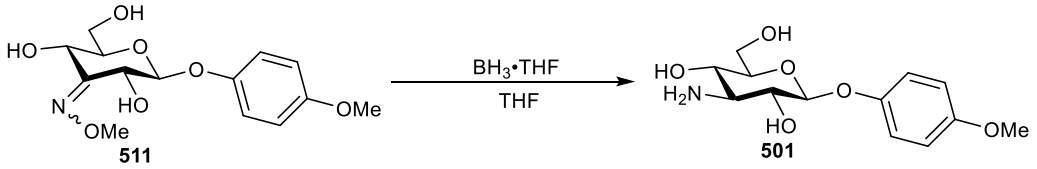

511 (302 mg, 0.964 mmol) was dissolved in THF (5 mL). 1M Borane-THF complex (5 mL, 4.82 mmol) was then added and the reaction was stirred overnight. MeOH is then added dropwise till the evolution of gas has ceased. The mixture is then concentrated in *vacuo.* and purified by flash chromatography to give **501** as a yellow solid (121 mg, 44% yield). ^{1}H NMR (300MHz, D_2O): δ 6.99 (d, *J* = 9.1 Hz, 2H), 6.86 (d, *J* = 9.1 Hz, 2H), 4.90 (d, *J* = 7.9 Hz, 1H), 3.78 (dd, *J* = 12.3, 2.3 Hz, 1H), 3.68 (s, 3H), 3.61 (dd, *J* = 12.3, 5.9 Hz, 1H), 3.49 (ddd, *J* = 8.8, 5.9, 2.4 Hz, 1H), 3.34-3.22 (m, 2H), 2.78 (t, *J* = 9.8 Hz, 1H). ^{13}C NMR (75MHz, D_2O): δ 154.6, 150.8, 118.1, 114.9, 101.5, 77.1, 72.4, 68.9, 60.5, 57.5, 55.7. LRMS (ESI): *m/z* calcd. for $C_{13}H_{19}NNaO_6$ $[M+Na]^+$ 308.3, found, 308.2.

***N*-gluconoamide-3-amino-3-deoxy-4-methoxyphenyl-β-D-gluconopyranoside (502)**

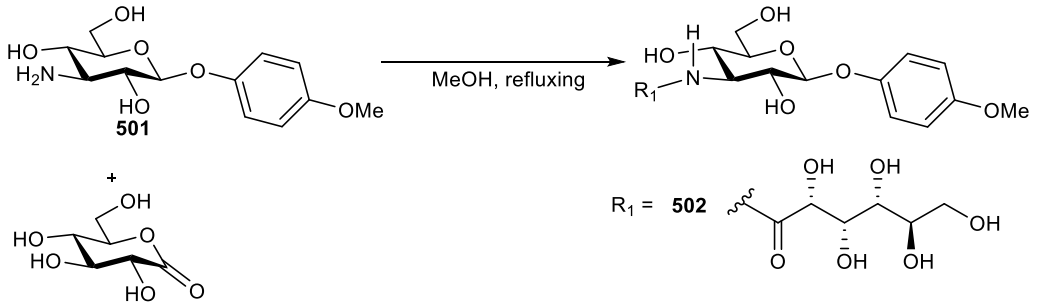

501 (50.7 mg, 0.178 mmol) and δ-gluconolactone (41.2 mg, 0.196 mmol) were dissolved in MeOH (10 mL) and the mixture is then refluxed overnight. The mixture is then concentrated in *vacuo.* and the resulting solid was recrystallized from boiling EtOH to give **502** as a white solid (25.6 mg, 31% yield). ^{1}H NMR (300MHz, D_2O): δ 7.00 (d, *J* = 9.1 Hz, 2H), 6.87 (d, *J* = 9.1 Hz, 2H), 5.01 (d, *J* = 7.8 Hz, 1H), 4.26 (d, *J* = 4.0 Hz, 1H), 4.03-3.97 (m, 1H), 3.94-3.91 (m, 1H), 3.80 (dd, *J* = 12.1, 1.6 Hz, 1H), 3.70 (s, 3H), 3.66-3.60 (m, 4H), 3.57-3.47 (m, 4H). ^{13}C NMR (75MHz, D_2O): δ 175.4, 154.7, 150.8, 118.2, 115.0, 101.6, 73.5, 71.9, 71.1, 70.7, 70.3, 69.4, 67.6, 62.6, 57.6, 57.0, 55.8. LRMS (ESI): *m/z* calcd. for $C_{19}H_{29}NNaO_{12}$ $[M+Na]^+$ 486.4, found, 486.7.

***N*-galactonoamide-3-amino-3-deoxy-4-methoxyphenyl-β-D-gluconopyranoside (503)**

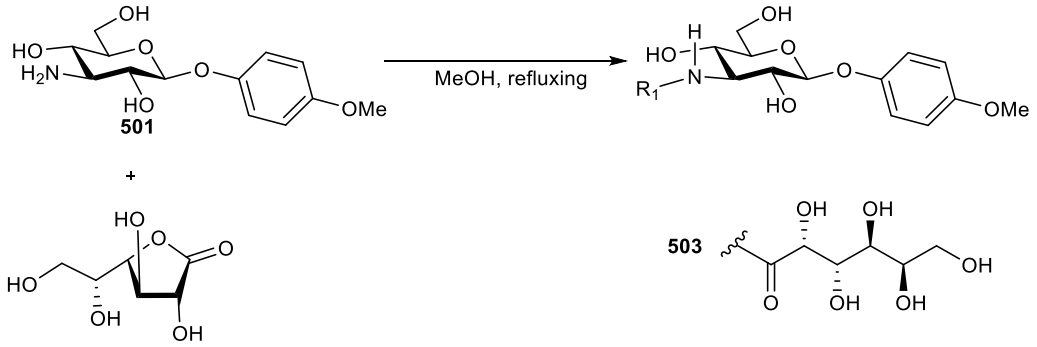

501 (115 mg, 0.403 mmol) and D-galactono-1,4-lactone (93.3 mg, 0.524 mmol) were dissolved in MeOH (10 mL) and the mixture is then refluxed overnight. The mixture is then concentrated in *vacuo.* and the resulting solid was recrystallized from boiling EtOH to give **503** as a white solid (52.3 mg, 28% yield). ^{1}H NMR (300MHz, D_2O): δ 6.97 (d, *J* = 9.0 Hz, 2H), 6.85 (d, *J* = 9.0 Hz, 2H), 4.98 (d, *J* = 7.6 Hz, 1H), 4.40 (d, *J* = 3.7 Hz, 1H), 3.94 (t, *J* = 2.9 Hz, 1H), 3.85-3.78 (m, 2H), 3.23 (s, 3H), 3.64 (dd, *J* = 12.2, 5.2 Hz, 1H) 3.59-3.51 (m, 6H). ^{13}C NMR (75MHz, D_2O): δ 176.6, 154.7, 150.7, 118.1, 115.0, 101.6, 77.1, 70.9, 70.5, 70.8, 70.5, 69.9, 63.1, 60.4, 57.1, 55.7. LRMS (ESI): *m/z* calcd. for $C_{19}H_{29}NNaO_{12}$ $[M+Na]^+$ 486.4, found, 486.5.

General procedure for the synthesis of *N*-cycloalkyl-D-glucoanamide

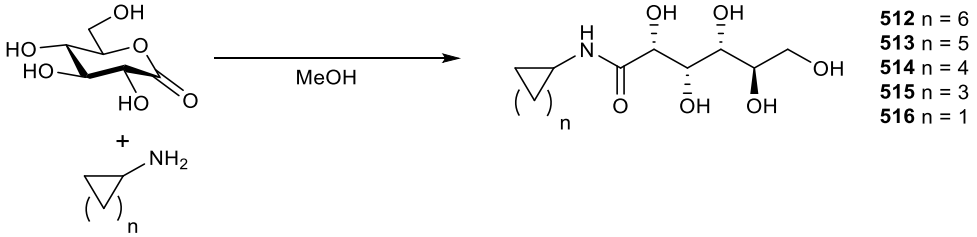

To a solution of D-gluconic acid-*δ*-lactone (998 mg, 5.61 mmol) in MeOH (30 mL) was added cycloalkylamine (1 eq.). The mixture was refluxed overnight then cooled in an ice bath. The precipitate was filtered off and washed with cold EtOH to afford a white powder.

***N*-cyclooctyl-D-gluconoamide (512)**

925 mg, 54% yield. ^{1}H NMR (400 MHz, D_2O): δ 4.12 (d, *J* = 4.1 Hz, 1H), 3.91 (dd, *J* = 4.0, 3.0 Hz, 1H), 3.80-3.75 (m, 1H), 3.67 (dd, *J* = 11.6, 2.8 Hz, 1H), 3.61-3.48 (m, 3H), 1.63-1.51 (m, 15H). ^{13}C NMR (100 MHz, D_2O): δ 172.4, 73.4, 72.1, 71.1, 70.3, 62.6, 49.8, 31.4, 31.4, 26.5, 25.0, 23.3. LRMS (ESI): *m/z* calcd. for $C_{14}H_{27}NNaO_6$ $[M+Na]^+$ 328.4, found, 328.6.

***N*-cycloheptyl-D-gluconoamide (513)**

834 mg, 51% yield. ^{1}H NMR (400 MHz, D_2O): δ 4.13 (d, *J* = 4.0 Hz, 1H), 3.94 (t, *J* = 3.4 Hz, 1H), 3.78-3.68 (m, 2H), 3.65-3.55 (m, 2H), 3.51 (dd, *J* = 11.6, 6.1 Hz 1H), 1.77-1.67 (m, 2H), 1.55-1.30 (m, 10H). ^{13}C NMR (100 MHz, D_2O): δ 172.5, 73.4, 72.1, 71.1, 70.3, 62.6, 50.9, 34.0, 34.0, 27.5, 23.7. LRMS (ESI): *m/z* calcd. for $C_{13}H_{25}NO_6$ $[M]^+$ 291.3, found, 291.2.

***N*-cyclohexyl-D-gluconoamide (514)**
498 mg, 32% yield. ^{1}H NMR (400 MHz, D_2O): δ 4.13 (d, *J* = 4.0 Hz, 1H), 3.93 (t, *J* = 3.0 Hz, 1H), 3.69 (dd, *J* = 11.6, 2.7 Hz 1H), 3.64-3.60 (m, 1H), 3.57 (dd, *J* = 7.8, 2.9 Hz, 1H), 3.52 (dd, *J* = 11.6, 6.1 Hz 2H), 1.73-1.56 (m, 4H), 1.51-1.45 (m, 1H), 1.23-0.97 (m, 5H). ^{13}C NMR (100 MHz, D_2O): δ 172.9, 73.4, 72.1, 71.0, 70.3, 62.6, 48.8, 31.9, 31.8, 24.9, 24.4. LRMS (ESI): *m/z* calcd. for $C_{12}H_{24}NO_6$ $[M+H]^+$ 278.3, found, 278.6.

***N*-cyclopentyl-D-gluconoamide (515)**
561 mg, 38% yield. ^{1}H NMR (400 MHz, D_2O): δ 4.13 (d, *J* = 4.0 Hz, 1H), 4.11-3.90 (m, 2H), 3.69 (dd, *J* = 11.6, 2.7 Hz 1H), 3.65-3.60 (m, 1H), 3.57 (dd, *J* = 7.7, 2.9 Hz 1H), 3.51 (dd, *J* = 11.6, 6.1 Hz 1H) 1.85-1.75 (m, 2H), 1.32-1.61 (m, 6H). ^{13}C NMR (100 MHz, D_2O): δ 173.4, 73.4, 72.1, 71.1, 70.3, 62.6, 51.2, 32.1, 32.0, 23.4. LRMS (ESI): *m/z* calcd. for $C_{11}H_{21}NNaO_6$ $[M+Na]^+$ 286.3, found, 286.1.

***N*-cyclopppropyl-D-gluconoamide (516)**
567 mg, 43% yield. ^{1}H NMR (400 MHz, D_2O): δ 4.13 (d, *J* = 4.0 Hz, 1H), 3.93 (t, *J* = 3.0 Hz 1H), 3.69 (dd, *J* = 11.6, 2.7 Hz 1H), 3.65-3.55 (m, 2H), 3.57 (dd, *J* = 7.7, 2.9 Hz 1H), 3.51 (dd, *J* = 11.6, 6.1 Hz 1H) 2.51-2.47 (m, 1H), 0.67-0.61 (m, 2H), 0.47-0.40 (m, 2H). ^{13}C NMR (100 MHz, D_2O): δ 176.1, 73.2, 71.9, 71.0, 70.4, 62.6, 21.8, 5.4, 5.4. LRMS (ESI): *m/z* calcd. for $C_9H_{17}KNO_6$ $[M+K]^+$ 274.3, found, 274.1.

General procedure for the synthesis of *N*-cycloalkyl-2,3,5-tri-*O*-benzyl-D-arabinoamide

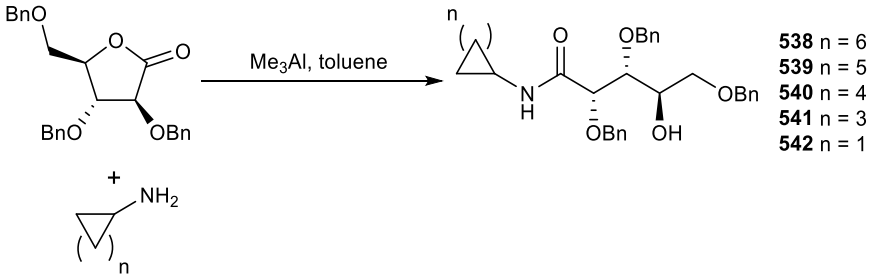

Cycloalkylamine (1.1 eq.) is dissolved in toluene (10 mL for 0.3 mmol of lactone) and trimethylaluminium (2 eq.) is added to the reaction and stirred for 1h. The ester (1 eq. in 5 mL of toluene) is then added and the reaction is then stirred overnight till the starting ester is fully consumed by TLC. The reaction is the quenched with 10% HCl dropwise and stirred for 30min till a white precipitate is formed. The precipitate is then filtered over Celite® and the mixture is portioned between EtOAc and water. The layers are separated and the aqueous layer is extracted with EtOAc (2x), dried with $MgSO_4$, filtered and concentrated in *vacuo.* The resulting syrup was then purified by flash chromatography.

***N*-cyclooctyl-2,3,5-tri-*O*-benzyl-D-arabinoamide (538)**
55.9 mg, 88% yield. ^{1}H NMR (300 MHz, $CDCl_3$): δ 7.40-7.00 (m, 15H), 6.75 (d, *J* = 8.5 Hz, 1H), 4.65 (d, *J* = 11.4 Hz, 1H), 4.55 (t, *J* = 11.6 Hz, 2H), 4.45- 4.35 (m, 3H), 4.27 (d, *J* = 2.0 Hz, 1H), 4.05 (dd, *J* = 8.8, 2.0 Hz, 1H), 3.92-3.87 (m, 2H), 3.60 (dd, *J* = 9.6, 3.2 Hz, 1H), 3.50 (dd, *J* = 9.6, 3.2 Hz, 1H), 1.70-1.40 (m, 15H). ^{13}C NMR (100 MHz, $CDCl_3$): δ 169.9, 137.8, 137.7, 137.0, 128.8, 128.7, 128.5, 128.4, 128.2, 128.2, 127.9, 127.9, 127.7, 110.0, 80.0, 74.7, 74.5, 73.3, 70.5, 69.3, 49.0, 31.8, 31.7, 27.2, 27.2, 25.2, 23.5. LRMS (ESI): *m/z* calcd. for $C_{34}H_{44}NO_5$ $[M+H]^+$ 546.7, found, 545.2.

***N*-cycloheptyl-2,3,5-tri-*O*-benzyl-D-arabinoamide (539)**
58.1 mg, 91% yield. ^{1}H NMR (300 MHz, $CDCl_3$): δ 7.40-7.10 (m, 13H), 6.75 (d, *J* = 8.3 Hz, 1H), 4.65 (d, *J* = 11.4 Hz, 1H), 4.59-4.50 (m, 2H), 4.45- 4.35 (m, 4H), 4.05 (dd, *J* = 8.8, 2.0 Hz, 1H), 3.95-3.85 (m, 2H), 3.60 (dd, *J* = 9.6, 3.2 Hz, 1H), 3.50 (dd, *J* = 9.5, 4.5 Hz, 1H), 1.85-1.77 (m, 2H), 1.60-1.20 (m, 11H). ^{13}C NMR (100 MHz, $CDCl_3$): δ 169.9, 137.9, 137.7, 137.0, 128.8, 128.7, 128.6, 128.5, 128.3, 128.2, 128.2, 127.9, 127.8, 127.7, 104.5, 80.0, 79.7, 74.7, 74.5, 73.3, 70.6, 69.4, 50.0, 35.8, 34.8, 28.0, 28.0, 25.2, 23.9, 23.9. LRMS (ESI): *m/z* calcd. for $C_{33}H_{41}NaNO_5$ $[M+Na]^+$ 554.7, found, 554.5.

***N*-cyclohexyl-2,3,5-tri-*O*-benzyl-D-arabinoamide (540)**
42.2 mg, 68% yield. ^{1}H NMR (300 MHz, $CDCl_3$): δ 7.36-7.17 (m, 15H), 7.16 (d, *J* = 8.7 Hz, 1H), 4.65 (d, *J* = 11.4 Hz, 1H), 4.56-4.52 (m, 2H), 4.43- 4.27 (m, 4H), 4.02 (dd, *J* = 8.9, 1.9 Hz, 1H), 4.01-4.00 (m, 1H), 3.60-3.58 (m, 1H), 3.57 (dd, *J* = 9.6, 3.3 Hz, 1H), 3.48 (dd, *J* = 9.6, 4.7 Hz, 1H), 1.77-1.03 (m, 10H). ^{13}C NMR (100 MHz, $CDCl_3$): δ 170.3, 137.8, 137.7, 137.0, 128.8, 128.7, 128.4, 128.4, 128.2, 127.9, 127.8, 127.7, 79.7, 79.6, 74.7, 74.5, 73.3, 70.5, 69.3, 47.7, 32.9, 32.8, 29.7, 25.4, 24.6. LRMS (ESI): *m/z* calcd. for $C_{32}H_{39}NaNO_5$ $[M+Na]^+$ 540.7, found, 540.9.

***N*-cyclopentyl-2,3,5-tri-*O*-benzyl-D-arabinoamide (541)**
44.1 mg, 73% yield. ^{1}H NMR (300 MHz, $CDCl_3$): δ 7.40-7.20 (m, 15H), 6.74 (d, *J* = 8.7 Hz, 1H), 4.71 (d, *J* = 11.5 Hz, 1H), 4.59-4.51 (m, 2H), 4.50- 4.32 (m, 4H), 4.20 (sextet, *J* = 6.9 Hz, 1H), 4.07-4.04 (m, 1H), 3.95-3.93 (m, 1H), 3.65-3.62 (m, 1H), 3.55 (dd, *J* = 9.6, 3.3 Hz, 1H), 3.54 (dd, *J* = 9.6, 4.7 Hz, 1H), 1.95-1.85 (m, 2H), 1.60-1.50 (m, 4H), 1.35-1.20 (m, 2H). ^{13}C NMR (100 MHz, $CDCl_3$): δ 170.8, 137.8, 137.7, 137.0, 128.7, 128.7, 128.4, 128.4, 128.2, 128.2, 127.9, 127.8, 127.7, 79.7, 74.7, 74.5, 73.3, 70.5, 69.3, 50.6, 33.1, 32.8, 23.6, 23.5. LRMS (ESI): *m/z* calcd. for $C_{31}H_{38}NO_5$ $[M+Na]^+$ 504.6, found, 504.2.

***N*-cyclopropyl-2,3,5-tri-*O*-benzyl-D-arabinoamide (542)**
33.7 mg, 59% yield. This compound was considered pure enough to be used crude to the next step.

General procedure for the synthesis of *N*-cycloalkyl-D-arabinoamide

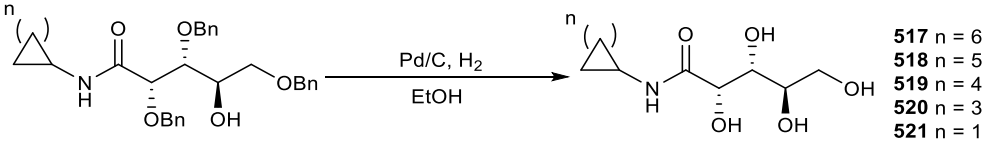

N-cycloalkyl-2,3,5-tri-*O*-benzyl-D-arabinoamide (1 eq.) is dissolved in EtOH (3 mL). Pd/C (10 mol %) is then added to reaction and the mixture is then exposed to 20 barr of hydrogen with vigorous stirring overnight. The reaction is then filtered over Celite® and concentrated in *vacuo*. The resulting syrup was recrystallized from MeOH/diethyl ether.

***N*-cyclooctyl-D-arabinoamide (517)**
22.8 mg, 94% yield. ^{1}H NMR (500 MHz, D_2O): δ 4.24 (d, *J* = 1.8 Hz, 1H), 3.82-3.78 (m, 1H), 3.73 (dd, *J* = 3.4, 2.8 Hz, 1H), 3.71-3.70 (m, 1H), 3.61 (dt, *J* = 6.2, 2.8 Hz, 1H), 3.53 (dd, *J* = 11.8, 6.2 Hz, 1H), 179-1.38 (m, 14H). ^{13}C NMR (100 MHz, D_2O): δ 173.4, 71.4, 70.7, 70.6, 62.9, 49.7, 31.4, 31.3, 26.5, 26.5, 25.0, 23.2, 23.1. LRMS (ESI): *m/z* calcd. for $C_{13}H_{25}NNaO_5$ $[M+Na]^+$ 298.4, found, 298.2.

***N*-cycloheptyl-D-arabinoamide (518)**
21.2 mg, 87% yield. ^{1}H NMR (500 MHz, D_2O): δ 4.20 (s, 1H), 3.69-3.66 (m, 2H), 3.60-3.55 (m, 1H), 3.49 (dd, *J* = 11.4, 6.3 Hz, 1H), 3.18-3.14 (m, 1H), 1.71-1.34 (m, 12H). ^{13}C NMR (100 MHz, D_2O): δ 173.4, 71.4, 70.6, 62.9, 50.7, 34.4, 33.9, 27.4, 23.6. LRMS (ESI): *m/z* calcd. for $C_{12}H_{23}NNaO_5$ $[M+Na]^+$ 284.3, found, 284.6.

***N*-cyclohexyl-D-arabinoamide (519)**
13.9 mg, 81% yield. ^{1}H NMR (500 MHz, D_2O): δ 4.21 (d, *J* = 1.6 Hz, 1H), 3.69-3.66 (m, 2H), 3.58 (dt, *J* = 6.2, 2.8 Hz, 1H), 3.48 (dd, *J* = 11.4, 6.3 Hz, 1H), 3.18-3.14 (m, 2H), 1.66-1.42 (m, 5H), 1.19-1.00 (m, 5H). ^{13}C NMR (100 MHz, D_2O): δ 173.9, 71.4, 70.6, 70.6, 62.9, 48.7, 31.9, 31.8, 24.8, 24.3. LRMS (ESI): *m/z* calcd. for $C_{12}H_{21}NKO_5$ $[M+K]^+$ 286.3, found, 286.5.

***N*-cyclopentyl-D-arabinoamide (520)**
19.6 mg, 86% yield. ^{1}H NMR (500 MHz, CD_3OD): δ 4.31 (s, 1H), 4.18-4.10 (m, 1H), 3.81-3.76 (m, 1H), 3.67-3.57 (m, 2H), 1.95-1.90 (m, 2H), 1.75-1.46 (m, 6H). ^{13}C NMR (100 MHz, D_2O): δ 174.3, 72.0, 71.3, 70.9, 63.5, 50.7, 32.2, 23.3, 23.3. LRMS (ESI): *m/z* calcd. for $C_{12}H_{20}NO_5$ $[M+H]^+$ 234.3, found, 234.8.

***N*-cyclopropyl-D-arabinoamide (521)**
11.2 mg, 92% yield. ^{1}H NMR (500 MHz, CD_3OD): δ mixture of rotamers: 4.29 (d, *J* = 1.3 Hz, 1H), 3.80-3.76 (m, 2H), 3.81-3.64-3.58 (m, 2H), 2.70-2.65 (m, 1H), 0.73-0.70 (m, 2H), 0.55-0.52 (m, 2H). ^{13}C NMR (100 MHz, D_2O): δ mixture of rotamers: 176.5, 175.3, 81.5, 74.2, 72.8, 72.0, 71.2, 70.9, 63.4, 59.5, 21.9, 21.8, 5.3, 5.3, 5.2, 5.2. LRMS (ESI): *m/z* calcd. for $C_8H_{15}NNaO_5$ $[M+Na]^+$ 228.2, found, 228.6.

Garner Aldehyde

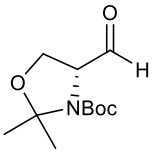

Garner aldehyde was prepared as previously described.[14] All spectral data was consistent with that reported in the literature.[14]

(S, *E*)-tert-butyl-4-(3-methoxy-3-oxoprop-1-en-1-yl)-2,2-dimethyloxazolidine-3-carboxylate (522)

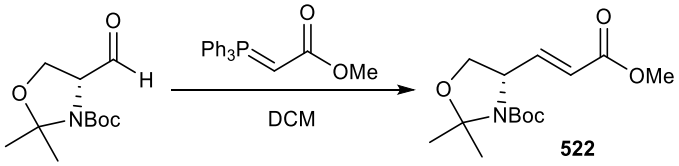

Garner aldehyde (1.67 g, 7.28 mmol) was dissolved in DCM (60 mL) and methyl (triphenylphosphoranylidene)acetate (3.14 g, 9.46 mmol) was added to the mixture. The reaction was stirred overnight and concentrated in *vacuo.* The mixture is then purified by flash chromatography to give **522** as a clear oil (1.66 g, 80% yield). ^{1}H NMR (300MHz, C_6D_6) major rotamer: δ 6.86 (dd, *J* = 15.6, 7.0 Hz, 1H), 5.90 (d, *J* = 15.6 Hz, 1H), 3.86 (t, *J* = 6.2 Hz, 1H), 3.45 (d, *J* = 6.8 Hz, 1H), 3.34 (s, 3H), 3.24 (d, *J* = 9.1Hz, 1H), 1.63 (s, 3H), 1.48 (s, 3H), 0.81 (s, 9H). Minor rotamer: δ 6.97 (dd, *J* = 15.6, 7.0 Hz, 1H), 6.09 (d, *J* = 15.6 Hz, 1H), 4.24 (t, *J* = 6.2 Hz, 1H), 3.46 (d, *J* = 6.8 Hz, 1H), 3.28 (s, 3H), 3.23 (d, *J* = 9.1Hz, 1H), 2.06 (s, 3H), 1.36 (s, 3H), 0.81 (s, 9H). ^{13}C NMR (75MHz, C_6D_6) mixture of rotamers: δ 165.7, 151.3, 146.1, 128.8, 128.0, 125.2, 122.0, 94.1, 79.4, 66.9, 57.9, 50.5, 27.9, 27.3, 26.8, 26.4, 23.8, 20.8. LRMS (ESI): *m/z* calcd. for $C_{14}H_{23}NNaO_5$ $[M+Na]^+$ 308.3, found, 308.8.

(R)-tert-butyl-4-((1*R*, 2*S*)-1,2-dihydroxy-3-methoxy-3-oxopropyl)-2,2-dimethyloxazolidine-3-carboxylate (523)

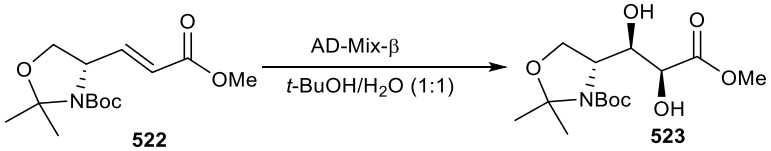

522 (3.06 g, 10.7 mmol) was dissolved in *t*-BuOH/H_2O (1:1, 100 mL). Methane sulfonamide (1.02 g, 10.7 mmol) and AD-mix-β (14.3 g) was added to the mixture and the reaction was stirred vigorously overnight. Sodium sulfite (233 mg) is added to the reaction and the reaction is stirred for 20 min. The reaction is diluted with DCM and the layers were separated. The aqueous layer is then re-extracted with DCM. The organic layer is dried with $MgSO_4$, filtered and concentrated in *vacuo.* The mixture is then purified by flash chromatography to give **523** as a clear oil (2.73 mg, 80% yield). ^{1}H NMR (300MHz, C_6D_6) mixture of rotamers: δ 4.71 (d, *J* = 4.8 Hz, 1H), 4.24 (d, *J* = 7.1Hz, 3H), 4.16 (dd, *J* = 12.8, 4.5 Hz, 2H), 3.98 (dd, *J* = 9.1, 4.9 Hz, 1H), 3.90-3.82 (m, 2H), 2.69 (d, *J* = 10.1 Hz, 1H), 1.55 (s, 3H), 1.50 (s, 3H), 1.47 (s, 9H). ^{13}C NMR (75MHz, C_6D_6): δ 171.4, 94.2, 82.0, 73.2, 70.4, 65.5, 61.5, 58.9, 28.3, 27.5, 24.0. LRMS (ESI): *m/z* calcd. for $C_{14}H_{25}NKO_7$ $[M+K]^+$ 354.8, found, 354.6.

General procedure for the synthesis of (2*S*, 3*R*, 4*R*)-4-amino-*N*-cycloalkyl-2,3,5-trihydroxypentanamide

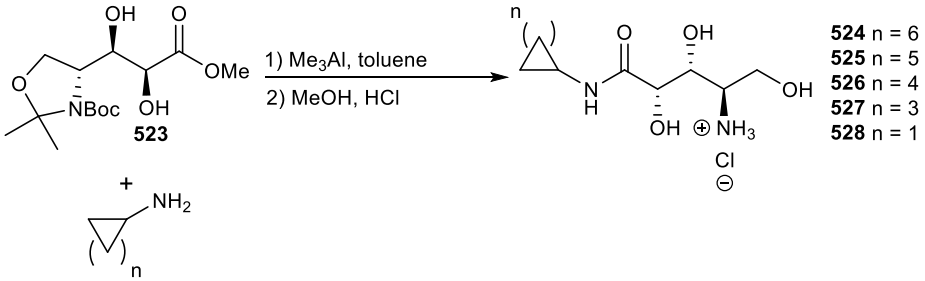

Cycloalkylamine (1.1 eq.) is dissolved in toluene (10 mL for 0.3 mmol of ester) and trimethylaluminium (2 eq.) is added to the reaction and stirred for 1h. The ester (1eq. in 5mL of toluene) is then added and the reaction is then stirred overnight till the starting ester is fully consumed by TLC. The reaction is the quenched with 10% HCl dropwise and stirred for 30min till a white precipitate is formed. The precipitate is then filtered over Celite® and the mixture is portioned between EtOAc and water. The layers are separated and the aqueous layer is extracted with EtOAc (2x), dried with $MgSO_4$, filtered and concentrated in *vacuo.* The resulting syrup is dissolved in 1:1 mixture of petroleum ether and EtOAc and passed through a pad of silica. The eluted product is then concentrated in *vacuo.* and dissolved in MeOH and 10% HCl is added till pH = 2. The reaction is stirred overnight and concentrated in *vacuo.* the resulting syrup is recrystallized from MeOH/diethyl ether to afford the product as a solid.

(2*S*, 3*R*, 4*R*)-4-amino-*N*-cyclooctyl-2,3,5-trihydroxypentanamide (524)
56.9 mg, 61% yield. ^{1}H NMR (300 MHz, D_2O): δ 4.12 (d, *J* = 4.1 Hz, 1H), 4.09 (dd, *J* = 4.0, 3.0 Hz, 1H), 3.88-3.84 (m, 1H), 3.83-3.77 (m, 1H), 3.73-3.67 (m, 2H), 3.48-3.42 (m, 1H), 1.70-1.30 (m, 14H). ^{13}C NMR (100 MHz, D_2O): δ 171.8, 71.6, 68.2, 67.9, 58.2, 55.3, 49.9, 31.5, 31.4, 26.5, 25.9, 25.1, 23.3, 22.9. LRMS (ESI): *m/z* calcd. for $C_{13}H_{27}ClN_2NaO_4$ $[M+Na]^+$ 333.8, found, 333.3.

(2*S*, 3*R*, 4*R*)-4-amino-*N*-cycloheptyl-2,3,5-trihydroxypentanamide (525)
67.7 mg, 76% yield. ^{1}H NMR (500 MHz, D_2O): δ 4.08 (d, *J* = 2.4 Hz, 1H), 4.06 (dd, *J* = 5.5, 2.3 Hz 1H), 3.83 (dd, *J* = 12.2, 4.1 Hz, 1H), 3.71-3.63 (m, 2H), 3.43-3.38 (m, 1H), 1.71-1.63 (m, 2H), 1.50-1.25 (m, 10H). ^{13}C NMR (100 MHz, D_2O): δ 171.9, 71.4, 68.1, 58.1, 55.2, 51.0, 34.0, 33.9, 27.4, 23.6. LRMS (ESI): *m/z* calcd. for $C_{12}H_{25}ClN_2O_4$ $[M]^+$ 296.8, found, 296.6.

(2*S*, 3*R*, 4*R*)-4-amino-*N*-cyclohexyl-2,3,5-trihydroxypentanamide (526)
49.2 mg, 57% yield. ^{1}H NMR (300 MHz, MeOD): δ 4.10 (d, *J* = 3.1 Hz, 1H), 4.05 (dd, *J* = 5.4, 3.1 Hz 1H), 3.91 (dd, *J* = 11.5, 4.3 Hz, 1H), 3.80-3.70 (m, 2H), 3.40-3.35 (m, 1H), 1.50-2.00 (m, 5H), 1.40-1.10 (m, 5H). ^{13}C NMR (100 MHz, D_2O): δ 172.3, 71.5, 68.1, 58.1, 55.2, 48.9, 31.9, 31.7, 24.8, 24.4. LRMS (ESI): *m/z* calcd. for $C_{11}H_{23}ClN_2O_4$ $[M]^+$ 282.8, found, 282.4.

(2*S*, 3*R*, 4*R*)-4-amino-*N*-cyclopentyl-2,3,5-trihydroxypentanamide (527)
16.9 mg, 21% yield. ^{1}H NMR (300 MHz, MeOD) major rotomer: δ 4.30 (d, *J* = 2.5 Hz, 1H), 4.19 (dd, *J* = 5.7, 2.5 Hz 1H), 4.12-4.09 (m, 1H), 4.05 (dd, *J* = 5.5, 3.2 Hz, 1H), 3.80-3.73 (m, 2H), 3.59-3.52 (m, 1H), 2.09-2.01 (m, 2H), 1.72-1.64 (m, 3H), 1.61-1.55 (m, 3H). Minor rotomer: δ 4.35 (d, *J* = 2.5 Hz, 1H), 4.15 (dd, *J* = 5.7, 2.5 Hz 1H), 4.13-4.12 (m, 1H), 4.05 (dd, *J* = 5.5, 3.2 Hz, 1H), 3.93-3.86 (m, 2H), 3.42-3.35 (m, 1H), 1.97-1.92 (m, 2H), 1.80-1.74 (m, 3H), 1.53-1.47 (m, 3H). ^{13}C NMR (100 MHz, MeOD) mix of rotomers: δ 172.5, 172.3, 71.5,72.0, 71.5, 71.1, 68.6, 68.2 68.1, 58.4, 58.3, 58.2, 55.8, 55.7, 55.6, 51.9, 51.4, 50.8, 32.1, 32.1, 30.6, 23.4, 23.4. LRMS (ESI): *m/z* calcd. for $C_{10}H_{21}ClN_2O_4$ $[M]^+$ 268.7, found, 282.3.

(2*S*, 3*R*, 4*R*)-4-amino-*N*-cyclopropyl-2,3,5-trihydroxypentanamide (528)
41.9 mg, 58% yield. ^{1}H NMR (300 MHz, MeOD): δ 4.35 (d, *J* = 2.4 Hz, 1H), 4.17 (dd, *J* = 5.9, 2.4 Hz 1H), 3.80-3.74 (m, 2H), 3.43-3.37 (m, 1H), 2.64-2.59 (m, 1H), 0.85-0.81 (m, 2H), 0.75-0.72 (m, 2H). ^{13}C NMR (100 MHz, MeOD): δ 172.4, 71.5, 68.1, 58.3, 55.6, 51.4, 22.9, 2.7. LRMS (ESI): *m/z* calcd. for $C_8H_{17}ClN_2NaO_4$ $[M+Na]^+$ 263.7, found, 263.5.

***N*-cyclooctyl-2,3,4,6-tetra-*O*-benzyl-D-gluconamide (530)**

Cyclooctylamine (0.03 mL, 0.212 mmol) is dissolved in toluene (10 mL) and trimethylaluminium (0.2 mL, 0.386 mmol) is added to the reaction and stirred for 1h. 2,3,4,6-tetra-*O*-benzyl-D-glucono-1,5-lactone (104 mg, 0.193 mmol) is then added and the reaction is then stirred overnight till the starting material is fully consumed by TLC. The reaction is the quenched with 10% HCl dropwise and stirred for 30 min till a white precipitate is formed. The precipitate is then filtered over Celite® and the mixture is portioned between EtOAc and water. The layers are separated and the aqueous layer is extracted with EtOAc (2x), dried with $MgSO_4$, filtered and concentrated in *vacuo.* The resulting syrup is then purified by flash chromatography to give **530** as a clear oil (91.2 mg, 71% yield). ^{1}H NMR (300 MHz, $CDCl_3$): δ 7.36-7.21 (m, 20H), 6.66 (d, *J* = 7.7 Hz, 1H), 4.72-4.50 (m, 8H), 4.26 (d, *J* = 3.3 Hz, 1H), 4.11 (dd, *J* = 5.7, 3.0, 1H), 4.00-3.93 (m, 2H), 3.87 (dd, *J* = 7.4, 5.8 Hz, 1H), 3.67(dd, *J* = 12.9, 3.3 Hz, 1H), 3.61(dd, *J* = 10.1, 5.3 Hz, 1H), 1.79-1.41 (m, 15H). ^{13}C NMR (100 MHz, $CDCl_3$): δ 169.5, 138.2, 138.1, 137.9, 136.8, 128.7, 128.5, 128.4, 128.3, 128.2, 128.2, 128.0, 127.9, 127.7, 127.7, 80.6, 80.1, 77.2, 75.1, 74.0, 73.4, 71.5, 71.1, 49.1, 32.1, 31.9, 27.2, 25.3, 23.5. LRMS (ESI): *m/z* calcd. for $C_{42}H_{51}NNaO_6$ $[M+Na]^+$ 688.8, found, 688.3.

***N*-cyclooctyl-2,3,4,6-tetra-*O*-benzyl-*n*-benzyl-5-amino-5-deoxy-D-gluconamide (531 and 532)**

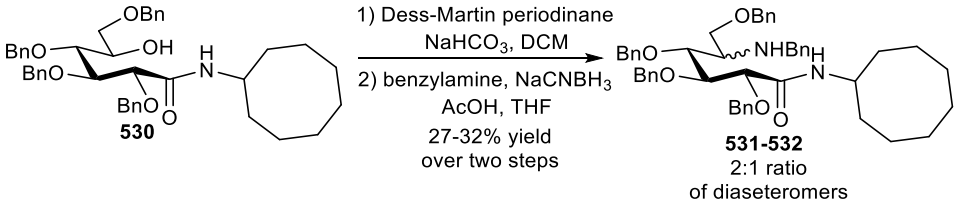

530 (51.2 mg, 0.0769 mmol) is dissolved in DCM (10 mL) and $NaHCO_3$ (25.9 mg, 0.308 mmol) is added. Dess-Martin periodinane (65.3 mg, 0.154 mmol) is then added and the reaction is stirred for 1h. The reaction mixture is then diluted with 10 mL of diethyl ether and then a 1:1:1 mixture of saturated $Na_2S_2O_3$ (5 mL), saturated $NaHCO_3$ (5 mL) and water (5 mL) is added slowly. The resulting biphasic mixture is stirred vigorously for 1h resulting in two clear layers. The layers are separated and the aqueous layer is extracted with diethyl ether (3x). The organic layers are then dried with $MgSO_4$, filtered and concentrated in *vacuo*. The resulting syrup is dissolved in THF (10 mL). Benzylamine (0.01 mL, 0.0923 mmol) and sodium cyanoborohydride (5.80 mg, 0.0923 mmol) is added to the reaction. Glacial AcOH is then added dropwise till pH = 2 and the reaction is refluxed overnight. The reaction is then cooled to rt and concentrated in *vacuo*. The resulting syrup is then purified by flash chromatography.

***N*-cyclooctyl-2,3,4,6-tetra-*O*-benzyl-*n*-benzyl-5-amino-5-deoxy-D-gluconamide (531)**
15.7 mg, 27% yield. ^{1}H NMR (300 MHz, $CDCl_3$): δ 7.26-7.19 (m, 25H), 6.66 (d, *J* = 7.4 Hz, 1H), 4.76 (d, *J* = 11.0 Hz, 1H), 4.67 (d, *J* = 11.0 Hz, 1H), 4.54-4.36 (m, 8H), 4.19 (dd, *J* = 7.9, 2.4 Hz, 1H), 4.11 (d, *J* = 2.4, 1H), 3.95-3.92 (m, 1H), 3.87 (dd, *J* = 8.1, 2.1 Hz, 1H), 3.73 (dt, J = 6.3, 1.8 Hz, 1H), 3.46 (dd, *J* = 9.0, 6.3 Hz, 1H), 3.34 (dd, *J* = 9.0, 6.3 Hz, 1H), 1.79-1.30 (m, 15H). ^{13}C NMR (100 MHz, $CDCl_3$): δ 169.1, 138.1, 138.1, 138.0, 136.5, 128.7, 128.7, 128.4, 128.4, 128.4, 128.2, 128.2, 128.0, 127.8, 127.7, 127.6, 80.4, 80.0, 78.2, 75.6, 74.9, 74.0, 73.2, 71.1, 69.3, 49.2, 32.1, 31.2, 27.2, 25.3, 23.5. LRMS (ESI): *m/z* calcd. for $C_{49}H_{59}N_2O_5$ $[M+H]^+$ 756.0, found, 756.4.

***N*-cyclooctyl-2,3,4,6-tetra-*O*-benzyl-*n*-benzyl-5-amino-5-deoxy-D-gluconamide (532)**
18.6 mg, 32% yield. ^{1}H NMR (300 MHz, $CDCl_3$): δ 7.34-7.19 (m, 25H), 6.66 (d, *J* = 8.3 Hz, 1H), 4.67-4.36 (m, 10H), 4.24 (d, *J* = 2.6, 1H), 4.09-4.07 (dd, *J* = 5.7, 2.8 Hz, 1H), 3.94-3.91 (m, 2H), 3.84 (dd, *J* = 7.6, 6.0 Hz, 1H), 3.64 (dd, *J* = 9.6, 2.7 Hz, 1H), 3.34 (dd, *J* = 9.8, 5.5 Hz, 1H), 1.73-1.34 (m, 15H).). ^{13}C NMR (100 MHz, $CDCl_3$): δ169.5, 138.2, 138.1, 137.8, 136.8, 128.7, 128.5, 128.5, 128.4, 128.3, 128.2, 128.2, 128.2, 128.0, 127.9, 127.7, 127.7, 80.6, 80.1, 77.2, 75.1, 74.0, 73.4, 71.5, 71.1, 49.2, 32.0, 31.8, 27.2, 25.3, 23.5. LRMS (ESI): *m/z* calcd. for $C_{49}H_{58}N_2NaO_5$ $[M+Na]^+$ 778.0, found, 778.2.

General procedure for the synthesis of *N*-cyclooctyl-5-amino-5-deoxy-D-gluconamides (533 and 534).

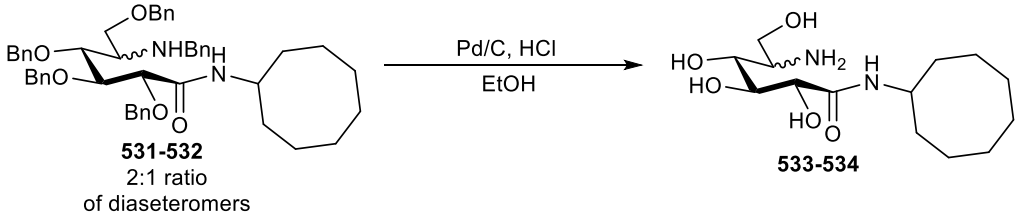

531-532
2:1 ratio
of diaseteromers

533-534

531 or **532** (1 eq.) is dissolved in EtOH (3 mL). Pd/C (10 mol %) is then added to reaction and the mixture is then exposed to 20 bar of hydrogen with vigorous stirring overnight. The reaction is then filtered over Celite® and concentrated in *vacuo.* The resulting syrup was recrystallized from MeOH/diethyl ether.

***N*-cyclooctyl-5-amino-5-deoxy-D-gluconamide (533)**
5.95 mg, 94% yield. ^{1}H NMR (300 MHz, D_2O): δ 4.10 (d, J = 2.4 Hz, 1H), 3.85 (dd, J = 6.6, 2.9 Hz 1H), 3.79-3.75 (m, 1H), 3.68-3.65 (m, 1H), 3.59 (dd, J = 6.6, 2.9 Hz, 1H), 3.54 (dd, J = 11.4, 4.6 Hz, 1H), 3.50 (dd, J = 11.4, 7.5 Hz, 1H), 1.64-1.34 (m, 15H). ^{13}C NMR (100 MHz, D_2O): δ 172.5, 71.8, 71.6, 71.3, 71.0, 62.7, 49.7, 31.3, 31.3, 26.4, 26.4, 25.0, 23.1. LRMS (ESI): *m/z* calcd. for $C_{14}H_{28}N_2NaO_5$ $[M+Na]^+$ 327.4, found, 327.7.

***N*-cyclooctyl-5-amino-5-deoxy-D-gluconamide (534)**
7.21 mg, 96% yield. ^{1}H NMR (300 MHz, D_2O): δ 4.13-4.05 (m, 2H), 3.87 (dd, J = 12.5, 3.3 Hz 1H), 3.80-3.75 (m, 1H), 3.75-3.65 (m, 1H), 3.47-3.40 (m, 1H), 1.70-1.30 (m, 14H). ^{13}C NMR (100 MHz, D_2O): δ 171.9, 71.6, 68.3, 58.2, 55.3, 49.9, 31.5, 31.4, 26.5, 25.1, 23.3. LRMS (ESI): *m/z* calcd. for $C_{14}H_{28}N_2KO_5$ $[M+K]^+$ 343.4, found, 343.3.

***N*-phenyl-D-gluconamide (535)**

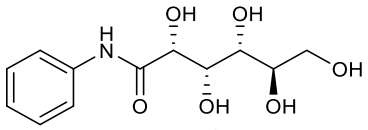

535

This compound was prepared by a fellow doctoral student Jennie Briard and was tested for IRI activity following the general experimental condition described previously.[15]

***N*-phenyl-2,3,5-tri-*O*-benzyl-D-arabinoamide (543)**

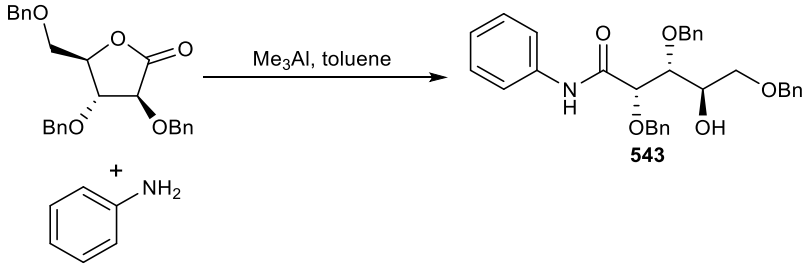

Aniline (0.012 mL, 0.131 mmol) was dissolved in toluene and trimethylaluminium (0.13 mL, 0.262 mmol) was added. The reaction was then stirred for 1h. 2,3,5-tri-*O*-benzyl-D-arabino-γ-lactone (49.8 mg, 0.119 mmol) was then added to the reaction and was stirred overnight. The reaction is the quenched with 10% HCl dropwise and stirred for 30min till a white precipitate is formed. The precipitate is then filtered over Celite® and the mixture is portioned between EtOAc and water. The layers are separated and the aqueous layer is extracted with EtOAc (2x), dried with $MgSO_4$, filtered and concentrated in *vacuo.* The resulting syrup is then purified by flash chromatography to give a **543** as a yellow oil (45.4 mg, 63% yield). ^{1}H NMR (300 MHz, $CDCl_3$): δ 8.51 (s, 1H), 7.50-7.00 (m, 20H), 4.75 (d, *J* = 11.3 Hz, 1H), 4.65 (d, *J* = 11.3 Hz, 1H), 4.51- 4.28 (m, 5H), 4.07 (dd, *J* = 8.9, 2.0 Hz, 1H), 4.00-3.97 (m, 1H), 3.65 (dd, *J* = 9.6, 3.2 Hz, 1H), 3.58 (dd, *J* = 9.6, 3.2 Hz, 1H). ^{13}C NMR (100 MHz, $CDCl_3$): δ 169.9, 137.6, 137.3, 137.2, 136.7, 129.0, 128.7, 128.5, 128.2, 128.0, 124.5, 119.5, 80.0, 79.9, 74.9, 74.8, 73.4, 70.4, 69.3. LRMS (ESI): *m/z* calcd. for $C_{39}H_{39}NNaO_5$ $[M+Na]^+$ 624.7, found, 624.5.

***N*-phenyl-D-arabinoamide (536)**

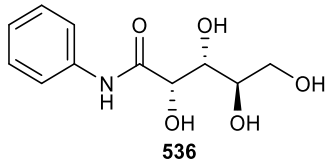

This compound was synthesized according to 'General procedure for the synthesis of *N*-cycloalkyl-D-arabinoamide' to give 88.9 mg in 97% yield. ^{1}H NMR (500 MHz, CD_3OD): δ 7.63 (d, *J* = 7.8 Hz, 2H), 7.33 (t, *J* = 6.9 Hz, 2H), 7.12 (t, *J* = 6.9 Hz, 1H), 4.50 (s, 1H), 3.95 (d, *J* = 8.3 Hz, 1H), 3.85 (d, *J* = 10.4 Hz, 1H), 3.74-3.65 (m, 2H). ^{13}C NMR (100 MHz, CD_3OD): δ 173.0, 137.6, 128.4, 124.0, 119.9, 72.2, 71.4, 71.2, 63.5. LRMS (ESI): *m/z* calcd. for $C_{11}H_{16}NO_5$ $[M+H]^+$ 242.2, found, 242.1.

(2*S*, 3*R*, 4*R*)-4-amino-*N*-phenyl-2,3,5-trihydroxypentanamide (537)

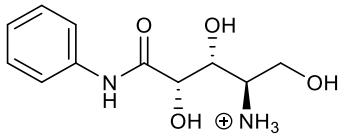

537

This compound was synthesized according to "General procedure for the synthesis of (2*S*, 3*R*, 4*R*)-4-amino-*N*-cycloalkyl-2,3,5-trihydroxypentanamide" to give 65.1 mg in 62% yield. ^{1}H NMR (300 MHz, D_2O): δ 7.44-7.40 (m, 3H), 7.29-7.27 (m, 2H), 4.18 (d, J = 2.3 Hz, 1H), 4.15 (dd, J = 5.6, 2.5 Hz, 1H), 3.71 (m, 2H), 3.47-3.43 (m, 1H). ^{13}C NMR (100 MHz, D_2O): δ 175.9, 130.0, 129.0, 122.8, 71.4, 68.2, 58.3, 55.3. LRMS (ESI): *m/z* calcd. for $C_{11}H_{18}ClN_2O_4$ $[M+H]^+$ 276.7, found, 276.9.

6.9.1 Spectroscopic Data

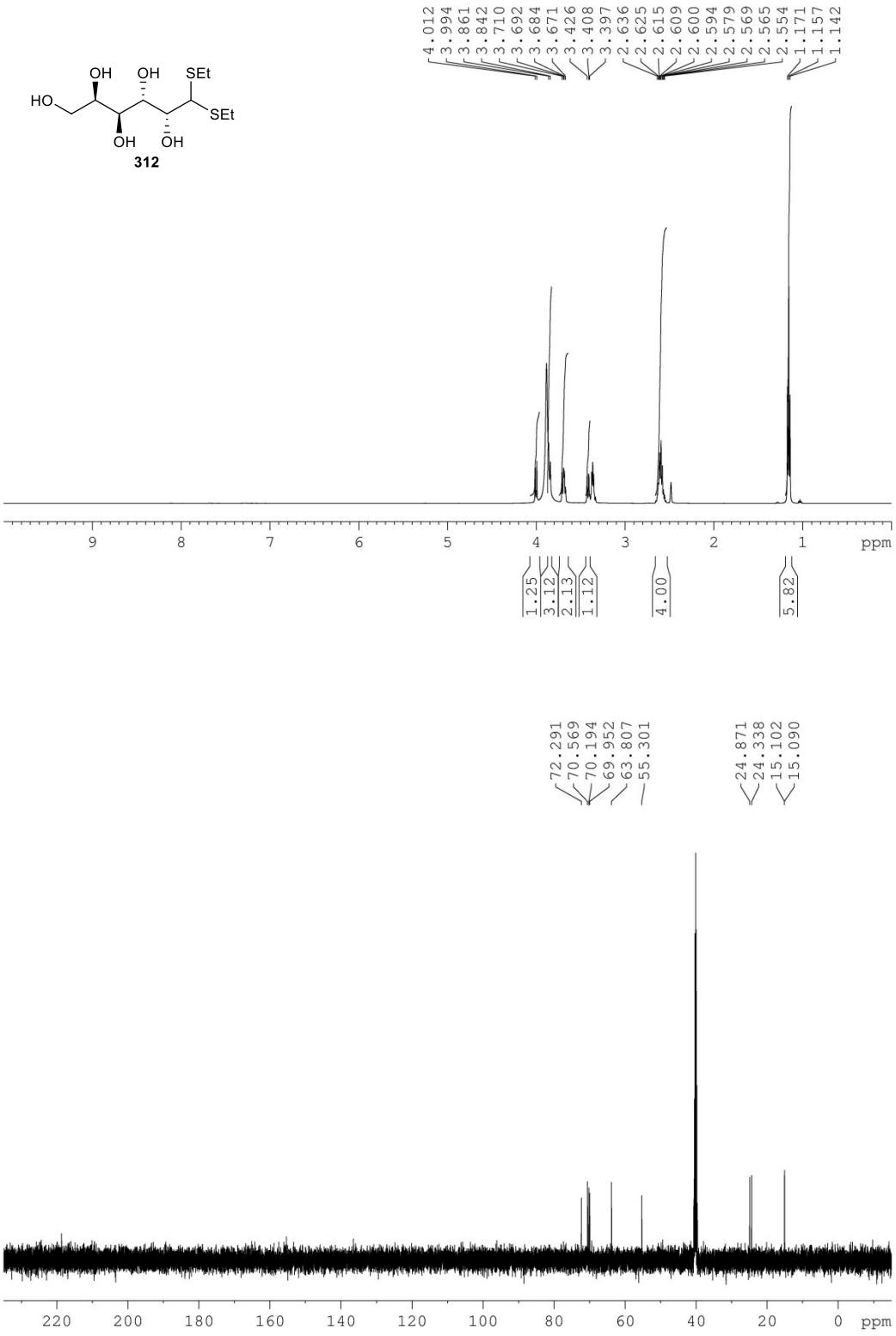

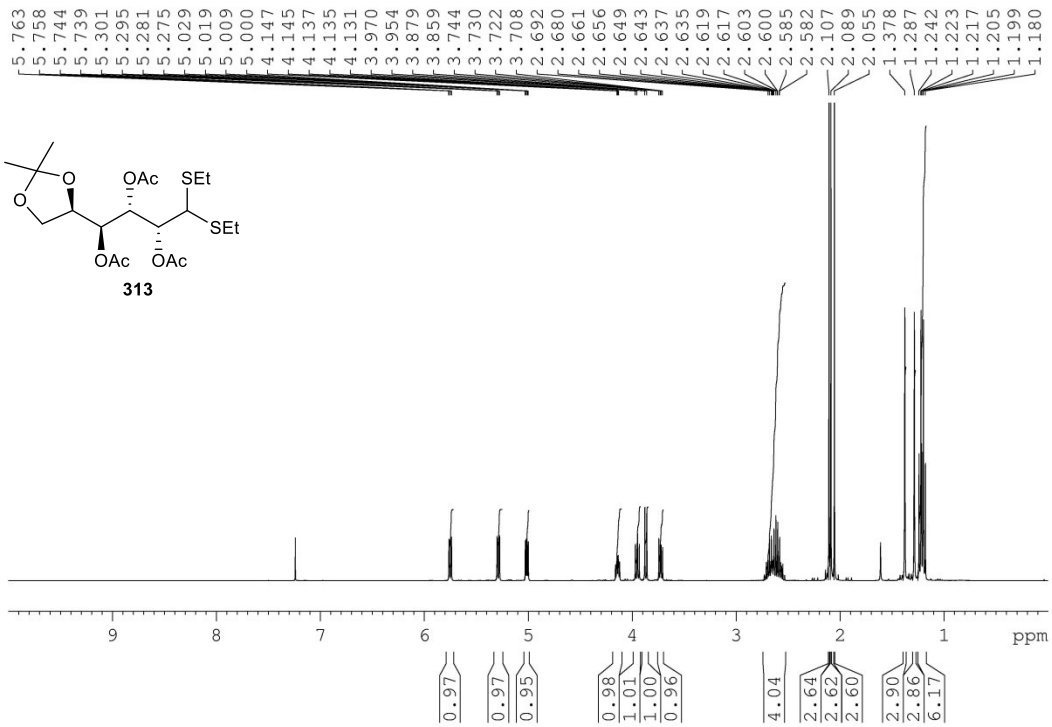
5.763
5.758
5.744
5.739
5.301
5.295
5.281
5.275
5.029
5.019
5.009
5.000
4.147
4.145
4.137
4.135
4.131
3.970
3.954
3.879
3.859
3.744
3.730
3.722
3.708
3.692
2.680
2.661
2.656
2.649
2.643
2.637
2.635
2.619
2.617
2.603
2.600
2.585
2.582
2.107
2.089
2.055
1.378
1.287
1.242
1.223
1.217
1.205
1.199
1.180
O
O
OAc
SEt
SEt
OAc
OAc
313
9
8
7
6
5
4
3
2
1
ppm
0.97
0.97
0.95
0.98
1.01
1.00
0.96
4.04
2.64
2.62
2.60
2.90
2.86
6.17

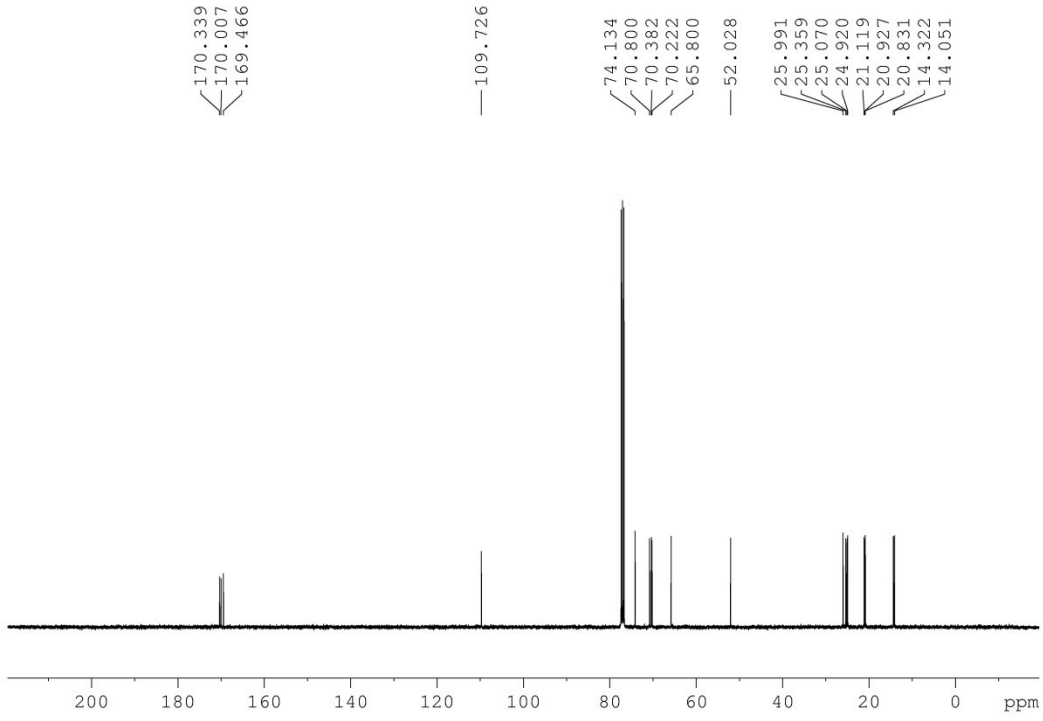
170.339
170.007
169.466
109.726
74.134
70.800
70.382
70.222
65.800
52.028
25.991
25.359
25.070
24.920
21.119
20.927
20.831
14.322
14.051
200
180
160
140
120
100
80
60
40
20
0
ppm

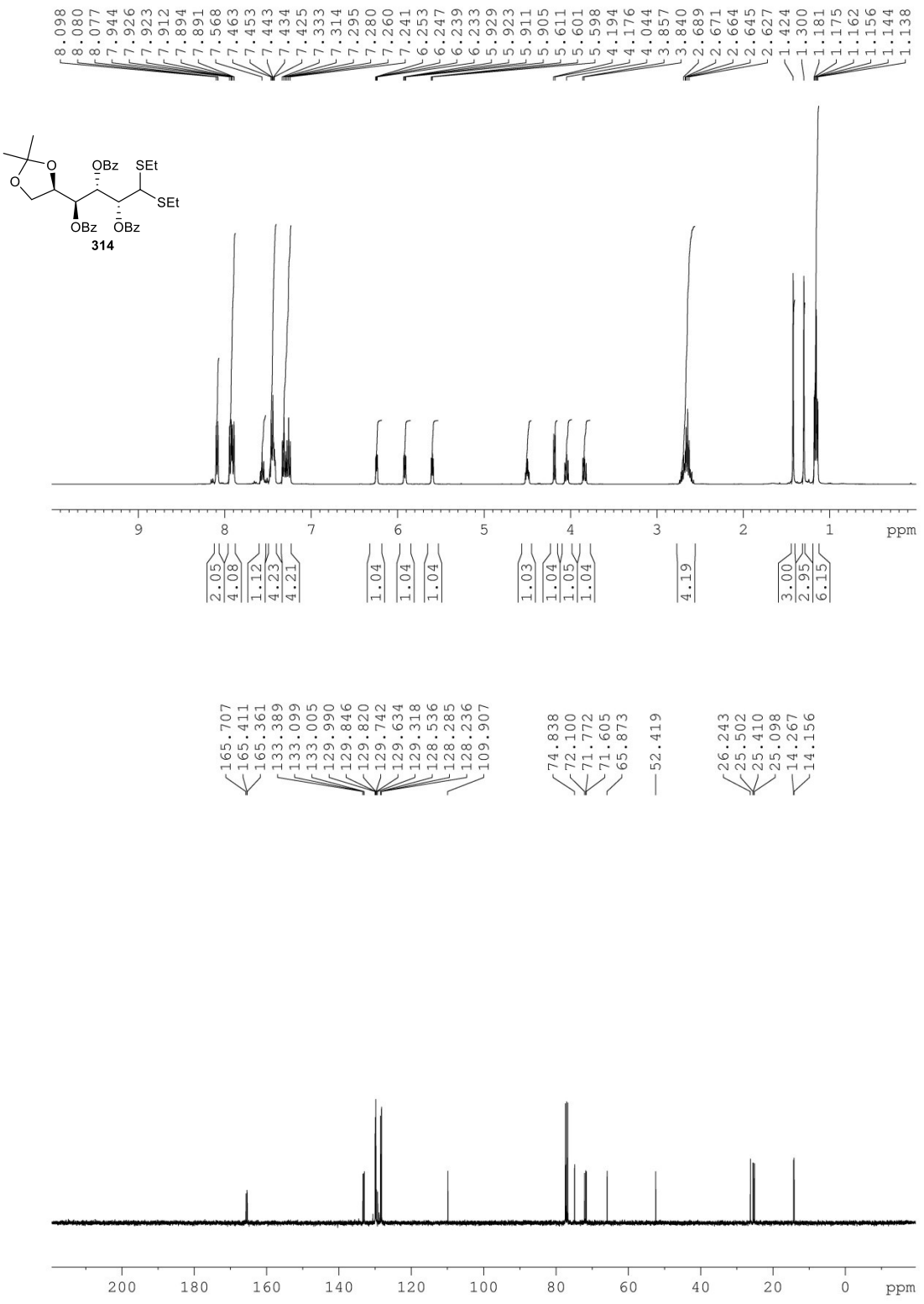
8.098
8.080
8.077
7.944
7.926
7.923
7.912
7.894
7.891
7.568
7.463
7.453
7.443
7.434
7.425
7.333
7.314
7.295
7.280
7.260
7.241
6.253
6.247
6.239
6.233
5.929
5.923
5.911
5.905
5.611
5.601
5.598
4.194
4.176
4.044
3.857
3.840
2.689
2.671
2.664
2.645
2.627
1.424
1.300
1.181
1.175
1.162
1.156
1.144
1.138
OBz
SEt
SEt
OBz
OBz
314
9
8
7
6
5
4
3
2
1
ppm
2.05
4.08
1.12
4.23
4.21
1.04
1.04
1.04
1.03
1.04
1.05
1.04
4.19
3.00
2.95
6.15
165.707
165.411
165.361
133.389
133.099
133.005
129.990
129.846
129.820
129.742
129.634
129.318
128.536
128.285
128.236
109.907
74.838
72.100
71.772
71.605
65.873
52.419
26.243
25.502
25.410
25.098
14.267
14.156
200
180
160
140
120
100
80
60
40
20
0
ppm

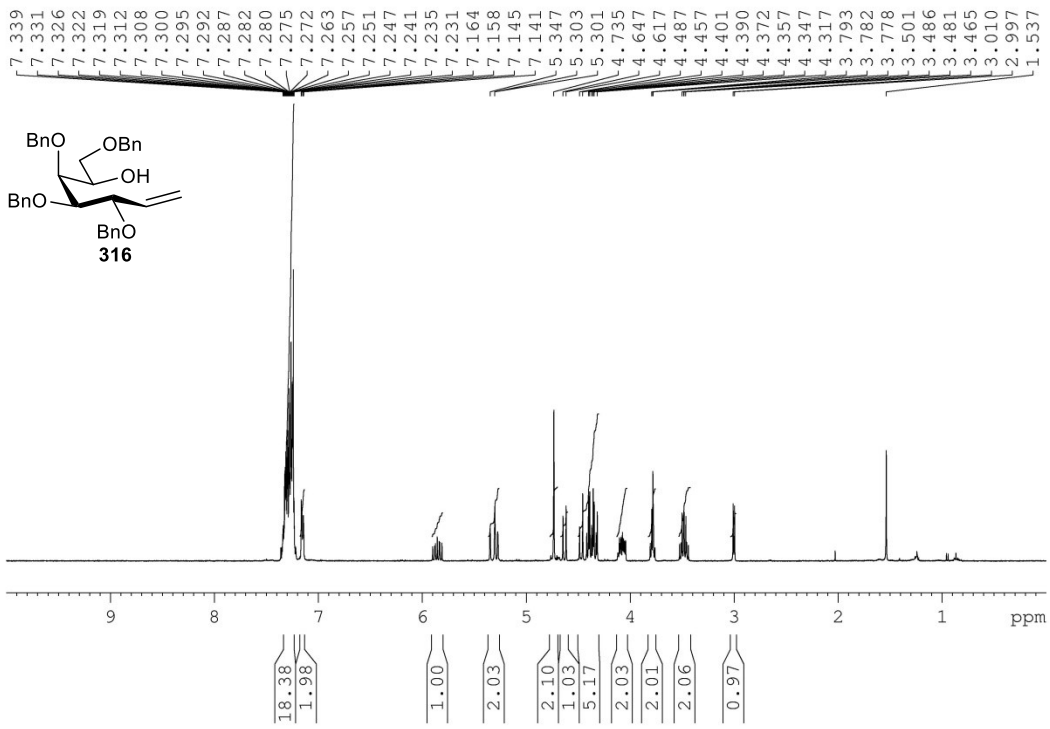
7.339
7.331
7.326
7.322
7.319
7.312
7.308
7.300
7.295
7.292
7.287
7.282
7.280
7.275
7.272
7.263
7.257
7.251
7.247
7.241
7.235
7.231
7.164
7.158
7.145
7.141
5.347
5.303
5.301
4.735
4.647
4.617
4.487
4.457
4.401
4.390
4.372
4.357
4.347
4.317
3.793
3.782
3.778
3.501
3.486
3.481
3.465
3.010
2.997
1.537
BnO
OBn
OH
BnO
BnO
316
9
8
7
6
5
4
3
2
1
ppm
18.38
1.98
1.00
2.03
2.10
1.03
5.17
2.03
2.01
2.06
0.97

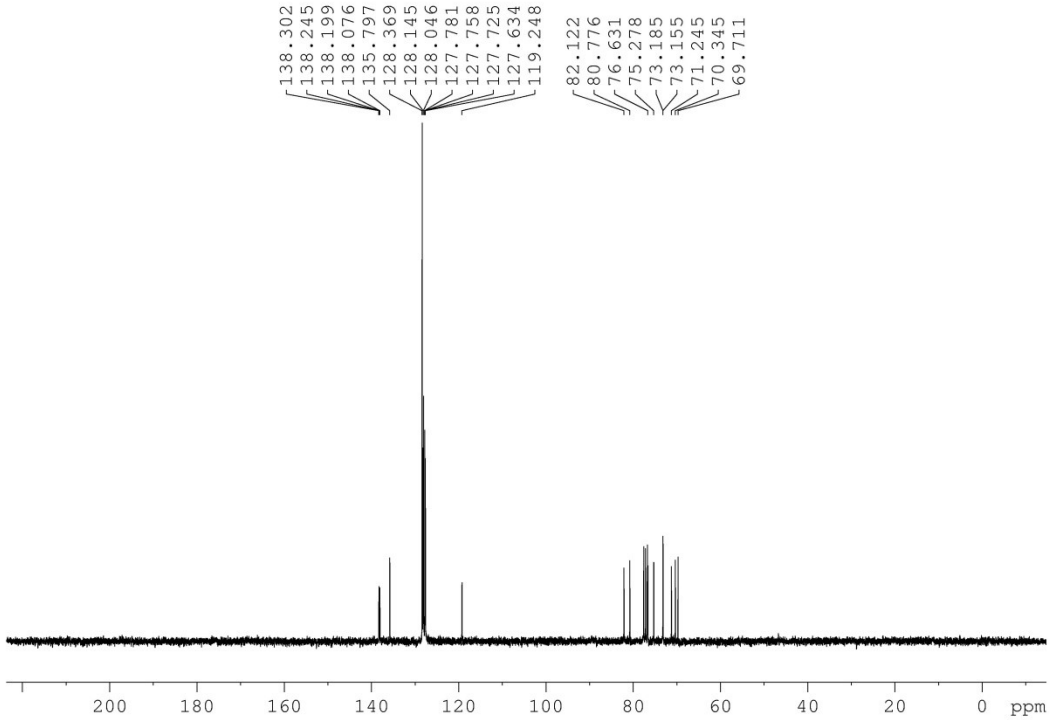
138.302
138.245
138.199
138.076
135.797
128.369
128.145
128.046
127.781
127.758
127.725
127.634
119.248
82.122
80.776
76.631
75.278
73.185
73.155
71.245
70.345
69.711
200
180
160
140
120
100
80
60
40
20
0
ppm

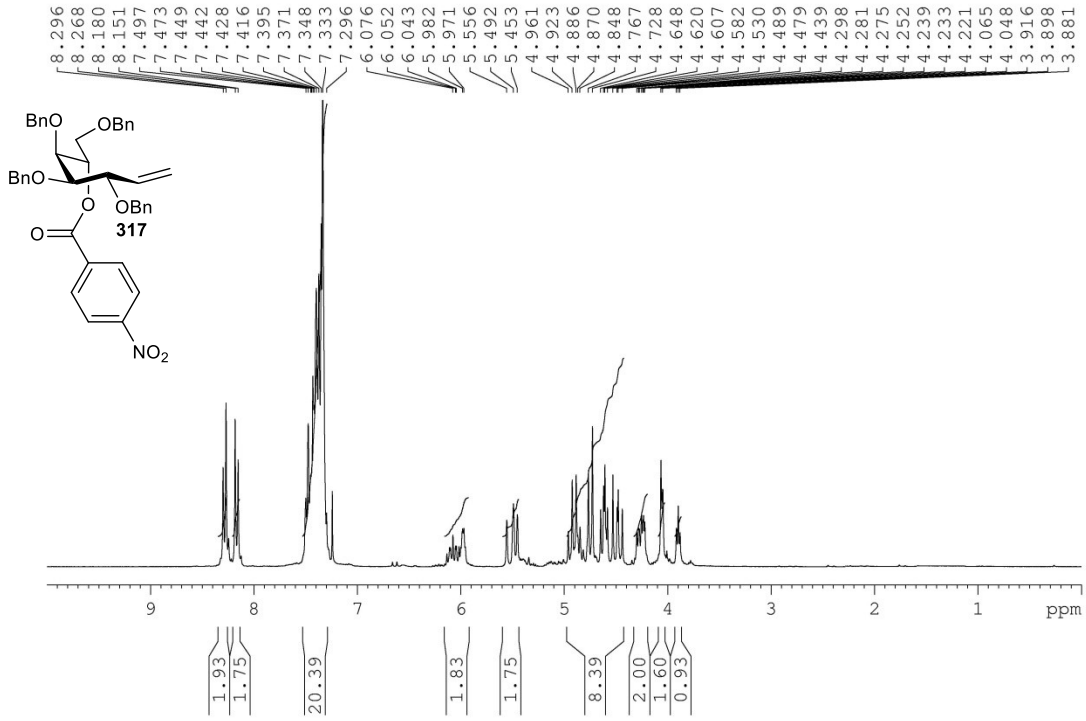
8.296
8.268
8.180
8.151
7.497
7.473
7.449
7.442
7.428
7.416
7.395
7.371
7.348
7.333
7.296
6.076
6.052
6.043
5.982
5.971
5.556
5.492
5.453
4.961
4.923
4.886
4.870
4.848
4.767
4.728
4.648
4.620
4.607
4.582
4.530
4.489
4.479
4.439
4.298
4.281
4.275
4.252
4.239
4.233
4.221
4.065
4.048
3.916
3.898
3.881
BnO
OBn
BnO
O
OBn
O
317
NO2
9
8
7
6
5
4
3
2
1
ppm
1.93
1.75
20.39
1.83
1.75
8.39
2.00
1.60
0.93

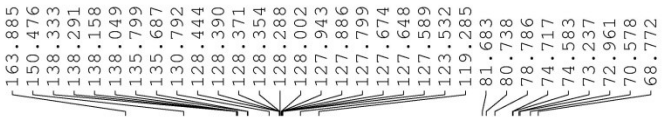
163.885
150.476
138.333
138.291
138.158
138.049
135.799
135.687
130.792
128.444
128.390
128.371
128.354
128.288
128.002
127.943
127.886
127.799
127.674
127.648
127.589
123.532
119.285
81.683
80.738
78.786
74.717
74.583
73.237
72.961
70.578
68.772

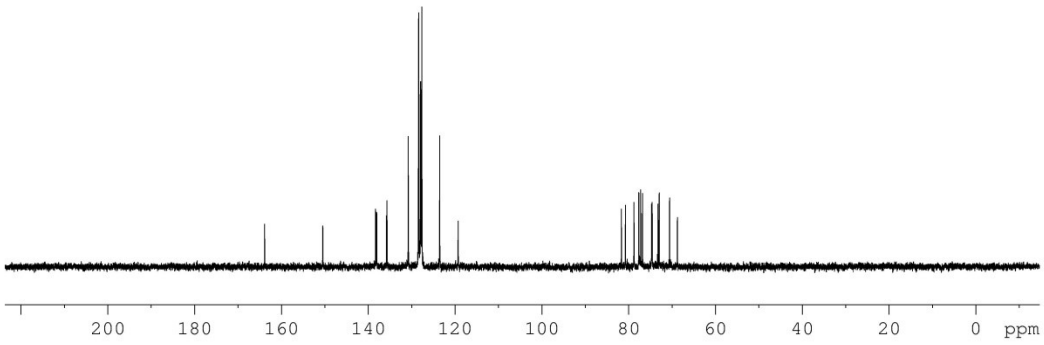
200
180
160
140
120
100
80
60
40
20
0
ppm

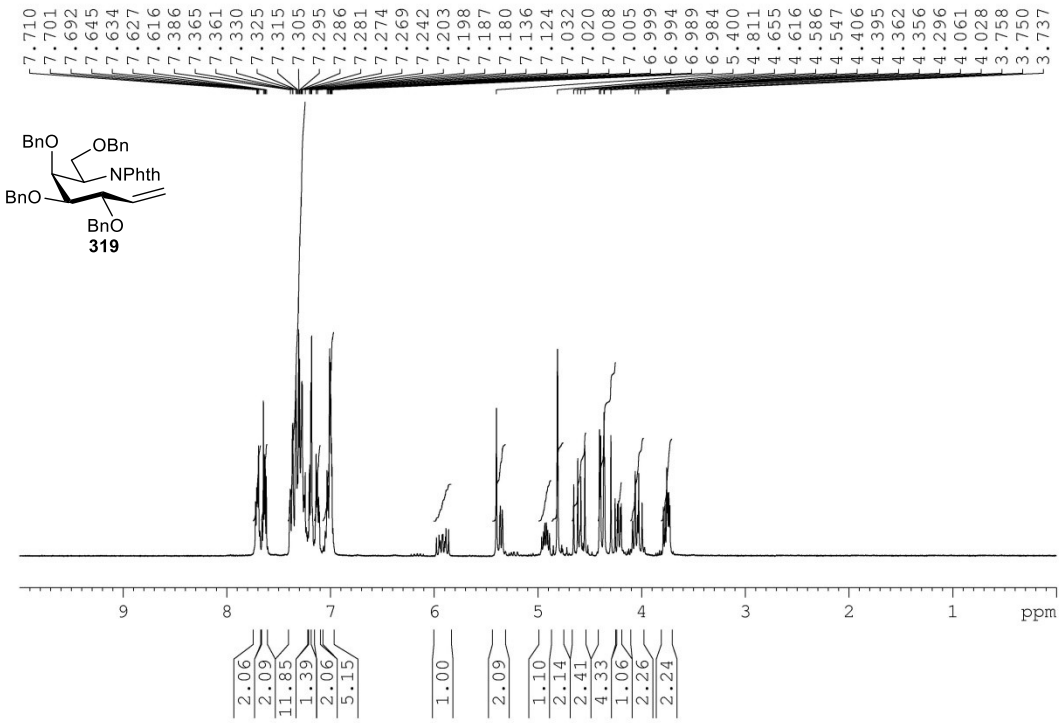
7.710
7.701
7.692
7.645
7.634
7.627
7.616
7.386
7.365
7.361
7.330
7.325
7.315
7.305
7.295
7.286
7.281
7.274
7.269
7.242
7.203
7.198
7.187
7.180
7.136
7.124
7.032
7.020
7.008
7.005
6.999
6.994
6.989
6.984
5.400
4.811
4.655
4.616
4.586
4.547
4.406
4.395
4.362
4.356
4.296
4.061
4.028
3.758
3.750
3.737
BnO
OBn
NPhth
BnO
BnO
319
9
8
7
6
5
4
3
2
1
ppm
2.06
2.09
11.85
1.39
2.06
5.15
1.00
2.09
1.10
2.14
2.41
4.33
1.06
2.26
2.24

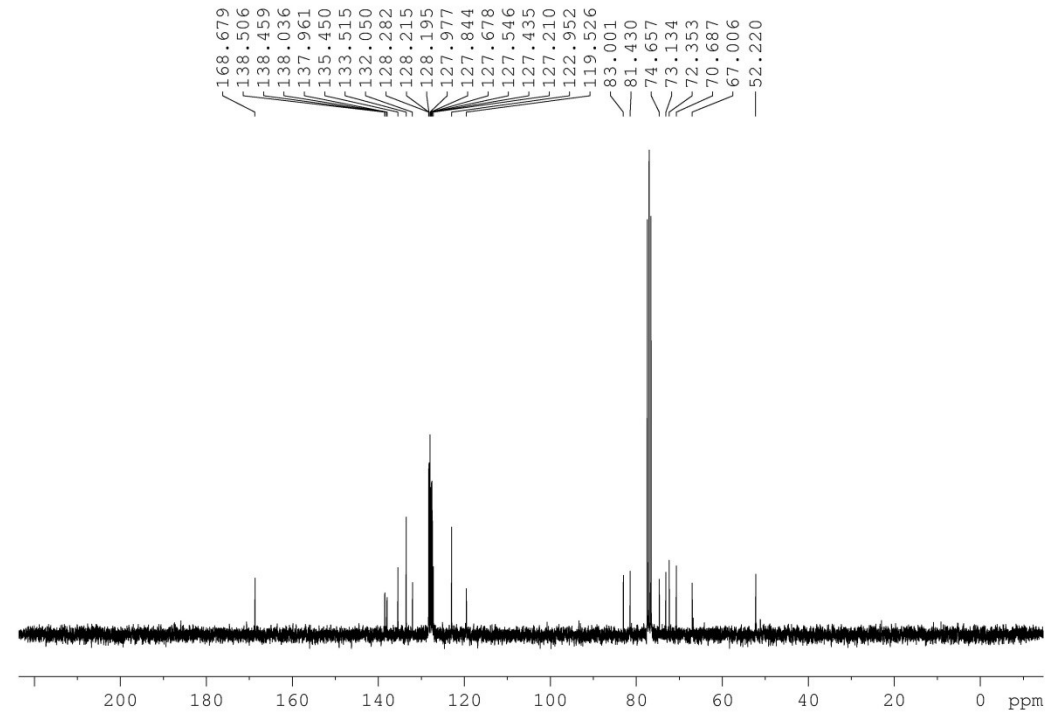
168.679
138.506
138.459
138.036
137.961
135.450
133.515
132.050
128.282
128.215
128.195
127.977
127.844
127.678
127.546
127.435
127.210
122.952
119.526
83.001
81.430
74.657
73.134
72.353
70.687
67.006
52.220
200
180
160
140
120
100
80
60
40
20
0
ppm

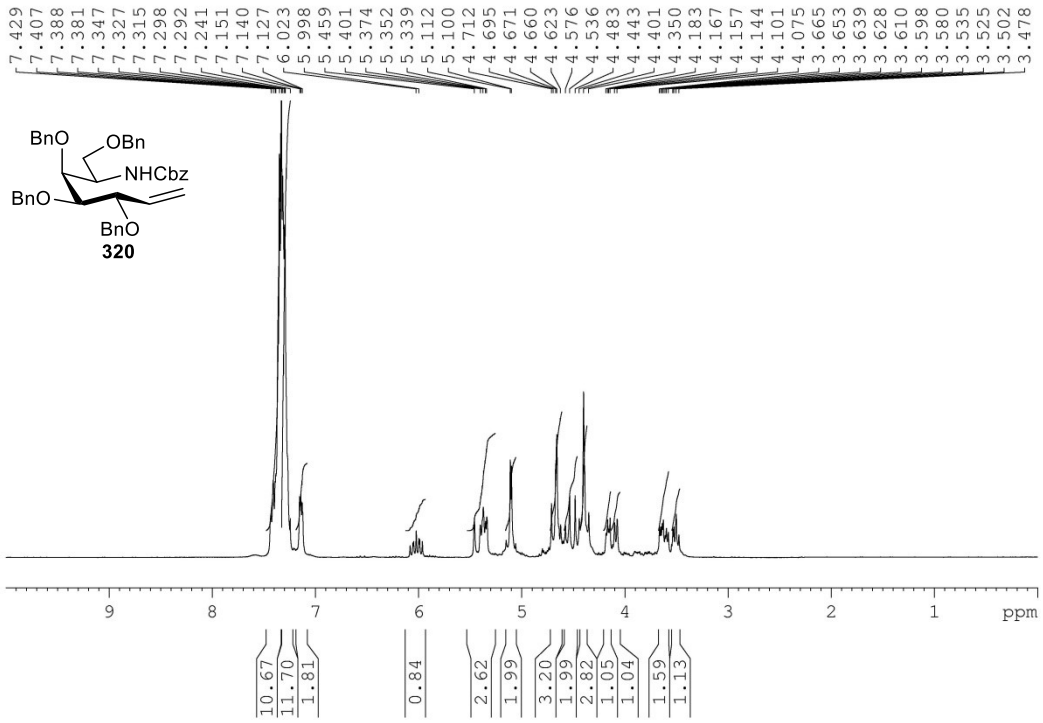
7.429
7.407
7.388
7.381
7.347
7.327
7.315
7.298
7.292
7.241
7.151
7.140
7.127
6.023
5.998
5.459
5.401
5.374
5.352
5.339
5.112
5.100
4.712
4.695
4.671
4.660
4.623
4.576
4.536
4.483
4.443
4.401
4.350
4.183
4.167
4.157
4.144
4.101
4.075
3.665
3.653
3.639
3.628
3.610
3.598
3.580
3.535
3.525
3.502
3.478
BnO
OBn
NHCbz
BnO
BnO
320
9
8
7
6
5
4
3
2
1
ppm
10.67
11.70
1.81
0.84
2.62
1.99
3.20
1.99
2.82
1.05
1.04
1.59
1.13

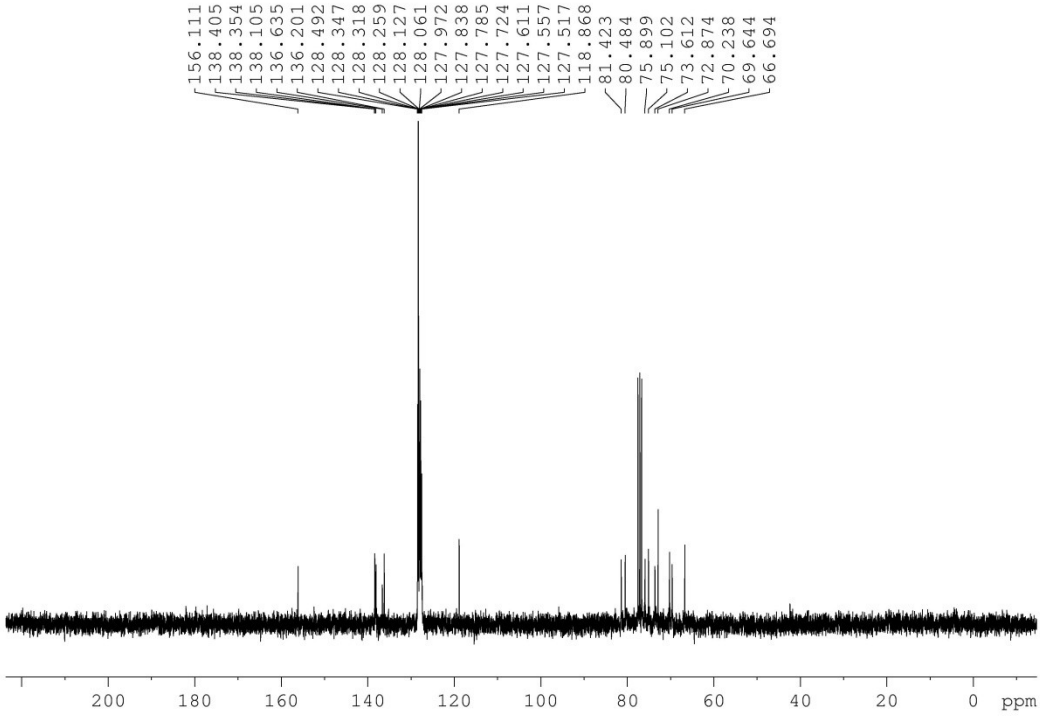
156.111
138.405
138.354
138.105
136.635
136.201
128.492
128.347
128.318
128.259
128.127
128.061
127.972
127.838
127.785
127.724
127.611
127.557
127.517
118.868
81.423
80.484
75.899
75.102
73.612
72.874
70.238
69.644
66.694
200
180
160
140
120
100
80
60
40
20
0
ppm

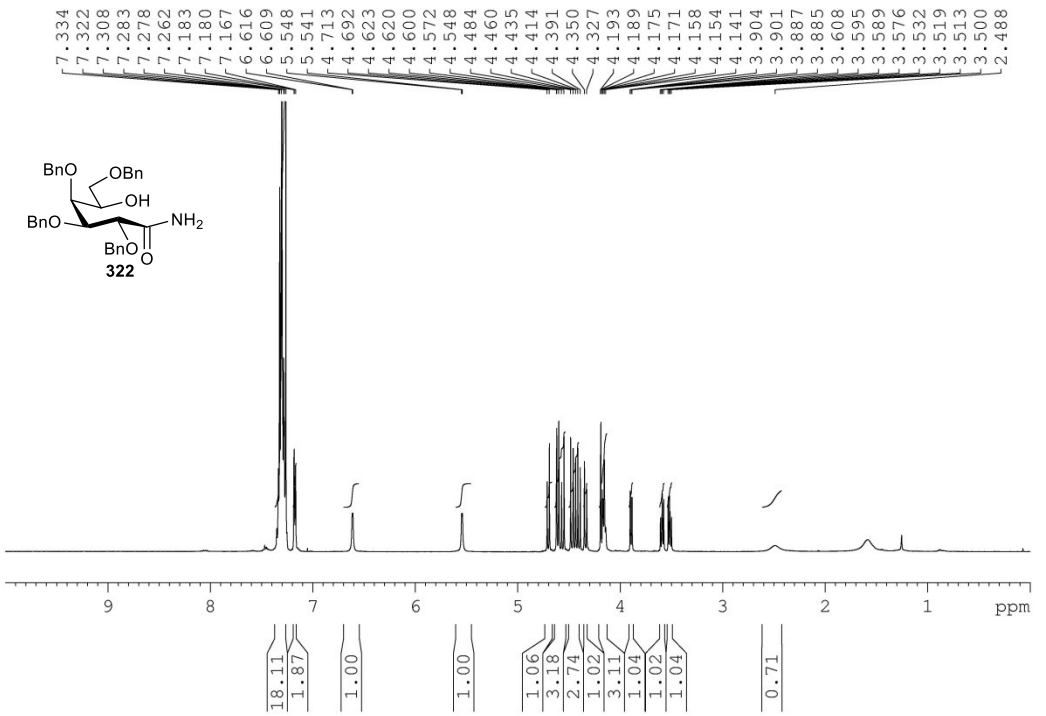
7.334
7.322
7.308
7.283
7.278
7.262
7.183
7.180
7.167
6.616
6.609
5.548
5.541
4.713
4.692
4.623
4.620
4.600
4.572
4.548
4.484
4.460
4.435
4.414
4.391
4.350
4.327
4.193
4.189
4.175
4.171
4.158
4.154
4.141
3.904
3.901
3.887
3.885
3.608
3.595
3.589
3.576
3.532
3.519
3.513
3.500
2.488
BnO
OBn
OH
BnO
NH2
BnO
O
322
9
8
7
6
5
4
3
2
1
ppm
18.11
1.87
1.00
1.00
1.06
3.18
2.74
1.02
3.11
1.04
1.02
1.04
0.71

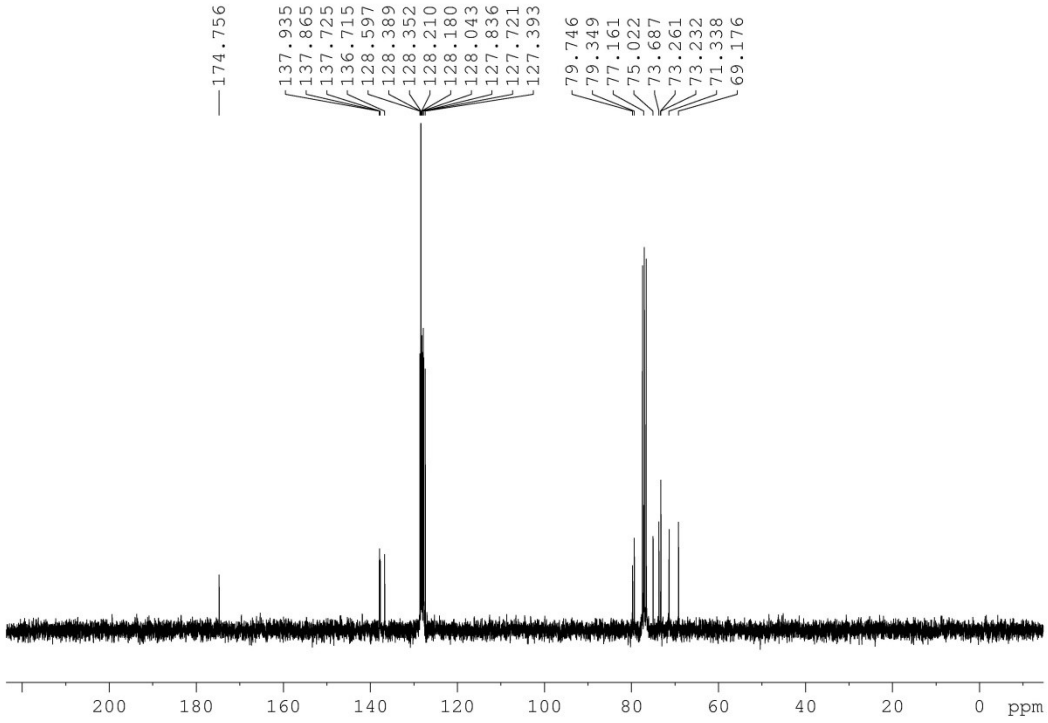
174.756
137.935
137.865
137.725
136.715
128.597
128.389
128.352
128.210
128.180
128.043
127.836
127.721
127.393
79.746
79.349
77.161
75.022
73.687
73.261
73.232
71.338
69.176
200
180
160
140
120
100
80
60
40
20
0
ppm

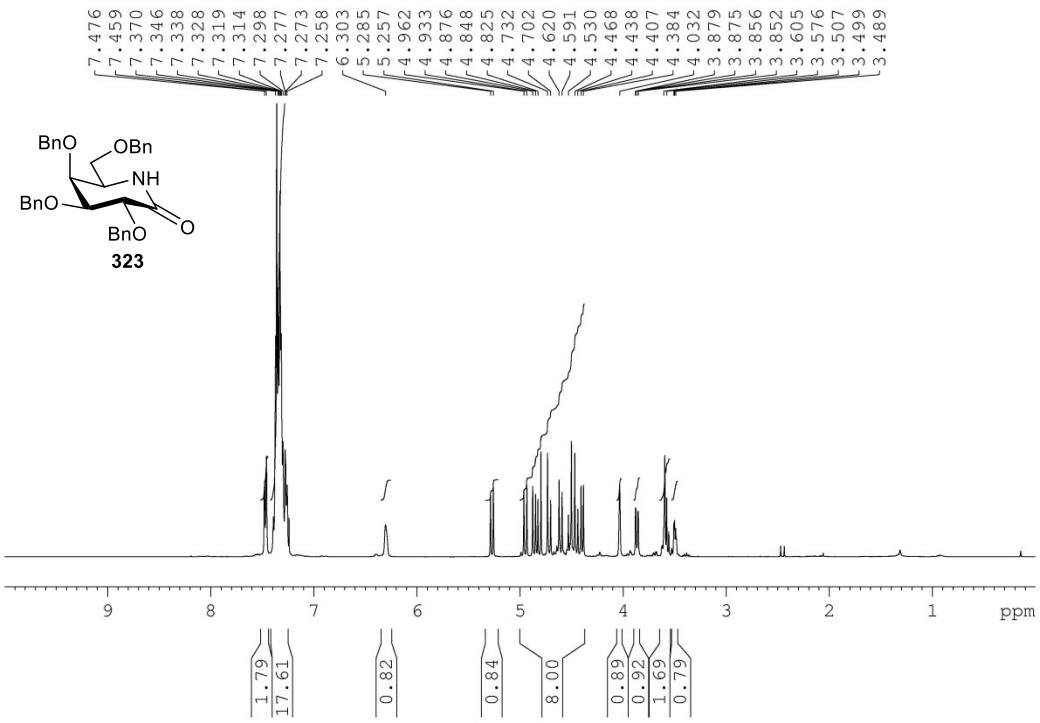
7.476
7.459
7.370
7.346
7.338
7.328
7.319
7.314
7.298
7.277
7.273
7.258
6.303
5.285
5.257
4.962
4.933
4.876
4.848
4.825
4.732
4.702
4.620
4.591
4.530
4.468
4.438
4.407
4.384
4.032
3.879
3.875
3.856
3.852
3.605
3.576
3.507
3.499
3.489
BnO
OBn
NH
BnO
BnO
O
323
9
8
7
6
5
4
3
2
1
ppm
1.79
17.61
0.82
0.84
8.00
0.89
0.92
1.69
0.79

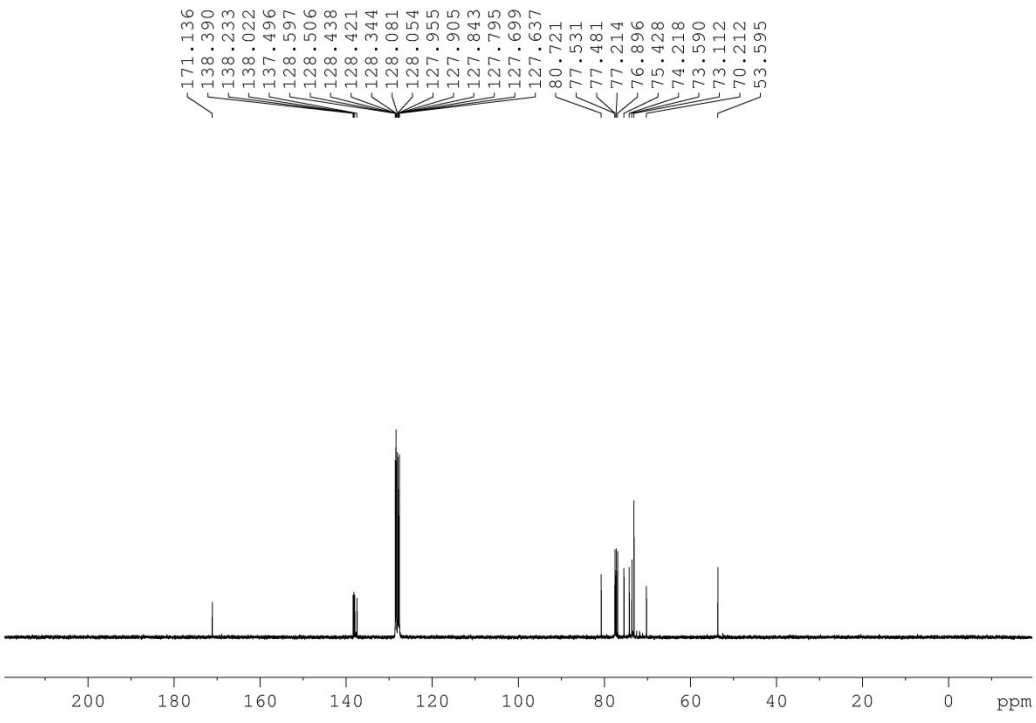
171.136
138.390
138.233
138.022
137.496
128.597
128.506
128.438
128.421
128.344
128.081
128.054
127.955
127.905
127.843
127.795
127.699
127.637
80.721
77.531
77.481
77.214
76.896
75.428
74.218
73.590
73.112
70.212
53.595
200
180
160
140
120
100
80
60
40
20
0
ppm

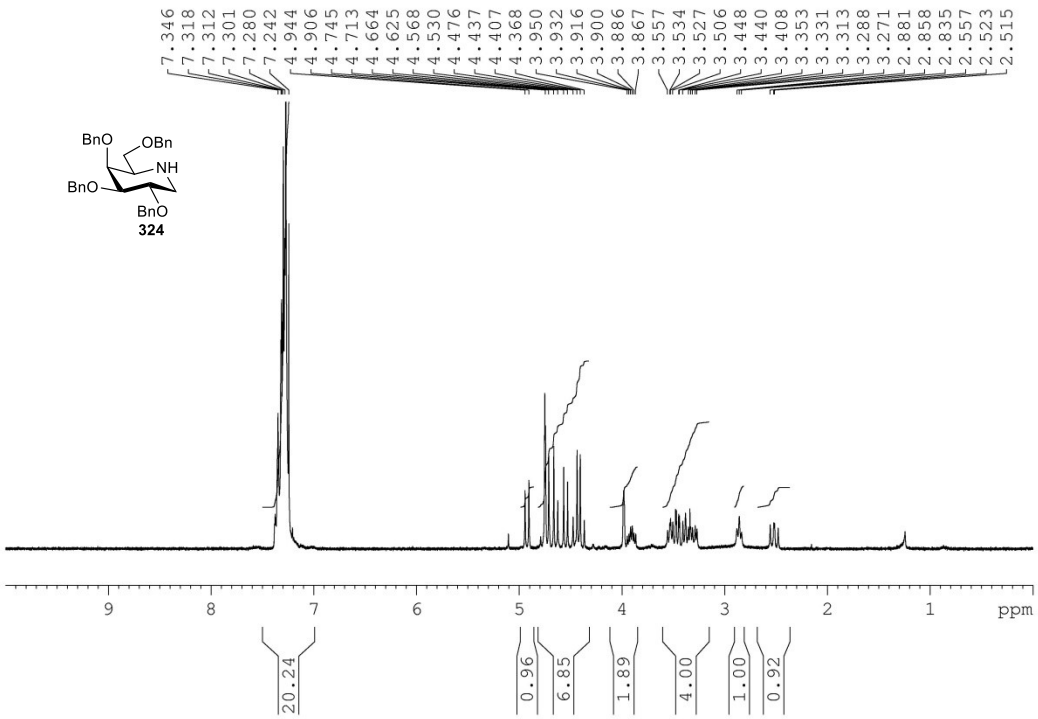
7.346
7.318
7.312
7.301
7.280
7.242
4.944
4.906
4.745
4.713
4.664
4.625
4.568
4.530
4.476
4.437
4.407
4.368
3.950
3.932
3.916
3.900
3.886
3.867
3.557
3.534
3.527
3.506
3.448
3.440
3.408
3.353
3.331
3.313
3.288
3.271
2.881
2.858
2.835
2.557
2.523
2.515
BnO
OBn
NH
BnO
BnO
324
9
8
7
6
5
4
3
2
1
ppm
20.24
0.96
6.85
1.89
4.00
1.00
0.92

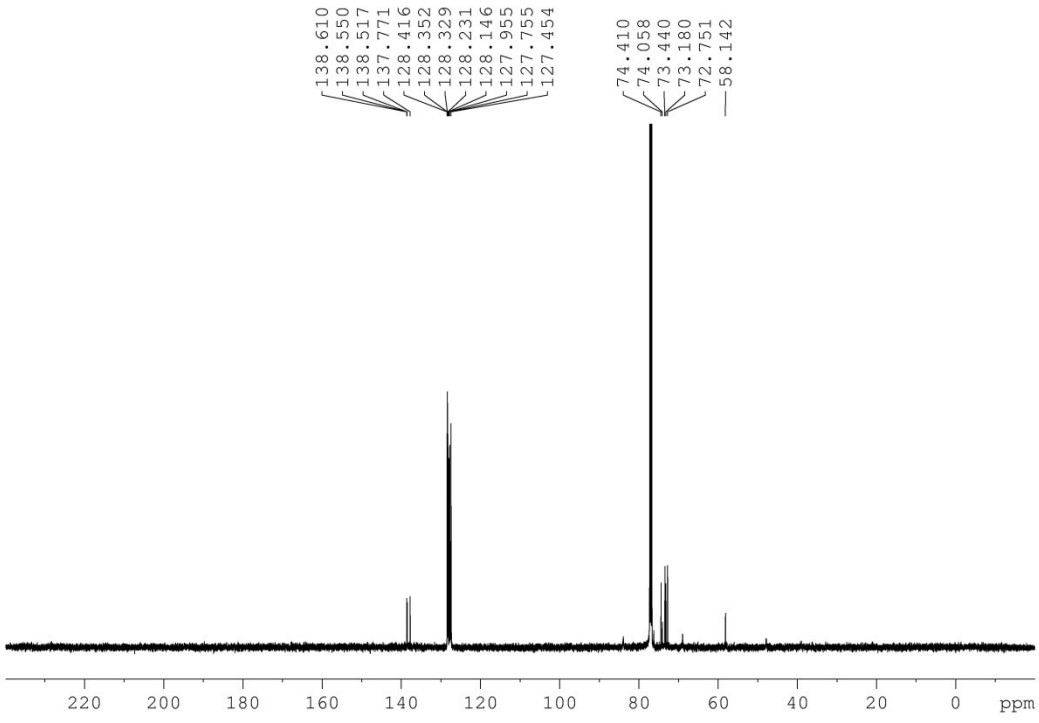
138.610
138.550
138.517
137.771
128.416
128.352
128.329
128.231
128.146
127.955
127.755
127.454
74.410
74.058
73.440
73.180
72.751
58.142
220
200
180
160
140
120
100
80
60
40
20
0
ppm

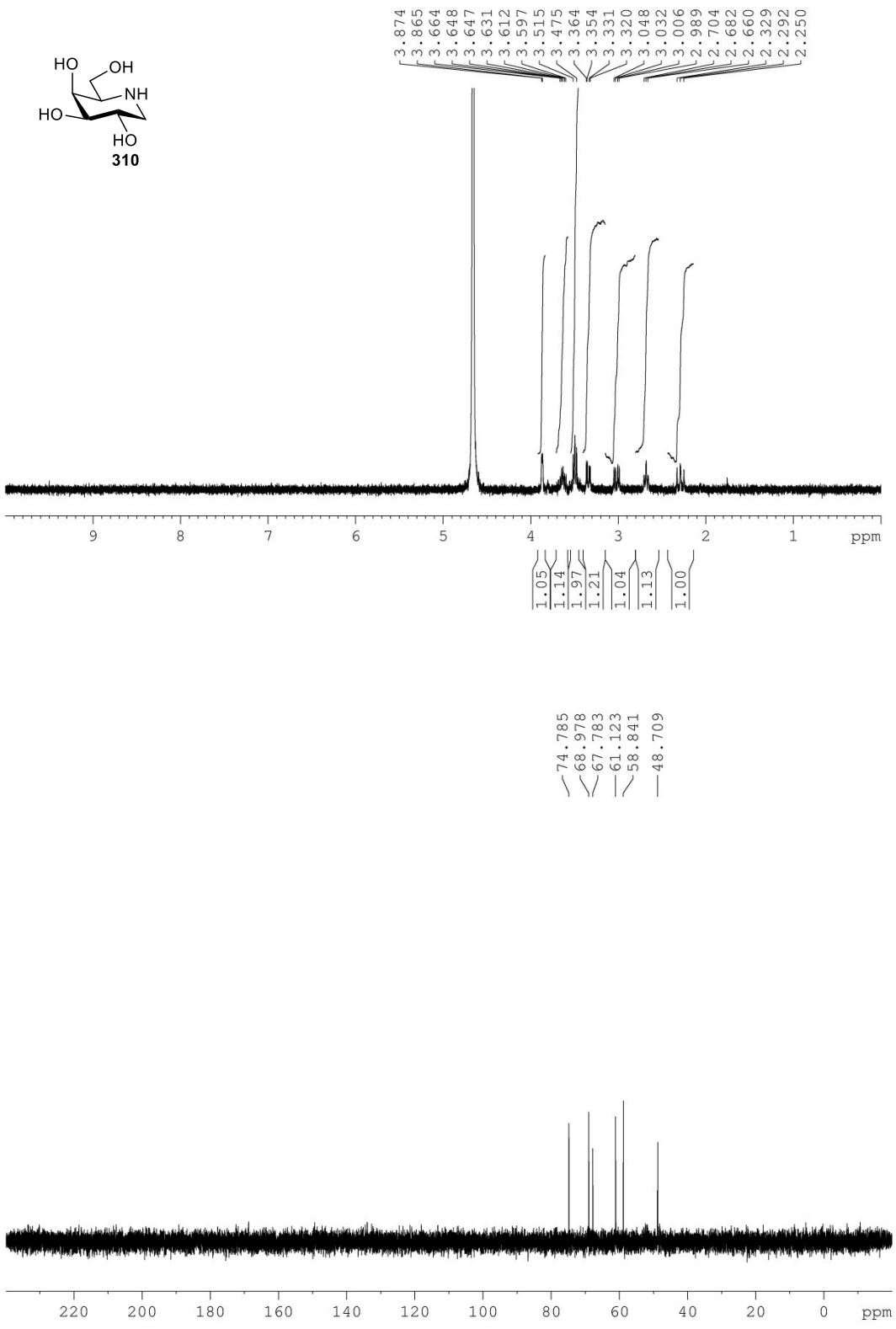
HO
OH
NH
HO
HO
310
3.874
3.865
3.664
3.648
3.647
3.631
3.612
3.597
3.515
3.475
3.364
3.354
3.331
3.320
3.048
3.032
3.006
2.989
2.704
2.682
2.660
2.329
2.292
2.250
9
8
7
6
5
4
3
2
1
ppm
1.05
1.14
1.97
1.21
1.04
1.13
1.00
74.785
68.978
67.783
61.123
58.841
48.709
220
200
180
160
140
120
100
80
60
40
20
0
ppm

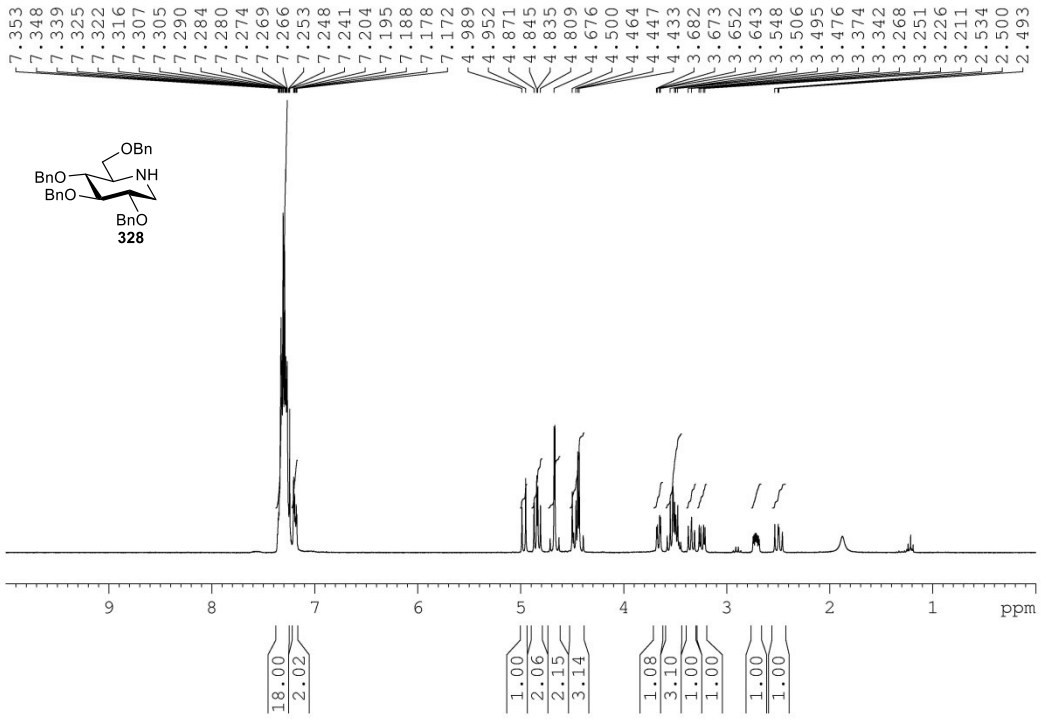
7.353
7.348
7.339
7.325
7.322
7.316
7.307
7.305
7.290
7.284
7.280
7.274
7.269
7.266
7.253
7.248
7.241
7.204
7.195
7.188
7.178
7.172
4.989
4.952
4.871
4.845
4.835
4.809
4.676
4.500
4.464
4.447
4.433
3.682
3.673
3.652
3.643
3.548
3.506
3.495
3.476
3.374
3.342
3.268
3.251
3.226
3.211
2.534
2.500
2.493
OBn
BnO
BnO
NH
BnO
328
9
8
7
6
5
4
3
2
1
ppm
18.00
2.02
1.00
2.06
2.15
3.14
1.08
3.10
1.00
1.00
1.00
1.00

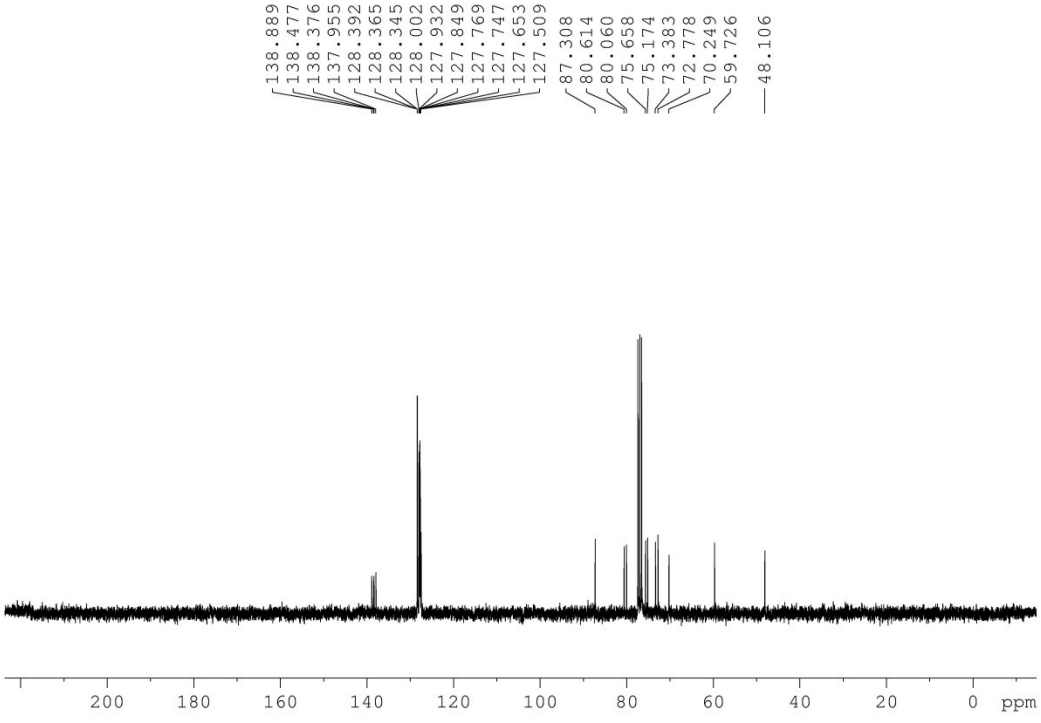
138.889
138.477
138.376
137.955
128.392
128.365
128.345
128.002
127.932
127.849
127.769
127.747
127.653
127.509
87.308
80.614
80.060
75.658
75.174
73.383
72.778
70.249
59.726
48.106
200
180
160
140
120
100
80
60
40
20
0
ppm

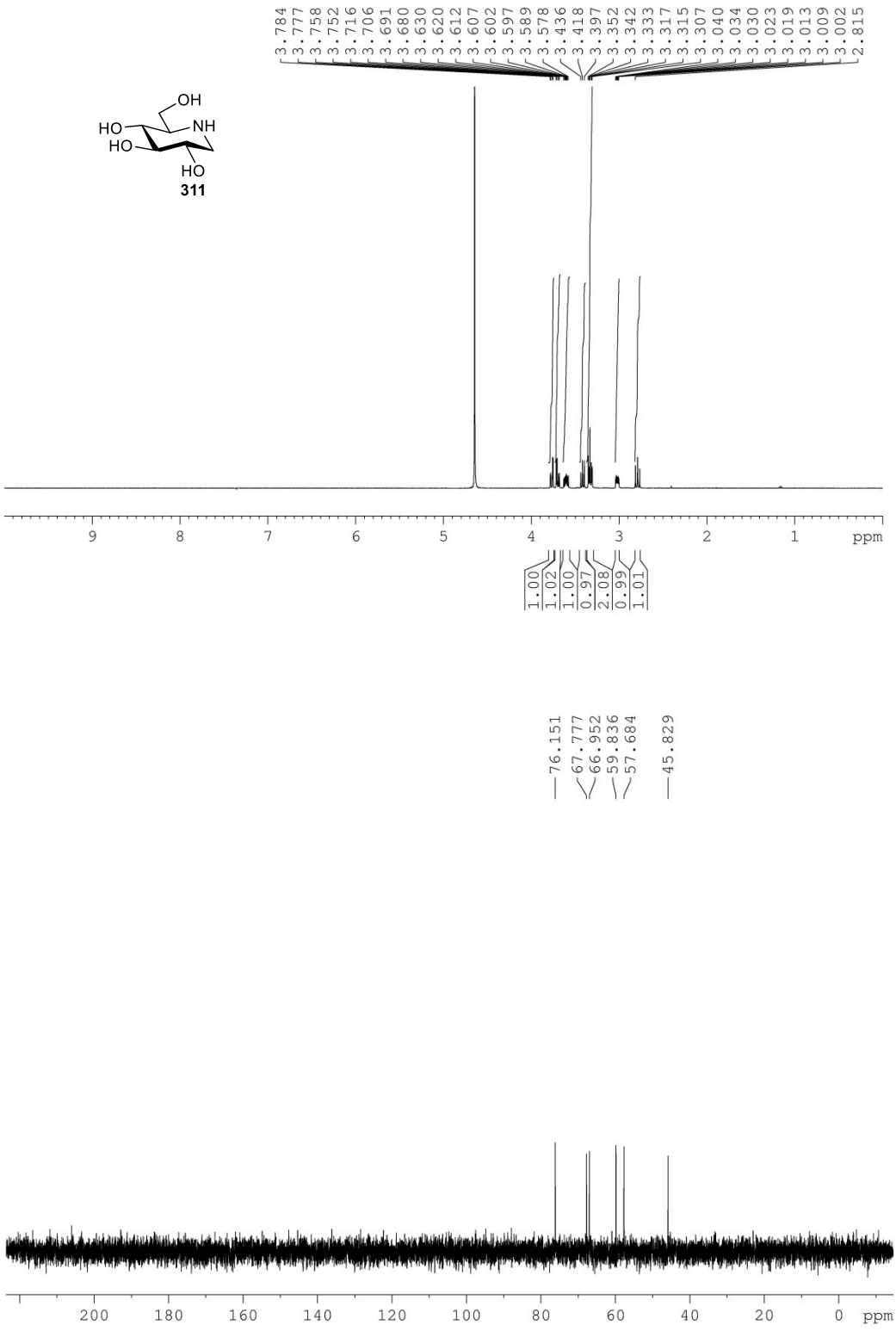
3.784
3.777
3.758
3.752
3.716
3.706
3.691
3.680
3.630
3.620
3.612
3.607
3.602
3.597
3.589
3.578
3.436
3.418
3.397
3.352
3.342
3.333
3.317
3.315
3.307
3.040
3.034
3.030
3.023
3.019
3.013
3.009
3.002
2.815
OH
HO
NH
HO
HO
311
9
8
7
6
5
4
3
2
1
ppm
1.00
1.02
1.00
0.97
2.08
0.99
1.01
76.151
67.777
66.952
59.836
57.684
45.829
200
180
160
140
120
100
80
60
40
20
0
ppm

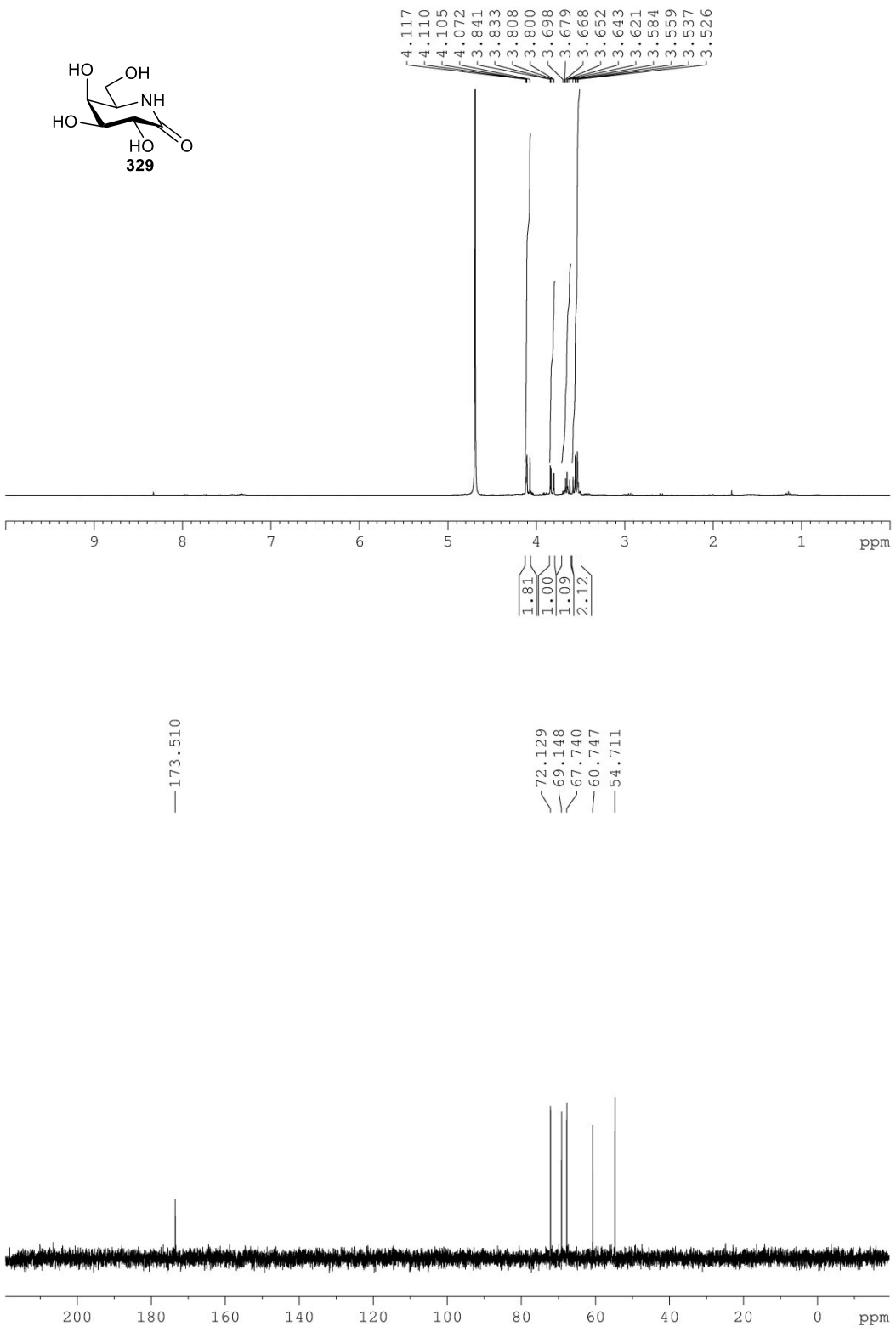
HO
OH
NH
HO
HO
O
329
4.117
4.110
4.105
4.072
3.841
3.833
3.808
3.800
3.698
3.679
3.668
3.652
3.643
3.621
3.584
3.559
3.537
3.526
9
8
7
6
5
4
3
2
1
ppm
1.81
1.00
1.09
2.12
173.510
72.129
69.148
67.740
60.747
54.711
200
180
160
140
120
100
80
60
40
20
0
ppm

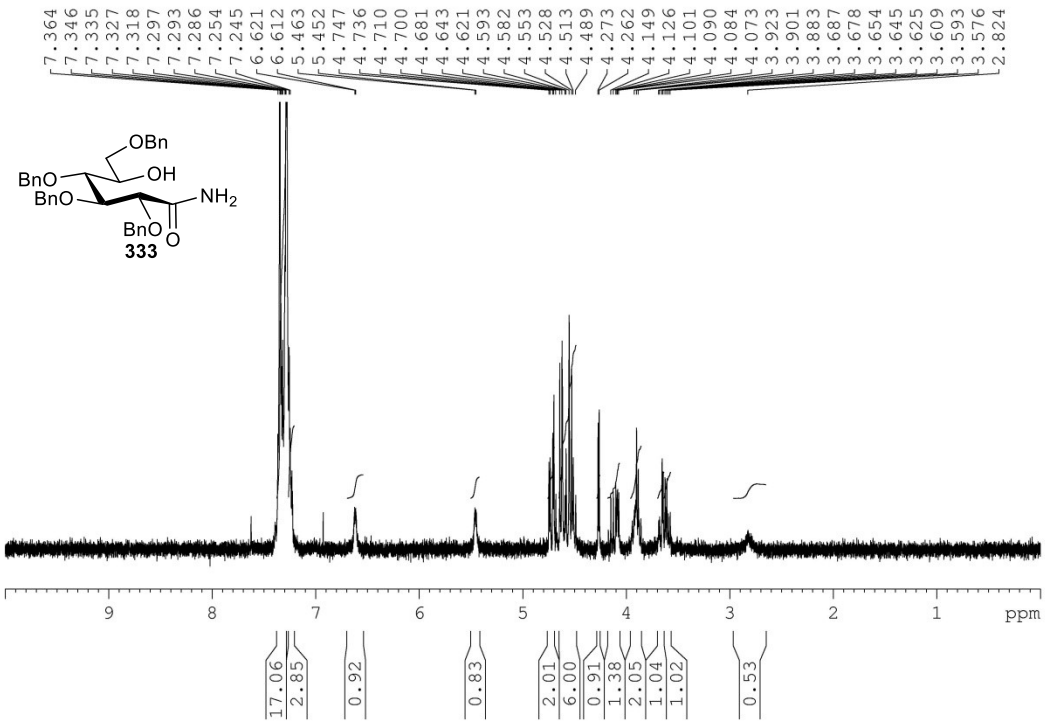
7.364
7.346
7.335
7.327
7.318
7.297
7.293
7.286
7.254
7.245
6.621
6.612
5.463
5.452
4.747
4.736
4.710
4.700
4.681
4.643
4.621
4.593
4.582
4.553
4.528
4.513
4.489
4.273
4.262
4.149
4.126
4.101
4.090
4.084
4.073
3.923
3.901
3.883
3.687
3.678
3.654
3.645
3.625
3.609
3.593
3.576
2.824
OBn
OH
BnO
BnO
NH2
BnO
O
333
9
8
7
6
5
4
3
2
1
ppm
17.06
2.85
0.92
0.83
2.01
6.00
0.91
1.38
2.05
1.04
1.02
0.53

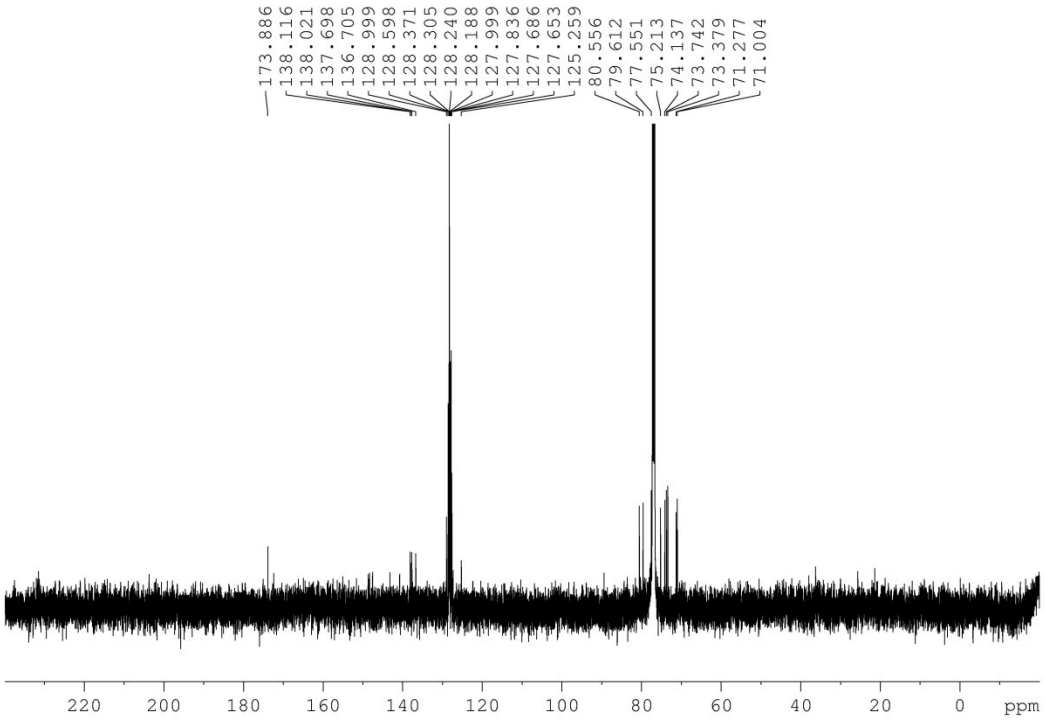
173.886
138.116
138.021
137.698
136.705
128.999
128.598
128.371
128.305
128.240
128.188
127.999
127.836
127.686
127.653
125.259
80.556
79.612
77.551
75.213
74.137
73.742
73.379
71.277
71.004
220
200
180
160
140
120
100
80
60
40
20
0
ppm

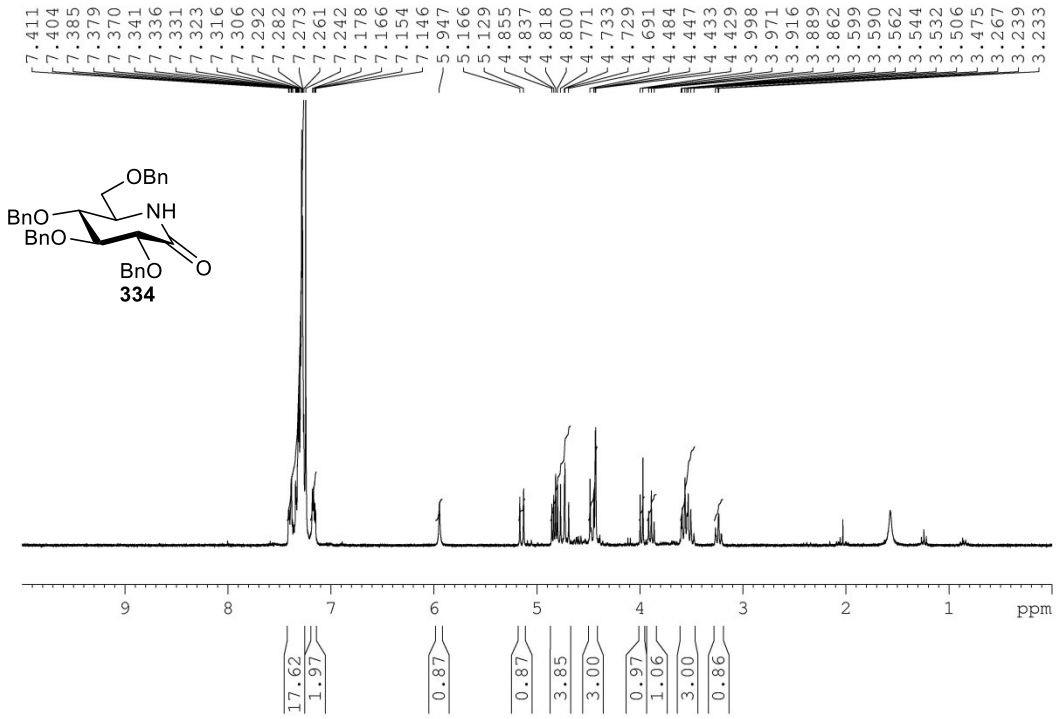
7.411
7.404
7.385
7.379
7.370
7.341
7.336
7.331
7.323
7.316
7.306
7.292
7.282
7.273
7.261
7.242
7.178
7.166
7.154
7.146
5.947
5.166
5.129
4.855
4.837
4.818
4.800
4.771
4.733
4.729
4.691
4.484
4.447
4.433
4.429
3.998
3.971
3.916
3.889
3.862
3.599
3.590
3.562
3.544
3.532
3.506
3.475
3.267
3.239
3.233
OBn
NH
BnO
BnO
BnO
O
334
9
8
7
6
5
4
3
2
1
ppm
17.62
1.97
0.87
0.87
3.85
3.00
0.97
1.06
3.00
0.86

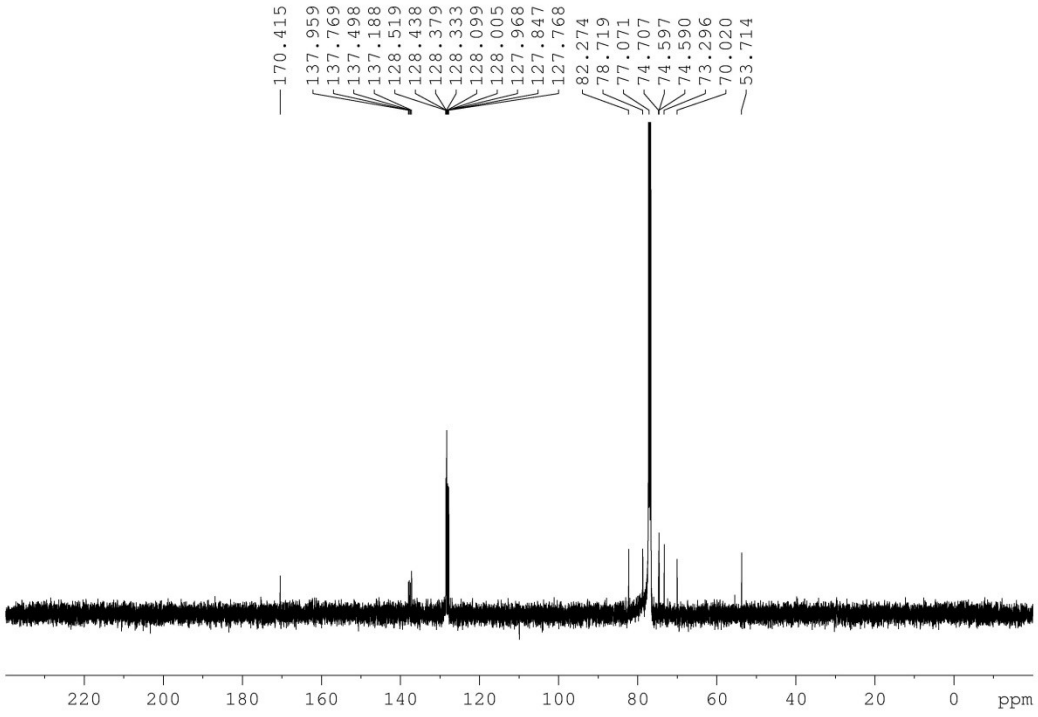
170.415
137.959
137.769
137.498
137.188
128.519
128.438
128.379
128.333
128.099
128.005
127.968
127.847
127.768
82.274
78.719
77.071
74.707
74.597
74.590
73.296
70.020
53.714
220
200
180
160
140
120
100
80
60
40
20
0
ppm

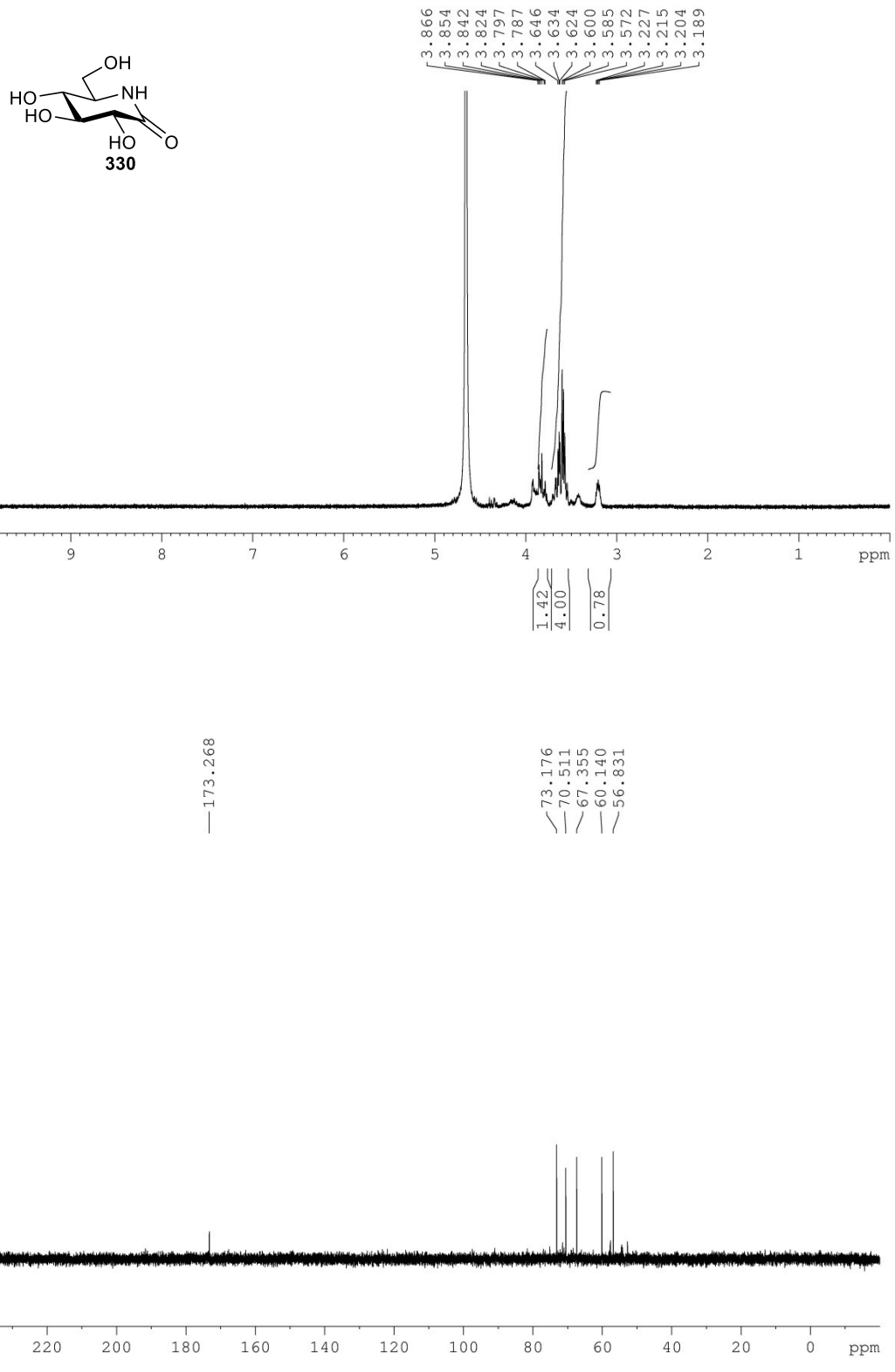
OH
HO
NH
HO
HO
O
330
3.866
3.854
3.842
3.824
3.797
3.787
3.646
3.634
3.624
3.600
3.585
3.572
3.227
3.215
3.204
3.189
9
8
7
6
5
4
3
2
1
ppm
1.42
4.00
0.78
173.268
73.176
70.511
67.355
60.140
56.831
220
200
180
160
140
120
100
80
60
40
20
0
ppm

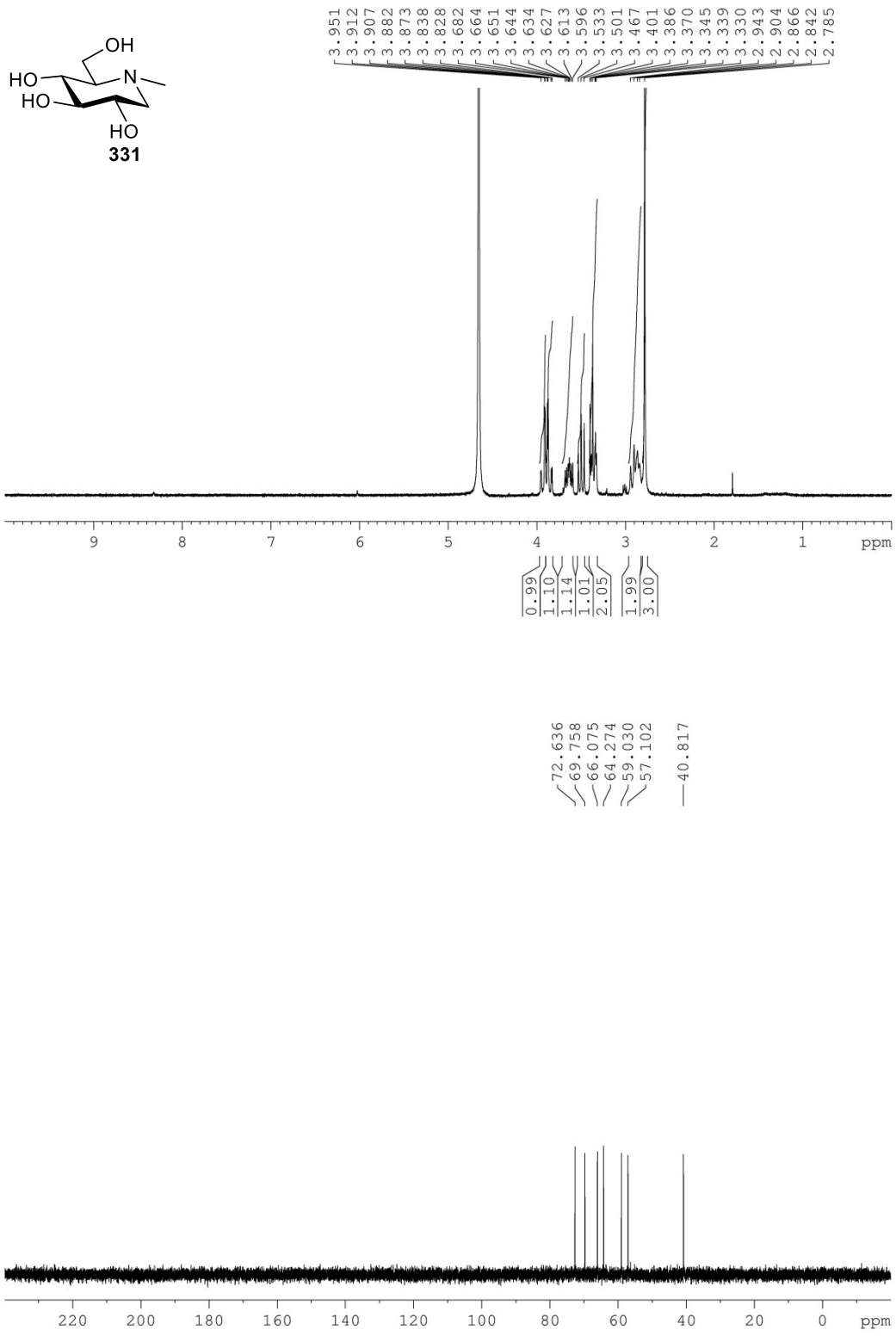
OH
HO
N
HO
HO
331
3.951
3.912
3.907
3.882
3.873
3.838
3.828
3.682
3.664
3.651
3.644
3.634
3.627
3.613
3.596
3.533
3.501
3.467
3.401
3.386
3.370
3.345
3.339
3.330
2.943
2.904
2.866
2.842
2.785
9
8
7
6
5
4
3
2
1
ppm
0.99
1.10
1.14
1.01
2.05
1.99
3.00
72.636
69.758
66.075
64.274
59.030
57.102
40.817
220
200
180
160
140
120
100
80
60
40
20
0
ppm

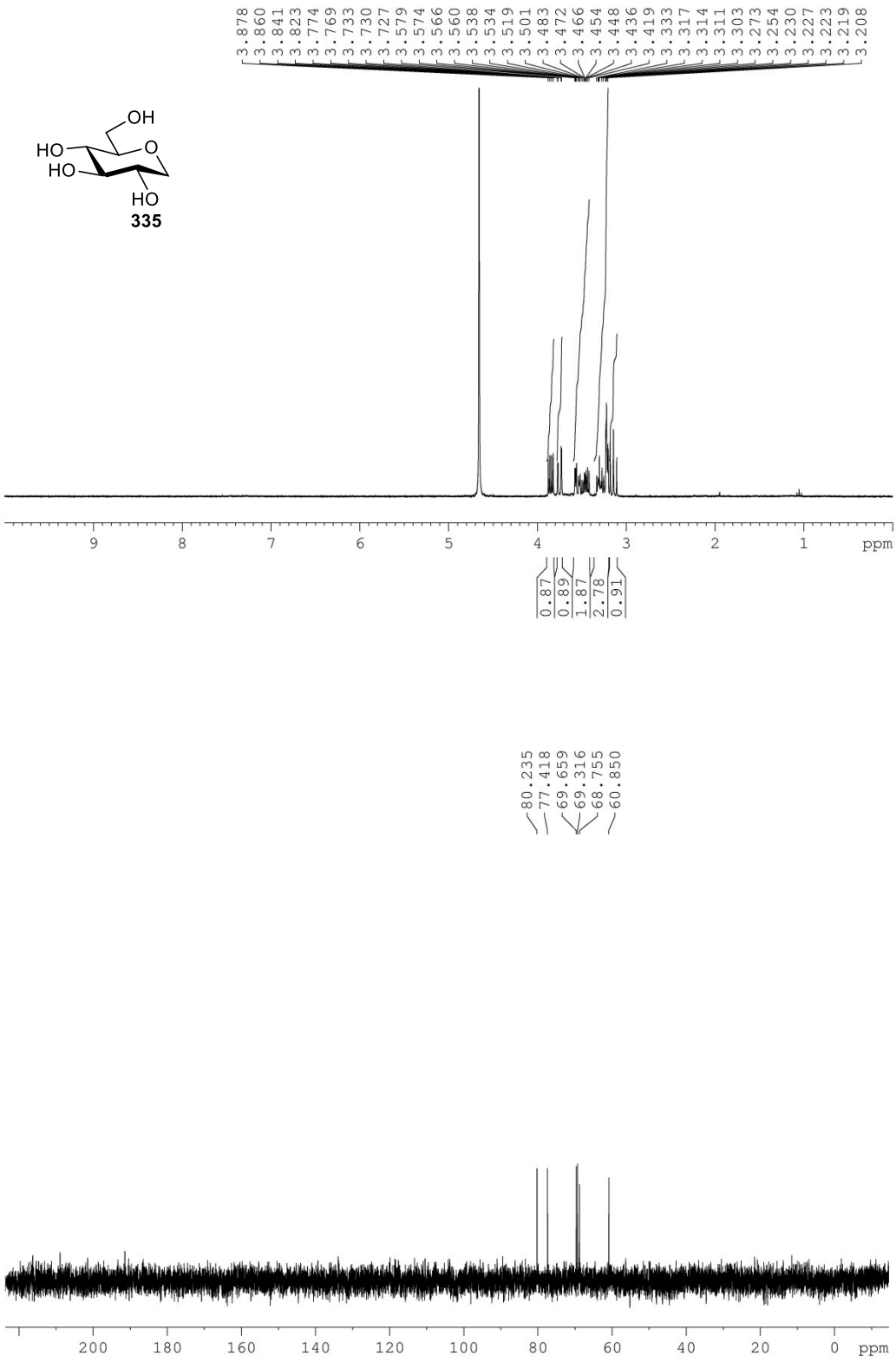
3.878
3.860
3.841
3.823
3.774
3.769
3.733
3.730
3.727
3.579
3.574
3.566
3.560
3.538
3.534
3.519
3.501
3.483
3.472
3.466
3.454
3.448
3.436
3.419
3.333
3.317
3.314
3.311
3.303
3.273
3.254
3.230
3.227
3.223
3.219
3.208
OH
HO
O
HO
HO
335
9
8
7
6
5
4
3
2
1
ppm
0.87
0.89
1.87
2.78
0.91
80.235
77.418
69.659
69.316
68.755
60.850
200
180
160
140
120
100
80
60
40
20
0
ppm

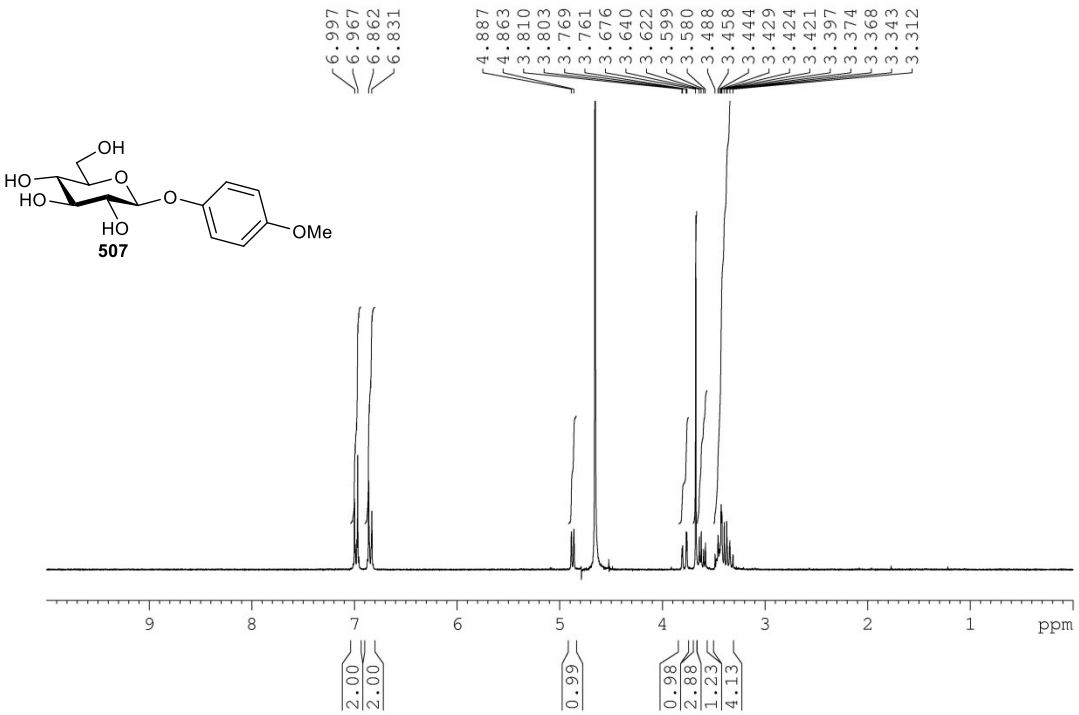
6.997
6.967
6.862
6.831
4.887
4.863
3.810
3.803
3.769
3.761
3.676
3.640
3.622
3.599
3.580
3.488
3.458
3.444
3.429
3.424
3.421
3.397
3.374
3.368
3.343
3.312
OH
HO
HO
HO
O
O
OMe
507
9
8
7
6
5
4
3
2
1
ppm
2.00
2.00
0.99
0.98
2.88
1.23
4.13

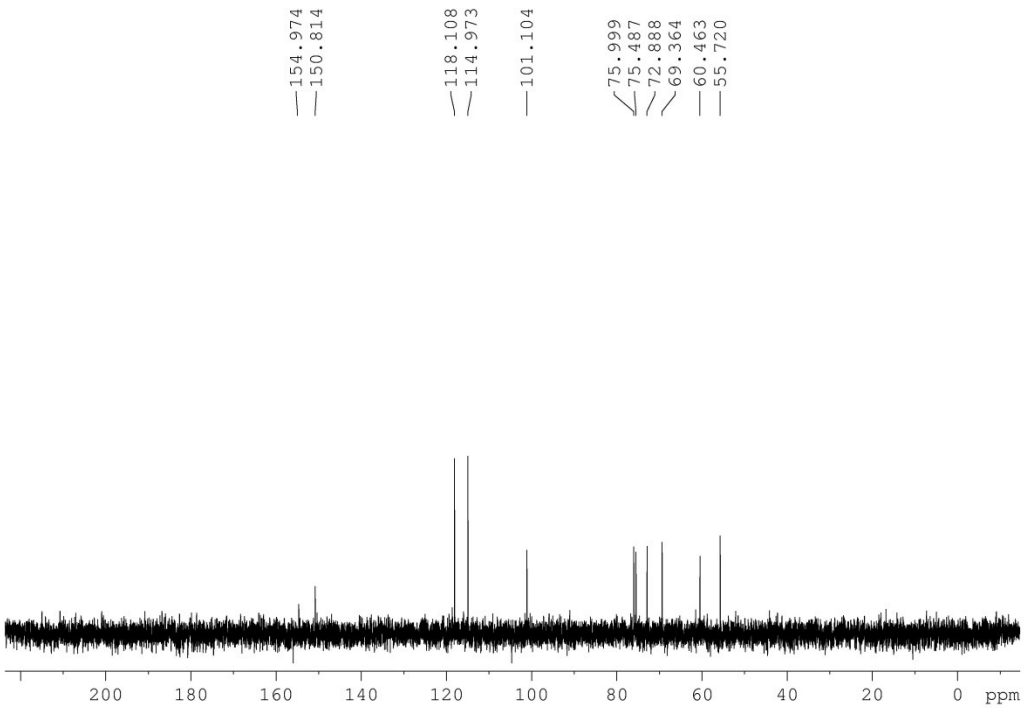
154.974
150.814
118.108
114.973
101.104
75.999
75.487
72.888
69.364
60.463
55.720
200
180
160
140
120
100
80
60
40
20
0
ppm

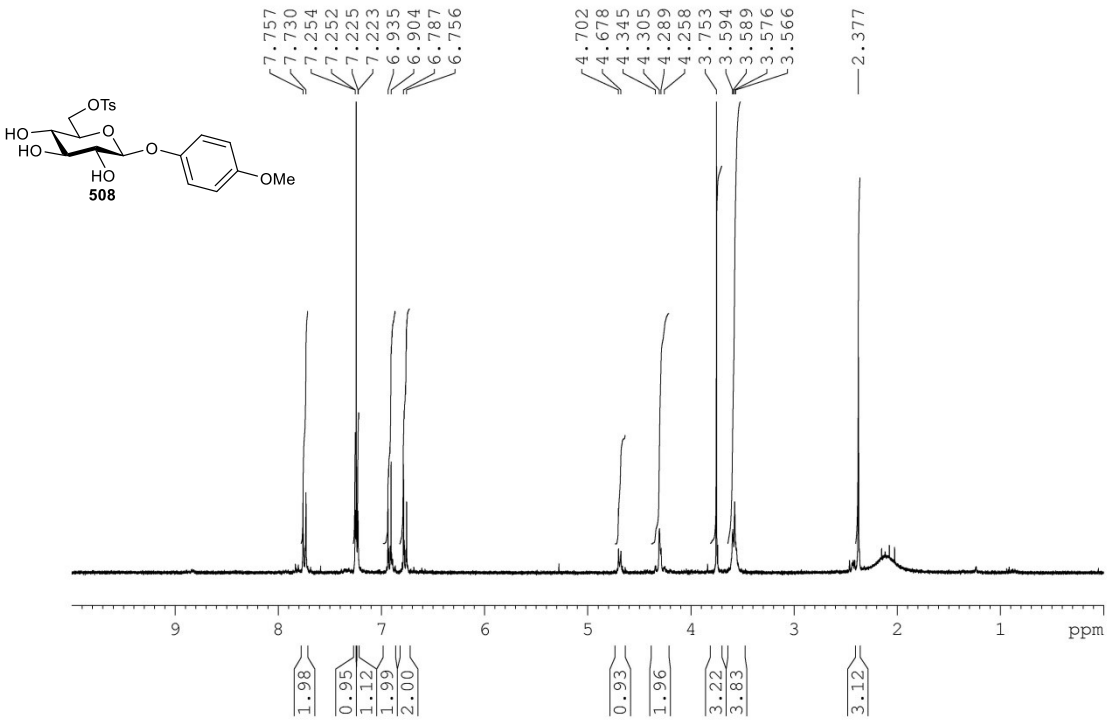
7.757
7.730
7.254
7.252
7.225
7.223
6.935
6.904
6.787
6.756
4.702
4.678
4.345
4.305
4.289
4.258
3.753
3.594
3.589
3.576
3.566
2.377
OTs
HO
HO
HO
O
O
OMe
508
9
8
7
6
5
4
3
2
1
ppm
1.98
0.95
1.12
1.99
2.00
0.93
1.96
3.22
3.83
3.12

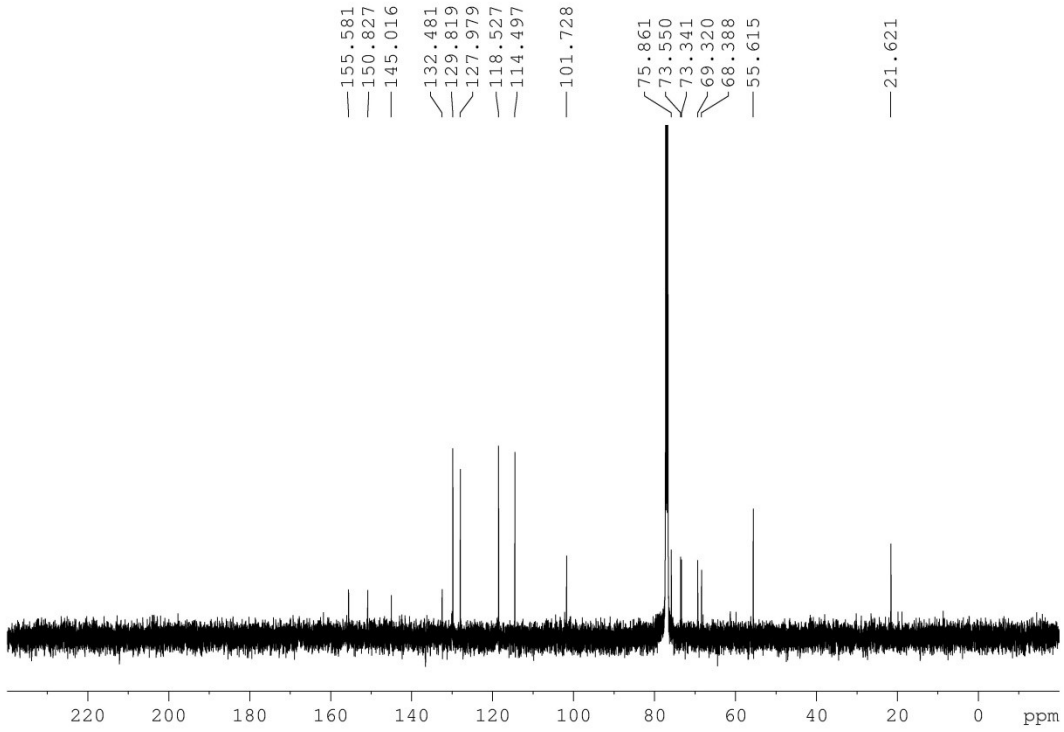
155.581
150.827
145.016
132.481
129.819
127.979
118.527
114.497
101.728
75.861
73.550
73.341
69.320
68.388
55.615
21.621
220
200
180
160
140
120
100
80
60
40
20
0
ppm

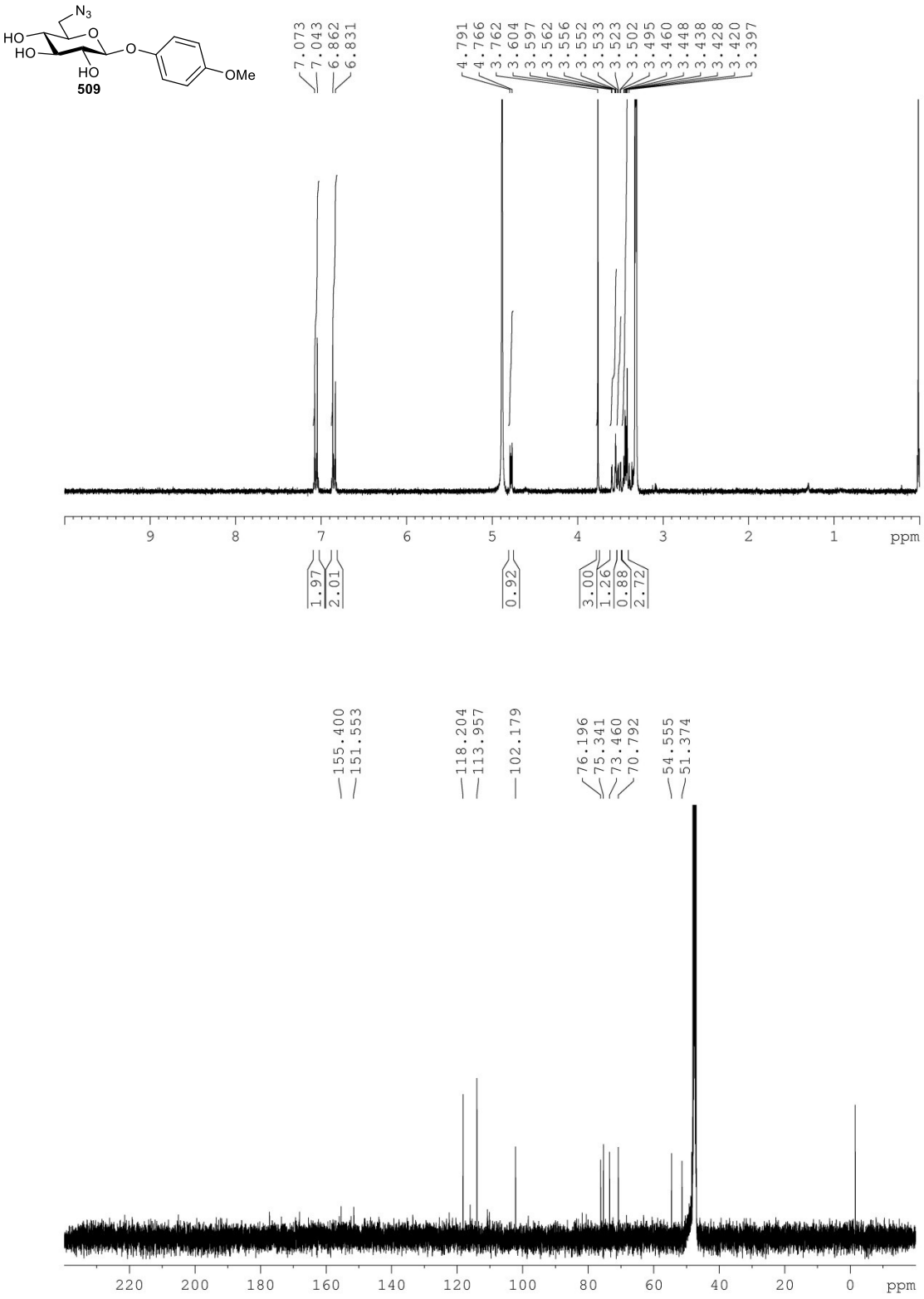
N3
HO
HO
HO
O
O
OMe
509
7.073
7.043
6.862
6.831
4.791
4.766
3.762
3.604
3.597
3.562
3.556
3.552
3.533
3.523
3.502
3.495
3.460
3.448
3.438
3.428
3.420
3.397
9
8
7
6
5
4
3
2
1
ppm
1.97
2.01
0.92
3.00
1.26
0.88
2.72
155.400
151.553
118.204
113.957
102.179
76.196
75.341
73.460
70.792
54.555
51.374
220
200
180
160
140
120
100
80
60
40
20
0
ppm

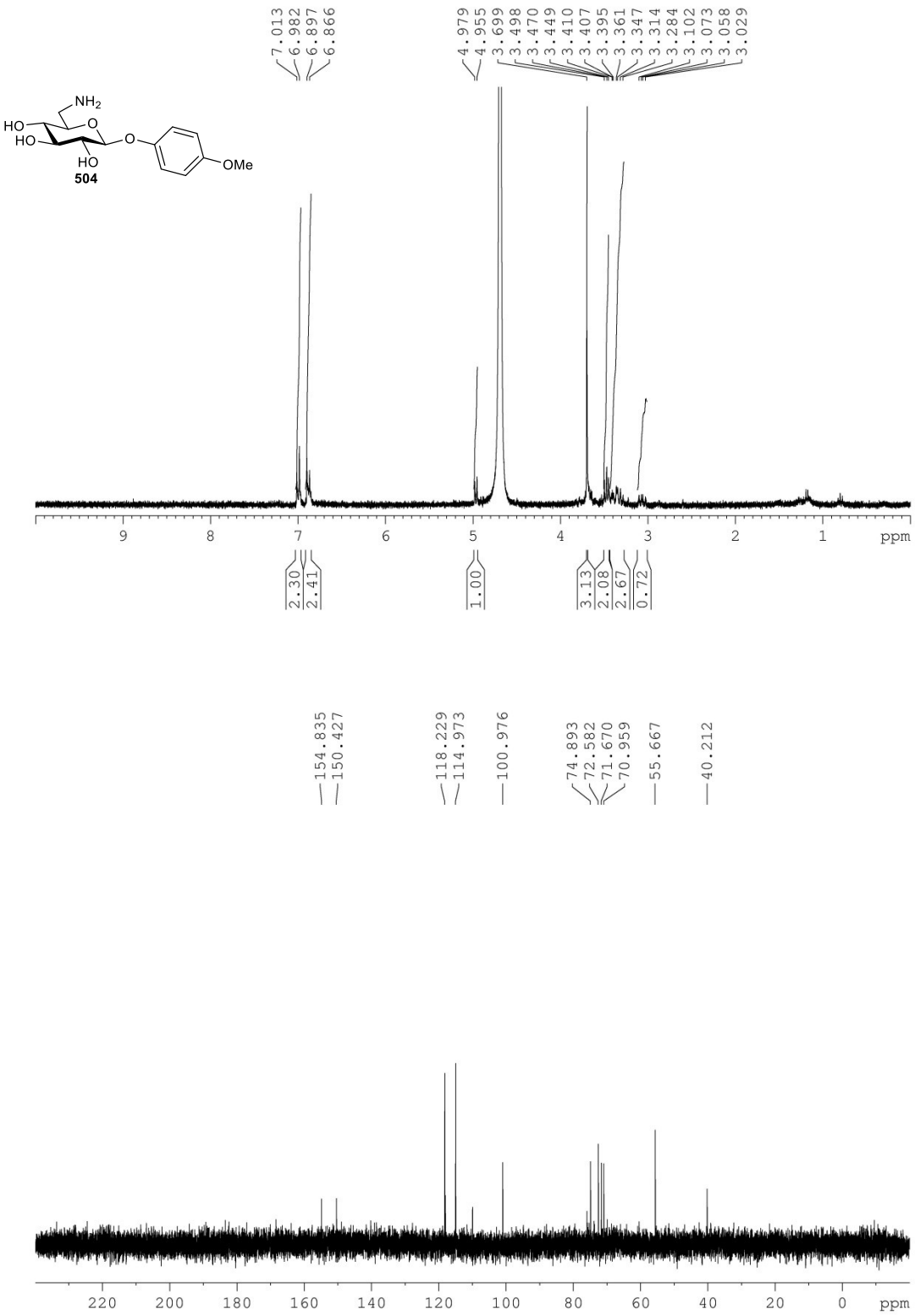
7.013
6.982
6.897
6.866
4.979
4.955
3.699
3.498
3.470
3.449
3.410
3.407
3.395
3.361
3.347
3.314
3.284
3.102
3.073
3.058
3.029
NH2
HO
HO
HO
O
O
OMe
504
ppm
2.30
2.41
1.00
3.13
2.08
2.67
0.72
154.835
150.427
118.229
114.973
100.976
74.893
72.582
71.670
70.959
55.667
40.212
ppm

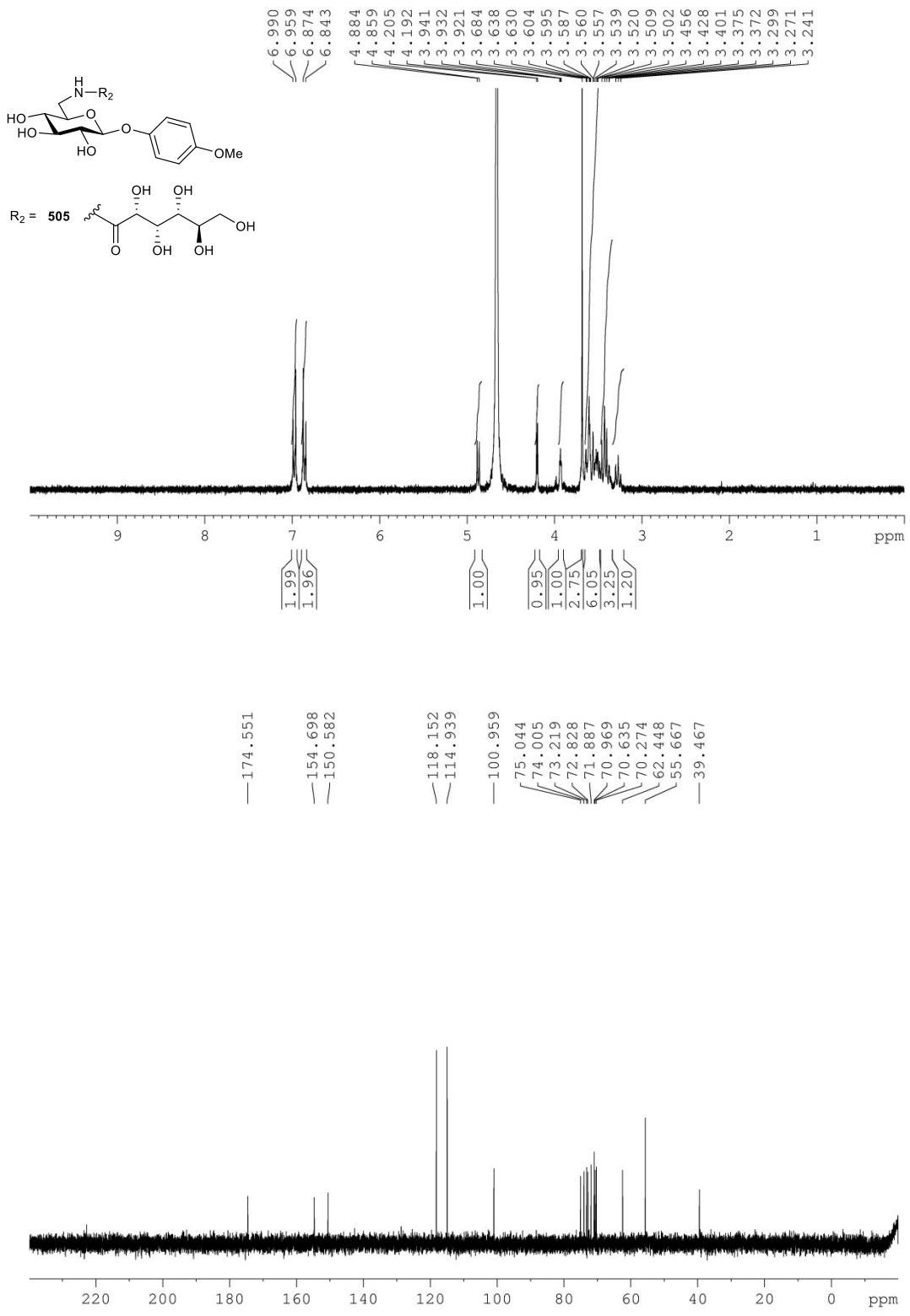
6.990
6.959
6.874
6.843
4.884
4.859
4.205
4.192
3.941
3.932
3.921
3.684
3.638
3.630
3.604
3.595
3.587
3.560
3.557
3.539
3.520
3.509
3.502
3.456
3.428
3.401
3.375
3.372
3.299
3.271
3.241
HO
HO
HO
O
O
N
H
R2
OMe
R2 = 505
OH
OH
OH
OH
OH
O
9
8
7
6
5
4
3
2
1
ppm
1.99
1.96
1.00
0.95
1.00
2.75
6.05
3.25
1.20
174.551
154.698
150.582
118.152
114.939
100.959
75.044
74.005
73.219
72.828
71.887
70.969
70.635
70.274
62.448
55.667
39.467
220
200
180
160
140
120
100
80
60
40
20
0
ppm

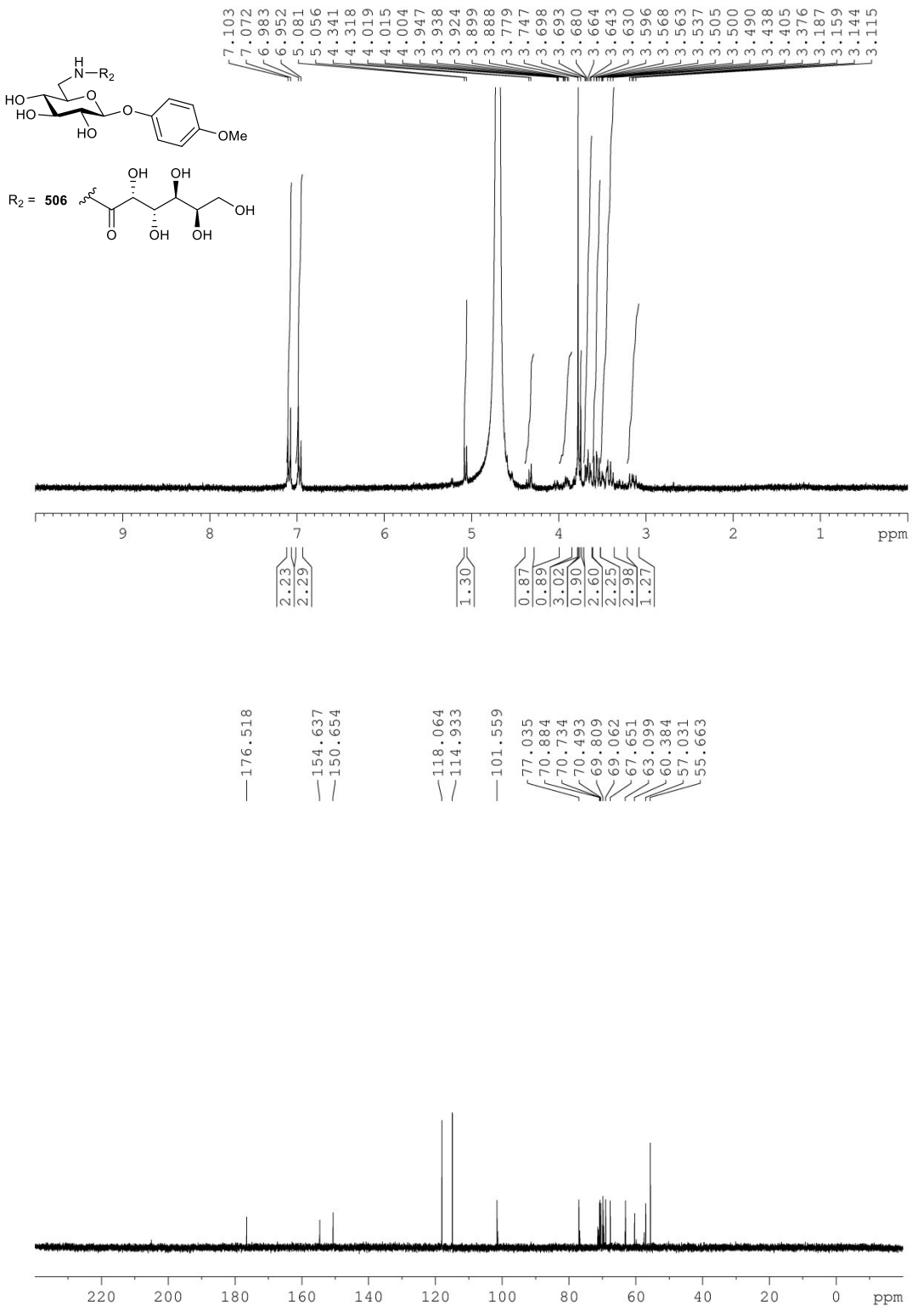
7.103
7.072
6.983
6.952
5.081
5.056
4.341
4.318
4.019
4.015
4.004
3.947
3.938
3.924
3.899
3.888
3.779
3.747
3.698
3.693
3.680
3.664
3.643
3.630
3.596
3.568
3.563
3.537
3.505
3.500
3.490
3.438
3.405
3.376
3.187
3.159
3.144
3.115
HO
HO
HO
O
O
OMe
H
N
R2
R2 = 506
OH
OH
OH
OH
OH
O
9
8
7
6
5
4
3
2
1
ppm
2.23
2.29
1.30
0.87
0.89
3.02
0.90
2.60
2.25
2.98
1.27
176.518
154.637
150.654
118.064
114.933
101.559
77.035
70.884
70.734
70.493
69.809
69.062
67.651
63.099
60.384
57.031
55.663
220
200
180
160
140
120
100
80
60
40
20
0
ppm

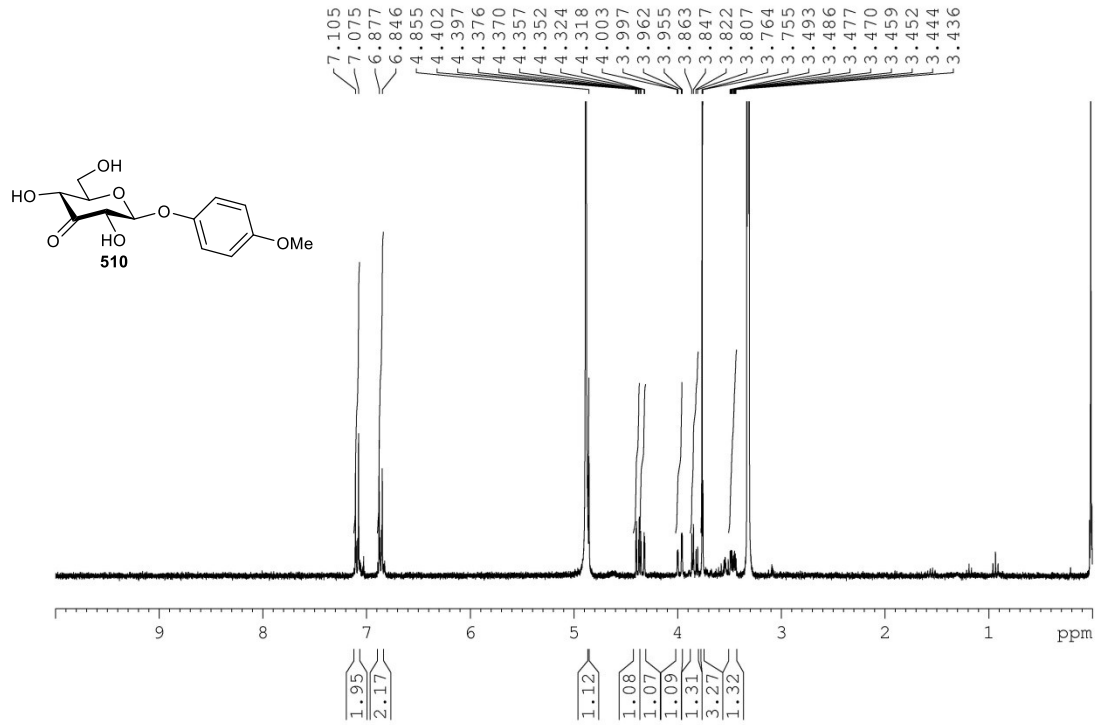
7.105
7.075
6.877
6.846
4.855
4.402
4.397
4.376
4.370
4.357
4.352
4.324
4.318
4.003
3.997
3.962
3.955
3.863
3.847
3.822
3.807
3.764
3.755
3.493
3.486
3.477
3.470
3.459
3.452
3.444
3.436
OH
HO
O
O
HO
O
OMe
510
9
8
7
6
5
4
3
2
1
ppm
1.95
2.17
1.12
1.08
1.07
1.09
1.31
3.27
1.32

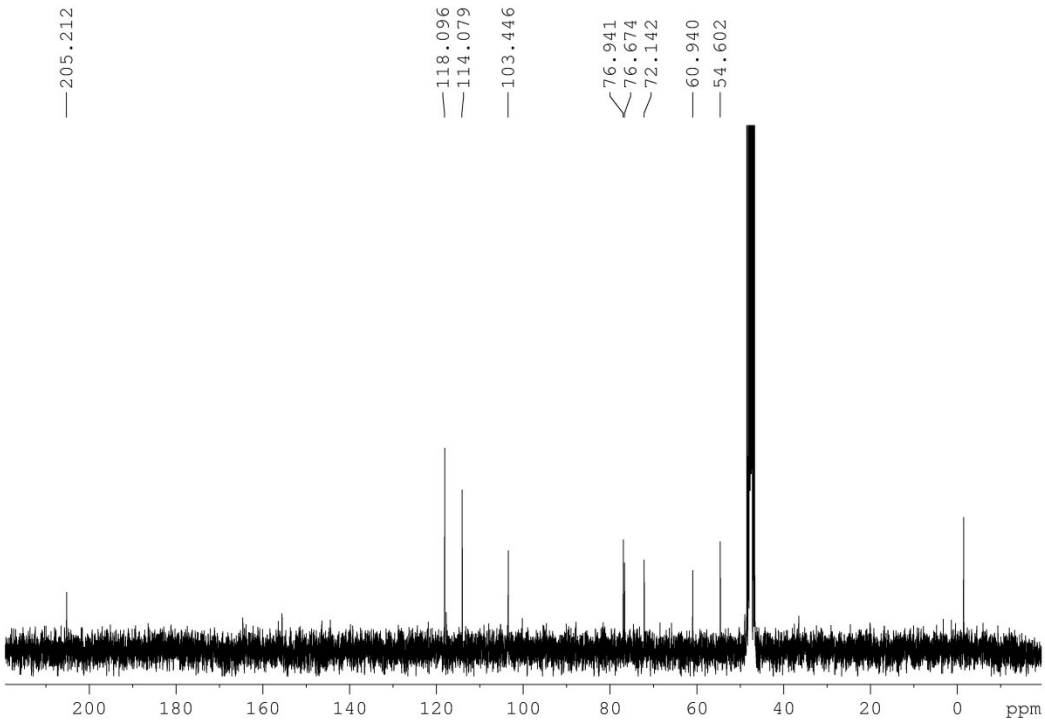
205.212
118.096
114.079
103.446
76.941
76.674
72.142
60.940
54.602
200
180
160
140
120
100
80
60
40
20
0
ppm

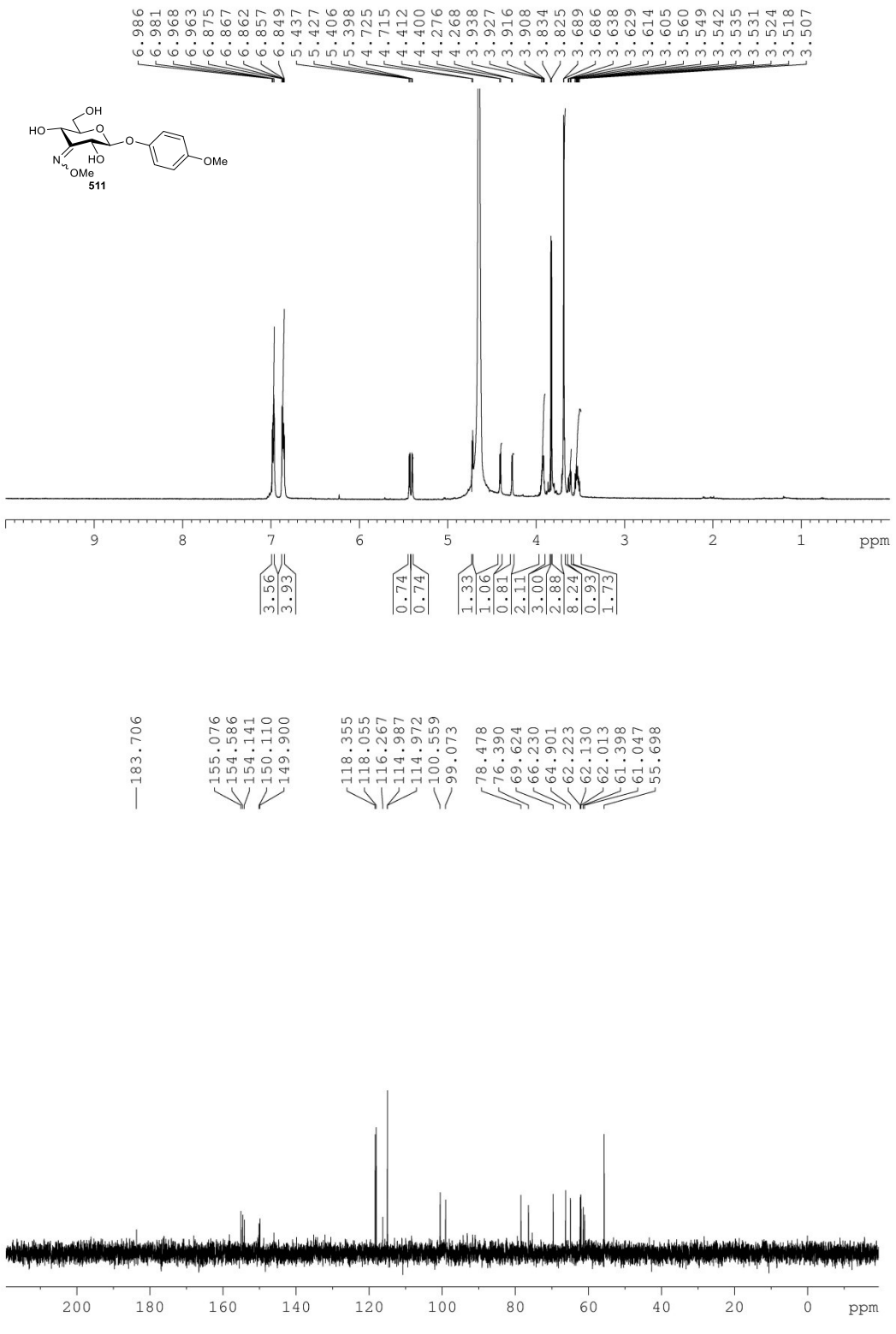
6.986
6.981
6.968
6.963
6.875
6.867
6.862
6.857
6.849
5.437
5.427
5.406
5.398
4.725
4.715
4.412
4.400
4.276
4.268
3.938
3.927
3.916
3.908
3.834
3.825
3.689
3.686
3.638
3.629
3.614
3.605
3.560
3.549
3.542
3.535
3.531
3.524
3.518
3.507
OH
HO
O
O
N
HO
OMe
OMe
511
9
8
7
6
5
4
3
2
1
ppm
3.56
3.93
0.74
0.74
1.33
1.06
0.81
2.11
3.00
2.88
8.24
0.93
1.73
183.706
155.076
154.586
154.141
150.110
149.900
118.355
118.055
116.267
114.987
114.972
100.559
99.073
78.478
76.390
69.624
66.230
64.901
62.223
62.130
62.013
61.398
61.047
55.698
200
180
160
140
120
100
80
60
40
20
0
ppm

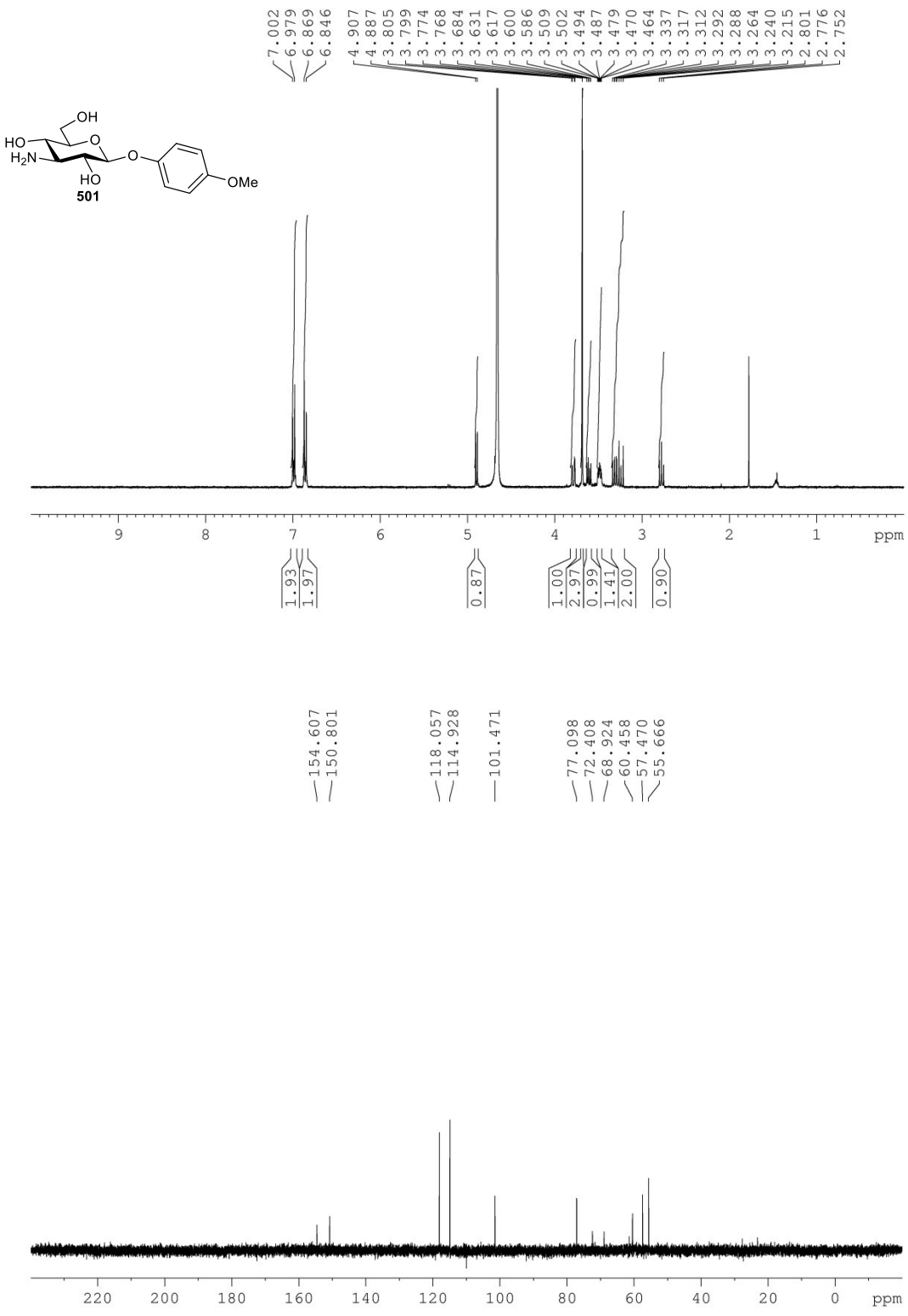
7.002
6.979
6.869
6.846
4.907
4.887
3.805
3.799
3.774
3.768
3.684
3.631
3.617
3.600
3.586
3.509
3.502
3.494
3.487
3.479
3.470
3.464
3.337
3.317
3.312
3.292
3.288
3.264
3.240
3.215
2.801
2.776
2.752
OH
HO
O
H2N
HO
O
OMe
501
9
8
7
6
5
4
3
2
1
ppm
1.93
1.97
0.87
1.00
2.97
0.99
1.41
2.00
0.90
154.607
150.801
118.057
114.928
101.471
77.098
72.408
68.924
60.458
57.470
55.666
220
200
180
160
140
120
100
80
60
40
20
0
ppm

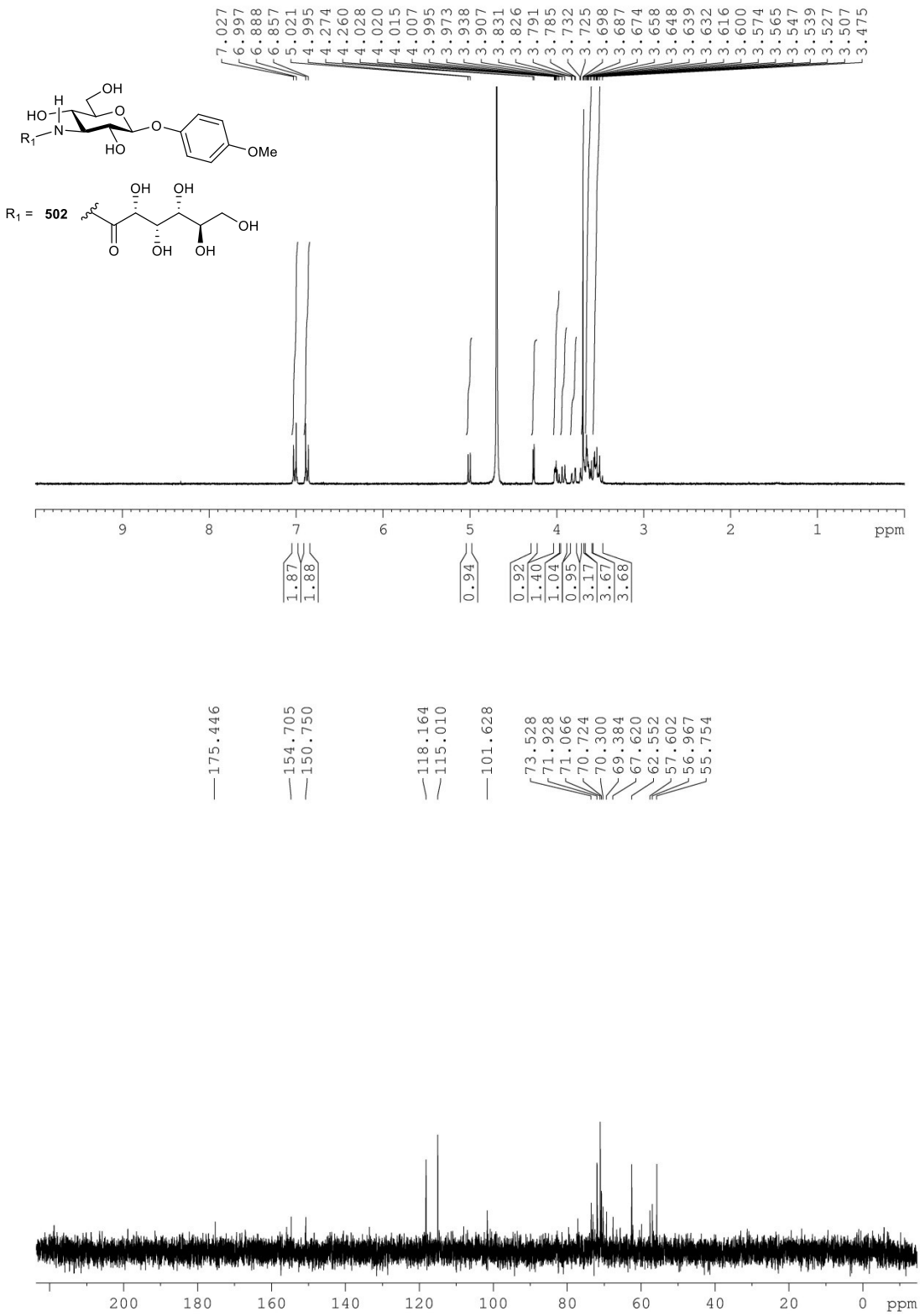
7.027
6.997
6.888
6.857
5.021
4.995
4.274
4.260
4.028
4.020
4.015
4.007
3.995
3.973
3.938
3.907
3.831
3.826
3.791
3.785
3.732
3.725
3.698
3.687
3.674
3.658
3.648
3.639
3.632
3.616
3.600
3.574
3.565
3.547
3.539
3.527
3.507
3.475
OH
H
HO
O
N
R1
HO
O
OMe
R1 = 502
OH
OH
OH
O
OH
OH
9
8
7
6
5
4
3
2
1
ppm
1.87
1.88
0.94
0.92
1.40
1.04
0.95
3.17
3.67
3.68
175.446
154.705
150.750
118.164
115.010
101.628
73.528
71.928
71.066
70.724
70.300
69.384
67.620
62.552
57.602
56.967
55.754
200
180
160
140
120
100
80
60
40
20
0
ppm

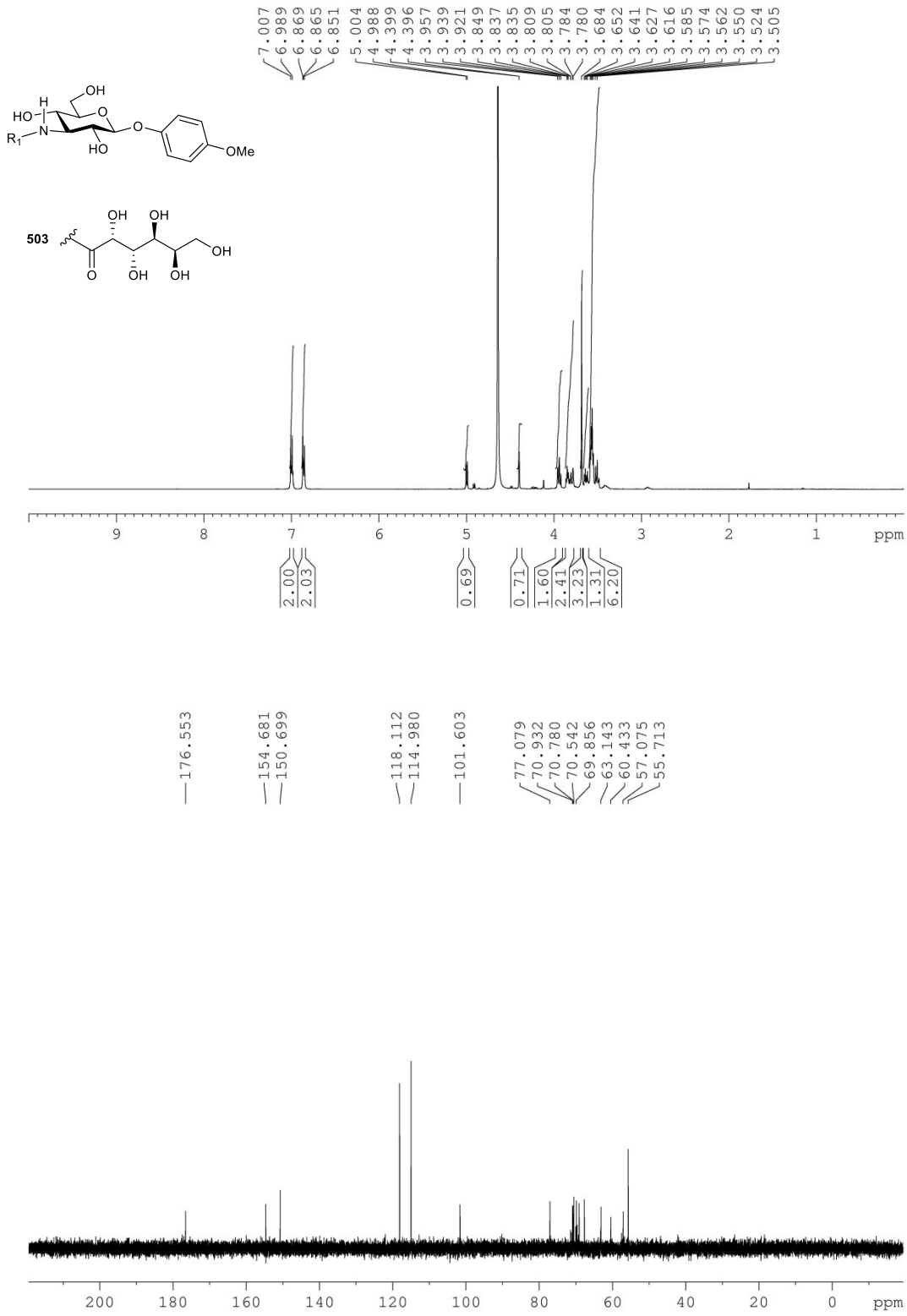
7.007
6.989
6.869
6.865
6.851
5.004
4.988
4.399
4.396
3.957
3.939
3.921
3.849
3.837
3.835
3.809
3.805
3.784
3.780
3.684
3.652
3.641
3.627
3.616
3.585
3.574
3.562
3.550
3.524
3.505
503
9
8
7
6
5
4
3
2
1
ppm
2.00
2.03
0.69
0.71
1.60
2.41
3.23
1.31
6.20
176.553
154.681
150.699
118.112
114.980
101.603
77.079
70.932
70.780
70.542
69.856
63.143
60.433
57.075
55.713
200
180
160
140
120
100
80
60
40
20
0
ppm

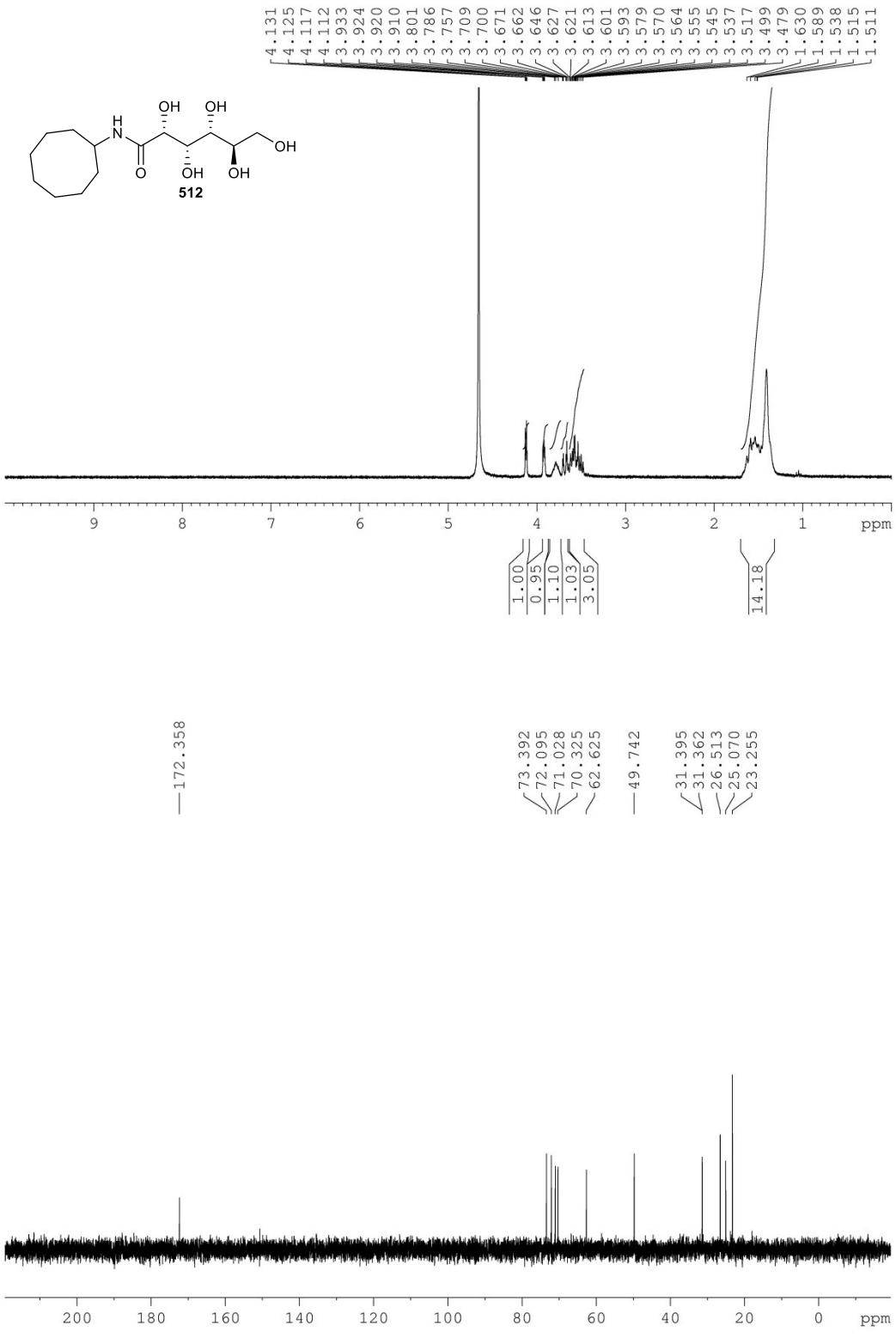
4.131
4.125
4.117
4.112
3.933
3.924
3.920
3.910
3.801
3.786
3.757
3.709
3.700
3.671
3.662
3.646
3.627
3.621
3.613
3.601
3.593
3.579
3.570
3.564
3.555
3.545
3.537
3.517
3.499
3.479
1.630
1.589
1.538
1.515
1.511
OH
OH
OH
OH
OH
H
N
O
512
9
8
7
6
5
4
3
2
1
ppm
1.00
0.95
1.10
1.03
3.05
14.18
172.358
73.392
72.095
71.028
70.325
62.625
49.742
31.395
31.362
26.513
25.070
23.255
200
180
160
140
120
100
80
60
40
20
0
ppm

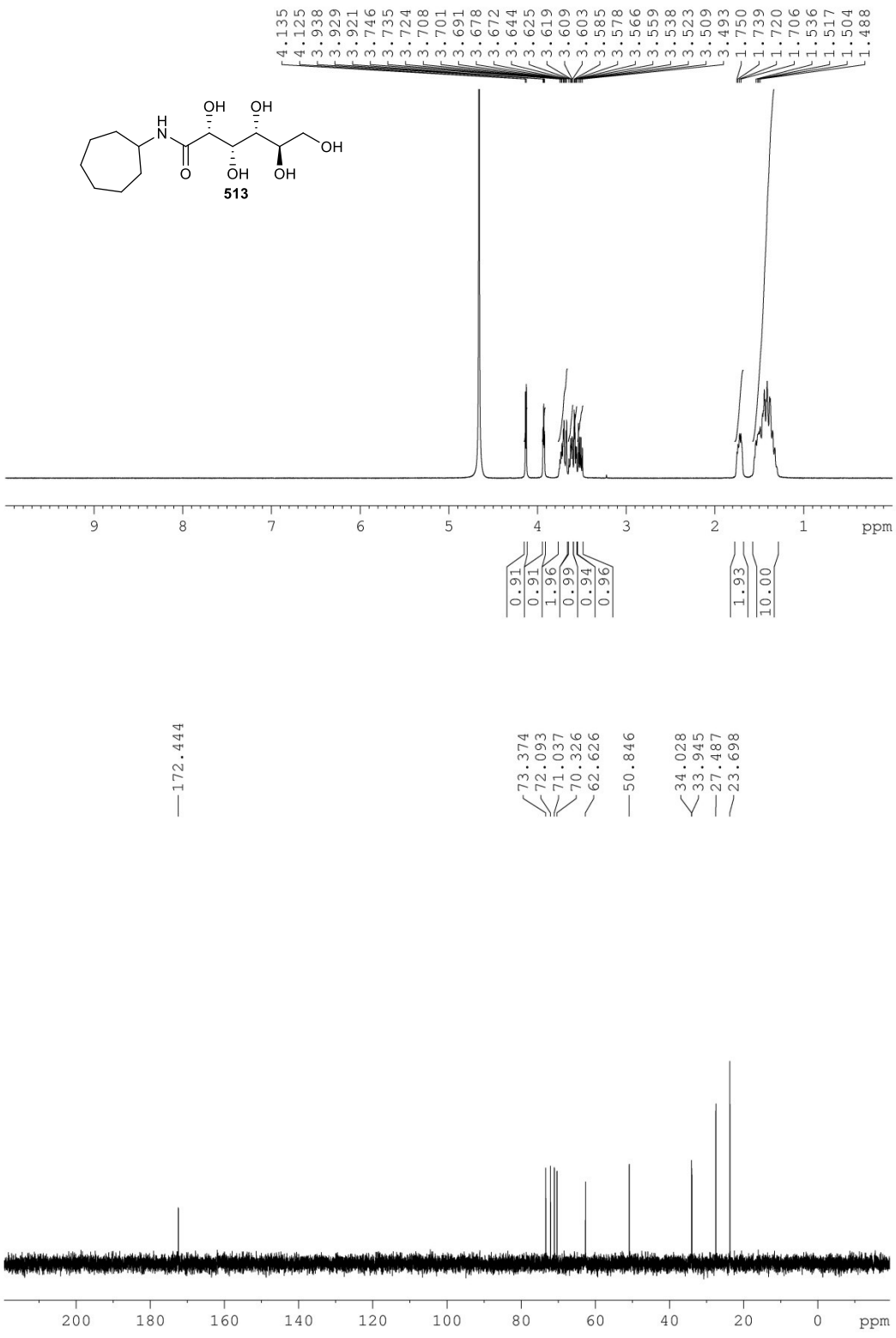
4.135
4.125
3.938
3.929
3.921
3.746
3.735
3.724
3.708
3.701
3.691
3.678
3.672
3.644
3.625
3.619
3.609
3.603
3.585
3.578
3.566
3.559
3.538
3.523
3.509
3.493
1.750
1.739
1.720
1.706
1.536
1.517
1.504
1.488
OH
OH
OH
OH
OH
H
N
O
513
9
8
7
6
5
4
3
2
1
ppm
0.91
0.91
1.96
0.99
0.94
0.96
1.93
10.00
172.444
73.374
72.093
71.037
70.326
62.626
50.846
34.028
33.945
27.487
23.698
200
180
160
140
120
100
80
60
40
20
0
ppm

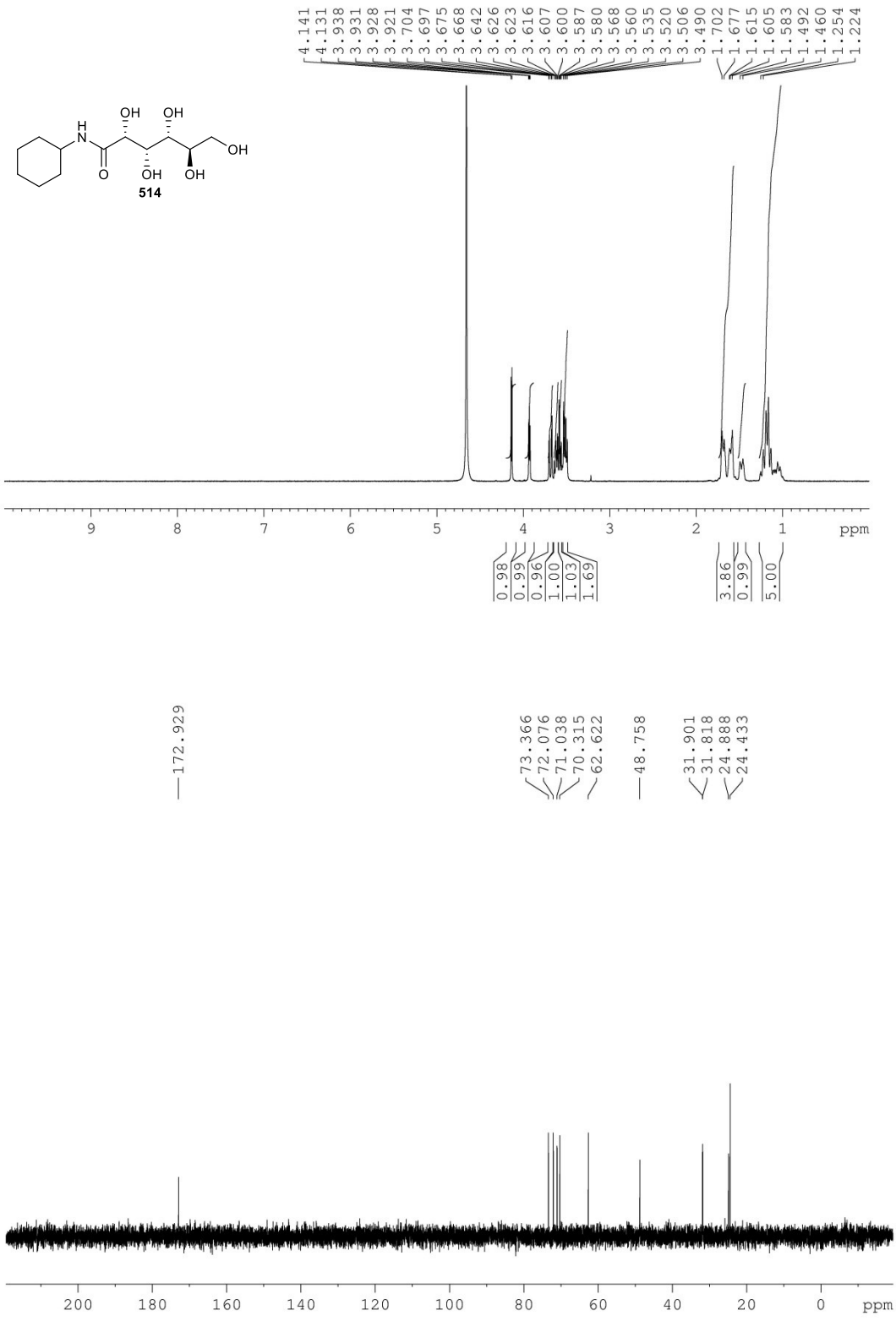
4.141
4.131
3.938
3.931
3.928
3.921
3.704
3.697
3.675
3.668
3.642
3.626
3.623
3.616
3.607
3.600
3.587
3.580
3.568
3.560
3.535
3.520
3.506
3.490
1.702
1.677
1.615
1.605
1.583
1.492
1.460
1.254
1.224
OH
OH
H
N
OH
O
OH
OH
514
9
8
7
6
5
4
3
2
1
ppm
0.98
0.99
0.96
1.00
1.03
1.69
3.86
0.99
5.00
172.929
73.366
72.076
71.038
70.315
62.622
48.758
31.901
31.818
24.888
24.433
200
180
160
140
120
100
80
60
40
20
0
ppm

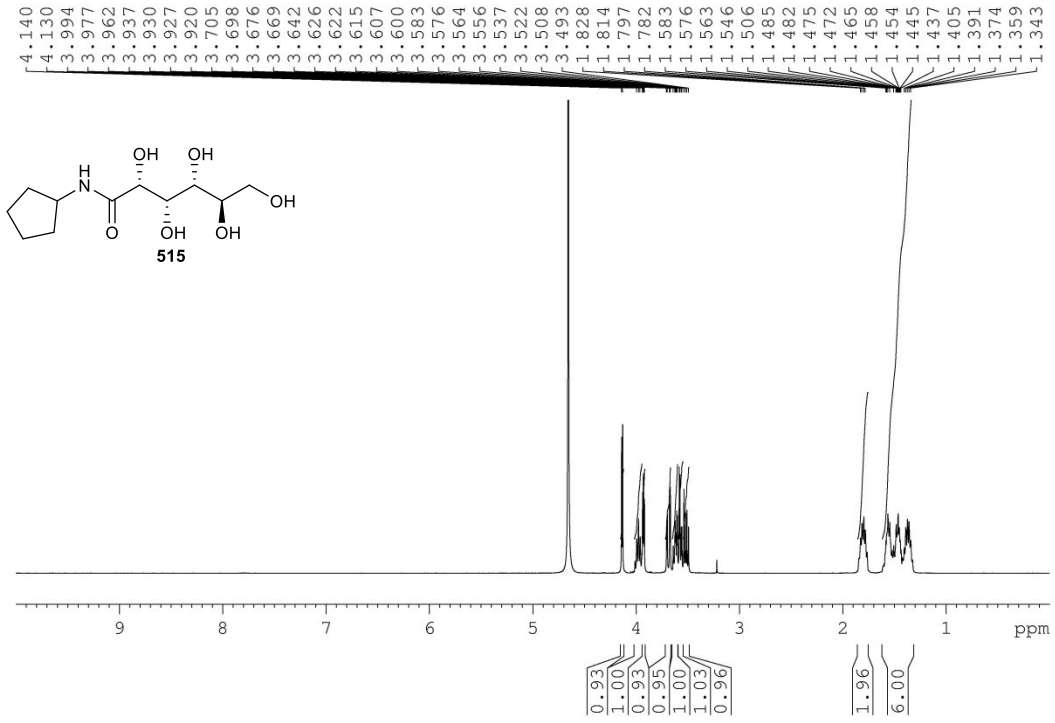
4.140
4.130
3.994
3.977
3.962
3.937
3.930
3.927
3.920
3.705
3.698
3.676
3.669
3.642
3.626
3.622
3.615
3.607
3.600
3.583
3.576
3.564
3.556
3.537
3.522
3.508
3.493
1.828
1.814
1.797
1.782
1.583
1.576
1.563
1.546
1.506
1.485
1.482
1.475
1.472
1.465
1.458
1.454
1.445
1.437
1.405
1.391
1.374
1.359
1.343
OH
OH
H
N
OH
O
OH
OH
515
9
8
7
6
5
4
3
2
1
ppm
0.93
1.00
0.93
0.95
1.00
1.03
0.96
1.96
6.00

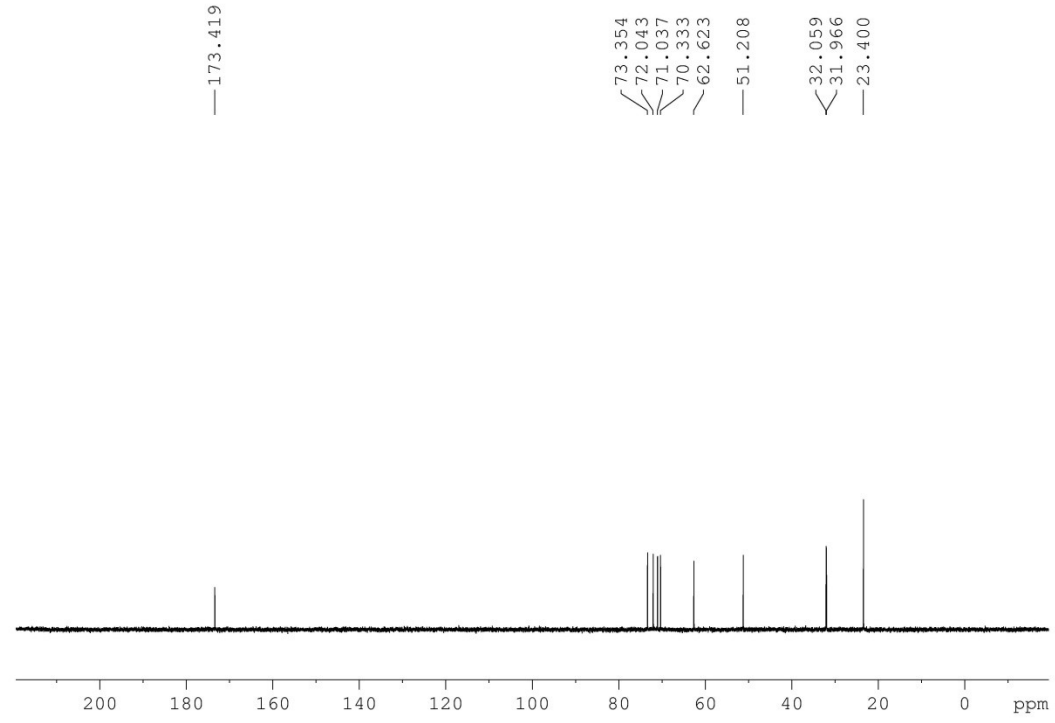
173.419
73.354
72.043
71.037
70.333
62.623
51.208
32.059
31.966
23.400
200
180
160
140
120
100
80
60
40
20
0
ppm

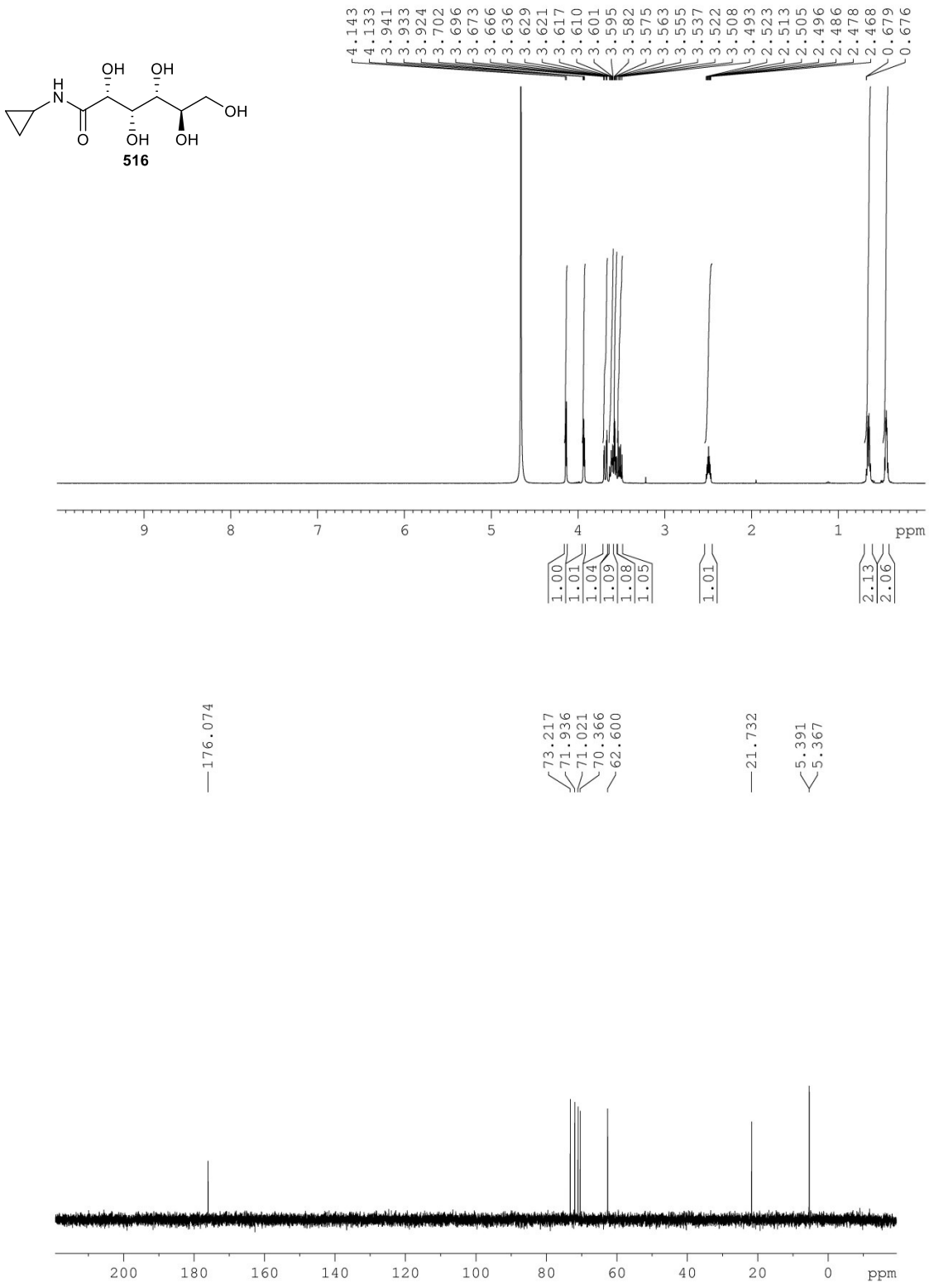
OH
OH
H
N
OH
O
OH
OH
516
4.143
4.133
3.941
3.933
3.924
3.702
3.696
3.673
3.666
3.636
3.629
3.621
3.617
3.610
3.601
3.595
3.582
3.575
3.563
3.555
3.537
3.522
3.508
3.493
2.523
2.513
2.505
2.496
2.486
2.478
2.468
0.679
0.676
9
8
7
6
5
4
3
2
1
ppm
1.00
1.01
1.04
1.09
1.08
1.05
1.01
2.13
2.06
176.074
73.217
71.936
71.021
70.366
62.600
21.732
5.391
5.367
200
180
160
140
120
100
80
60
40
20
0
ppm

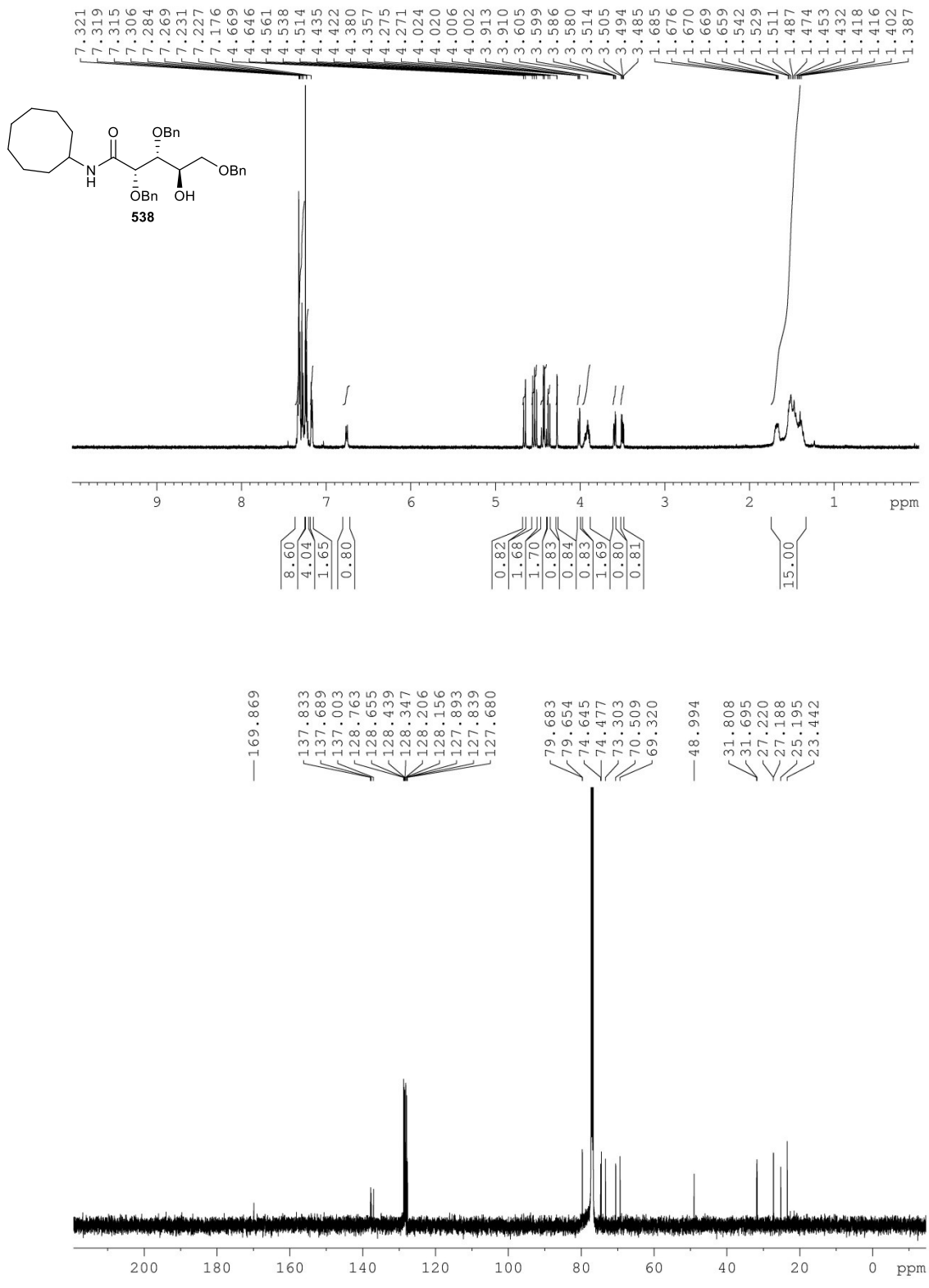
7.321
7.319
7.315
7.306
7.284
7.269
7.231
7.227
7.176
4.669
4.646
4.561
4.538
4.514
4.435
4.422
4.380
4.357
4.275
4.271
4.024
4.020
4.006
4.002
3.913
3.910
3.605
3.599
3.586
3.580
3.514
3.505
3.494
3.485
1.685
1.676
1.670
1.669
1.659
1.542
1.529
1.511
1.487
1.474
1.453
1.432
1.418
1.416
1.402
1.387
O
OBn
N
H
OBn
OBn
OH
538
9
8
7
6
5
4
3
2
1
ppm
8.60
4.04
1.65
0.80
0.82
1.68
1.70
0.83
0.84
0.83
1.69
0.80
0.81
15.00
169.869
137.833
137.689
137.003
128.763
128.655
128.439
128.347
128.206
128.156
127.893
127.839
127.680
79.683
79.654
74.645
74.477
73.303
70.509
69.320
48.994
31.808
31.695
27.220
27.188
25.195
23.442
200
180
160
140
120
100
80
60
40
20
0
ppm

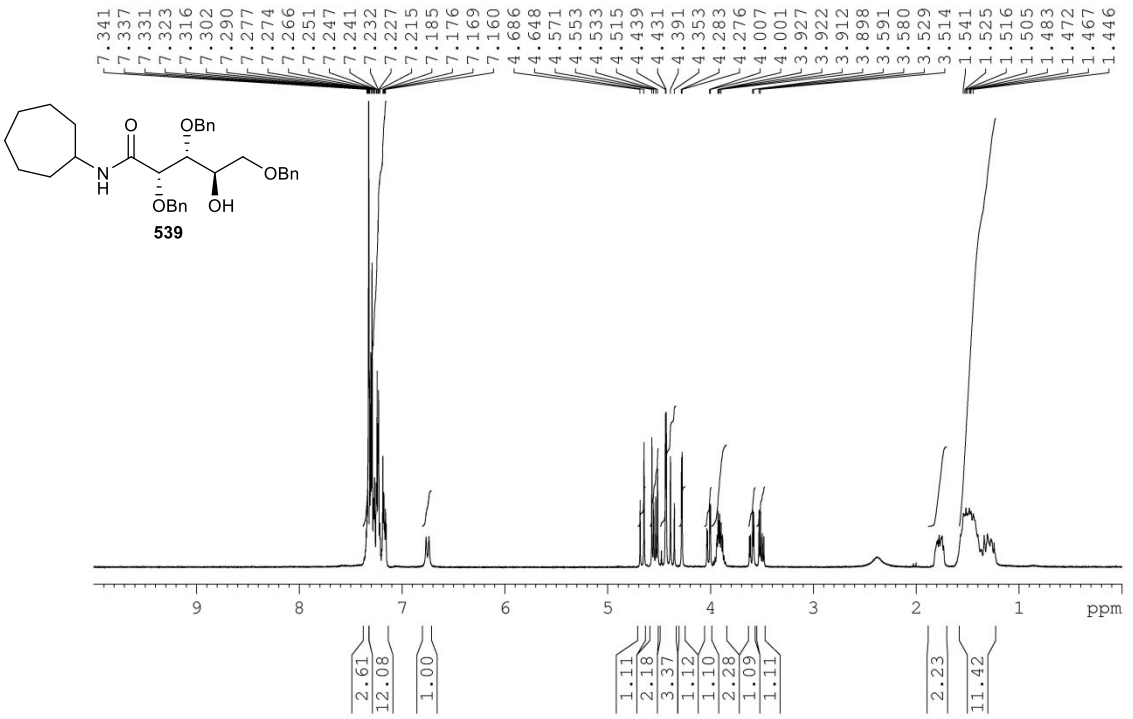
7.341
7.337
7.331
7.323
7.316
7.302
7.290
7.277
7.274
7.266
7.251
7.247
7.241
7.232
7.227
7.215
7.185
7.176
7.169
7.160
4.686
4.648
4.571
4.553
4.533
4.515
4.439
4.431
4.391
4.353
4.283
4.276
4.007
4.001
3.927
3.922
3.912
3.898
3.591
3.580
3.529
3.514
1.541
1.525
1.516
1.505
1.483
1.472
1.467
1.446
O
OBn
N
H
OBn
OBn
OBn
OH
539
9
8
7
6
5
4
3
2
1
ppm
2.61
12.08
1.00
1.11
2.18
3.37
1.12
1.10
2.28
1.09
1.11
2.23
11.42

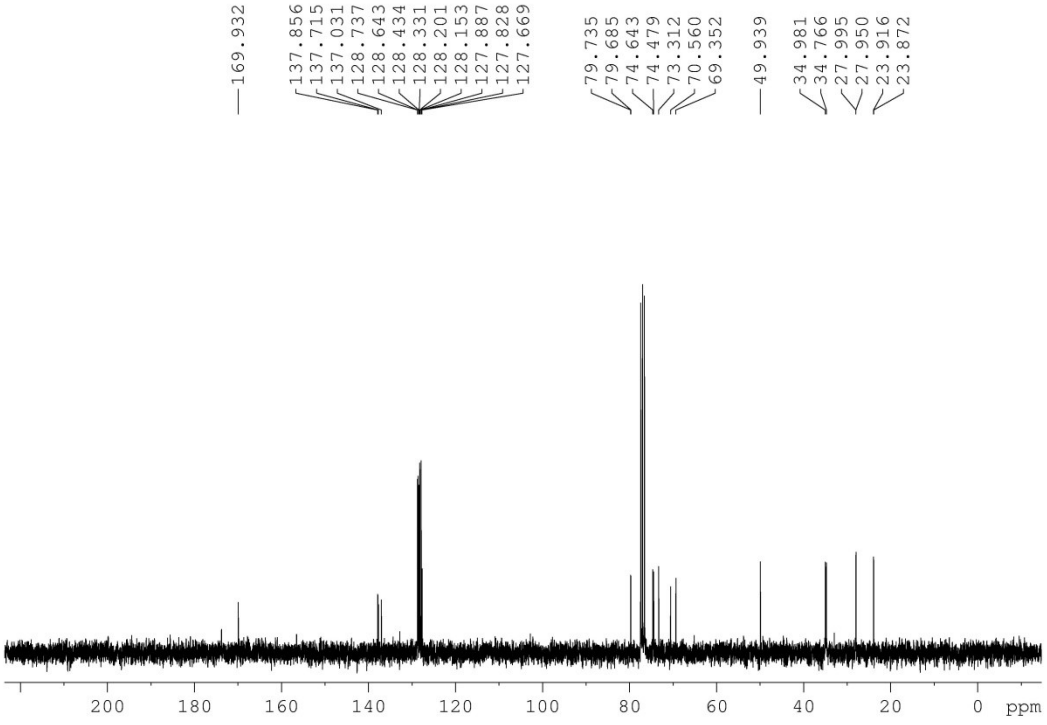
169.932
137.856
137.715
137.031
128.737
128.643
128.434
128.331
128.201
128.153
127.887
127.828
127.669
79.735
79.685
74.643
74.479
73.312
70.560
69.352
49.939
34.981
34.766
27.995
27.950
23.916
23.872
200
180
160
140
120
100
80
60
40
20
0
ppm

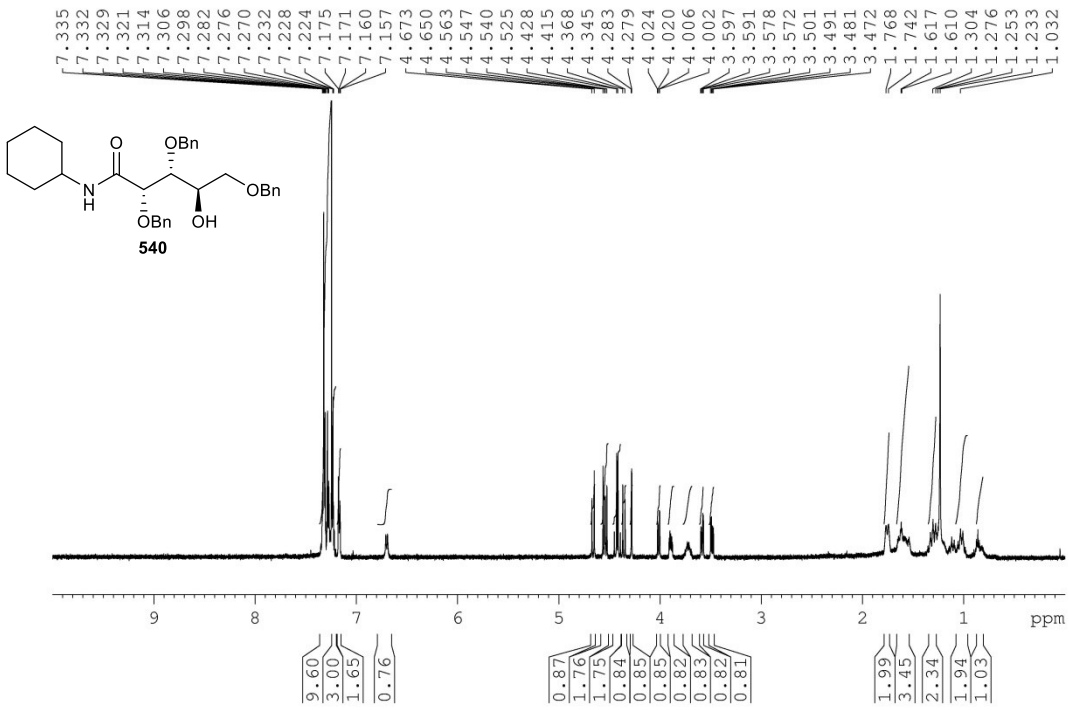
7.335
7.332
7.329
7.321
7.314
7.306
7.298
7.282
7.276
7.270
7.232
7.228
7.224
7.175
7.171
7.160
7.157
4.673
4.650
4.563
4.547
4.540
4.525
4.428
4.415
4.368
4.345
4.283
4.279
4.024
4.020
4.006
4.002
3.597
3.591
3.578
3.572
3.501
3.491
3.481
3.472
1.768
1.742
1.617
1.610
1.304
1.276
1.253
1.233
1.032
O
OBn
N
H
OBn
OBn
OH
540
9
8
7
6
5
4
3
2
1
ppm
9.60
3.00
1.65
0.76
0.87
1.76
1.75
0.84
0.85
0.85
0.82
0.83
0.82
0.81
1.99
3.45
2.34
1.94
1.03

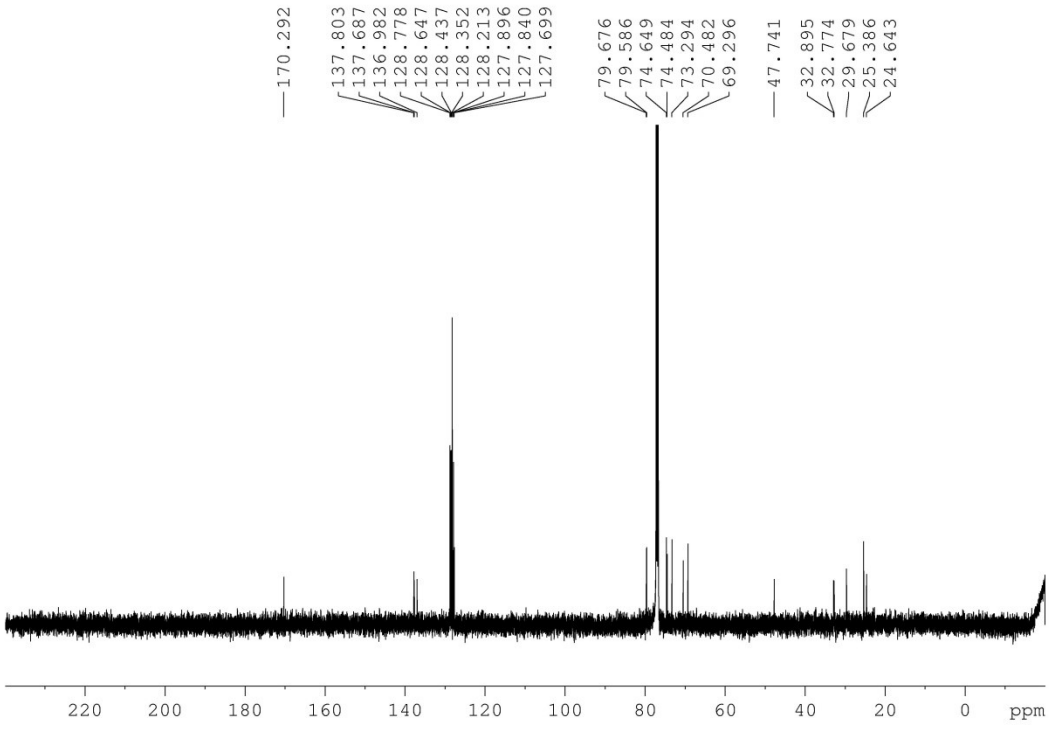
170.292
137.803
137.687
136.982
128.778
128.647
128.437
128.352
128.213
127.896
127.840
127.699
79.676
79.586
74.649
74.484
73.294
70.482
69.296
47.741
32.895
32.774
29.679
25.386
24.643
220
200
180
160
140
120
100
80
60
40
20
0
ppm

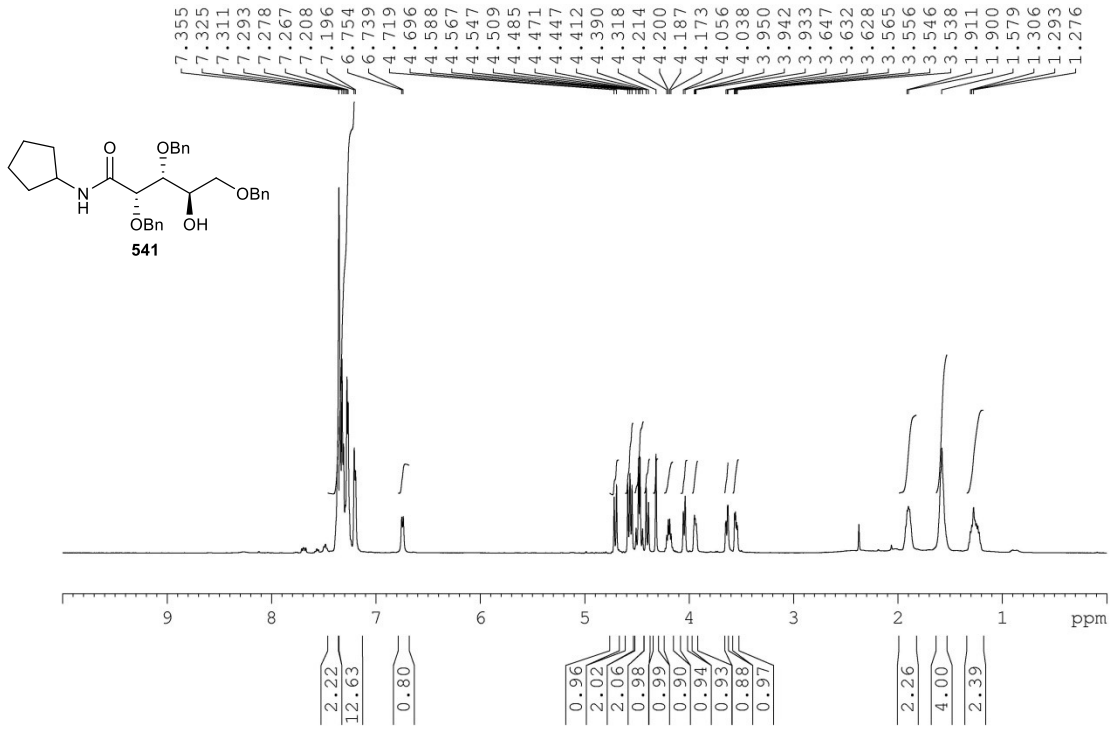
7.355
7.325
7.311
7.293
7.278
7.267
7.208
7.196
6.754
6.739
4.719
4.696
4.588
4.567
4.547
4.509
4.485
4.471
4.447
4.412
4.390
4.318
4.214
4.200
4.187
4.173
4.056
4.038
3.950
3.942
3.933
3.647
3.632
3.628
3.565
3.556
3.546
3.538
1.911
1.900
1.579
1.306
1.293
1.276
O
OBn
N
H
OBn
OBn
OH
541
9
8
7
6
5
4
3
2
1
ppm
2.22
12.63
0.80
0.96
2.02
2.06
0.98
0.99
0.90
0.94
0.93
0.88
0.97
2.26
4.00
2.39

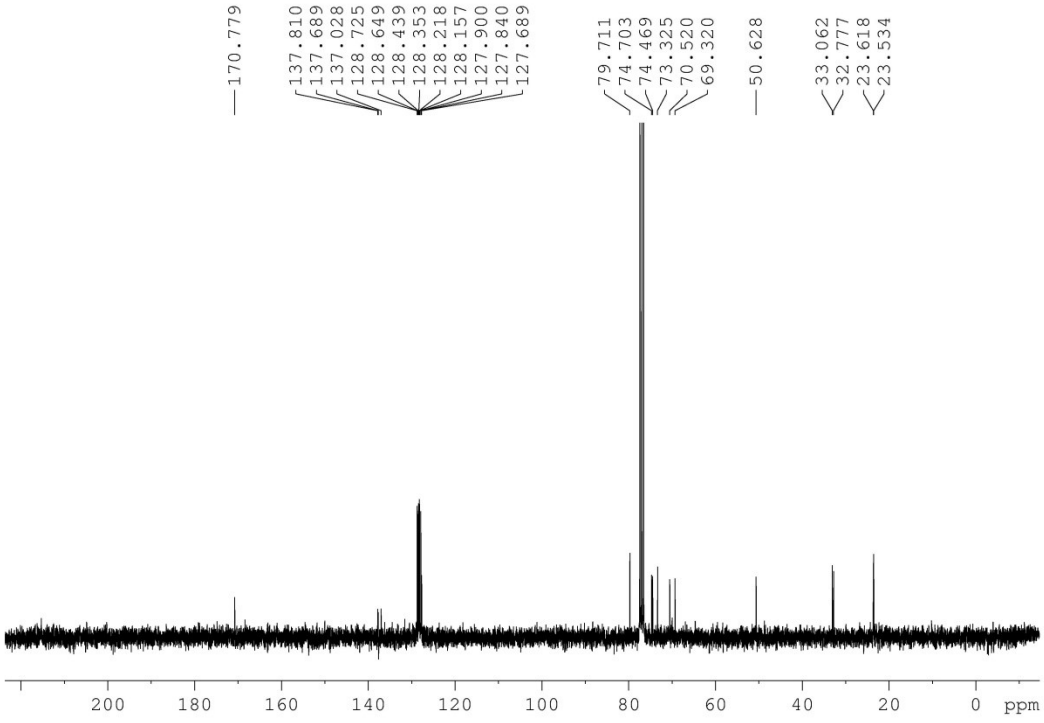
170.779
137.810
137.689
137.028
128.725
128.649
128.439
128.353
128.218
128.157
127.900
127.840
127.689
79.711
74.703
74.469
73.325
70.520
69.320
50.628
33.062
32.777
23.618
23.534
200
180
160
140
120
100
80
60
40
20
0
ppm

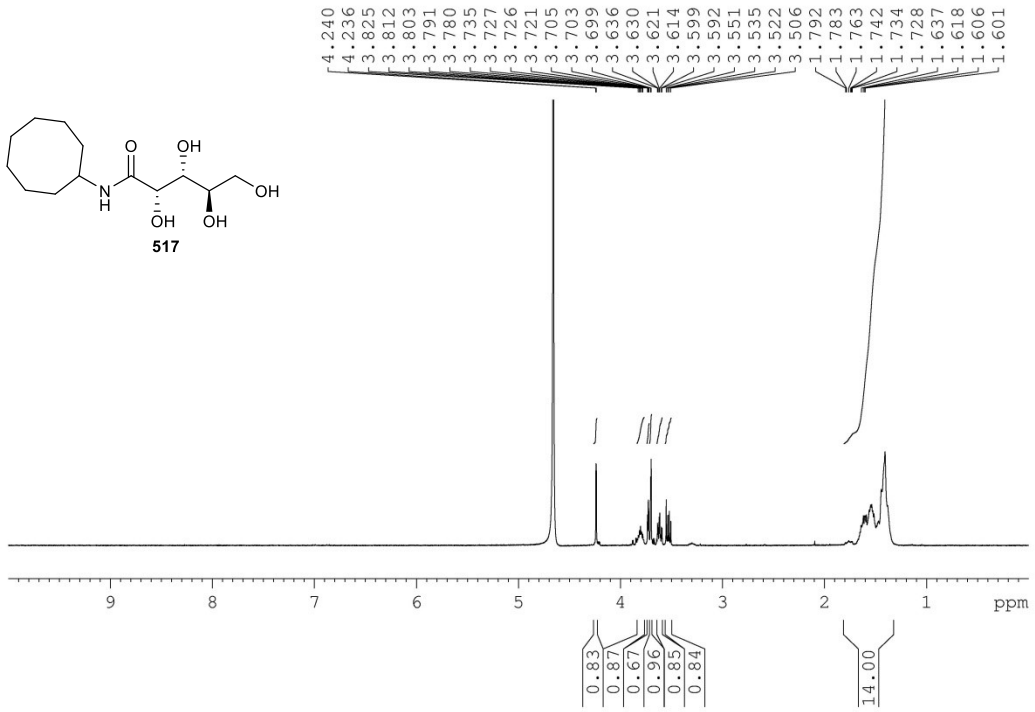
4.240
4.236
3.825
3.812
3.803
3.791
3.780
3.735
3.727
3.726
3.721
3.705
3.703
3.699
3.636
3.630
3.621
3.614
3.599
3.592
3.551
3.535
3.522
3.506
1.792
1.783
1.763
1.742
1.734
1.728
1.637
1.618
1.606
1.601
O
OH
N
H
OH
OH
OH
517
9
8
7
6
5
4
3
2
1
ppm
0.83
0.87
0.67
0.96
0.85
0.84
14.00

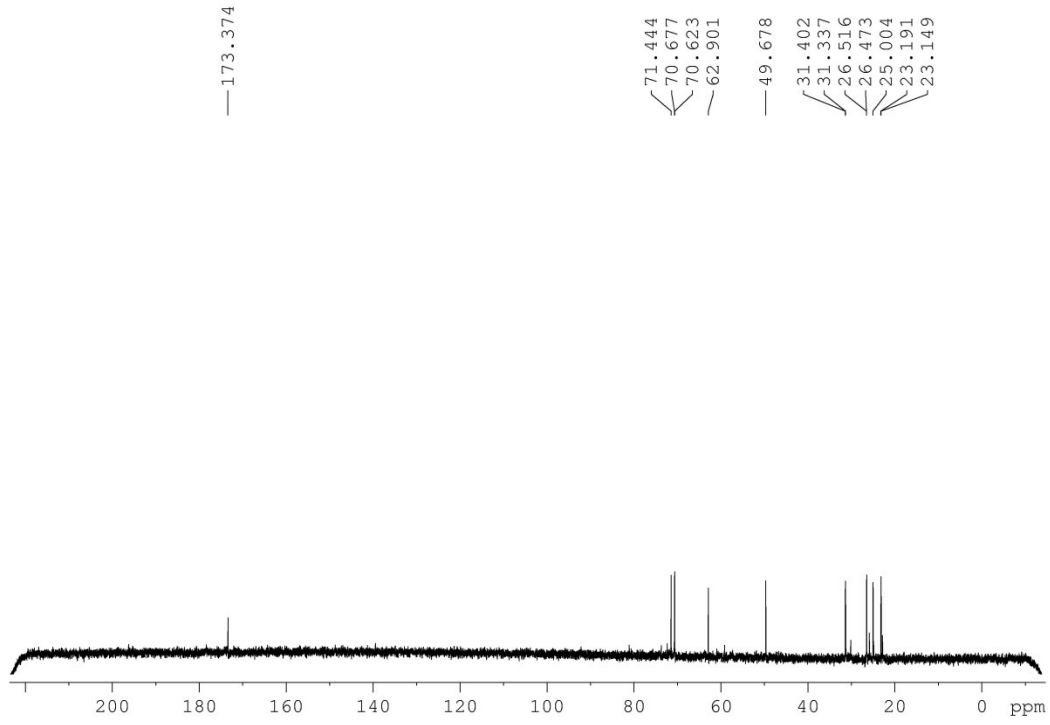
173.374
71.444
70.677
70.623
62.901
49.678
31.402
31.337
26.516
26.473
25.004
23.191
23.149
200
180
160
140
120
100
80
60
40
20
0
ppm

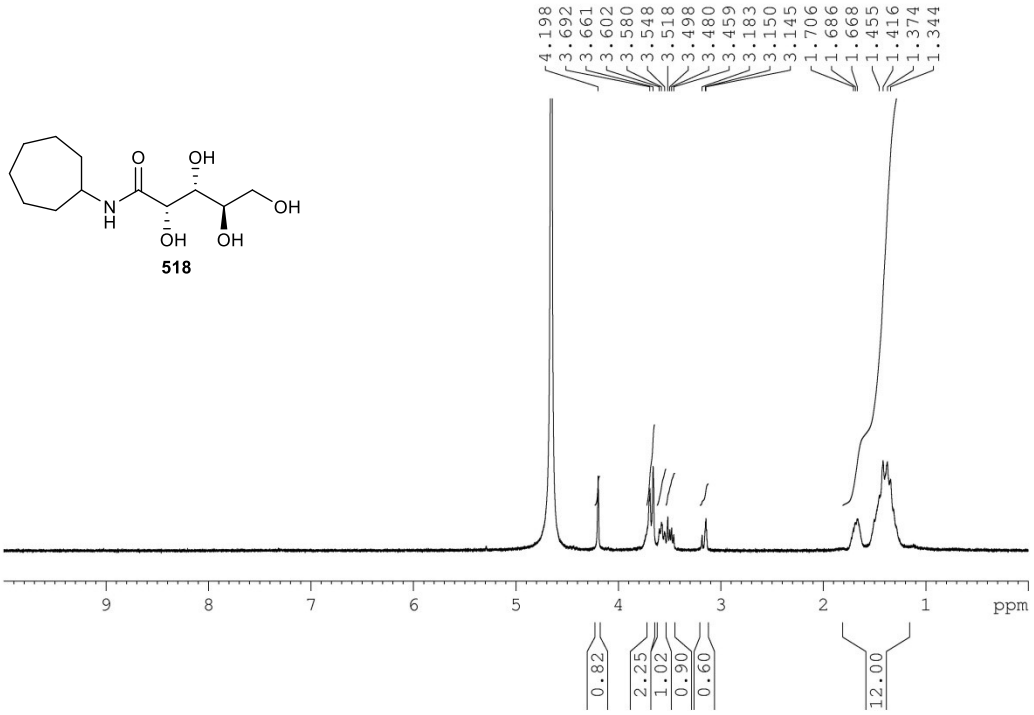
4.198
3.692
3.661
3.602
3.580
3.548
3.518
3.498
3.480
3.459
3.183
3.150
3.145
1.706
1.686
1.668
1.455
1.416
1.374
1.344
O
OH
N
H
OH
OH
OH
518
9
8
7
6
5
4
3
2
1
ppm
0.82
2.25
1.02
0.90
0.60
12.00

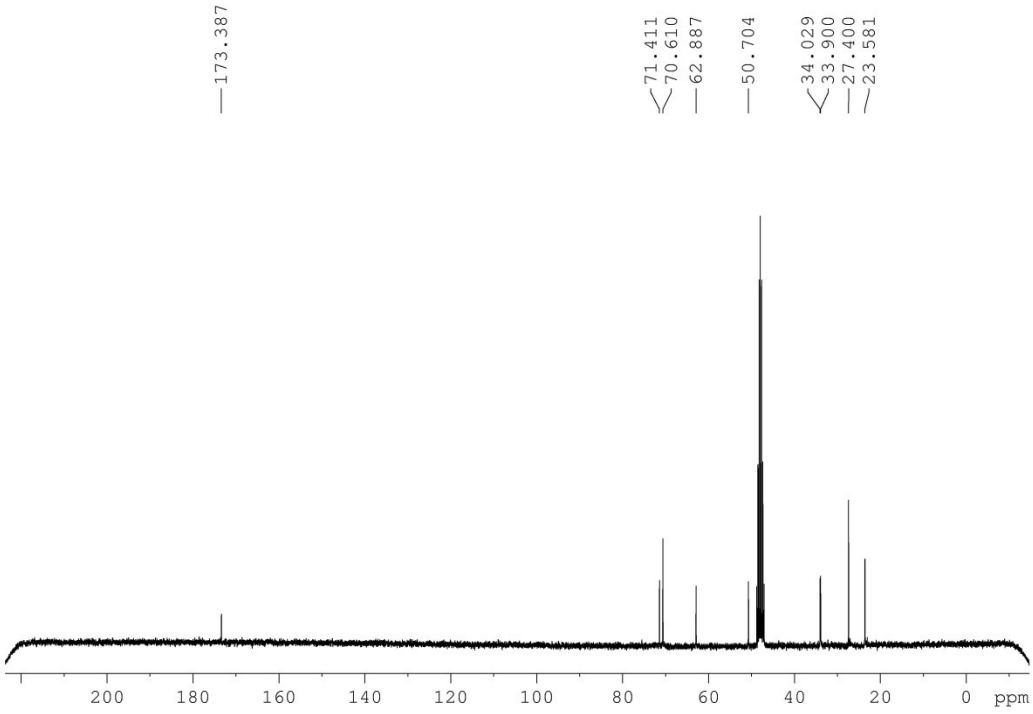
173.387
71.411
70.610
62.887
50.704
34.029
33.900
27.400
23.581
200
180
160
140
120
100
80
60
40
20
0
ppm

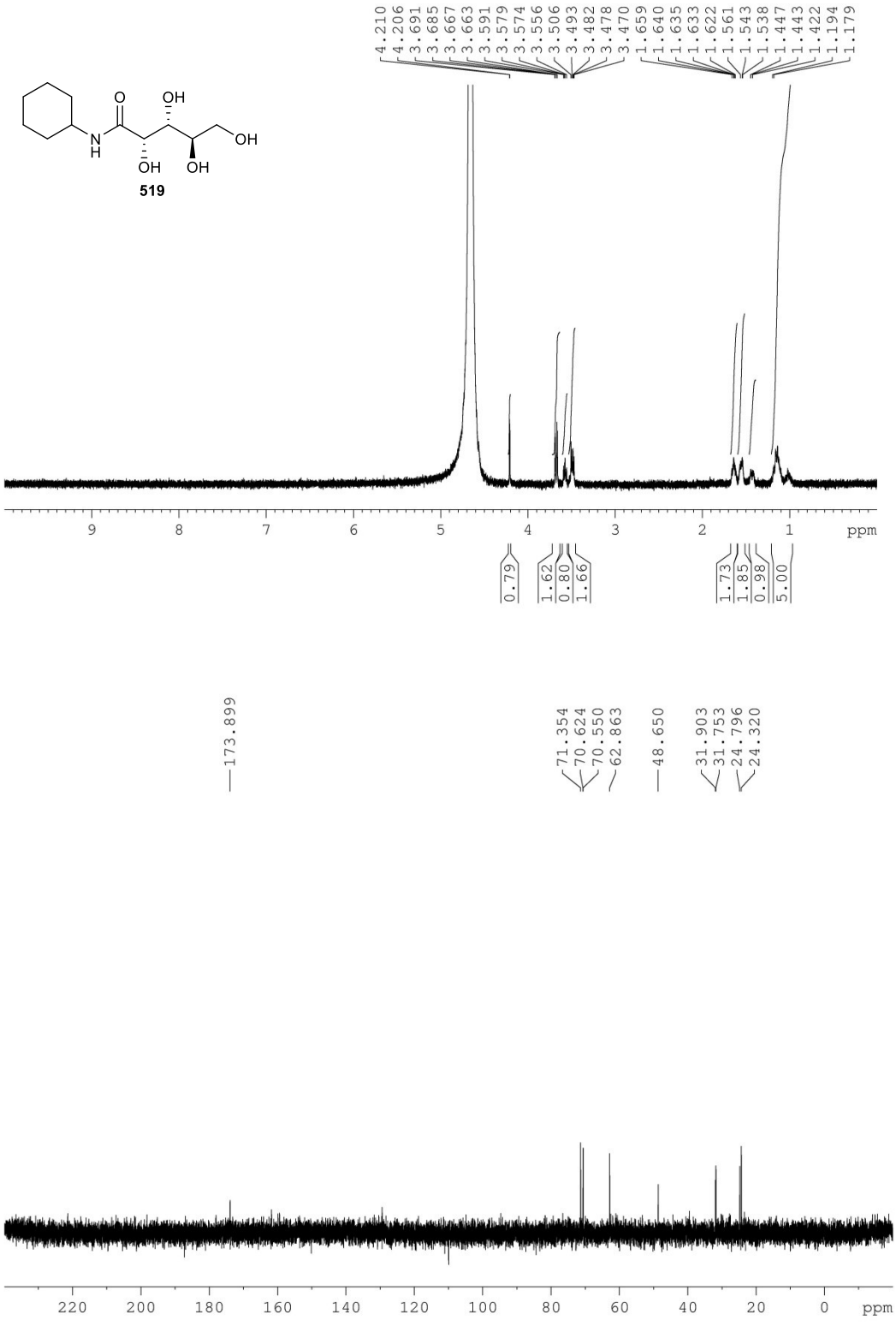
519
4.210
4.206
3.691
3.685
3.667
3.663
3.591
3.579
3.574
3.556
3.506
3.493
3.482
3.478
3.470
1.659
1.640
1.635
1.633
1.622
1.561
1.543
1.538
1.447
1.443
1.422
1.194
1.179
ppm
0.79
1.62
0.80
1.66
1.73
1.85
0.98
5.00
173.899
71.354
70.624
70.550
62.863
48.650
31.903
31.753
24.796
24.320
ppm

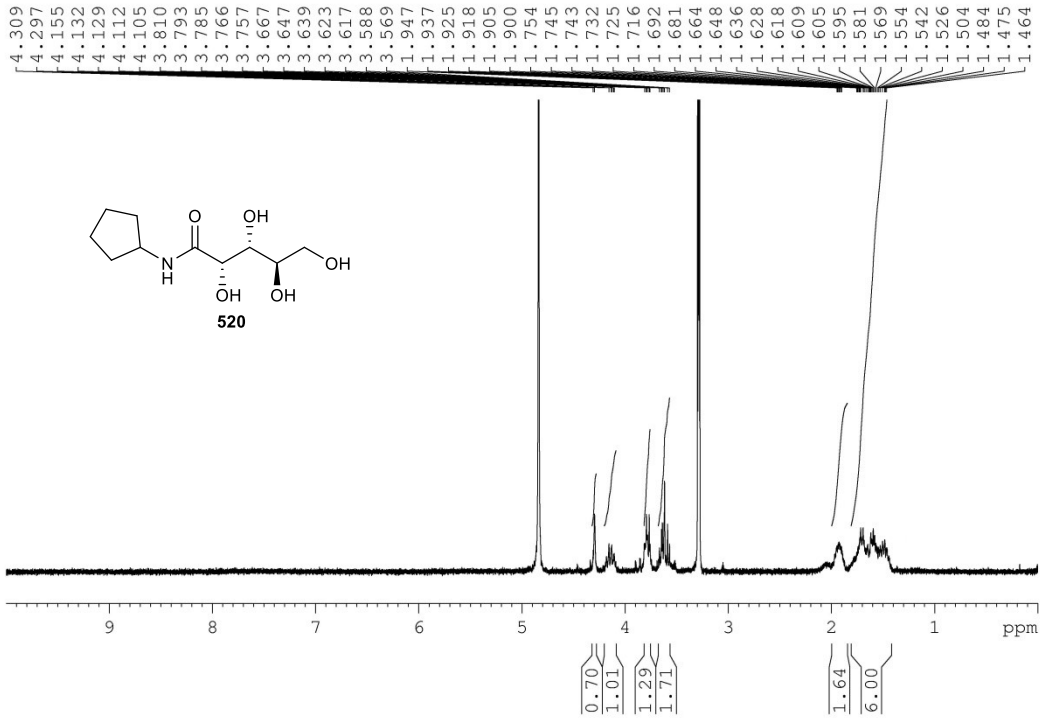
4.309
4.297
4.155
4.132
4.129
4.112
4.105
3.810
3.793
3.785
3.766
3.757
3.667
3.647
3.639
3.623
3.617
3.588
3.569
1.947
1.937
1.925
1.918
1.905
1.900
1.754
1.745
1.743
1.732
1.725
1.716
1.692
1.681
1.664
1.648
1.636
1.628
1.618
1.609
1.605
1.595
1.581
1.569
1.554
1.542
1.526
1.504
1.484
1.475
1.464
O
OH
N
H
OH
OH
OH
520
9
8
7
6
5
4
3
2
1
ppm
0.70
1.01
1.29
1.71
1.64
6.00

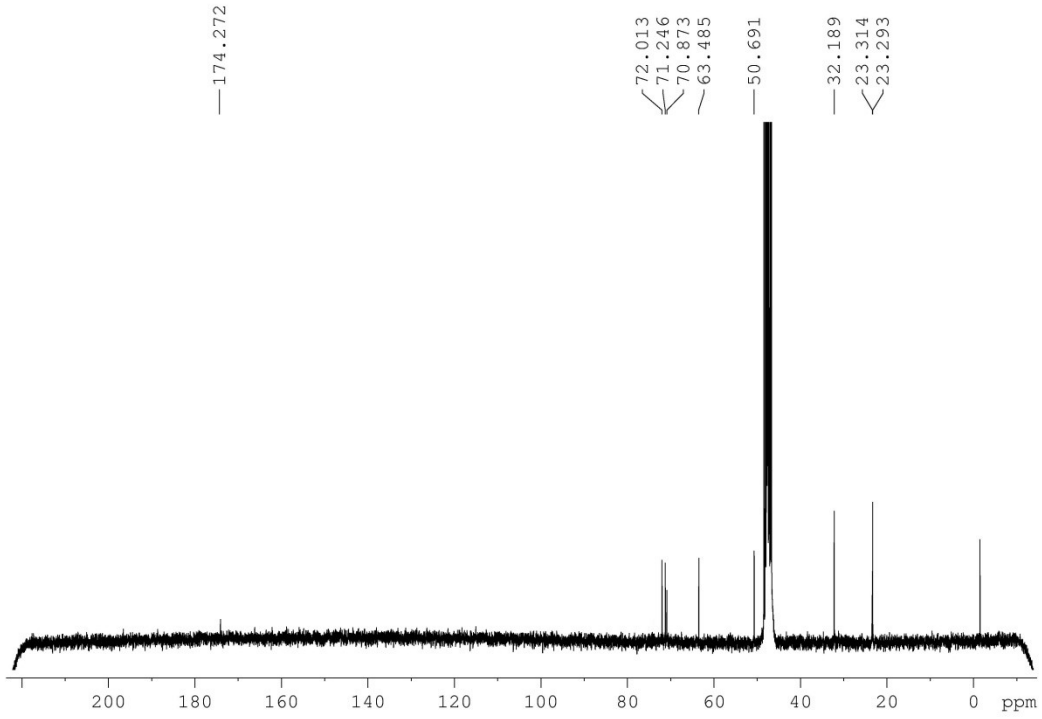
174.272
72.013
71.246
70.873
63.485
50.691
32.189
23.314
23.293
200
180
160
140
120
100
80
60
40
20
0
ppm

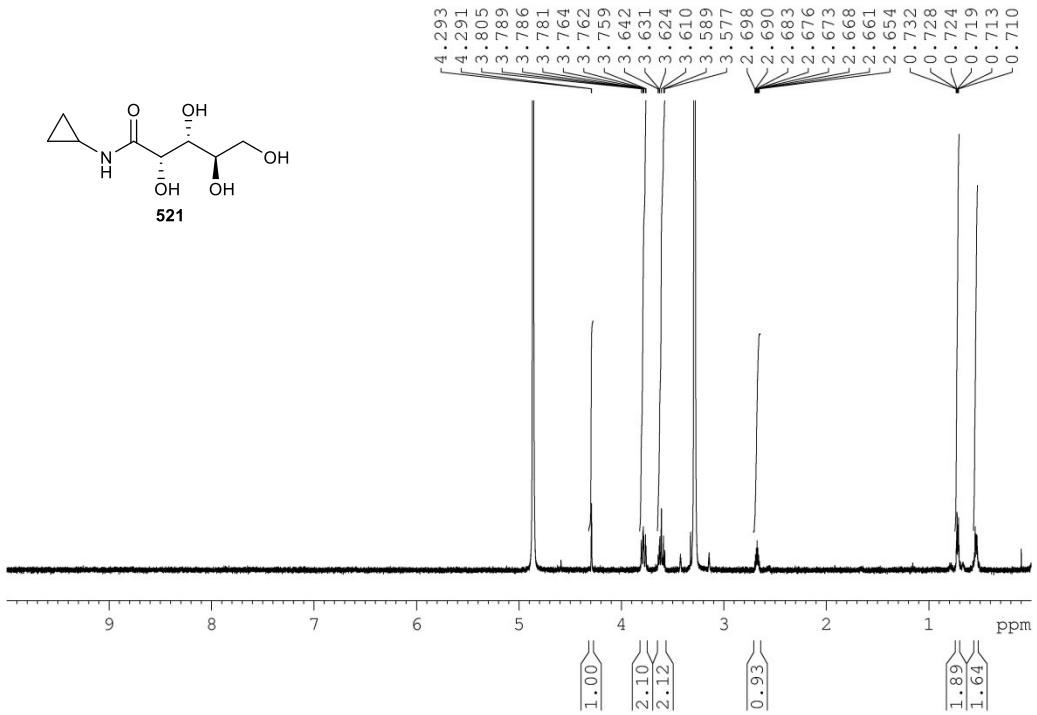
4.293
4.291
3.805
3.789
3.786
3.781
3.764
3.762
3.759
3.642
3.631
3.624
3.610
3.589
3.577
2.698
2.690
2.683
2.676
2.673
2.668
2.661
2.654
0.732
0.728
0.724
0.719
0.713
0.710
O
OH
N
H
OH
OH
OH
521
9
8
7
6
5
4
3
2
1
ppm
1.00
2.10
2.12
0.93
1.89
1.64

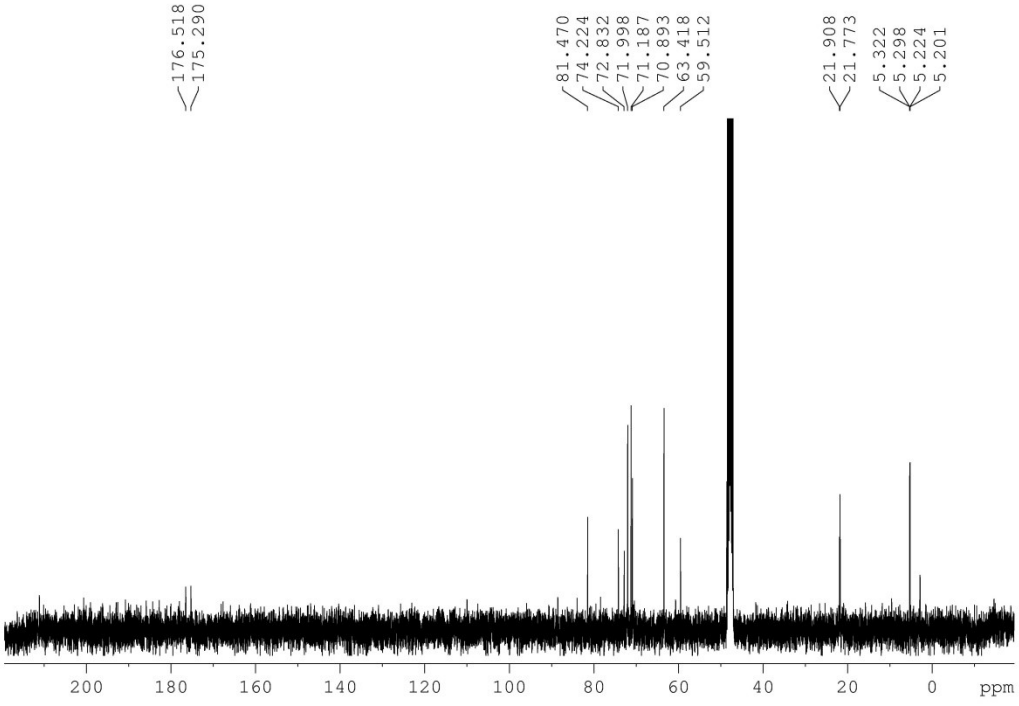
176.518
175.290
81.470
74.224
72.832
71.998
71.187
70.893
63.418
59.512
21.908
21.773
5.322
5.298
5.224
5.201
200
180
160
140
120
100
80
60
40
20
0
ppm

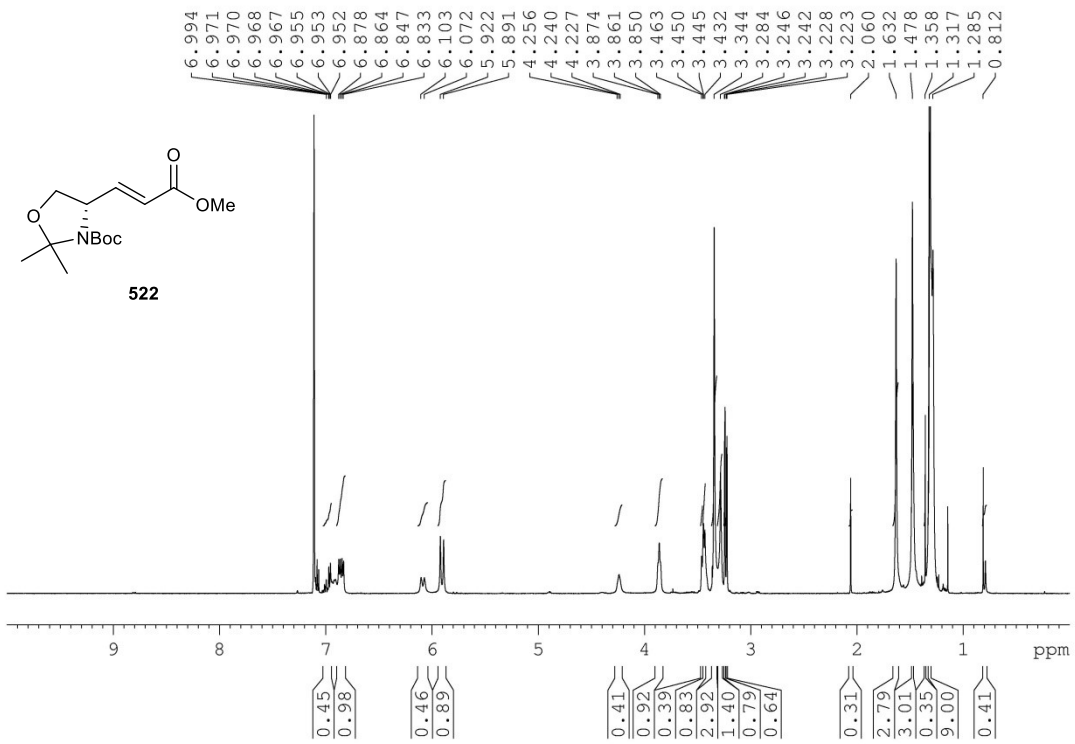
6.994
6.971
6.970
6.968
6.967
6.955
6.953
6.952
6.878
6.864
6.847
6.833
6.103
6.072
5.922
5.891
4.256
4.240
4.227
3.874
3.861
3.850
3.463
3.450
3.445
3.432
3.344
3.284
3.246
3.242
3.228
3.223
2.060
1.632
1.478
1.358
1.317
1.285
0.812
O
OMe
O
NBoc
522
9
8
7
6
5
4
3
2
1
ppm
0.45
0.98
0.46
0.89
0.41
0.92
0.39
0.83
2.92
1.40
0.79
0.64
0.31
2.79
3.01
0.35
9.00
0.41

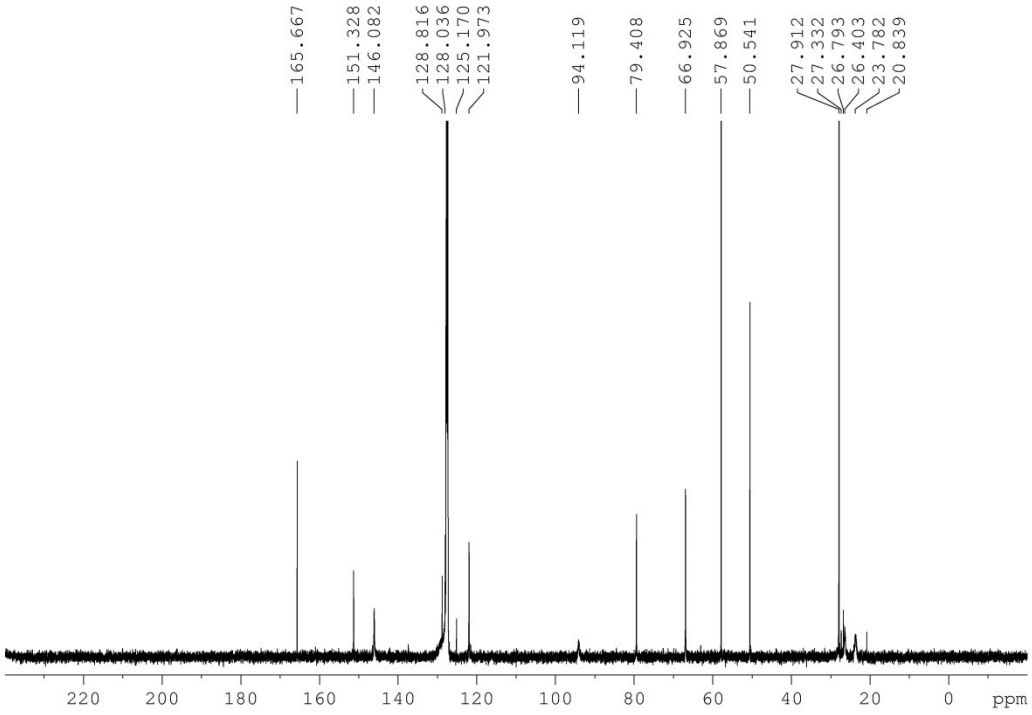
165.667
151.328
146.082
128.816
128.036
125.170
121.973
94.119
79.408
66.925
57.869
50.541
27.912
27.332
26.793
26.403
23.782
20.839
220
200
180
160
140
120
100
80
60
40
20
0
ppm

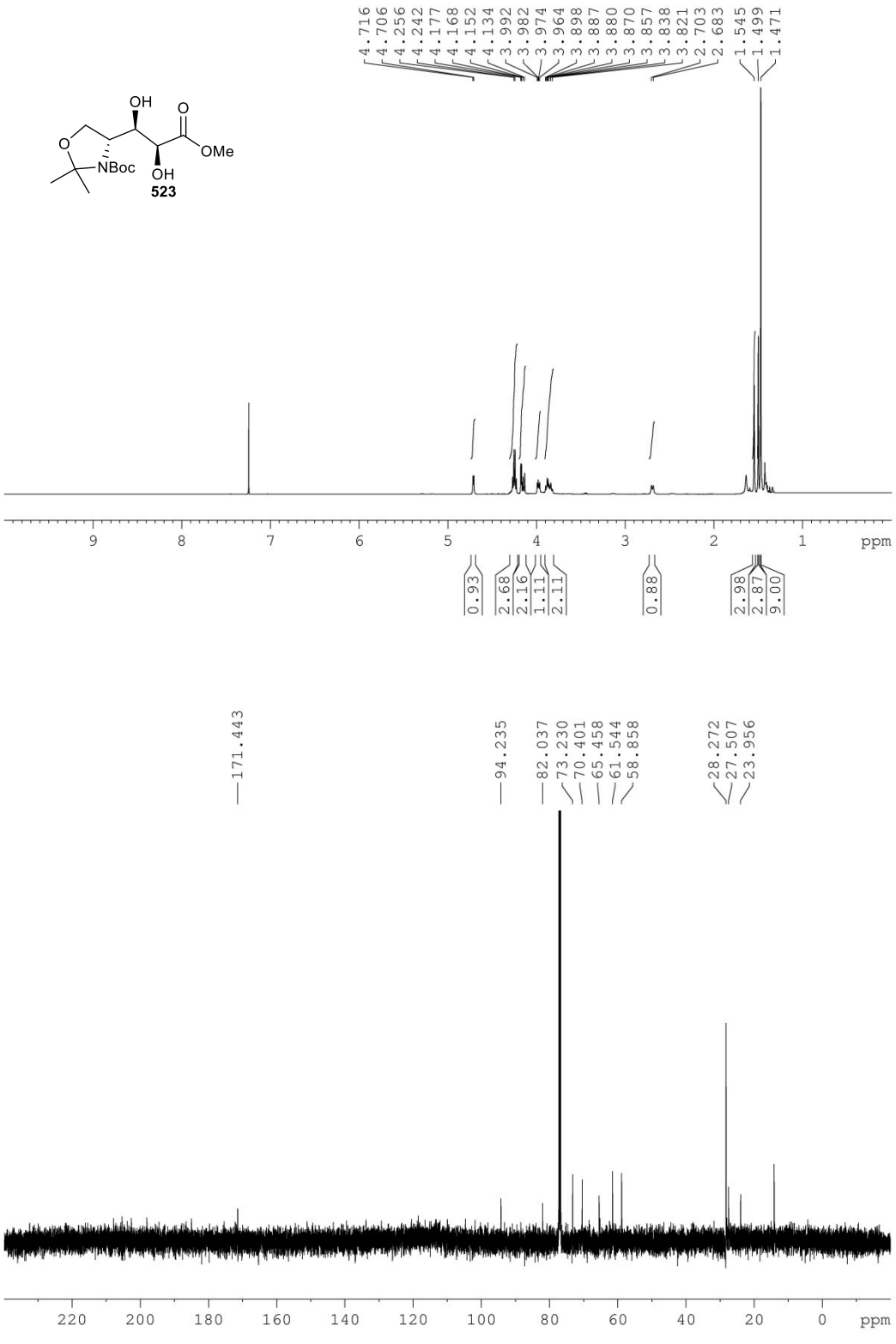
4.716
4.706
4.256
4.242
4.177
4.168
4.152
4.134
3.992
3.982
3.974
3.964
3.898
3.887
3.880
3.870
3.857
3.838
3.821
2.703
2.683
1.545
1.499
1.471
OH
O
OMe
O
NBoc
OH
523
9
8
7
6
5
4
3
2
1
ppm
0.93
2.68
2.16
1.11
2.11
0.88
2.98
2.87
9.00
171.443
94.235
82.037
73.230
70.401
65.458
61.544
58.858
28.272
27.507
23.956
220
200
180
160
140
120
100
80
60
40
20
0
ppm

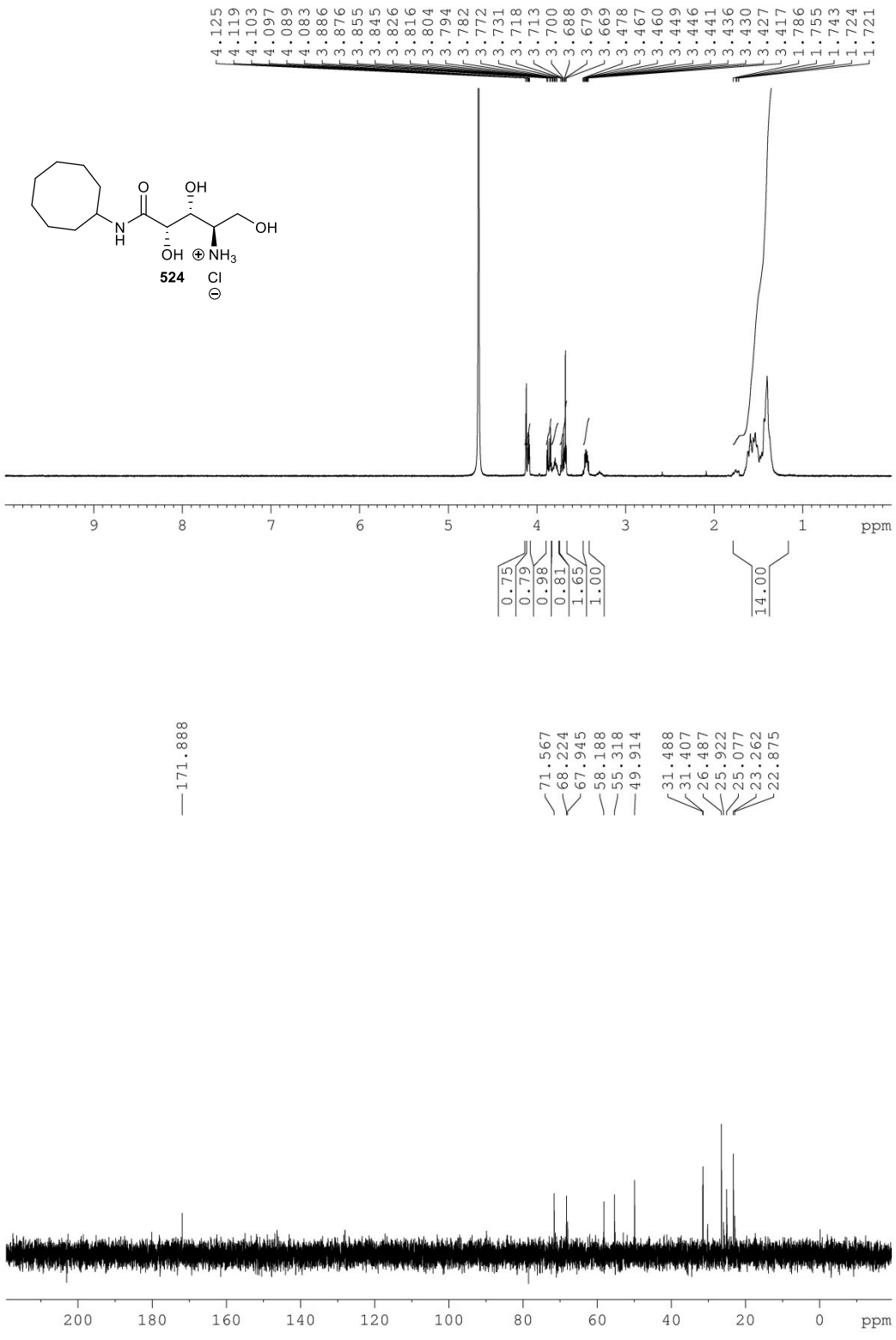
4.125
4.119
4.103
4.097
4.089
4.083
3.886
3.876
3.855
3.845
3.826
3.816
3.804
3.794
3.782
3.772
3.731
3.718
3.713
3.700
3.688
3.679
3.669
3.478
3.467
3.460
3.449
3.446
3.441
3.436
3.430
3.427
3.417
1.786
1.755
1.743
1.724
1.721
O
OH
N
H
OH
OH
⊕NH3
524
Cl
⊖
9
8
7
6
5
4
3
2
1
ppm
0.75
0.79
0.98
0.81
1.65
1.00
14.00
171.888
71.567
68.224
67.945
58.188
55.318
49.914
31.488
31.407
26.487
25.922
25.077
23.262
22.875
200
180
160
140
120
100
80
60
40
20
0
ppm

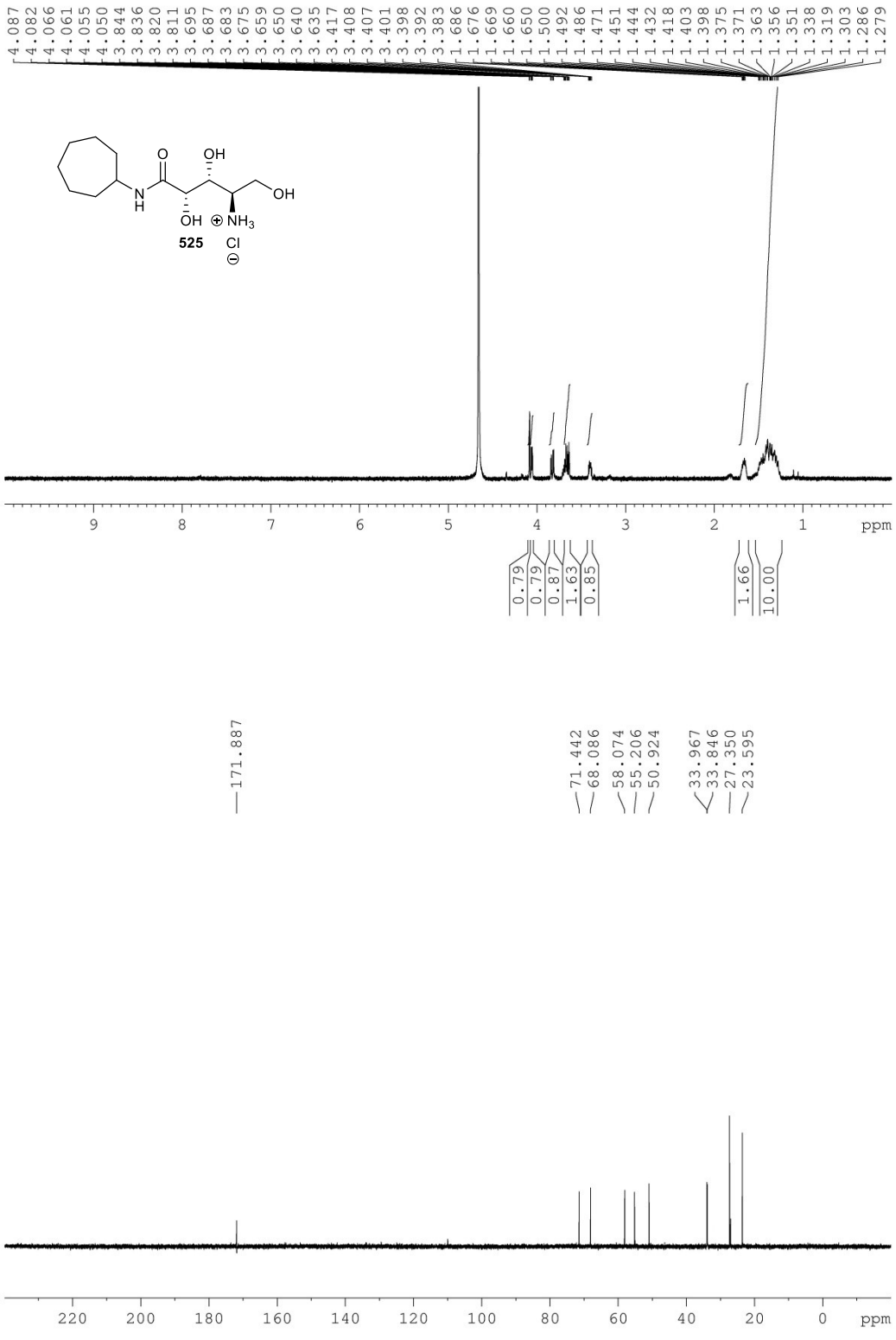
4.087
4.082
4.066
4.061
4.055
4.050
3.844
3.836
3.820
3.811
3.695
3.687
3.683
3.675
3.659
3.650
3.640
3.635
3.417
3.408
3.407
3.401
3.398
3.392
3.383
1.686
1.676
1.669
1.660
1.650
1.500
1.492
1.486
1.471
1.451
1.444
1.432
1.418
1.403
1.398
1.375
1.371
1.363
1.356
1.351
1.338
1.319
1.303
1.286
1.279
O
OH
N
H
OH
OH
NH3
525
Cl
ppm
0.79
0.79
0.87
1.63
0.85
1.66
10.00
171.887
71.442
68.086
58.074
55.206
50.924
33.967
33.846
27.350
23.595
ppm

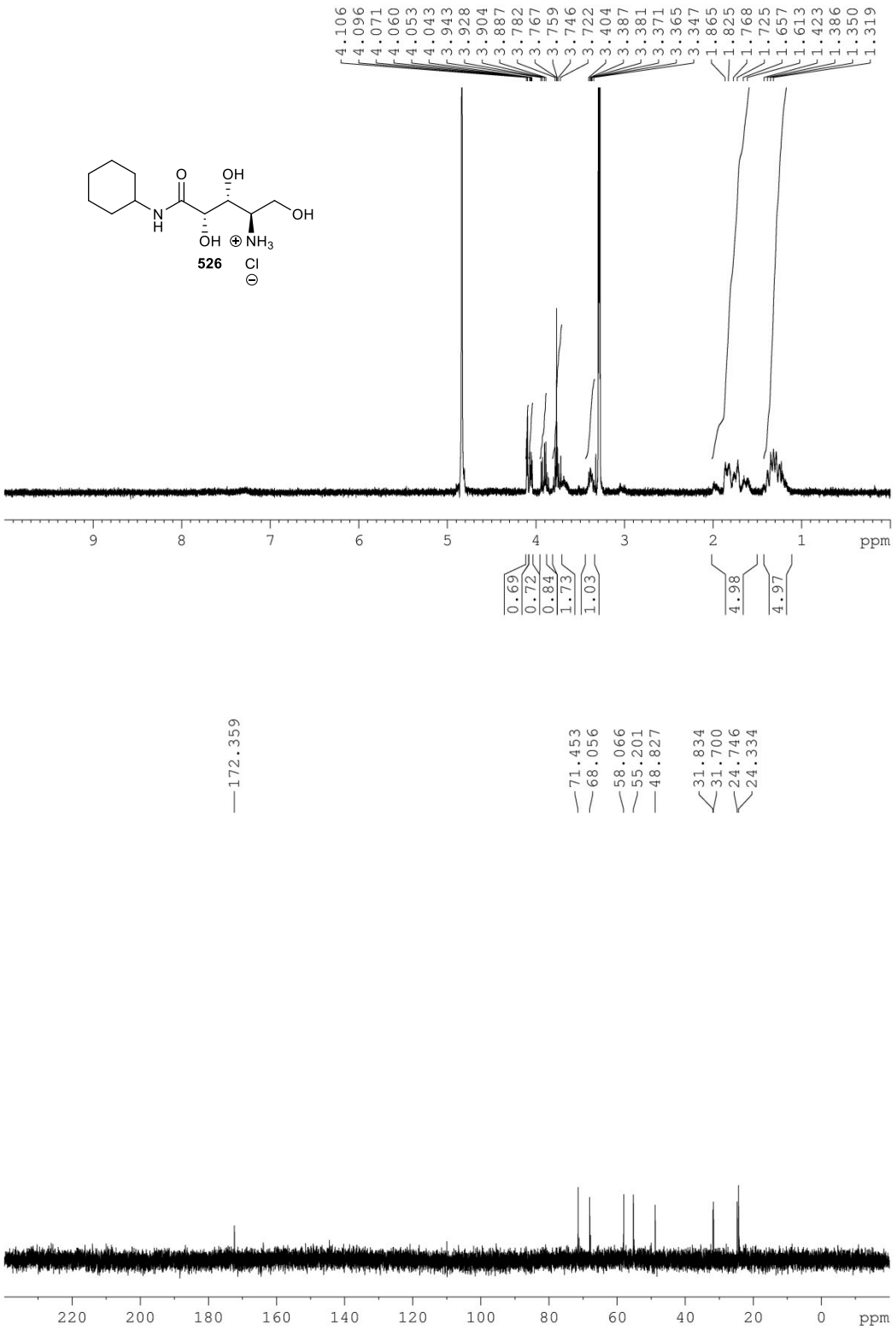
4.106
4.096
4.071
4.060
4.053
4.043
3.943
3.928
3.904
3.887
3.782
3.767
3.759
3.746
3.722
3.404
3.387
3.381
3.371
3.365
3.347
1.865
1.825
1.768
1.725
1.657
1.613
1.423
1.386
1.350
1.319
O
OH
N
H
OH
OH
NH3
526
Cl
9
8
7
6
5
4
3
2
1
ppm
0.69
0.72
0.84
1.73
1.03
4.98
4.97
172.359
71.453
68.056
58.066
55.201
48.827
31.834
31.700
24.746
24.334
220
200
180
160
140
120
100
80
60
40
20
0
ppm

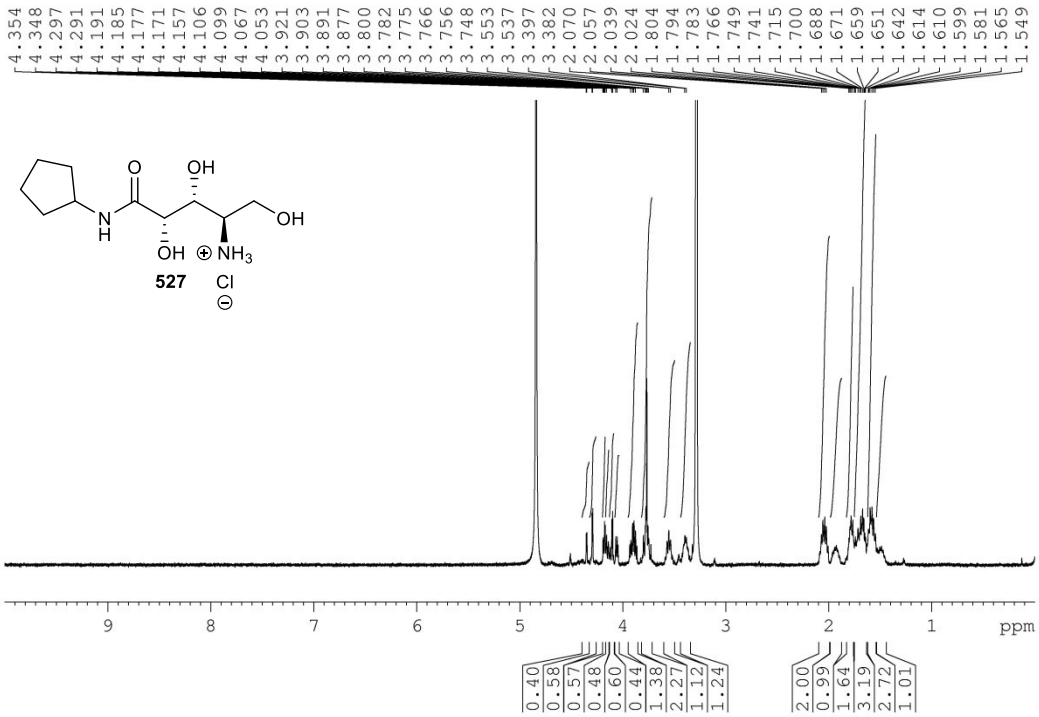
4.354
4.348
4.297
4.291
4.191
4.185
4.177
4.171
4.157
4.106
4.099
4.067
4.053
3.921
3.903
3.891
3.877
3.800
3.782
3.775
3.766
3.756
3.748
3.553
3.537
3.397
3.382
2.070
2.057
2.039
2.024
1.804
1.794
1.783
1.766
1.749
1.741
1.715
1.700
1.688
1.671
1.659
1.651
1.642
1.614
1.610
1.599
1.581
1.565
1.549
O
OH
N
H
OH
OH
NH3
527
Cl
9
8
7
6
5
4
3
2
1
ppm
0.40
0.58
0.57
0.48
0.60
0.44
1.38
2.27
1.12
1.24
2.00
0.99
1.64
3.19
2.72
1.01

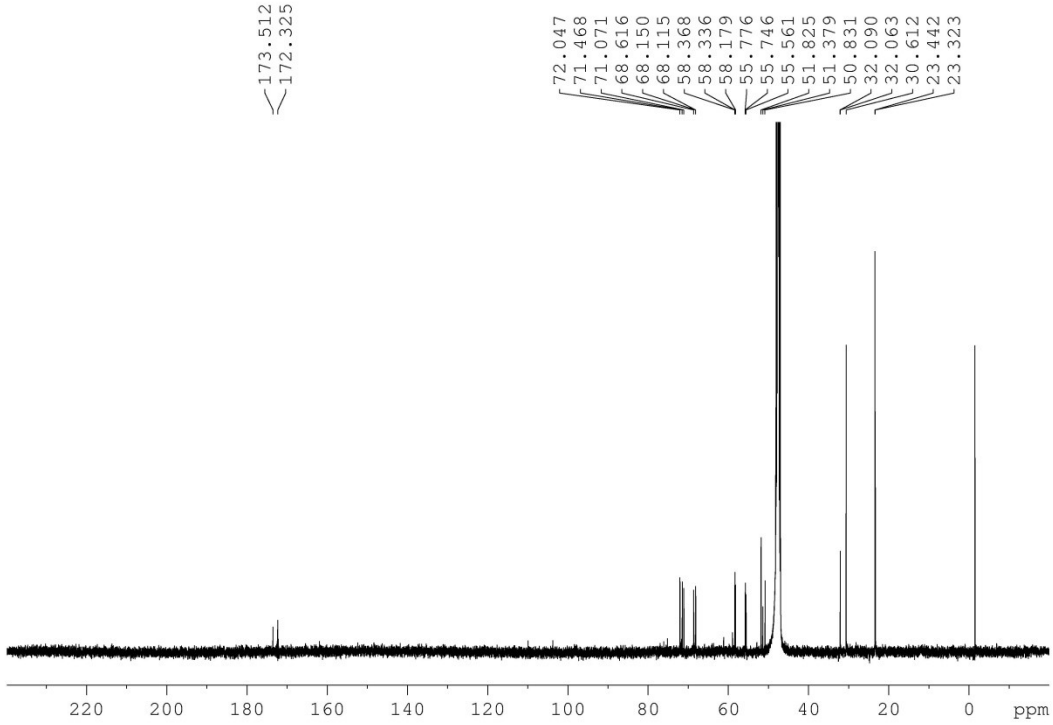
173.512
172.325
72.047
71.468
71.071
68.616
68.150
68.115
58.368
58.336
58.179
55.776
55.746
55.561
51.825
51.379
50.831
32.090
32.063
30.612
23.442
23.323
220
200
180
160
140
120
100
80
60
40
20
0
ppm

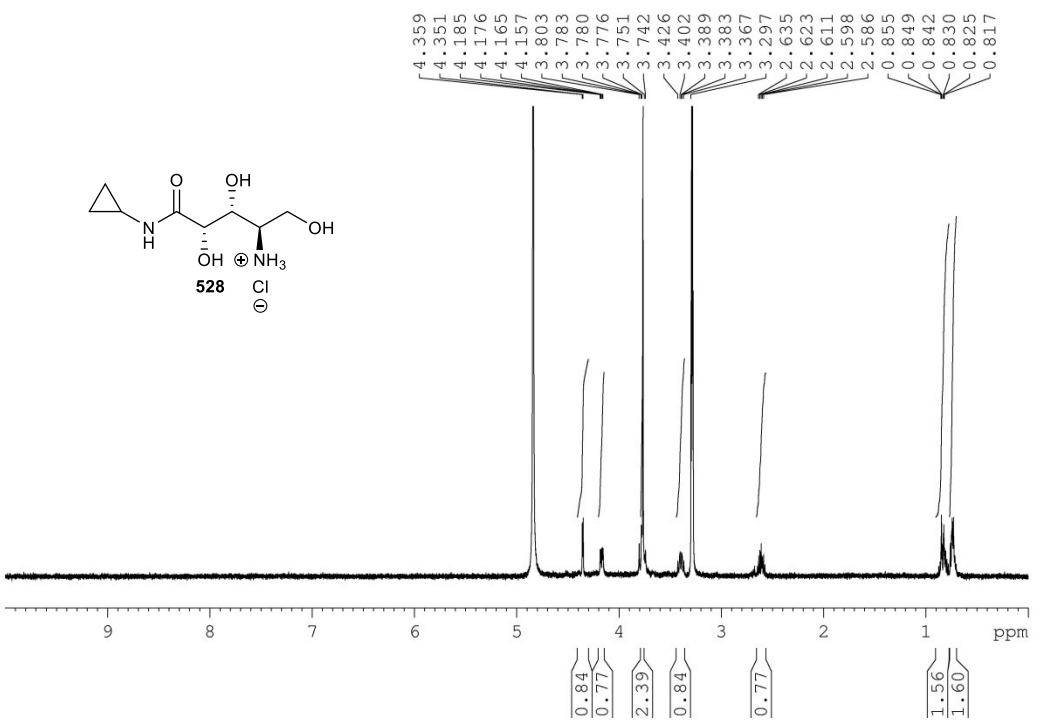
4.359
4.351
4.185
4.176
4.165
4.157
3.803
3.783
3.780
3.776
3.751
3.742
3.426
3.402
3.389
3.383
3.367
3.297
2.635
2.623
2.611
2.598
2.586
0.855
0.849
0.842
0.830
0.825
0.817
O
OH
N
H
OH
NH3
OH
528
Cl
9
8
7
6
5
4
3
2
1
ppm
0.84
0.77
2.39
0.84
0.77
1.56
1.60

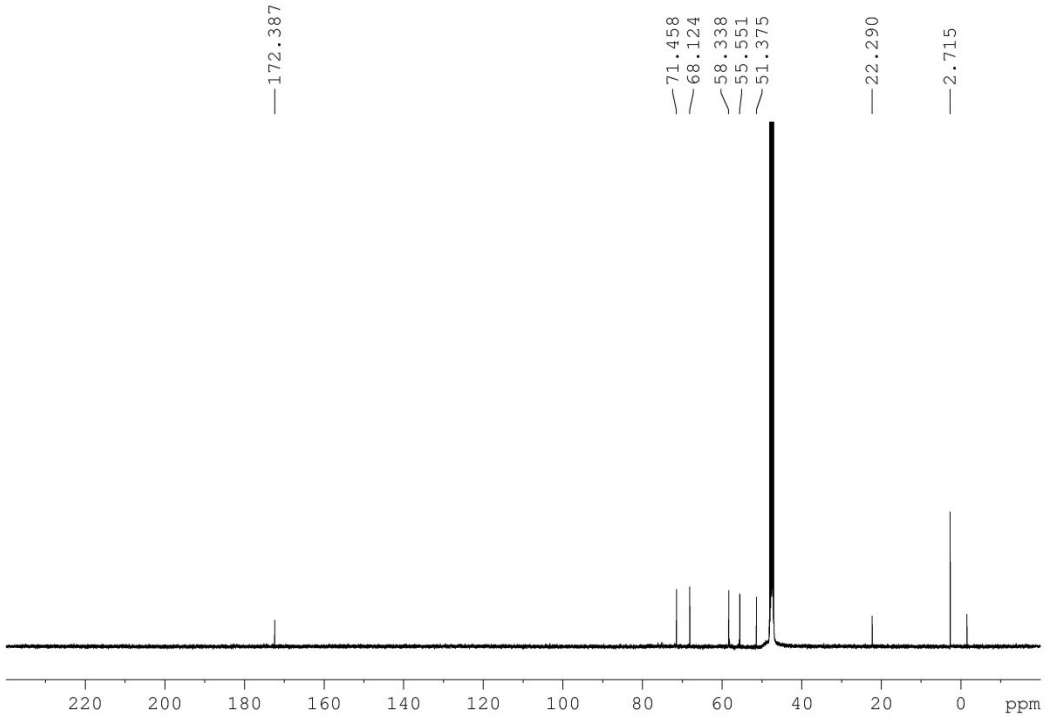
172.387
71.458
68.124
58.338
55.551
51.375
22.290
2.715
220
200
180
160
140
120
100
80
60
40
20
0
ppm

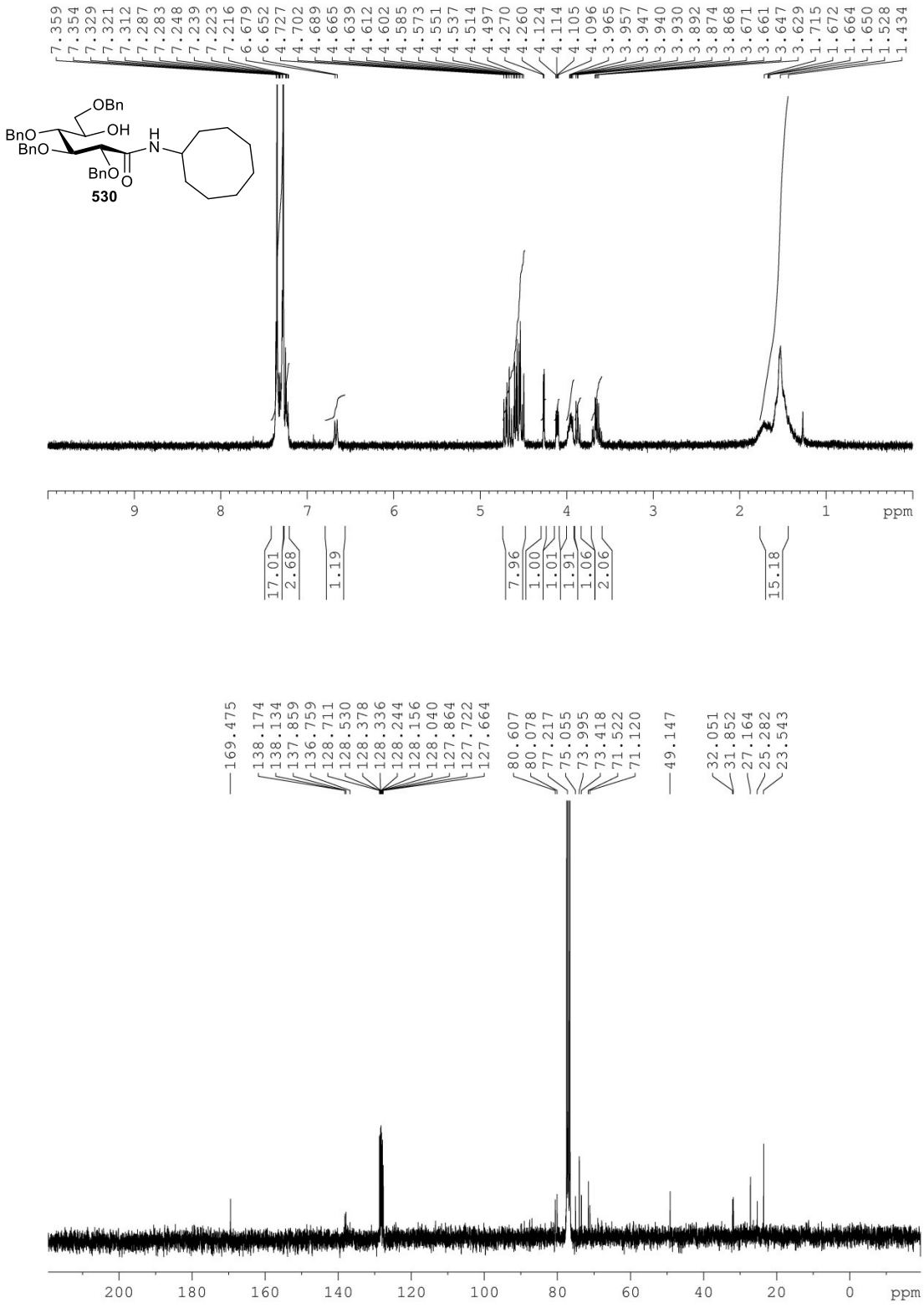
7.359
7.354
7.329
7.321
7.312
7.287
7.283
7.248
7.239
7.223
7.216
6.679
6.652
4.727
4.702
4.689
4.665
4.639
4.612
4.602
4.585
4.573
4.551
4.537
4.514
4.497
4.270
4.260
4.124
4.114
4.105
4.096
3.965
3.957
3.947
3.940
3.930
3.892
3.874
3.868
3.671
3.661
3.647
3.629
1.715
1.672
1.664
1.650
1.528
1.434
OBn
OH
BnO
BnO
BnO
H
N
O
530
9
8
7
6
5
4
3
2
1
ppm
17.01
2.68
1.19
7.96
1.00
1.01
1.91
1.06
2.06
15.18
169.475
138.174
138.134
137.859
136.759
128.711
128.530
128.378
128.336
128.244
128.156
128.040
127.864
127.722
127.664
80.607
80.078
77.217
75.055
73.995
73.418
71.522
71.120
49.147
32.051
31.852
27.164
25.282
23.543
200
180
160
140
120
100
80
60
40
20
0
ppm

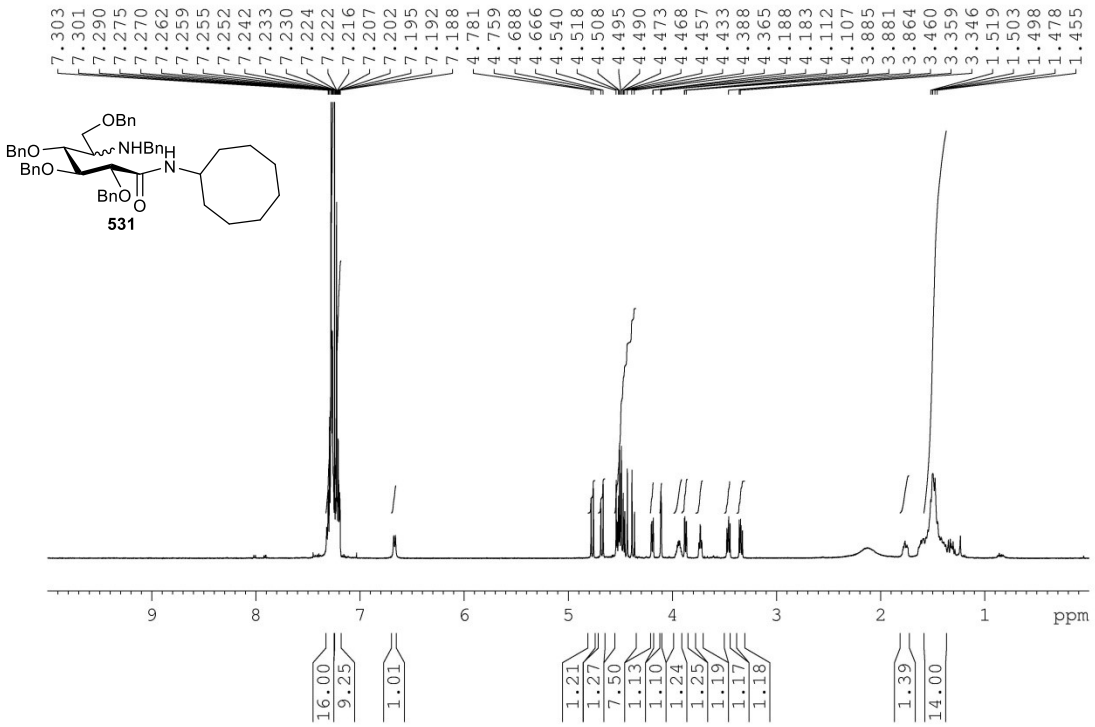
7.303
7.301
7.290
7.275
7.270
7.262
7.259
7.255
7.252
7.242
7.233
7.230
7.224
7.222
7.216
7.207
7.202
7.195
7.192
7.188
4.781
4.759
4.688
4.666
4.540
4.518
4.508
4.495
4.490
4.473
4.468
4.457
4.433
4.388
4.365
4.188
4.183
4.112
4.107
3.885
3.881
3.864
3.460
3.359
3.346
1.519
1.503
1.498
1.478
1.455
OBn
BnO
NHBn
H
N
BnO
BnO
O
531
9
8
7
6
5
4
3
2
1
ppm
16.00
9.25
1.01
1.21
1.27
7.50
1.13
1.10
1.24
1.25
1.19
1.17
1.18
1.39
14.00

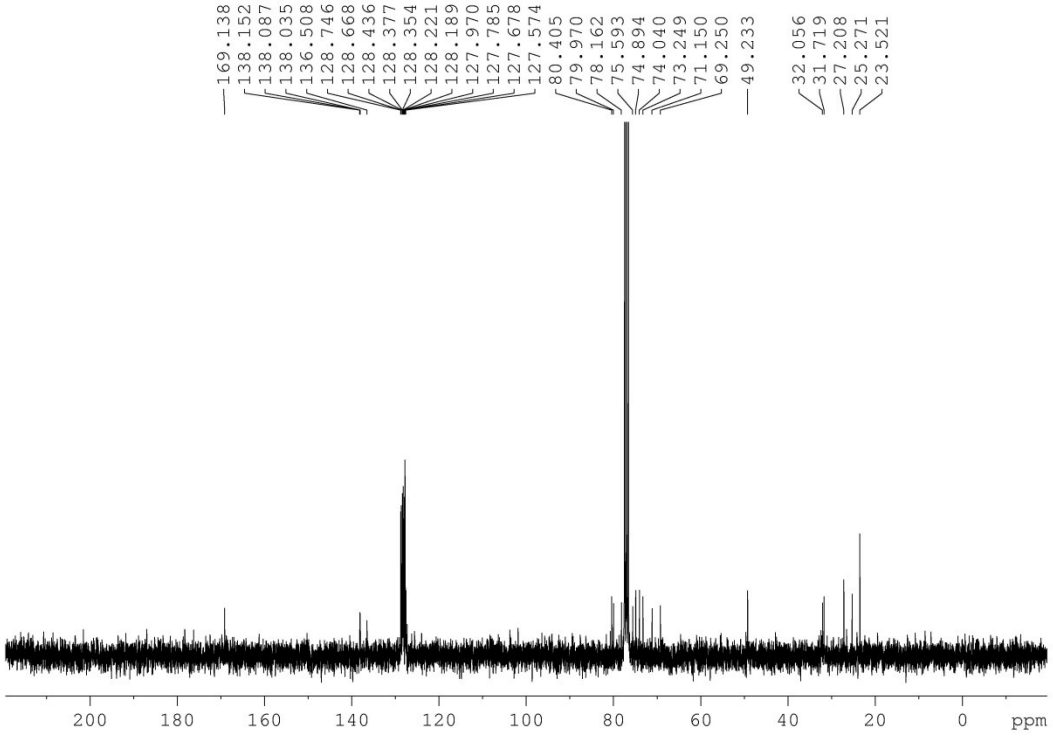
169.138
138.152
138.087
138.035
136.508
128.746
128.668
128.436
128.377
128.354
128.221
128.189
127.970
127.785
127.678
127.574
80.405
79.970
78.162
75.593
74.894
74.040
73.249
71.150
69.250
49.233
32.056
31.719
27.208
25.271
23.521
200
180
160
140
120
100
80
60
40
20
0
ppm

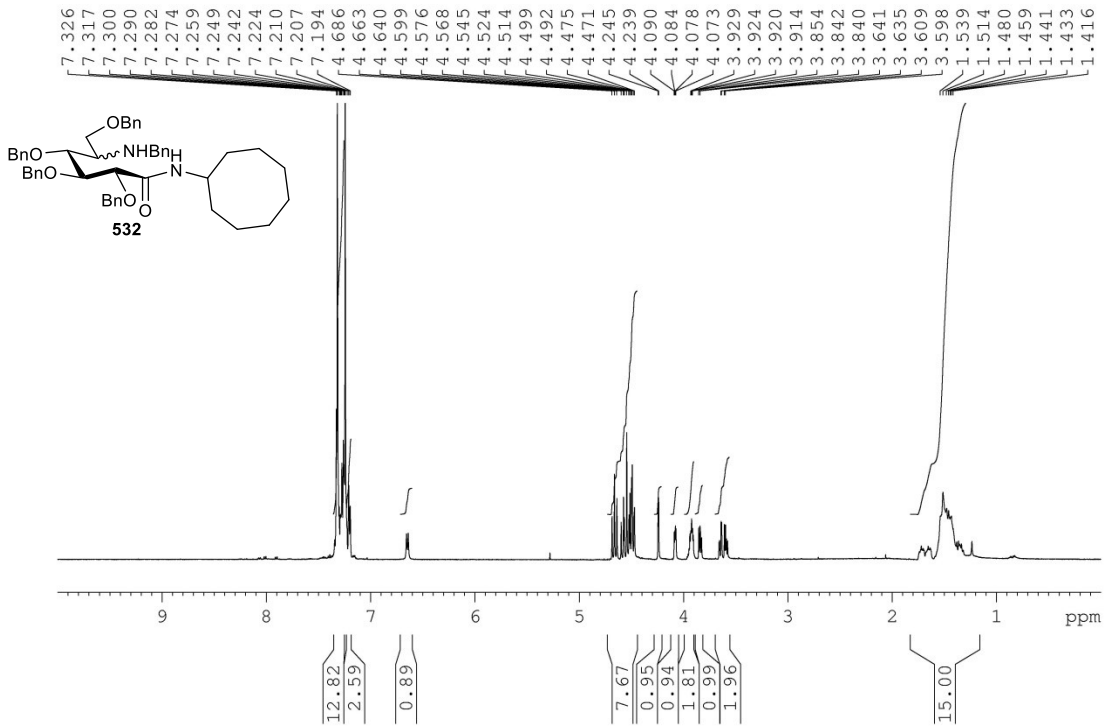
7.326
7.317
7.300
7.290
7.282
7.274
7.259
7.249
7.242
7.224
7.210
7.207
7.194
4.686
4.663
4.640
4.599
4.576
4.568
4.545
4.524
4.514
4.499
4.492
4.475
4.471
4.245
4.239
4.090
4.084
4.078
4.073
3.929
3.924
3.920
3.914
3.854
3.842
3.840
3.641
3.635
3.609
3.598
1.539
1.514
1.480
1.459
1.441
1.433
1.416
OBn
NHBn
H
N
BnO
BnO
BnO
O
532
9
8
7
6
5
4
3
2
1
ppm
12.82
2.59
0.89
7.67
0.95
0.94
1.81
0.99
1.96
15.00

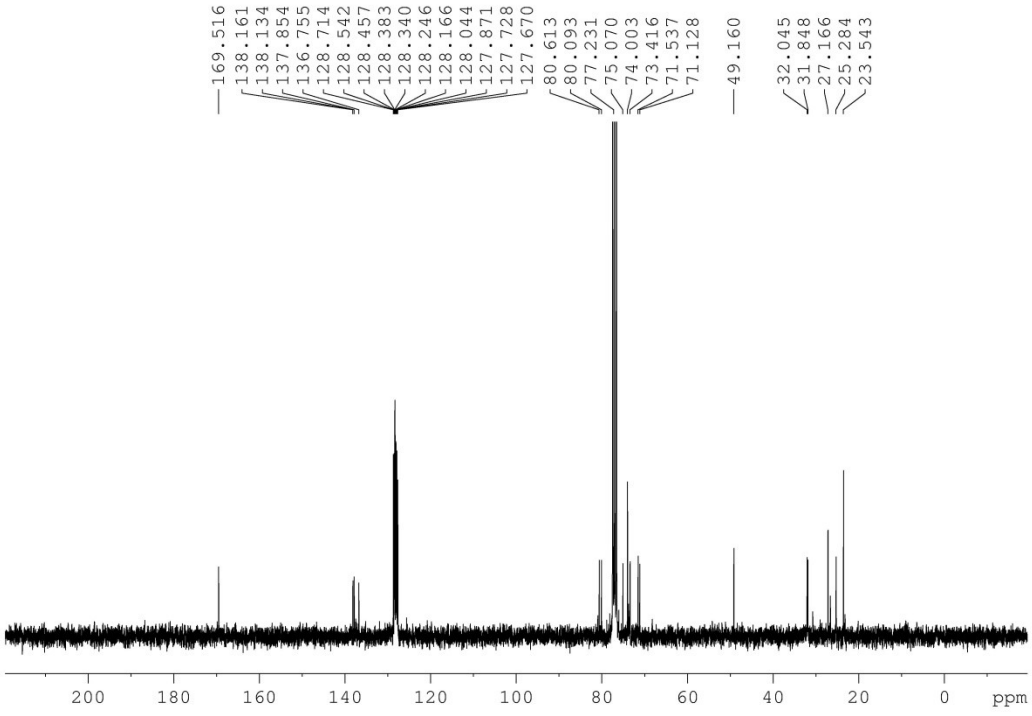
169.516
138.161
138.134
137.854
136.755
128.714
128.542
128.457
128.383
128.340
128.246
128.166
128.044
127.871
127.728
127.670
80.613
80.093
77.231
75.070
74.003
73.416
71.537
71.128
49.160
32.045
31.848
27.166
25.284
23.543
200
180
160
140
120
100
80
60
40
20
0
ppm

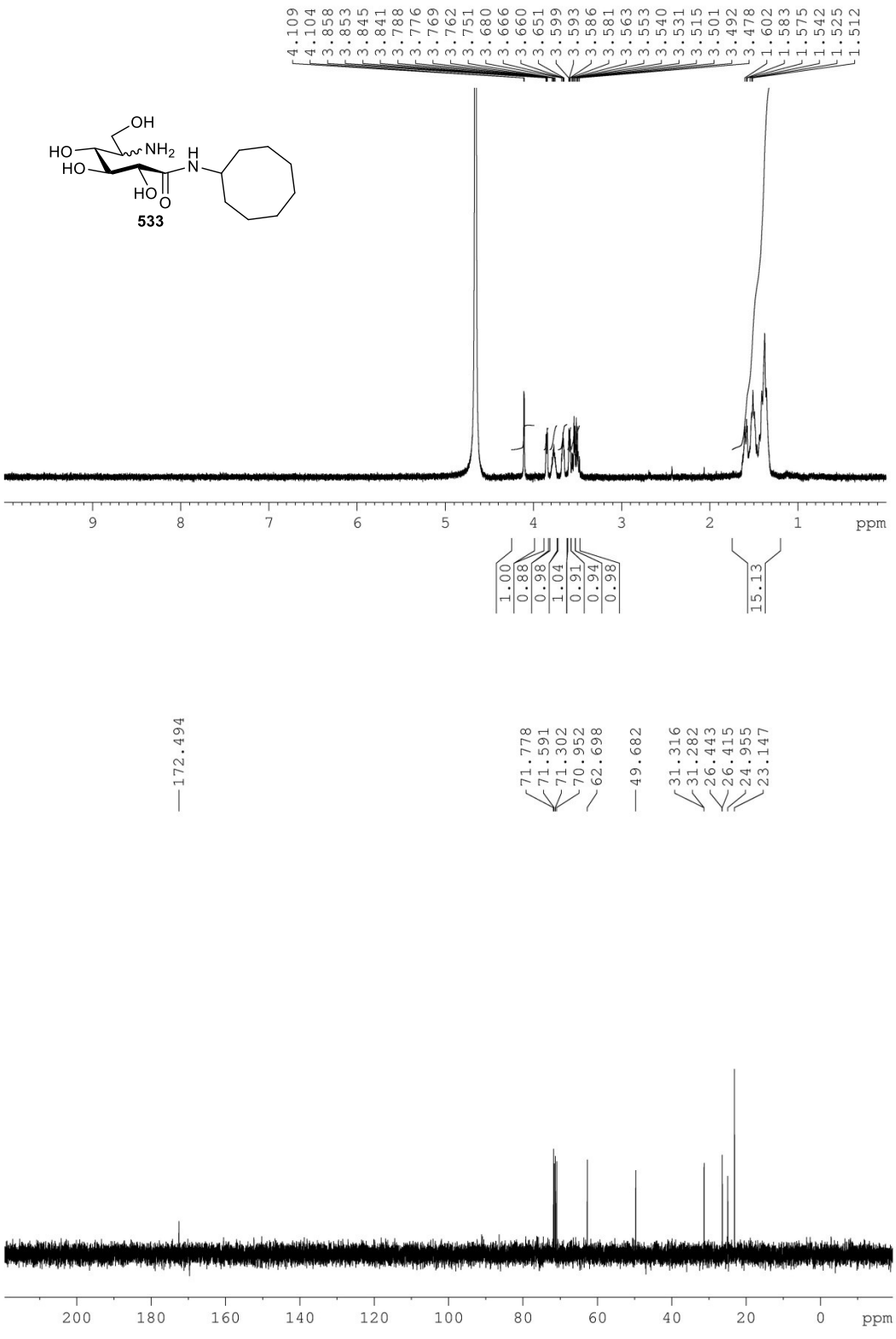
4.109
4.104
3.858
3.853
3.845
3.841
3.788
3.776
3.769
3.762
3.751
3.680
3.666
3.660
3.651
3.599
3.593
3.586
3.581
3.563
3.553
3.540
3.531
3.515
3.501
3.492
3.478
1.602
1.583
1.575
1.542
1.525
1.512
OH
HO
NH2
H
N
HO
HO
O
533
9
8
7
6
5
4
3
2
1
ppm
1.00
0.88
0.98
1.04
0.91
0.94
0.98
15.13
172.494
71.778
71.591
71.302
70.952
62.698
49.682
31.316
31.282
26.443
26.415
24.955
23.147
200
180
160
140
120
100
80
60
40
20
0
ppm

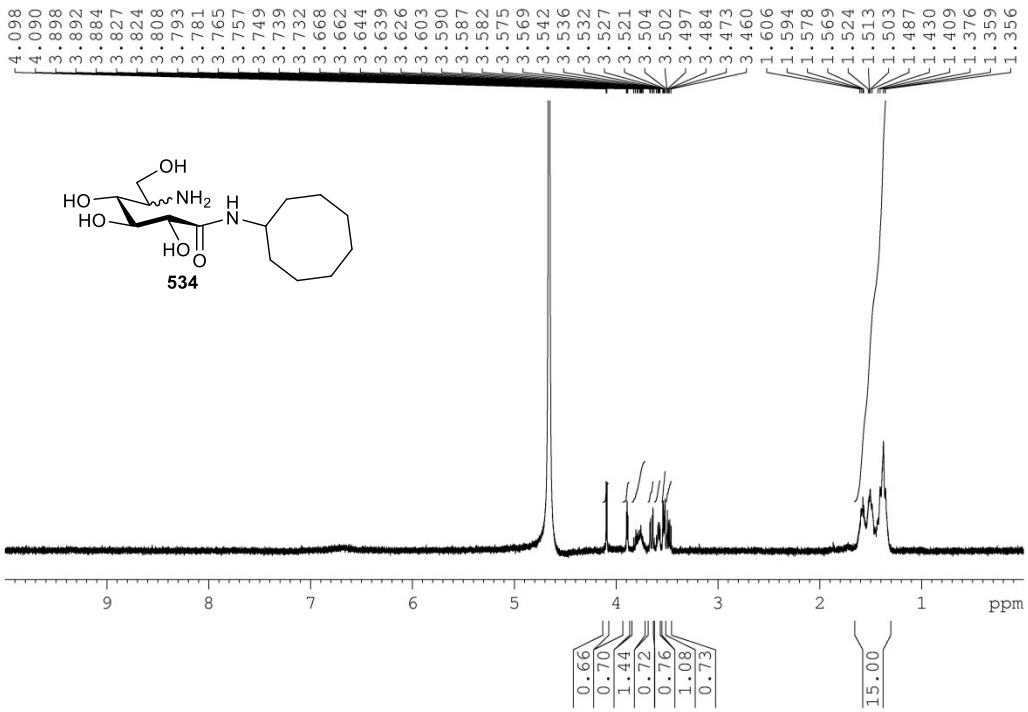
4.098
4.090
3.898
3.892
3.884
3.827
3.824
3.808
3.793
3.781
3.765
3.757
3.749
3.739
3.732
3.668
3.662
3.644
3.639
3.626
3.603
3.590
3.587
3.582
3.575
3.569
3.542
3.536
3.532
3.527
3.521
3.504
3.502
3.497
3.484
3.473
3.460
1.606
1.594
1.578
1.569
1.524
1.513
1.503
1.487
1.430
1.409
1.376
1.359
1.356
OH
HO
NH2
H
N
HO
HO
O
534
9
8
7
6
5
4
3
2
1
ppm
0.66
0.70
1.44
0.72
0.76
1.08
0.73
15.00

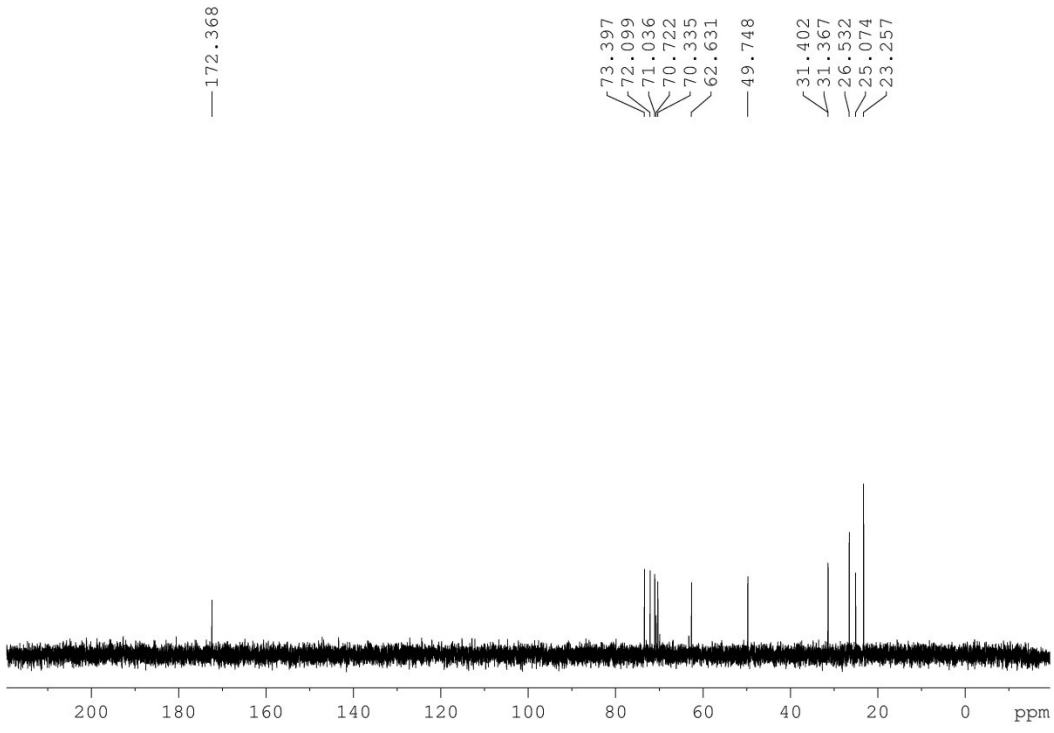
172.368
73.397
72.099
71.036
70.722
70.335
62.631
49.748
31.402
31.367
26.532
25.074
23.257
200
180
160
140
120
100
80
60
40
20
0
ppm

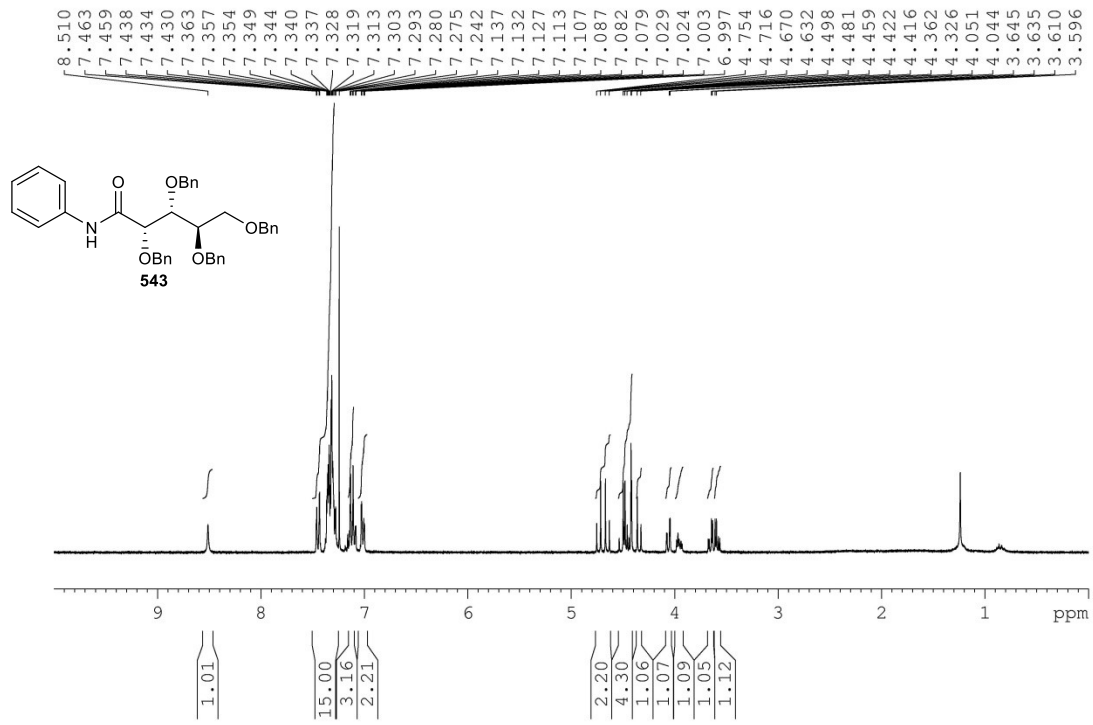
8.510
7.463
7.459
7.438
7.434
7.430
7.363
7.357
7.354
7.349
7.344
7.340
7.337
7.328
7.319
7.313
7.303
7.293
7.280
7.275
7.242
7.137
7.132
7.127
7.113
7.107
7.087
7.082
7.079
7.029
7.024
7.003
6.997
4.754
4.716
4.670
4.632
4.498
4.481
4.459
4.422
4.416
4.362
4.326
4.051
4.044
3.645
3.635
3.610
3.596
O
OBn
N
H
OBn
OBn
OBn
543
9
8
7
6
5
4
3
2
1
ppm
1.01
15.00
3.16
2.21
2.20
4.30
1.06
1.07
1.09
1.05
1.12

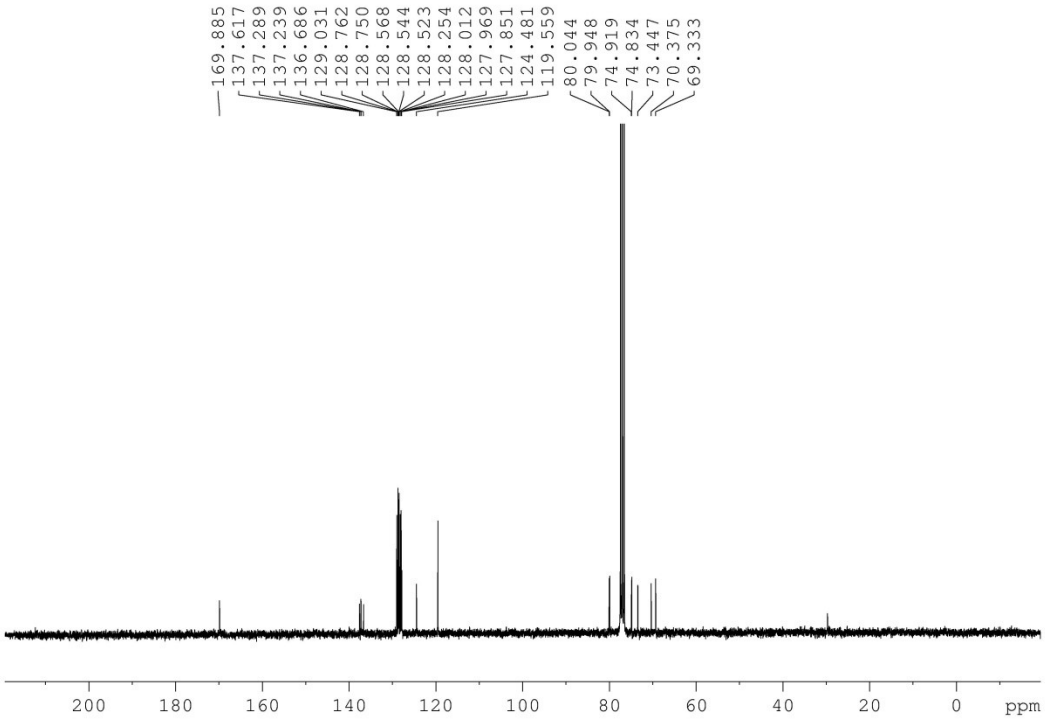
169.885
137.617
137.289
137.239
136.686
129.031
128.762
128.750
128.568
128.544
128.523
128.254
128.012
127.969
127.851
124.481
119.559
80.044
79.948
74.919
74.834
73.447
70.375
69.333
200
180
160
140
120
100
80
60
40
20
0
ppm

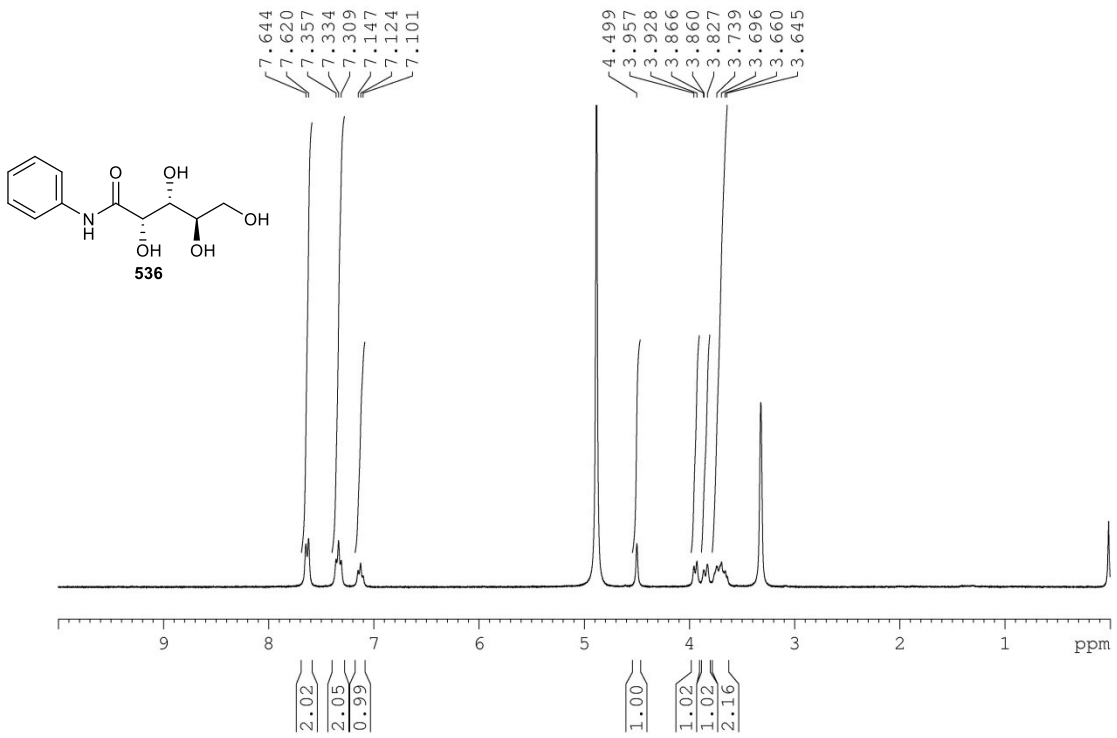
7.644
7.620
7.357
7.334
7.309
7.147
7.124
7.101
4.499
3.957
3.928
3.866
3.860
3.827
3.739
3.696
3.660
3.645
O
OH
N
H
OH
OH
OH
536
9
8
7
6
5
4
3
2
1
ppm
2.02
2.05
0.99
1.00
1.02
1.02
2.16

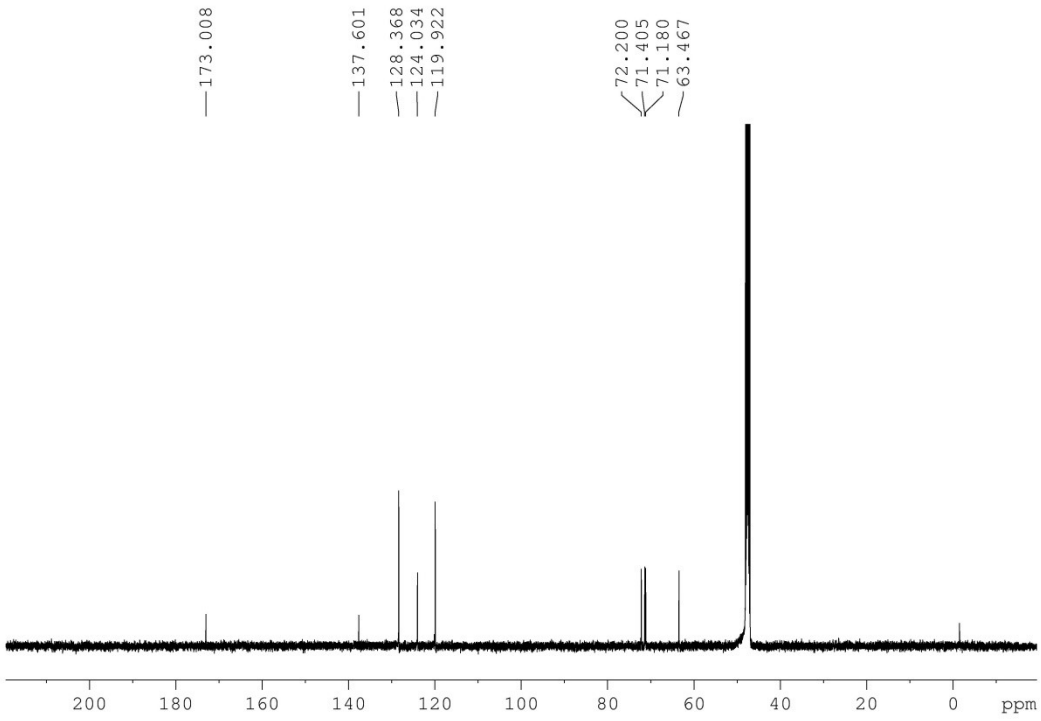
173.008
137.601
128.368
124.034
119.922
72.200
71.405
71.180
63.467
200
180
160
140
120
100
80
60
40
20
0
ppm

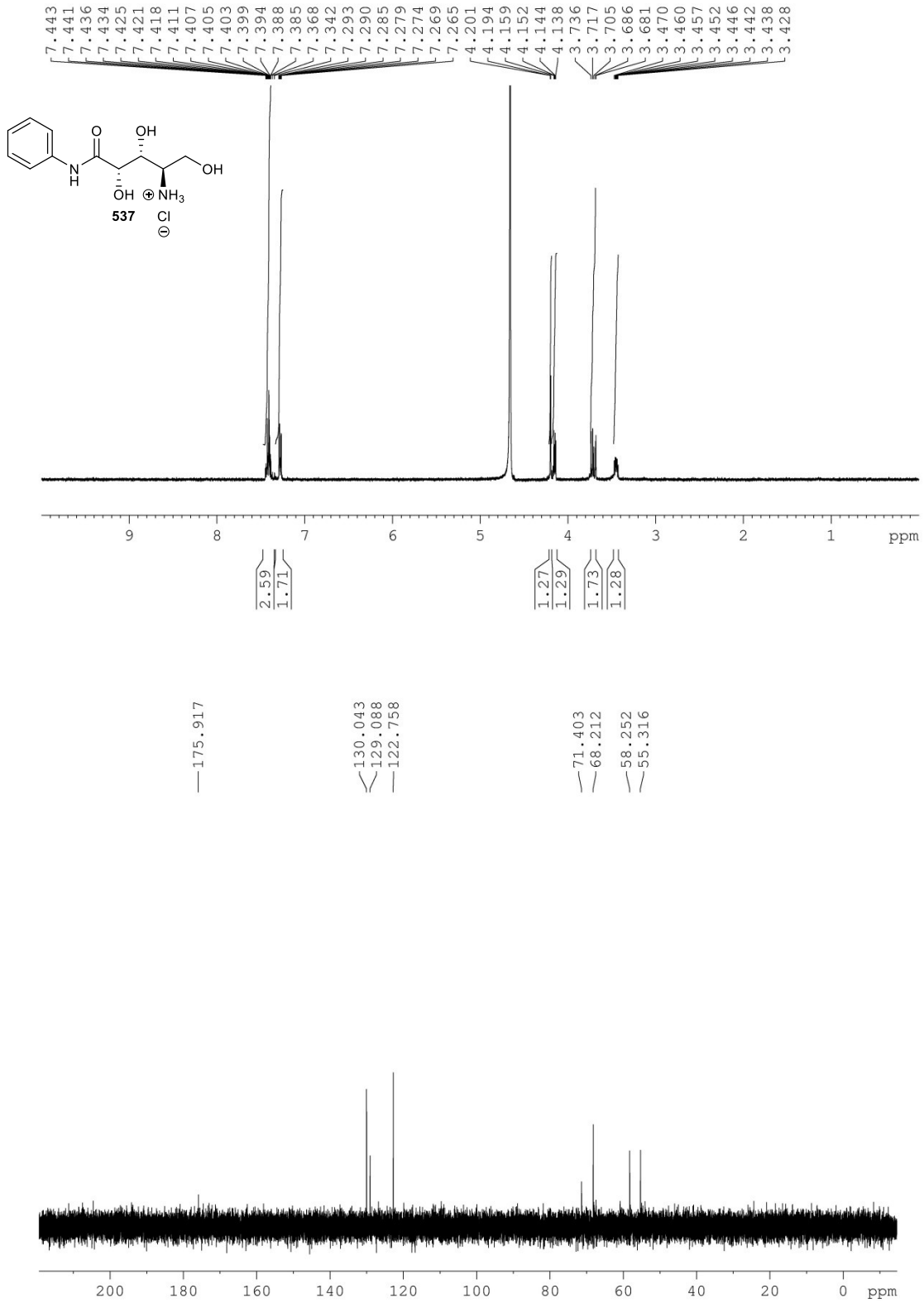
7.443
7.441
7.436
7.434
7.425
7.421
7.418
7.411
7.407
7.405
7.403
7.399
7.394
7.388
7.385
7.368
7.342
7.293
7.290
7.285
7.279
7.274
7.269
7.265
4.201
4.194
4.159
4.152
4.144
4.138
3.736
3.717
3.705
3.686
3.681
3.470
3.460
3.457
3.452
3.446
3.442
3.438
3.428
O
OH
N
H
OH
OH
NH3
537
Cl
9
8
7
6
5
4
3
2
1
ppm
2.59
1.71
1.27
1.29
1.73
1.28
175.917
130.043
129.088
122.758
71.403
68.212
58.252
55.316
200
180
160
140
120
100
80
60
40
20
0
ppm

7.0 References

1. Knight, C. A.; Hallett, J.; DeVries, A. L., *Cryobiology.* **1988,** 25, 55-60.

2. Jackman, J.; Noestheden, M.; Moffat, D.; Pezacki, J. P.; Findlay, S.; Ben, R. N., *Biochem. Biophys. Res. Commun.* **2007,** 354, 340-344.

3. Chakrabartty, A.; Hew, C. L., *Eur. J. Biochem.* **1991,** 202, 1057-1063.

4. Capicciotti, C. J. The Rational Design of Potent Ice Recrystallization Inhibitors for Use as Novel Cryoprotectants. 2014, Ph. D. Dissertation, University of Ottawa.

5. Chaytor, J. L.; Tokarew, J. M.; Wu, L. K.; Leclère, M.; Tam, R. Y.; Capicciotti, C. J.; Guolla, L.; von Moos, E.; Findlay, C. S.; Allan, D. S.; Ben, R. N., *Glycobiology* **2012,** 22, 123-133.

6. Rubinstein, P.; Dobrila, L.; Rosenfield, R. E.; Adamson, J. W.; Migliaccio, G.; Migliaccio, A. R.; Taylor, P. E.; Stevens, C. E., *Proc. Natl Acad. Sci. U. S. A.* **1995,** 92, 10119-10122.

7. Sutherland, D. R.; Anderson, L.; Keeney, M.; Nayar, R.; Chin-Yee, I. A. N., *J. Hematother. Stem Cell Res.* **1996,** 5, 213-226

8. Keeney, M.; Chin-Yee, I.; Weir, K.; Popma, J.; Nayar, R.; Robert Sutherland, D. *Commun. Clin. Cytom.* **1998**, 34, 61-70.

9. Maeda, T.; Nishimura, S.-I., *Chem. Eur. J.* **2008,** 14, 478-487.

10. Martin, O. R.; Saavedra, O. M.; Xie, F.; Liu, L.; Picasso, S.; Vogel, P.; Kizu, H.; Asano, N., *Bioorg. Med. Chem.* **2001,** 9, 1269-1278.

11. Overkleeft, H. S.; van Wiltenburg, J.; Pandit, U. K., *Tetrahedron* **1994,** 50, 4215-4224.

12. Wennekes, T.; van den Berg, R. J. B. H. N.; Donker, W.; van der Marel, G. A.; Strijland, A.; Aerts, J. M. F. G.; Overkleeft, H. S., *J. Org. Chem.* **2007,** 72, 1088-1097.

13. Wennekes, T.; Meijer, A. J.; Groen, A. K.; Boot, R. G.; Groener, J. E.; van Eijk, M.; Ottenhoff, R.; Bijl, N.; Ghauharali, K.; Song, H.; O'Shea, T. J.; Liu, H.; Yew, N.; Copeland, D.; van den Berg, R. J.; van der Marel, G. A.; Overkleeft, H. S.; Aerts, J. M., *J. Med. Chem.* **2009,** 53, 689-698.

14. Dondoni, A.; Perrone, D., *Org. Syn.* **2000,** 77, 64-71.

15. Ben, R.; Capicciotti, C. J. *20150157010*, 2015.

Conclusions

The overall aim for this thesis was the synthesis of novel small molecule ice recrystallization inhibitors and the elucidation of the structural features required for potent IRI activity. These molecules have potential use as novel cryoprotectants and also as inhibitors of formation of gas hydrates which are an ice-like solid. In particular, the goals of this study were: (1) examine the role of hydrogen bond donation at the endocyclic position within a pyranose ring towards IRI activity; (2) Use of recently discovered small molecule IRIs towards inihibiing gas hydrate formation to determine structural features required to inhibit both processes; and (3) synthesis of non-surfactant like small molecule IRIs through the combination of structural features required for potent IRI activity.

The first goal was achieved through the synthesis of azasugars which possessed an amine in place of the ring oxygen. Amines were hypothesized to be protonated at a pH of 7.4 (pH of PBS) and thus possibly only act as hydrogen bond donors. Structure-function work suggested that the presence of hydrogen bond donation at the endocyclic position maybe important to IRI activity. The azasugars possessed moderate to potent IRI activity. Analogues of the azasugars with possibly decreased ability to act as hydrogen bond donors exhibited decreased IRI activity as compared to the azasugars. These results suggested that hydrogen bond donation at the endocyclic position maybe important to IRI activity. If these amines are protonated, the negative counterion may also be playing a role in hydration and IRI activity. Furthermore, the low cytotoxicity towards the metabolic activity of Hep G2 cells of the D-glucose based azasugar suggested its further exploration as a novel cryoprotectant.

Secondly, recently developed small molecule IRIs such as the azasugars, carbohydrate-based surfactants and hydrogelators possessing long alkyl chains were investigated for their ability to inhibit gas hydrate formation. The effectiveness of the small molecules was measured using a differential scanning calorimeter to track the cumulative heat of reaction generated from the formation of a sI gas hydrate. The small molecules were compared to PVP 10 which is a commercial inhibitor. The resulted suggested that some of the small molecules were superior to the commercial inhibitor at much lower weight percent concentrations. However, an overall analysis revealed that IRI activity was not a good predictor of the ability to inhibit gas hydrate formation. It was demonstrated that the small molecules do not possess the ability to bind to ice (TH activity) and thus, it was suggested that they possibly do not bind to gas hydrates either.

The last goal of this thesis was achieved by first examining the structural features of recently developed small molecule IRIs. These included presence of long alkyl chains, an amide linkage, the presence of an open-alditol chains, the presence of an amine at C3 on a pyranose ring and a pyranose ring possessing an aryl ring at the anomeric carbon. The combination of long alkyl chains to a polar carbohydrate head has led to a surfactant-like nature to some of these compounds which can be detrimental to cell membranes during cryopreservation. Thus, the remaining structural motifs were combined to generate a series of disaccharides where open-alditol chains of D-glucose and D-galactose were linked to the pyranose ring of β-PMP-Glc by an amide bond either at the C3 or C6 position on the pyranose ring. These disaccharides produced only one potent inhibitor of ice recrystallization. This disaccharide possessed the open-alditol chain of D-galactose linked to the pyranose ring of β-PMP-Glc via an amide at the C3 position.

Given that *N*-alkyl-D-aldonamides possessed unprecedented IRI activity, the use of other hydrophobic moieties attached to an open-alditiol chain required further exploration. Furthermore, it has been demonstrated that a delicate balance between hydrophobicity and hydrophilicity impacts IRI activity. Based on this, a series of *N*-cycloalkyl and *N*-phenyl-aldonamides were synthesized and investigated for their IRI activity. The use of different cycloalkyl groups as the hydrophobic moiety did not impact IRI activity. Additionally, modification to the open-alditol chain of D-glucose such as removal of a hydroxyl group or replacement of a hydroxyl group to an amine also resulted in minimal impact on IRI activity. However, *N*-phenyl-D-arabonamide was found to possess potent IRI activity. Further kinetic investigation of this activity demonstrated this compound to be one of the more potent inhibitors of ice recrystallization discovered by the Ben laboratory. Lastly, the use of these novel small molecules IRIs towards cryopreservation of hematopoietic stem cells was also explored. Overall, these compounds failed to demonstrate an improvement over the commercially utilized 10% DMSO cryoprotectants solution.

Overall, these studies promote the further investigation of other novel small molecule IRIs towards inhibiting ice recrystallization and gas hydrate formation. The success demonstrated by some of the molecules studied within this thesis will facilitate future studies in this field.

Claims to Original Research

1. IRI, TH and cytotoxicity profiles of azasugars and its analogues.
2. Use of small molecule IRIs to inhibit gas hydrate formation.
3. Syntheis, IRI activity and analysis of cryopreservative ability of disaacharides possessing open-alditol chains of D-glucose and D-galactose were linked to the pyranose ring of β-PMP-Glc by an amide bond either at the C3 or C6 position on the pyranose ring. Addtionally, a similar analysis of *N*-cycloalkyl-D-aldonamides and *N*-phenyl-D-aldonamides

Publications

Tonelli, D.; Capicciotti, C. J.; Doshi, M.; Ben, R. N., *RSC Adv.* **2015,** 5, 21728-21732.

Capicciotti, C. J.; Doshi, M.; Ben, R. N., Ice Recrystallization Inhibitors: From Biological Antifreezes to Small Molecules. In *Recent Developments in the Study of Recrystallization*, Wilson, P., Ed. InTech: New York, 2013; pp 177-224.